

Modelling pumped-storage effects on thermal structure, ice cover and water quality of lakes and reservoirs in a changing climate

Thèse N° 9211

Présentée le 4 février 2019

à la Faculté de l'environnement naturel, architectural et construit
Laboratoire de physique des systèmes aquatiques - Chaire Margaretha Kamprad
Programme doctoral en génie civil et environnement

pour l'obtention du grade de Docteur ès Sciences

par

ULRIKE KOBLER

Acceptée sur proposition du jury

Prof. U. von Gunten, président du jury
Prof. A. J. Wüest, Dr M. Schmid, directeurs de thèse
Prof. M. Leppäranta, rapporteur
Dr M. Perroud, rapporteuse
Prof. A. Schleiss, rapporteur

2019

*The only way to know how a complex system will behave – after you modify it –
is to modify it and see how it behaves.*

George E. P. Box

Acknowledgements

When I was invited for the job interview to Kastanienbaum four years ago, I got a perfect impression on why so many people like working at Eawag: it was not only a perfect day without any clouds and an amazing view at Lake Lucerne and the surrounding mountains, but it was also the community feeling, which one could grasp during the coffee break on the terrace. So I was really pleased, when I heard from Martin that I got this PhD position.

Martin, ich möchte dir ein grosses Danke aussprechen für deine Unterstützung während dieser vier Jahre meines Doktorats. Danke für die vielen Stunden in denen du mit mir Lösungsvorschläge diskutiert und Ideen gewälzt hast, und dass, du mich weiter motiviert hast, wenn ich kaum noch Licht am Ende des Tunnels gesehen habe. Ausserdem möchte ich mich für deine Unterstützung bei der Feldarbeit bedanken.

Johny, danke für deine Unterstützung, deinen Einsatz und deine guten Ratschläge vor allem betreffend der Publikationen. Ich bin sehr dankbar, dass ich dich als meinen Doktorvater habe und ich auf deine vieljährigen Erfahrungen zurückgreifen konnte.

Bei der SBB AG möchte ich mich bedanken, dass sie dieses Doktorat überhaupt ermöglicht haben und mir dabei sehr viel Freiheit gelassen haben. Besonders gilt mein Dank Jana Lutz und Andreas Eggimann, die mir immer rasch mit Antworten zur Verfügung standen.

Bei der Feldarbeit durfte ich auf die Hilfe von Michi Schurter, dem ich jetzt leider nicht mehr persönlich danke sagen kann, zählen.

Auch Michi Plüss möchte ich für seinen Einsatz bei der Feldarbeit ein grosses Danke aussprechen: danke, dass du immer die Ruhe in Person warst, und dass du dich mit mir aufs Eis gewagt hast.

In diesem Zusammenhang möchte ich mich auch beim Etzelwerk-Team bedanken, das uns immer bei der Feldarbeit begleitet hat und mich während der vorangegangenen Kaffeepausen oft zum Lachen brachte.

Patrick Kathriner danke, dass du für dieses Projekt die Laborarbeit erledigt hast und dir Zeit genommen hast mich für meine Lehrtätigkeit vorzubereiten.

Für die Unterstützung bei administrativen Dingen (und beim Geldwechsel um an die nächste Tasse Kaffee zu gelangen) möchte ich euch, Eliane, Patricia, Nadja, Luzia und Michelle, danken.

I would also like to thank Eric de Goede and Rob Uittenbogaard for their help regarding Delft3D.

Zudem danke ich Christine Levy und Felix Keller für ihre Zeit mir die Eisdickenbestimmung mit dem Georadar näher zu bringen.

Philipp, danke, dass du immer ein offenes Ohr für meine Probleme hattest und dir auch oft die Zeit genommen hast Lösungen dafür zu finden.

Many thanks also go to Adrian, who shared his expertise on Simstrat and PEST, perfectly organised our bike to work group over these four years, and was often making me smile.

Fabian, danke, dass du dich um meine Simstrat-Problemchen gekümmert hast, und auch sonst möchte ich dir danken für deine ruhige Art, die mich manchmal auch anstecken konnte, gewisse Situationen nicht zu ernst zu nehmen.

Davide, thanks for being such a great and funny office mate, for your support with the set-up of GLM, and for discussing with me.

To the other members of the Modelling Group I would like to say thank you for discussing many issues and your constructive criticism.

Auch bei den Mitgliedern des KB-Forums, Beat, Patricia, Karin, Pädi, Dani und Andreas möchte ich mich bedanken für die gemeinsame Arbeit. Dank gilt in diesem Zusammenhang auch Anna, die mir in der Position als PhD-Repräsentantin nachfolgt.

I would also like to thank all my friends for keeping me sane throughout these four years, animating me to go out, and for just being there whenever I needed someone to talk to.

Particularly, I would like to thank Rohini, for being such a good friend, giving me some insights in the Indian cuisine, chatting about something else than work during coffee breaks, and teaching me how to successfully master difficult times!

To all other fellow PhD students and co-workers: thank you for making these four years of my PhD in KB extra special.

Zum Abschluss möchte ich mich nun bei meiner Familie bedanken. Danke Papa, dass du mir das Studium in Wien ermöglich hast, dass du nach dem Verlust unserer Mutter immer bereit gestanden bist, wenn es mal schwierig wurde und dass du mich mit deinem Gespür für grafisches Design infiziert hast.

Gudrun, Reinmar und Erich, danke, dass ihr so grossartig seid, mich über schwierige Zeiten getröstet habt, mir immer mal wieder eine Motivationsspritze verpasst habt, und einfach nur da seid, wenn es darauf ankommt.

Elena und Severin, danke, dass ich noch nicht zu „uncool“ bin eure grosse Schwester zu sein. Danke Karin, dass ich Teil dieser zweiten Familie sein darf.

Ein Dank gilt auch den weiteren Mitgliedern meiner Familie, allen voran meinen grossartigen Tanten, Martha, Monika und Ulrike, und meiner Oma, Angela, ihr seid immer für mich da und nur einen Anruf entfernt.

Christof, danke, dass du mir, wenn ich es mal brauche die Leviten liest, mich motivierst, für mich Dinge tust, die du eigentlich gar nicht magst, und mich zum Lachen bringst!

Kastanienbaum, 31 October 2018

Abstract

New renewable electricity is nowadays often generated by photovoltaics and wind. Yet, their intermittent nature calls for energy storage, which is today still provided to ~95% by pumped-storage (PS) hydropower plants. However, PS is known to affect abiotic and biotic characteristics of the two connected water bodies. Thus, a two-dimensional laterally-averaged hydrodynamic and water quality model was set up to assess the impacts on water quality and temperature in a first step. Then, this analysis was extended to evaluate the additional effect of climate change, which also modifies abiotic and biotic characteristics. For this purpose, 150-years long synthetic time series of meteorological conditions for current (1998-2012) and future climate (2078-2092) were generated with a weather generator. To assess the robustness of projected impacts on the ice cover of the upper reservoir (Sihlsee) three one-dimensional, vertical hydrodynamic models were additionally set up.

To attribute effects to either the PS flows or to water withdrawal from the hypolimnion, two reference scenarios were defined: one with deep-water withdrawal (NoPS) and another one with surface outflow (QNat). While the hypolimnetic temperature differs by $<1\text{ }^{\circ}\text{C}$ comparing present PS and NoPS, the temperature differences can reach up to $\sim 10\text{ }^{\circ}\text{C}$ for the comparison with QNat. Thus, the effects at Sihlsee are mainly shaped by the deep-water withdrawal. The hypolimnetic warming will be further amplified by climate change with an increase, e.g. for September, of $< 0.6\text{ }^{\circ}\text{C}$ for QNat compared to $\sim 2.5\text{ }^{\circ}\text{C}$ for the extended PS operation.

The major hypolimnetic temperature dissimilarities between QNat and all other PS scenarios further result in different dynamics of stratification, oxygen depletion and nutrient release from sediments. Climate change, in case of QNat, further strengthens and prolongs summer stratification, which consequently leads to declining dissolved oxygen and increasing phosphate concentrations in the hypolimnion. This effect can partly be counteracted by deep-water withdrawal and PS operation.

While the comparison of present with both reference scenarios yields no major differences for the ice-covered period, the ice thickness is projected to decline by $\sim 30\%$ along with an earlier ice-off by ~ 1 month for the extended PS scenario. Climate change generally results in an additional thinning and shortening of the ice-covered period. This trend is supported by the results of the one-dimensional models. For the extended PS operation, future climate could even result in a complete disappearance of the ice cover at Sihlsee, which is not supported by all models, as the two-dimensional model shows different impacts for segments closer to the PS intake/outlet.

Overall, the results highlight the importance of the PS intake/outlet position, and of a clear definition of the reference state for the environmental impact assessment. This seems to be crucial for existing reservoirs, as the choice of the reference state could result in a different assessment of the ecological effects and subsequently requirements and costs for compensation measures. Moreover, the findings show that future climate should be considered for the planning of new and recommissioning of existing PS hydropower plants, which will be in place for many decades.

Keywords

Reservoir modelling; recommissioning pumped-storage operations; hydropower; lake ice; lake stratification; lake stability; weather generator; climate scenarios; CE-QUAL-W2; GLM; Simstrat; MyLake;

Zusammenfassung

Immer mehr Elektrizität wird durch Photovoltaik- oder Windanlagen produziert. Jedoch ist diese zeitlich veränderlich und erfordert elektrische Speicherkapazität, die auch heute in den meisten Fällen durch Pumpspeicherung (PS) bereitgestellt wird. Allerdings wirkt sich die PS auf abiotische und biotische Faktoren der verbundenen Gewässer aus. Daher wurde ein zweidimensionales hydrodynamisches und Wasserqualitätsmodell aufgesetzt. Da der Klimawandel die verbundenen Gewässer ebenfalls verändert, wurde das Modell erweitert. Dazu wurden 150-jährige Zeitreihen für aktuelle (1998-2012) und künftige (2078-2092) meteorologische Daten mit einem Wettergenerator erzeugt. Um zu überprüfen, wie aussagekräftig die Ergebnisse des zweidimensionalen Modells betreffend der Eisdecke des oberen Speichersees (Sihlsee) sind, wurden zusätzlich drei weitere ein-dimensionale hydrodynamische Modelle erstellt.

Vergleicht man den aktuellen PS-Betrieb mit zwei unterschiedlichen Referenzszenarien ergeben sich Temperaturdifferenzen (ΔT) im Hypolimnion von $< 1^\circ\text{C}$ (Referenz mit Tiefenwasserentnahme) und $\sim 10^\circ\text{C}$ (Referenz mit Oberflächenabfluss, QNat). Daher wird die Temperatur im Hypolimnion des Sihlsees hauptsächlich durch die Tiefenwasserentnahme beeinflusst. Für die PS-Erweiterung entstehen ΔT im Hypolimnion von $\sim 2^\circ\text{C}$. Zusätzlich beeinflusst das künftige Klima die Temperatur im Hypolimnion, z.B. ergeben sich für September $\Delta T < 0.6^\circ\text{C}$ für QNat und $\sim 2.5^\circ\text{C}$ für die PS-Erweiterung.

Die grossen ΔT im Hypolimnion zwischen QNat und allen anderen PS-Szenarien verändern auch die Schichtung, die Sauerstoffzehrung und die Nährstoffrücklösung aus dem Sediment. Für QNat bedeutet die Berücksichtigung des Klimawandels, dass die sommerliche Schichtung verstärkt und verlängert wird, was zu verringertem Sauerstoffgehalt und zunehmenden Phosphatkonzentrationen im Hypolimnion führt. Dieser Effekt kann durch die Tiefenwasserentnahme und den PS-Betrieb zum Teil kompensiert werden.

Für die PS-Erweiterung im aktuellen Klima findet das Ende der Eisbedeckung um ~ 1 Monat früher statt und die Dicke verringert sich um $\sim 30\%$. Alle anderen Szenarien gleichen sich im aktuellen Klima. Hingegen ergeben sich unabhängig vom Szenario für das künftige Klima dünnere Eisdecken und kürzere eisbedeckte Perioden, was durch die eindimensionalen Modelle bestätigt wurde. Im Falle der PS-Erweiterung könnte die Eisbedeckung sogar völlig ausbleiben. Allerdings wird diese Aussage nicht von allen Modellen bestätigt. Zudem würde beim zweidimensionalen Modell die Eisbedeckung in der Nähe der Entnahmestelle stärker beeinflusst.

Die Ergebnisse unterstreichen die zentrale Bedeutung der Entnahme-/Rückgabentiefe. Für bestehende Speicherseen stellt sich ausserdem die Frage, wie ein Referenzzustand zu definieren

ist. Denn abhängig von der Definition ergeben sich grössere oder kleinere Unterschiede, die in weiterer Folge über die Kosten der Kompensationsmassnahmen entscheiden. Des Weiteren heben die Untersuchungen hervor, dass bei der Umweltverträglichkeitsprüfung von Neubauten oder Erweiterungen von PS-Kraftwerken künftige Klimaszenarien zu berücksichtigen sind.

Stichwörter

Modellierung von Speicherseen; Erweiterung von Pumpspeicherkraftwerken; Wasserkraft; Seeeis; Schichtung und Stabilität von Seen; Wettergenerator; Klimaszenarien; CE-QUAL-W2; GLM; Simstrat; MyLake;

Contents

Acknowledgements	v
Abstract	ix
Zusammenfassung.....	xi
Contents	13
Chapter 1 Introduction	15
1.1 Pumped-storage effects.....	16
1.2 Climate change effects.....	18
1.3 Development of local climate projections.....	20
1.4 Lake and ice modelling	21
1.5 Study site.....	23
1.6 Approach and outline.....	25
Chapter 2 Effects of lake-reservoir pumped-storage operations on temperature and water quality	27
2.1 Overview.....	27
2.2 Introduction.....	28
2.3 Study site.....	30
2.4 Materials and methods.....	32
2.5 Results	35
2.6 Discussion	37
2.7 Conclusions.....	43
Chapter 3 Supplementary information to Chapter 2.....	45
3.1 Overview.....	45
3.2 Model forcing and initial conditions	46
3.3 Available observations at Sihlsee and Upper Lake Zurich and model calibration	52
3.4 Results at Upper Lake Zurich.....	62
3.5 Specifications of pumped-storage hydropower plants in literature review.....	66
Chapter 4 Combined effects of pumped-storage operation and climate change on thermal structure and water quality	67
4.1 Overview.....	67
4.2 Introduction.....	68
4.3 Study sites.....	70
4.4 Materials and methods.....	71
4.5 Results	73
4.6 Discussion	80
4.7 Conclusions.....	83

Chapter 5	Supplementary information to Chapter 4	85
5.1	Overview	85
5.2	Additional information on model description and study site	86
5.3	Calibration and validation of the weather generator VG	89
5.4	Additional results Sihlsee	96
5.5	Results Upper Lake Zurich	98
Chapter 6	Ensemble modelling of ice cover for a reservoir affected by pumped-storage operation and climate change	105
6.1	Overview	105
6.2	Introduction	106
6.3	Study site	108
6.4	Methodology	108
6.5	Results	114
6.6	Discussion	122
6.7	Conclusions	124
Chapter 7	Supplementary material to Chapter 6	127
7.1	Overview	127
7.2	Selected segments in CE-QUAL-W2	128
7.3	Meteorological forcing	129
7.4	Adaptation GLM	130
7.5	Sensitivity analysis	131
7.6	Additional information model calibration	142
7.7	Temporal dynamics lake ice projections	145
7.8	Additional information on the effects due to PS operation and climate change	149
Chapter 8	Conclusions	151
8.1	Achieved results	151
8.2	Outlook	153
References		155
Curriculum Vitae		163

Chapter 1 Introduction

Greenhouse gas emissions increased from 2000 to 2010 more rapidly than in the previous three decades (IPCC 2014). The most effective mitigation measure is to implement more renewable energy (IPCC 2014). Decreasing costs, increasing performance and incentives for investments in renewable energy technologies entailed a globally increasing share of the newly added electricity generating capacity. In 2016, renewables accounted for ~62% of the net addition to the global power generating capacity (REN21 2017). This increase was mainly due to a growing proportion of wind, hydro and solar power generation.

One of the drawbacks of electricity production with renewable technologies, such as wind and solar, is their intermittency, which can be overcome by electric storage capacity. Still today, the most widely used electrical energy storage is provided through pumped-storage (PS) hydropower plants, which accounted for ~95% by the end of 2016 (REN21 2017). These PS hydropower plants typically connect two or more water bodies, and are operated in the two modes of generating and pumping. During times of overproduction or low price levels, electricity can be used to pump water from the lower to the upper water body, thus, increasing the potential energy. During times of high electricity demand, water can be released from the upper water body to generate electricity.

However, PS operations are known to affect the upper and the lower water bodies, which are related to this type of electricity generation and storage. Due to expensive investments, PS hydropower plants are also intended to be operated for many decades within which climate change could further modify the connected water bodies. Yet, the coupled effects due to PS operation and climate change have not been studied. Moreover, the modifications of ice cover due to PS operation have up to now not been quantified. To address these remaining questions in this thesis, numerical models will be utilised in combination with local climate projections. Therefore, the current state of knowledge is briefly reviewed in the following with respect to (i) PS effects, (ii) climate change effects, (iii) the development of local climate projections, as well as (iv) lake and ice modelling.

1.1 Pumped-storage effects

PS operations modify physical and geochemical (abiotic) as well as ecological (biotic) properties of the connected water bodies. Abiotic effects include changes of water temperature, stratification, water level fluctuations (WLF), sediment resuspension, oxygen and nutrient cycling as well as inorganic suspended solids (ISS) concentrations, which further affect light penetration (Bonalumi et al. 2011). The creation of strong currents, especially close to turbine outlets, may induce changes in lake-internal circulation patterns (Anderson 2006). WLF might, moreover, change the conditions of sediment pore water (Wildman et al. 2010). Modified water temperature and mixing patterns as well as WLF can also affect the formation, stability and break-up of ice cover (Liu and Wu 1999; Solvang et al. 2012).

Biotic PS impacts are less studied but supposed to include effects on organisms and on interactions between species (Helland et al. 2011; Stanford and Hauer 1992) through modifying the food web, habitat area, population dynamics and nutrient levels. A direct impact of intensified WLF is the stranding of juvenile fish in littoral zones during dewatering (Bell et al. 2008). WLF, moreover, can cause freezing, desiccation and direct physical stress in the littoral zone, affecting abundance and diversity of littoral sessile macrophytes and benthic algae. Changes in ISS concentration can also affect primary production, and indirectly dissolved oxygen (DO) (Hirsch et al. 2017). PS impacts on ice cover can affect ecology as well, e.g., by impacting light availability (Laybourn-Parry et al. 2012). Finally, organisms from reservoirs connected by PS operations can get entrained (e.g., Hauck and Edson 1976; Potter et al. 1982; Anderson 2010). This also enables alien species to spread from a downstream to an upstream reservoir (Harby et al. 2013).

The assessment of PS effects can be based on (i) in-situ observations before and after PS commissioning or (ii) modeling studies. An example for the in-situ approach was performed at Lake Oconee. There, the water column was completely mixed in summer since PS operation, whereas beforehand temperature differences between epi- and hypolimnion had ranged between 5 and 13 °C (Potter et al. 1982). At Twin Lakes, in-situ observations indicated reduced residence time, cooling of both water bodies and weakened stratification due to PS operation (USBR 1993).

In recent years, some model assessments of PS effects have been published. Yet, most of them focused on impacts on temperature and stratification. Exemplarily, Bonalumi et al. (2012), who investigated a PS operation between Lago Bianco and Lago di Poschiavo, found that both water bodies would mostly be warmed. They could, moreover, show that a large fraction of the warming of Lago di Poschiavo would occur due to frictional warming of the PS flows. In addition, they projected significantly reduced ice-covered periods at Lago Bianco, which was only qualitatively described due to lack of observational data. Furthermore, Ramos-Fuertes et al. (2018) showed that projections of PS operation for a Spanish reservoir would result in a homogenisation and heating at intermediate depths of the water column, and the advancement of mixing by ~1 month. Moreover, Bermúdez et al. (2017) found that PS impact depends on

reservoir geometry, as their temperature projections showed stronger effects for the narrower lower reservoir. Aside from these strong effects, another model assessment for Lake Elsinore projected only minor overall impacts on timing and strength of summer stratification (Anderson 2010). However, these projections showed a seasonal variation with a pronounced effect in May.

Local effects, i.e., close to the PS intake/outlet, have also been studied. For example, Müller et al. (2016) investigated whether the turbulence induced by PS cycles could hinder particles from settling. They found that while generating could affect the flow field to a distance of up to 150 m, pumping mode only influenced it in the vicinity of the PS intake/outlet. Furthermore, they stated that, dependent on the discharge and on the lake's topography, the PS generating flow could introduce large eddy flow fields in the lower reservoir of their studied PS hydropower plant. Therefore, they recommended the application of PS cycles to avoid settling of turbidity currents and consequently the filling up of reservoirs.

In addition to the modification of temperature other water quality parameters, such as ISS, DO, and nutrient concentrations, are affected by PS operations. These changes result from two different mechanisms: (i) the exchange of water masses, and (ii) indirect effects due to altered mixing and stratification dynamics. If the water quality of two water bodies is significantly different, the exchange of water between them could potentially change their water quality (Bonalumi et al. 2012). The importance of this effect scales with the ratio of the exchanged water masses and the volumes of the basins.

Moreover, the intrusion depth of PS flows is of high ecological relevance: if a nutrient-laden PS flow intrudes close to the surface, primary production is fuelled, whereas if it intrudes below the euphotic zone, nutrients are not directly available for primary production (Bermúdez et al. 2017; Bonalumi et al. 2012). Furthermore, a direct effect of the PS intake/outlet locations has been shown: the lower they were located the higher the PS impacts became (Bonalumi et al. 2012), which is also supported by the findings for two connected drinking water reservoirs in South Korea (Park et al. 2017).

Although the reported effects on temperature and water quality are diverse and site specific, a life cycle assessment of PS hydropower plants indicated overall lower impacts in all considered categories when compared to battery storage (Immendoerfer et al. 2017), highlighting their relevance for the implementation of new renewable electricity.

1.2 Climate change effects

Within the long periods for which concessions of PS hydropower plants are granted, significant climate change must be expected. The additional effects due to climate change might amplify or weaken those of PS operations, but these relationships have so far not been studied. Thus, the following section provides an excerpt of available literature on observed and projected climate change effects. This section is, however, not encompassing all effects that could arise from climate change, as these can vary among different sites. Yet, the most important modifications are summarized in this section.

For a wide variety of lakes around the globe, climate change has been shown to result in (i) a warming of lake surface water temperatures (O'Reilly et al. 2015; Woolway et al. 2017), (ii) an increased overall water temperature of some tenths of a degree per decade (Kraemer et al. 2015; Persson et al. 2005), and (iii) a pronounced warming of the epilimnion compared to smaller temperature changes in the hypolimnion (Butcher et al. 2015; Kraemer et al. 2015; Livingstone 2003). The latter can be explained by increased resistance to vertical mixing, although the overall thermal input would rise due to climate change (Butcher et al. 2015). Hypolimnetic temperatures are shaped by the complex interaction between heat exchange and stratification, and more distinctly by thermocline depth and water clarity (Butcher et al. 2015).

The reported warming of water temperature was in good agreement with observations of surface air temperatures. Schmid et al. (2014) showed, e.g., that surface equilibrium temperatures are expected to increase by 70 to 85% of the air temperature increase, if all other meteorological forcing remained constant. For specific lakes, changes in other meteorological variables can have an impact as well. For example, at Lakes Constance (Fink et al. 2014) and Zurich (Schmid and Köster 2016), an excess warming was observed, most of which could be attributed to enhanced solar radiation.

Observations, additionally, revealed that some changes occurred rapidly (e.g., Woolway et al. 2017). In the late 1980s a rapid change of air temperature resulted in a corresponding increase of lake surface water temperature. The causes are discussed in literature: some studies traced it back to the alteration of atmospheric circulation patterns (e.g., North et al. 2013), and others claimed that it resulted from a random coincidence of several forcing factors acting on temperature in the same direction (e.g., Reid et al. 2016).

Some studies also claimed that the projected changes were regionally coherent (Woolway et al. 2017), while others suggested that lake characteristics, such as morphometry and local geographic settings, could possibly mediate climate change effects (O'Reilly et al. 2015). Further reasons for differential warming include the alteration of lake internal processes, such as the timing of lake stratification, and changes of other components of the meteorological forcing (Schmid and Köster 2016; Woolway et al. 2017).

Another aspect that has been observed aside from temperature changes is the increasing strength and duration of summer stratification (Butcher et al. 2015; Dokulil et al. 2010; Ficker et al. 2017).

Stratification itself is shaped by external drivers (i.e. heat exchange and wind) as well as lake characteristics (i.e. morphometry and light penetration). Mixing regimes could also be altered due to long-term climate change (Ficker et al. 2017).

The changes of summer stratification dynamics further resulted in reduced hypolimnetic DO content due to increasing resistance to mixing (Ficker et al. 2017; Xia et al. 2014). This has even led to increasing frequency of hypoxia and anoxia (Ficker et al. 2017; North et al. 2014). The decreasing DO concentrations, furthermore, ensue nutrient release from sediments and affect the lake productivity (Delpla et al. 2009).

Moreover, climate change implies ecological changes. Among others, the modification of summer stratification dynamics can lead to (i) alterations of food-webs, (ii) changing habitat quality and availability, and (iii) differences of species abundance (Ficke et al. 2007; Rühland et al. 2015). Regarding fish, physiological functions, such as thermal tolerance, growth, metabolism, food consumption and reproductive success, could be affected (Ficke et al. 2007; Jeppesen et al. 2012). In addition, prolonged summer stratification, receding water levels and less frequent overturns might favour the development of particular primary producers (Ficke et al. 2007). Climate change has also been shown to (i) favour the development of harmful cyanobacterial blooms (Huisman et al. 2018), and (ii) advance spring phytoplankton bloom (Schlabing et al. 2014).

For the winter period, climate change has resulted in (i) shortened inverse stratification, (ii) reduced ice-covered period, and (iii) declining ice thicknesses (Benson et al. 2012; Leppäranta 2014; Magee et al. 2016). Due to decreasing ice thicknesses the buoyancy of the ice cover would be reduced. This could, in turn, result in more frequent white ice formation that could partly counteract the decrease of black ice thicknesses (Leppäranta 2014). Moreover, thinner ice could lead to increased frequency of ice breakage due to wind loads and could consequently increase the probability of open water conditions.

The physical changes in winter also led to changes of biogeochemical and ecological aspects. Due to the increased probability of open water conditions more aeration can take place (Butcher et al. 2015), thus, resulting in reduced nutrient release from sediments. For some fish species, changes in winter phenology might result in earlier breeding and thus, an increasing body size due to the earlier ice-off (Hovel et al. 2016; Shuter et al. 2012). With the declining ice-covered season under-ice algal blooms might occur more rarely (Moore et al. 2009).

Climate can also affect catchment related processes, like (i) the frequency and intensity of extreme events (e.g. heavy rainfall, intensification of evapotranspiration, alterations of glacial melting, variation of snow cover) and (ii) the modification of biogeochemical processes (Dokulil 2014). In particular, climate change could lead to increasing phosphorus and ISS release from the watershed during extreme precipitation events as well as nitrogen losses due to enhanced denitrification (Me et al. 2018; Mooij et al. 2005). As climate change alters inflow temperatures, the intrusion dynamics could be affected as well (Fink et al. 2016; Răman Vinnă et al. 2018).

1.3 Development of local climate projections

The assessment of local climate change effects on lakes and reservoirs requires considering processes at smaller scales than those of general circulation models. The available downscaling methods are divided into two groups: dynamical approaches and statistical methods. The first approach applies the output from general circulation models as boundary conditions for producing outputs of higher resolution (Fowler et al. 2007), which allows, for instance, regional climate features like orographic precipitation and extreme climate events.

Statistical downscaling, on the other hand, summarizes statistical techniques to transfer global changes to smaller scales. These methods can also be utilized to downscale regional projections to local scales (Keller et al. 2017). For Switzerland, climate projections are available for the network of MeteoSwiss stations as well as separated for three distinct regions: north-eastern, north-western and southern Switzerland (CH2011 2011). These climate projections were already applied for assessing the impacts on aspects concerning cryosphere, hydrology, biodiversity, forests, agriculture, energy and health (CH2014 2014).

The projections, given in CH2011 (2011), are based on the delta-change technique, which modifies local weather observations by the application of an additive or a multiplicative term. This adaption term is taken from the output of climate models (Keller et al. 2017). Keller et al. (2017) describe the disadvantages of the delta-change method. These include the limitation to the record length of observations as well as incapability of changing variability, extremes and temporal structure. To overcome the latter issue one could use a weather generator, which allows creating an ensemble of realizations of climate.

Many weather generators have been developed in recent years. Some examples that have been tested for Switzerland are given in Keller et al. (2015) and Peleg et al. (2017). While Keller et al. (2015) highlights the general difficulty to represent extreme events with a weather generator, Peleg et al. (2017) were able to reasonably well reproduce these extremes. Another weather generator, called VG, was developed for assessing climate effects on lakes (Schlabing et al. 2014), and is based on a single vector-autoregressive process. In combination with a one-dimensional hydrodynamic model, VG was able to reproduce current climate effects for Lake Constance. Due to the successful application at Lake Constance, VG was used for producing synthetic time series of current and future climate. Annual time series of projected air temperature changes for 2085, north-eastern Switzerland, and the A2 emission scenario from CH2011 (2011) were utilised to drive VG.

1.4 Lake and ice modelling

To assess effects on lake or reservoir temperature, a variety of hydrodynamic models are available. Most of these models include the computation of ice thicknesses, and some of them can be coupled to water quality models of different complexity. This section gives a brief overview of available models and their previous utilization for impact assessments.

In general, the applicable hydrodynamic descriptions range from box models to three-dimensional, more physically based representations. Box models may be used in the context of paleo-climatic simulations. There it is crucial to correctly compute the thermal inertia of inland water bodies, and to reduce computation time due to the consideration of typically long time series (Stepanenko et al. 2013). One-dimensional models can be considered sufficient for many limnological studies, where detailed information on the temperature profile becomes necessary. The advantage of three-dimensional hydrodynamic models is that they can resolve spatial dynamics. Menshutkin et al. (2013) highlights the necessity of three-dimensional models, particularly, for large lakes, where phenomena like baroclinic Kelvin and Poincare wave formation need to be considered. However, three-dimensional models require more computation time and spatially resolved data for calibration.

Exemplarily, a thorough comparison of eight hydrodynamic models was presented by Stepanenko et al. (2013). They compared a box and a two-layer model (FLake) to six one-dimensional vertical models (Hostetler, CLM4-LISSS, MINLAKE96, LAKE, Simstrat and LAKEoneD). The focus of their study was to determine the relevant processes necessary for coupling lake models to general circulation models or numerical weather predictions, where lakes could introduce feedbacks on local climate and meteorology.

As of today, many hydrodynamic models independent of their complexity were equipped already with ice models to allow for a year round simulation of mid-latitude lakes. For example, Oveisy et al. (2012) introduced an ice model to the three-dimensional Estuary and Lake Computer Model (ELCOM), which showed reasonable agreement with observations. Also de Goede et al. (2014) implemented an ice model to Delft3D, considering thermodynamic aspects and the motion of the ice sheet. Just recently, Simstrat was equipped with a lake ice model based on the description of Saloranta and Andersen (2007). Most of the implemented ice models follow the mathematical concepts described in Maykut and Untersteiner (1969)¹, Semptner (1976)¹, Saloranta and Andersen (2007)² and Rogers et al. (1995)³. A general and comprehensive overview of lake ice modelling is given in Leppäranta (2014).

In some publications, these combined hydrodynamic and ice models were used to assess climate change effects. For example, the comparative study by Yao et al. (2014) showed effects of future climate conditions not only on lake temperature, but also on ice cover for the period 2010-2100. For this purpose, they compared the results of four models: Hostetler, Minlake, Simple Ice Model

¹ Implemented in CE-QUAL-W2

² Simstrat and MyLake

³ ELCOM and GLM

and General Lake Model (GLM). Additionally, MyLake was applied for assessing climate change impacts. Exemplarily, Gebre et al. (2014a) projected significant changes for the thermal structure of lakes, which would further result in decreasing ice duration and thickness towards the end of the 21st century in the Nordic-Baltic region.

Many hydrodynamic models were also coupled with water quality models for the evaluation of different management strategies. Menshutkin et al. (2014) and Mooij et al. (2010) reviewed examples of these coupled models. One of the mentioned models, the dynamic reservoir simulation model (DYRESM) was coupled with the computational aquatic ecosystem dynamics model (CAEDYM). As an example, DYRESM-CAEDYM was applied by Trolle et al. (2008), who analysed several management scenarios to meet the requirements of the European Water Framework Directive. Mooij et al. (2010) highlighted that CAEDYM was, hitherto, mainly used for assessing nutrient cycling, effects of increased nutrient loading on algal blooms and changes to phytoplankton succession, as well as for identifying conditions that favour cyanobacteria.

A directly coupled laterally-averaged hydrodynamic and water quality model (CE-QUAL-W2), was, exemplarily, used for the computation of nutrient and sediment dynamics of reservoirs (Mooij et al. 2010). Additionally, the environmental fluid dynamics code (EFDC), was coupled to water quality models, such as the water quality simulation program for eutrophication (WASP/EUTRO5). This coupled model was, for example, successfully tested by Zou et al. (2006). GLM in combination with the Aquatic Ecodynamics model (AED2) was also applied for the assessment of temperature and DO dynamics. Exemplarily, Weber et al. (2017) optimised the operation of selective withdrawal at the Grosse Dhuenn drinking water reservoir.

As mentioned in Section 1.1, the assessment of PS effects through modelling focused up to now on the assessment of lake temperature and stratification. Most of the used models were based on two- (Bonalumi et al. 2012; Ramos-Fuertes et al. 2018) or three-dimensional hydrodynamic models (Anderson 2010; Bermúdez et al. 2017).

1.5 Study site

The two water bodies investigated in the present study, Upper Lake Zurich and Sihlsee (Figure 1.1), are already today connected by a hydropower plant with a small PS capacity. In the process of the concession renewal, which is expected for 2019, the Swiss Federal Railways (SBB AG) as the owner of the power plant investigated different options for increased PS between the two lakes. The funding of this thesis, granted by SBB AG, therefore, gives the opportunity to focus on scientifically interesting challenges and how these can be tackled.

The upper water body, Sihlsee (47.1225°N, 8.7856°E) is the reservoir with the largest surface area in Switzerland. It is a dimictic reservoir, with an ice cover in winter. The maximum ice thickness typically reaches ~0.20 m. Sihlsee has a surface area of 11.30 km² and a maximum volume of 96.1×10⁶ m³. At maximum water level, it has a length of 8.5 km, a width of 2.5 km, and a maximum depth of 23 m, with an average depth of 9 m (Basler & Hofmann AG 2014). Its operating level varies between 889.34 and 876.84 m a.s.l. The retention time scale is ~135 days.

The tributaries of Sihlsee are Minster (40%), Sihl (21%), Grossbach (7%), Eubach (6%) and some smaller creeks (26%). The values in brackets indicate the areal contribution of each catchment to the whole watershed area of ~156.5 km². The long-term monthly mean discharge of Minster, which is the main tributary, ranges from 1.22 to 5.32 m³ s⁻¹ for the period 1981-2000. The intake of the PS hydropower plant at Sihlsee is located at an elevation of ~870 m a.s.l. This intake is also used as outlet in case of pumping.

Before this study, there has been no monitoring of temperature or water quality parameters in Sihlsee, and only few publications concerning this artificial lake had been published. For instance, sediment core analyses (Ammann 1987) showed that most of the deposited material in Sihlsee is delivered by the River Minster. A more recent study investigated greenhouse gas emissions (CO₂, CH₄ and N₂O) from the lake (Diem et al. 2012).

The lower basin of the PS scheme, Upper Lake Zurich (47.2117°N, 8.8675°E), is a natural lake. It can be characterised as monomictic. It has a surface area of 20.25 km² and a maximum volume of 470×10⁶ m³. It is 10.5 km long, 2.5 km wide and 48 m deep, with an average depth of 23 m (Amt für Umwelt Kanton St. Gallen 2018). The lake surface is at an altitude of ~406 m a.s.l. and has an average retention time of ~70 days. The lake level is controlled at the outflow in Zurich and therefore relatively stable.

The tributaries of Upper Lake Zurich are Linthkanal, including the discharge from Walensee and the Linthebene (83%), Jona (5%), Wägitaler Aa (5%) as well as minor inflows from the surrounding area of the Upper Lake Zurich (7%). Again, the values in brackets indicate the contribution to the entire watershed of ~1564 km². The monthly averaged discharge of Linthkanal measured at the outflow of Walensee ranges from 16.3 to 86.8 m³ s⁻¹ (values were estimated for February and July 2014, respectively). At Upper Lake Zurich, the elevation of the PS outlet, which is also used as intake, is at ~403 m a.s.l.

Upper Lake Zurich is monitored due to its relevance for Lower Lake Zurich, which is used as drinking water source for roughly one million people (Gammeter and Forster 2002; Schildknecht et al. 2013). Another important feature of Upper Lake Zurich is the conservation area, called “Bätzimatt”, which is habitat for three species of macrophytes, *Ceratophyllum demersum*, *Potamogeton pusillus* and *Ranunculus circinatus*. All of them are on the IUCN red list of endangered species (AQUAPLUS 2013).

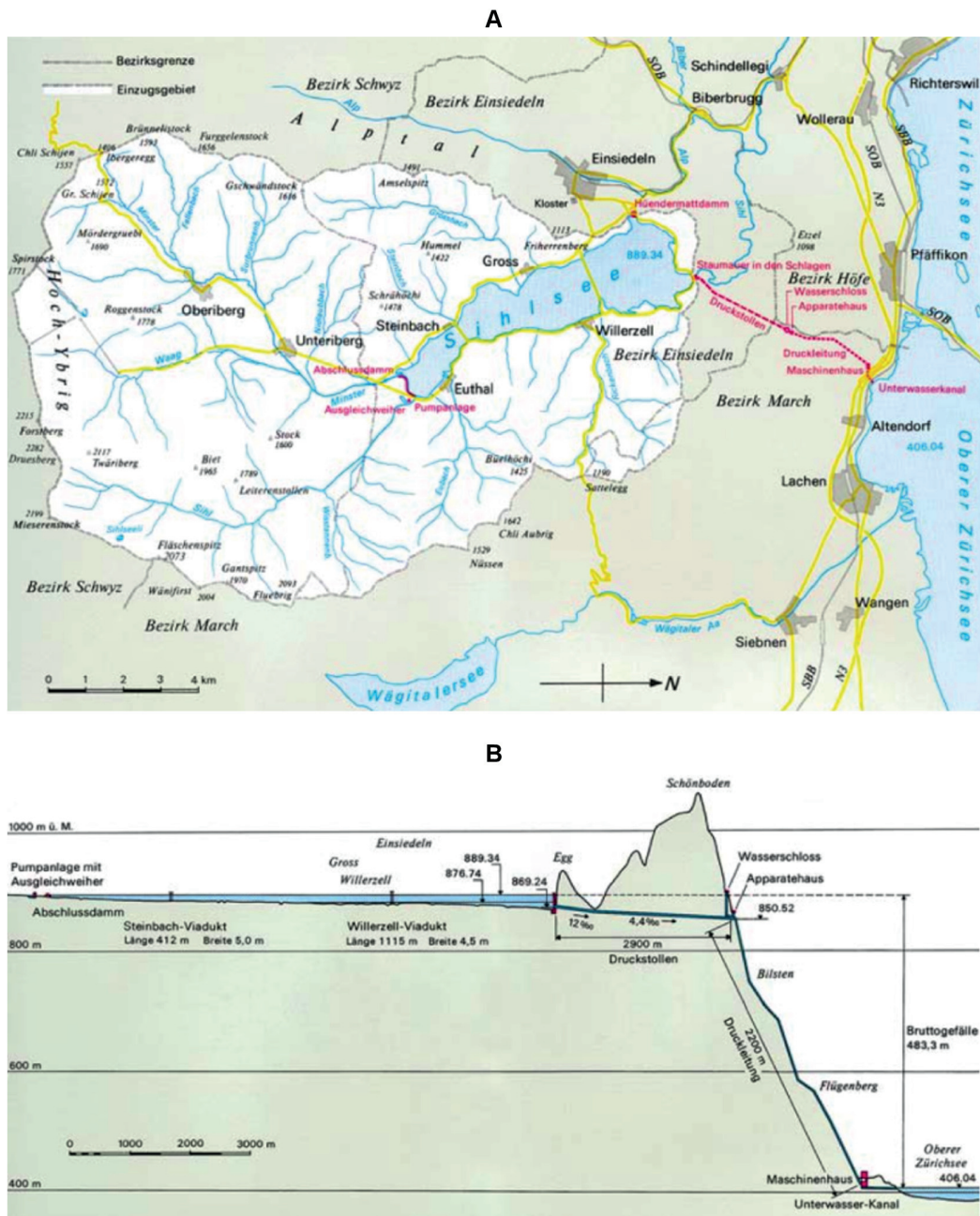


Figure 1.1 (A) Plan view and (B) cross section of Etzelwerk (Source: SBB AG (2006), Das Etzelwerk, Faltblatt.).

1.6 Approach and outline

Although the PS effects on temperature and stratification have been assessed in several publications (Anderson 2010; Bonalumi et al. 2012; Ramos-Fuertes et al. 2018), the impact on water quality and lake ice has not been quantified. Additionally, when PS operations are extended the definition of a reference state for the environmental impact assessment is not clearly defined. Moreover, Bonalumi et al. (2012) could show pronounced PS effects for the warm years of their studied period, suggesting that the effects of PS operation could be enhanced due to climate change. Yet, the assessment of the combined effects has also not been studied. Furthermore, the question of the reliability of a model itself remains. Thus, the main research questions of this dissertation can be summarized as follows:

- How will temperature, water quality and ice cover be affected by PS operation?
- How do temperature, DO and nutrient projections of two differently defined reference scenarios compare to the current PS operation?
- Are the effects of PS operation aggravated or weakened by climate change?
- Should the development of PS operations consider the additional effect of climate change?
- How reliable are the projections, particularly, those for the ice-covered period?

The first and the second research question are addressed in Chapter 2, by setting up and calibrating a laterally-averaged two-dimensional hydrodynamic and water quality model to assess the effects of two PS and two reference scenarios. Chapter 3 provides supplementary information to Chapter 2. In Chapter 4, the calibrated two-dimensional model is utilized to run simulations for VG-generated 10×15-year-long synthetic time series of future and current climate. This will allow answering research questions three and four. The supplementary material of Chapter 4 is given in Chapter 5. To solve the last research question, two additional one-dimensional models, accounting for deep-water withdrawal and ice formation, are set up and calibrated in Chapter 6. Chapter 7 contains the supplementary information of Chapter 6. In Chapter 8, the main findings of this dissertation are presented along with aspects that would be interesting to investigate in the future.

Chapter 2

Effects of lake-reservoir pumped-storage operations on temperature and water quality⁴

2.1 Overview

As has been highlighted in Chapter 1, PS hydropower plants are expected to make an important contribution to energy storage in the next decades with growing market shares of “new renewable” electricity. Yet, PS operations have been shown to affect the water quality of the connected water bodies through the water exchange between them and through the deep-water withdrawal from the upper water body. Thus, this chapter focuses on the assessment of the importance of these two processes in the context of recommissioning a PS hydropower plant. To this end, different scenarios were simulated with a modified version of the numerical, two-dimensional hydrodynamic and water quality model CE-QUAL-W2. The comparison of present and extended PS operations showed significant impacts of the water exchange between the two water bodies on the seasonal dynamics of temperatures, stratification, nutrients, and ice cover, especially in the smaller upper reservoir. Yet, the comparison of the present PS scenario and the reference scenario with deep-water withdrawal resulted in only minor effect of the water exchange. On the other side, the comparison with the near-natural reference revealed that deep-water withdrawal strongly decreases the strength of summer stratification in the upper reservoir, further shortening its duration by ~1.5 months, consequently improving oxygen availability, and reducing the accumulation of nutrients in the hypolimnion. These findings highlight the importance of assessing the effects of different options for water withdrawal depths in the design of PS hydropower plants, as well as the relevance of defining a reference state when a PS facility is to be recommissioned.

⁴ This chapter is based on the scientific article “Effects of lake-reservoir pumped-storage operations on temperature and water quality” by U. G. Kobler, A. Wüest and M. Schmid published in *Sustainability*. The fieldwork, simulations and the analysis presented hereafter are original and were performed by the author of the thesis.

2.2 Introduction

The share of “new renewables”, such as photovoltaic and wind power plants, to the electricity production is increasing globally as a consequence of political decisions to reduce greenhouse gas emissions (Barbour et al. 2016; EU Commission 2011). At the end of 2016, 2017 GW of renewable power capacity were installed globally (REN21 2017), with parts of ~300 GW and ~490 GW from photovoltaic and wind power, respectively. The integration of these “new renewables” to the electrical grid is challenging due to their intermittency (Evans et al. 2012) and entails network load stability problems resulting from decentralized production (Ibrahim et al. 2008). Electricity storage addresses a large part of these timing and stability issues.

Even today, the most efficient technologies for storing electric energy are still pumped-storage (PS) hydropower plants, which also provide ancillary services such as voltage support and various forms of reserve capacity to fine-tune the matching of supply and demand and to ensure reliability (REN21 2017). Worldwide, >300 PS hydropower plants were installed with a total capacity of ~150 GW by the end of 2016, and plans existed for another 40 GW by 2020 (REN21 2017), with overall energy efficiencies reaching up to 87% and an individual size of up to 3000 MW (Rehman et al. 2015). Thus, within the last few years, PS operations regained attention, and overviews of proposed PS hydropower plants have been presented in various studies (Barbour et al. 2016; Deane et al. 2010).

However, PS operations modify physical and geochemical (abiotic) as well as ecological (biotic) properties of the connected water bodies. Abiotic effects include changes of water temperature, stratification, water level fluctuations, sediment resuspension, oxygen and nutrient cycling in the water column as well as modifications of inorganic suspended sediment, which accordingly alter light penetration (Bonalumi et al. 2011). Additionally, lake-internal circulation patterns (Anderson 2006) as well as ice cover (Liu and Wu 1999; Solvang et al. 2012) may be affected.

Biotic PS impacts are, in general, less studied but can include effects such as stranding of juvenile fish in littoral zones during dewatering (Bell et al. 2008), entrainment of organisms (Hauck and Edson 1976), and spreading of alien species from downstream to upstream (Harby et al. 2013).

Assessing PS impacts for different scenarios is typically undertaken by the application of numerical models. Models of different complexity have previously been applied for studying impacts of reservoir management on water quality. These range from one-dimensional models such as GLM-AED (Weber et al. 2017), DYRESM-CAEDYM (Romero et al. 2004) or MyLake (Gebre et al. 2014b), to three-dimensional models such as the Environmental Fluid Dynamics Code (Anderson 2010), Delft3D (Bermúdez et al. 2017) or ELCOM-CAEDYM (Romero et al. 2004; van der Linden et al. 2015). Models of lower complexity have the advantage of shorter computation times, allowing for large numbers of simulations, e.g., for the purpose of parameter estimation or scenario simulations, but may not be able to adequately reproduce the effects of local inflows on basin-scale dynamics and water quality, especially for large local discharges as they are typically introduced by PS operations. Three-dimensional models can resolve these

spatial dynamics, but their computational demand, especially when coupled to water quality models, still precludes their application to long-term studies and for purposes where a large number of simulations is required. Furthermore, spatially resolved observational data are often not available to calibrate the three-dimensional processes.

For our case, the simulation of a coupled lake–reservoir system over a time scale of 15 years and with a potential future application to climate change scenarios, the two-dimensional, laterally averaged hydrodynamic and water quality model CE-QUAL-W2 is a good compromise between spatial resolution and computational demand. It has previously been applied to numerous case studies for reservoir management (Kuo et al. 2006; Liu et al. 2009), among which also another case study of a lake and a reservoir coupled by PS (Bonalumi et al. 2012).

When planning a new or extending an existing PS scheme, environmental effects need to be projected and minimized during the planning phase (Harby et al. 2013; Hirsch et al. 2017). For this purpose, a reference state needs to be defined. This could be the natural state without a reservoir. However, in the case of existing reservoirs, which are often used for multiple purposes, such as for flood protection and recreation (Harby et al. 2013), reservoir removal could have relevant ecological and socio-economic effects, and might therefore not be a realistic option (Bellmore et al. 2017). Hence, other artificial reference states can be considered to analyse the impacts of PS extension or for recommissioning present PS operation.

This study aimed to assess the impacts on temperature, stratification as well as water quality in a natural lake and a reservoir connected by a PS hydropower plant. We analysed: (a) its extension; and (b) two reference scenarios without PS operation. Both reference scenarios keep the dam, but they differ in withdrawal depth of the outflow which, either remains at the current depth of the residual flow outlet in the hypolimnion or is moved up to the surface. The first reference scenario allowed to individually assess the impacts of water exchange due to PS, while the second corresponded to a “quasi-natural” behaviour of the reservoir. We hypothesized that the impacts of PS operations are partially caused by the exchange of water between the two water bodies, and partially by the depth of water removal from the upper reservoir. To disentangle these effects, the scenarios were simulated using the 2D-model CE-QUAL-W2 and compared to the present PS operation.

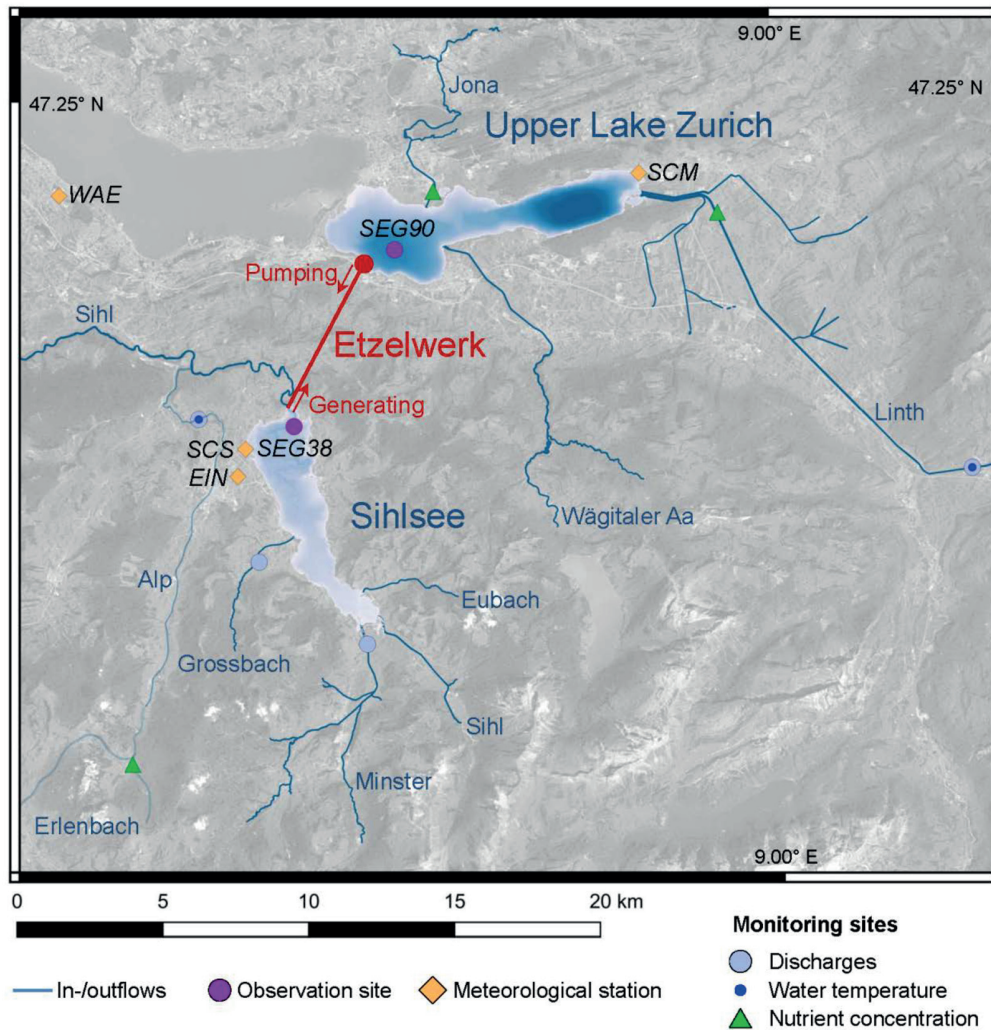


Figure 2.1 Overview of study site: Etzelwerk with its two connected water bodies Sihlsee (upper reservoir; 8.5 km long and 2.5 km wide) and Upper Lake Zurich (lower lake; 10.5 km long and 2.5 km wide). Meteorological stations refer to: EIN: Einsiedeln; WAE: Wädenswil; SCM: Schmerikon (all MeteoSwiss); and SCS: Segelclub Sihlsee. The MeteoSwiss station at Zurich Fluntern (SMA) is outside the graph (coordinates: 8.56573°E, 47.37789°N). Observation sites correspond with the deepest points of model segments 38 (SEG38) and 90 (SEG90), for which model results were generated.

2.3 Study site

Etzelwerk, a PS hydropower plant located in Switzerland, was chosen as the study site. It was built in the 1930s and is operated between Sihlsee and Upper Lake Zurich (Figure 2.1). Its current concession runs out at the end of 2022. For its renewal, several options for extending the PS operation have been considered: 525 (265) MW, 250 (80) MW and 150 (60) MW for the generating (pumping) mode. Additionally, a reference state was defined as a base for the required mitigation measures.

Sihlsee is the artificial upper reservoir of the Etzelwerk PS hydropower plant (Figure 2.1). At maximum water level, it is 23 m deep, has a surface area of 11.3 km² and a volume of 96.1×10⁶ m³. The water level varies by 12.5 m between 889.34 and 876.84 m a.s.l., thus the storage capacity is ~89.4×10⁶ m³. The catchment area is 156.5 km², with the major tributaries Minster (40% of catchment), Sihl (21%), Grossbach (7%) and Eubach (6%). The grid location of inflows, outflows and PS flows is depicted in Figure 3.1. The current hydraulic residence time is ~135 days. Since no previous observations were available, temperature, oxygen and nutrient concentrations were monitored in Sihlsee during 2014–2016 as a base for model calibration. The observations were made at SEG38 and are summarized in Section 3.3.

Upper Lake Zurich is the lower lake of this PS hydropower plant and is of natural origin (Figure 2.1). Its surface elevation varies by ~1.0 m between 405.5 and 406.5 m a.s.l. At highest water level, it has a maximum depth of 48 m, a surface area of 20.25 km² and a volume of 470×10⁶ m³. The catchment area (1564 km²) is about one order of magnitude larger than that of Sihlsee. The main tributaries contributing to this catchment are Linth (83%, including the discharge from Walensee and Linthebene), Jona (5%) and Wägitaler Aa (5%). The average water residence time is ~70 days. Additional information on bathymetry and model forcing can be found in Section 3.2, and an overview of the physical and chemical properties of Upper Lake Zurich (monitored by a routine program at SEG90) is given Section 3.3.

Epilimnion temperatures at both lakes are rather similar. Hypolimnion temperatures at Sihlsee can reach up to <17 °C in summer, whereas those at Upper Lake Zurich remain below 6 °C. During the stagnation phase, suboxic or anoxic conditions develop in the hypolimnia of both lakes. Mean annual nitrate concentrations differ significantly between Sihlsee (~230 µg N L⁻¹) and Upper Lake Zurich (~660 µg N L⁻¹), respectively, while mean total phosphorus concentrations are similar in both water bodies, even though higher peak concentrations are reached in Sihlsee after flood events.

The average annual water balances (calculated for the period 1997–2015) of both water basins are given in Table 2.1. The extended PS operation would increase the water exchange between the two water bodies from 214 to 778×10⁶ m³ s⁻¹ for the PS generating flow and from 26 to 590×10⁶ m³ s⁻¹ for the PS pumping flow (Table 2.1). The seasonality of the artificial PS flows is shown in Figure 3.2. For both reference scenarios, no PS flows were considered. The hydraulic residence time of Sihlsee is, therefore, increased to ~150 days in both reference scenarios and reduced to ~40 days in the extended PS scenario.

Table 2.1 Annual water balance of the two water bodies of Etzelwerk. Sum of all inflows, outflows and artificial flows for present and extended PS operation as well as for the two reference scenarios NoPS and QNat (details given in Section 2.4.2). A correction term was required to close the water balance for Sihlsee, described in Section 3.2.

	Sihlsee			Upper Lake Zurich		
	Present PS	Extended PS	Reference Scenarios	Present PS	Extended PS	Reference Scenarios
	[10 ⁶ m ³ year ⁻¹]					
Sum of inflows	235	235	235	2410	2410	2410
Sum of outflows	-32	-32	-220	-2598	-2598	-2410
Correction term	-15	-15	-15	0	0	0
PS generating flow	-214	-778	0	214	778	0
PS pumping flow	26	590	0	-26	-590	0

2.4 Materials and methods

2.4.1 Model description

The simulations were run with the model CE-QUAL-W2, version 3.71 (Cole and Wells 2013), developed in a cooperation of the US Corps of Engineers and the Portland State University. It is a two-dimensional laterally averaged hydrodynamic and water quality model. The two water bodies are directly connected in the model, i.e., the volumes of head race tunnel and penstock are neglected. In effect, this volume needs to be flushed at every PS flow inversion before water is effectively transferred between the two water bodies. For the present PS, this accounts for ~5% and ~13% of the generating and pumping flows, respectively. Thus, the volume exchanged between the two water bodies is slightly overestimated. Frictional losses were considered, with an assumption of 90% and 80% efficiency level for generating and pumping, respectively. The effect of this frictional warming was, however, minor.

The model forcing includes meteorological, hydrological and water quality forcing as well as bathymetrical data. A detailed description including initial conditions is given in Section 3.2. All simulations were run for the period 1997–2012, whereas years 2013–2015 and 1997–2015 were used for calibration of Sihlsee and Upper Lake Zurich, respectively. The first year of each period was considered as spin-up phase, and not included in the results. The results shown for Sihlsee were generated at model segment 38 (SEG38), and those for Upper Lake Zurich at model segment 90 (SEG90) (Figure 2.1). These segments correspond to the observation locations at the two water bodies. A detailed description of the PS scenarios follows in Section 2.4.2.

The model considered an hourly time step and the model variables comprise: water temperature, dissolved oxygen, inorganic suspended solids, phosphate, ammonium, sum of nitrate and nitrite, dissolved and particulate organic matter (labile and refractory), algae (two groups) and zooplankton.

The model was calibrated against observations through a manual trial and error calibration. Parameter values were either set according to recommendations from literature or tuned to match observations (details in Section 3.3). The identified parameter set, the comparison between observed and simulated profiles and time series as well as the computed mean absolute error (MAE) and mean error (ME) of temperature, dissolved oxygen, total phosphorus and the sum of nitrate and nitrite are given in Section 3.3.

The root mean square errors (RMSEs) for the entire calibration period for the overall water column, the epilimnion and the hypolimnion are shown in Table 2.2. The RMSE of temperature is <1 °C for both water bodies, which is comparable to the range of ~ 0.7 – 2.1 °C achieved in a recent multi-lake comparative analyses using the 1D-model GLM (Bruce et al. 2018). The MAEs (Table 3.3) for the entire water column of 0.71 °C for Sihlsee and 0.65 °C for Upper Lake Zurich are within the range of ~ 0.3 – 0.9 °C that resulted from 70 previous applications of CE-QUAL-W2 (Cole and Wells 2013). RMSEs for dissolved oxygen are comparable to the value of 1.05 mg L⁻¹ in a recent study on reducing thermal pollution downstream with the additional objective to avoid hypoxia (Weber et al. 2017), and again within the range typically achieved with CE-QUAL-W2 for similar applications (Cole and Wells 2013; Deliman and Gerald 2002). The same is true for nutrient concentrations, where, for example, Deliman and Gerald (2002) showed RMSEs of 570 µg N L⁻¹ for the sum of nitrate and nitrite and 40 µg P L⁻¹ for total phosphorus; and Smith et al. (2014) presented RMSEs in the hypolimnion of ≤ 100 µg N L⁻¹ for the sum of nitrate and nitrite and ≤ 16 µg P L⁻¹ for total phosphorus as well as RMSEs in the epilimnion of ≤ 40 µg N L⁻¹ and ≤ 7 µg P L⁻¹ for the sum of nitrate and nitrite and total phosphorus, respectively. RMSEs of the sum of nitrate and nitrite presented in two further studies, which both focussed on projecting the response to nutrient reduction scenarios, were ~ 100 µg N L⁻¹ for both epi- and hypolimnion (Liu et al. 2009) and ≤ 590 µg N L⁻¹ (Kuo et al. 2006) for the entire water column.

Table 2.2 Root mean square error (RMSE) of temperature, dissolved oxygen, the sum of nitrate and nitrite as well as total phosphorus computed for the entire water column, the epilimnion and the hypolimnion of Sihlsee and Upper Lake Zurich.

Variable	Unit	Sihlsee 2014–2015			Upper Lake Zurich 1998–2015		
		Entire Water Column	Epilimnion ¹	Hypolimnion ²	Entire Water Column	Epilimnion ¹	Hypolimnion ³
Temperature	[°C]	0.94	0.93	0.94	0.93	0.78	0.98
Dissolved oxygen	[mg L ⁻¹]	1.15	1.07	1.38	1.26	0.99	1.16
Sum nitrate and nitrite	[µg N L ⁻¹]	76	69	89	114	142	114
Total phosphorus	[µg P L ⁻¹]	4.45	2.74	6.51	4.13	3.90	3.96

¹ Uppermost 5 m of the water column. ² Lowermost 5 m of the water column. ³ All depths ≥ 20 m.

2.4.2 Pumped-storage scenarios

Here, we present the results of simulations corresponding to present PS operations, the largest PS extension scenario and two reference scenarios considering no PS flows.

The present PS scenario represents the current state, where water is withdrawn from the hypolimnion of Sihlsee for both generating electricity (~135 MW installed capacity) and the residual flow to River Sihl. Water from Upper Lake Zurich is pumped up to Sihlsee (~65 MW installed capacity) and discharged to its hypolimnion. At Upper Lake Zurich, intake and outlet of the PS hydropower plant are placed within the epilimnion.

The extended PS is operated with installed capacities of 525 MW and 265 MW for generating and pumping, respectively. The basic hourly dataset for this scenario was provided by the Swiss Federal Railways and considered monthly-averaged net inflows to Sihlsee. It was adapted to account for hourly instead of monthly mean natural inflows, to allow assessing the influence of floods and low flows (details are given in Section 3.4).

For the first reference scenario (NoPS) water is withdrawn from the hypolimnion through the present outlet of River Sihl's residual flow. The discharge of River Sihl downstream the dam is based on a regime analysis of observed outflows, before the dam was built (LIMNEX AG, 2016, personal communication), representing a near-natural effluent for River Sihl downstream of the dam.

For the second reference scenario (QNat), the discharge to River Sihl is similar to that of NoPS, but released from the epilimnion, where water is discharged over a weir (crest at 887.4 m a.s.l., Figure 3.1). This outflow corresponds to the "theoretical" natural state of the lake, if the dam were of natural origin.

The current PS generating flow approximately equals the sum of inflows for Sihlsee, but contributes <10% to the total inflows of Upper Lake Zurich (Table 2.1). The pumping flow accounts for ~10% of the natural inflows at Sihlsee and for ~1% at Upper Lake Zurich. Consequently, the impacts of the PS operations are much more important for Sihlsee, and we focus the discussion of the results on this reservoir. Results for Upper Lake Zurich are presented in Section 3.4.

2.4.3 Aggregation of results

From the simulated temperatures and concentrations of dissolved oxygen and nutrients, we calculated means, minima and maxima of all years included in the studied period (1998–2012) for each day of the year. The simulations were aggregated separately for the epilimnion (represented by the uppermost 5 m of the water column) and the hypolimnion (represented by the lowermost 5 m of the water column). The differences between scenarios were calculated at every depth and then aggregated for either the epi- or the hypolimnion. The aggregation included the computation of mean and standard deviation for each season.

The durations of summer and inverse winter stratification were defined as the longest uninterrupted periods with temperature differences $>0.2\text{ }^{\circ}\text{C}$ and $<-0.2\text{ }^{\circ}\text{C}$ between the upper- and the lowermost layer. Schmidt stability was calculated according to Idso (1973) for each day and its mean value was calculated for each month. Ice-on was defined as the first day in winter, when ice thickness at SEG38 was $>0\text{ m}$, and ice-off as the first day in spring without ice at SEG38.

2.5 Results

Figure 2.2 depicts the mean and extrema for temperature, dissolved oxygen and nutrients for all considered PS scenarios, and Figure 2.3 shows a boxplot of their seasonal differences between either one of the two reference scenarios QNat and NoPS or the extended PS scenario and the present PS scenario. In both figures, the results are presented separately for the epi- and the hypolimnion.

In summer and autumn (May–December), epilimnion temperatures of Sihlsee are $\sim 1.6\text{ }^{\circ}\text{C}$ lower in the reference scenario QNat compared to all other scenarios. Hypolimnion temperatures for QNat are reduced by up to $10\text{--}11\text{ }^{\circ}\text{C}$ in late August compared to the other scenarios. These large temperature differences result from hypolimnetic water withdrawal, which draws the thermocline and warmer epilimnion water downwards. This highlights the strong effect of deep-water withdrawal on the temperature regime of Sihlsee. In contrast, the hypolimnion temperature differences between the extended and the present PS operation generally range within $\sim 3\text{ }^{\circ}\text{C}$, and those between the present PS operation and NoPS are $<1\text{ }^{\circ}\text{C}$ for most of the summer. In both cases, the hypolimnion of Sihlsee is warmed during summer due to pumping of epilimnion water from Upper Lake Zurich.

In winter and spring (December–May), epilimnetic temperatures are similar for all scenarios except for the extended PS scenario, where they increase by $\sim 1.6\text{ }^{\circ}\text{C}$. These differences are shaped by enhanced PS pumping flow during winter and result also in a significantly shortened ice-covered period (Figure 2.4 A) along with start and end dates of summer and inverse stratification, for the extended PS scenario. These further results in a decreasing ice thickness from $\sim 30\text{--}34\text{ cm}$ to $\sim 23\text{ cm}$ for the extended PS scenario (Figure 2.4 C). Inverse stratification is

also shortened by ~50 days (later start and earlier end) due to the pumping of comparably warm water from Upper Lake Zurich.

The deep-water withdrawal of present PS, extended PS and NoPS reference scenarios affects stratification (Figure 2.4 A) and water column stability (Figure 2.4 B) accordingly. Summer stratification is prolonged for QNat by ~40–50 days since water temperatures are much cooler for this scenario in autumn and more time is needed to cool the water column sufficiently to initiate mixing. For extended PS, summer stratification is prolonged by ~10–15 days, caused by earlier stratification start due to earlier ice-off (Figure 2.4 A).

Schmidt stability is for most months smallest in the extended PS scenario (Figure 2.4 B). Thus, enhanced PS pumping flow generally decreases water column stability. In the simulations this leads occasionally (three times in 12 years) to temperature differences <0.5 °C between the upper- and lowermost layer, and, thus, strong wind events can initiate almost complete mixing of the water column in summer. This does not occur in the near-natural reference scenario QNat. The other three scenarios show major differences from August to October, where Schmidt stability is decreased by factors of up to ~3.3 compared to the reference scenario QNat.

Dissolved oxygen concentrations in the epilimnion are mainly driven by equilibration with the atmosphere and primary production and do not differ much between the scenarios, only the shorter ice-covered period slightly raises concentrations in spring for the extended PS scenario. Conversely, large differences arise in the hypolimnion, where the prolonged stratification in the reference scenarios QNat increases the time available for oxygen depletion due to the decomposition of organic matter. This leads to maximum differences of ~ 8 mg L⁻¹ in late October when hypolimnetic oxygen concentrations reach their minimum in QNat, but are already partially replenished by seasonal mixing in the other scenarios. In addition, PS introduces oxygen-rich water from the epilimnion of Upper Lake Zurich to the hypolimnion of Sihlsee, counteracting oxygen depletion during both summer stratification and inverse winter stratification, which is particularly the case for the extended PS scenario (Figure 2.3). Following the Swiss Water Protection Ordinance (GSchV 1998), dissolved oxygen concentrations in lakes should always exceed a threshold of 4 mg L⁻¹. In the near-natural reference scenario QNat, simulated concentrations fall below this threshold every year, on average during ~90 days. This value is reduced to ~33 days (in 14 out of 15 years) for the reference NoPS, and ~22 days (11 years) for the present PS scenario. For the extended PS scenario, hypolimnetic dissolved oxygen concentrations below 4 mg L⁻¹ were simulated only in one year for an uninterrupted period of ~3 days, which is still less than for the other scenarios in that specific year.

Nutrient concentrations are also affected by both the exchange of water in the PS scenarios and the changes in stratification due to the withdrawal depth. The sum of nitrate and nitrite concentrations is increased by a factor of ~1.2–4 in the extended PS scenario, as the prevailing concentrations are higher by factor of ~3 in Upper Lake Zurich compared to Sihlsee. Similarly, phosphate concentrations increase during winter (November–April) by ~2–6 µg P L⁻¹. For present PS, these effects are much smaller, as the PS pumping flow is only 5% of that in the

extended PS. The prolonged stratification in the reference scenario QNat allows more time for the accumulation of nutrients in the hypolimnion from mineralization at the sediment surface. Until late October, nutrient concentrations are increased by up to $\sim 80 \mu\text{g N L}^{-1}$ and $\sim 7 \mu\text{g P L}^{-1}$ for the sum of nitrate and nitrite and phosphate, respectively, compared to the present PS scenario. Seasonal mixing propagates the effects on nutrient concentrations from the hypo- to the epilimnion. Thus, concentrations are raised in the reference scenario QNat from April to December by up to $2.3 \mu\text{g P L}^{-1}$ and $21 \mu\text{g N L}^{-1}$ for phosphate and the sum of nitrate and nitrite, respectively.

2.6 Discussion

At Sihlsee, extended PS operation is projected to result, compared to the present PS, in: (a) an increase of hypolimnion temperature by $\sim 2^\circ\text{C}$ during summer due to pumping surface water from Upper Lake Zurich; (b) warming of surface water by $\sim 1.6^\circ\text{C}$ during winter and spring mostly due to enhanced mixing; (c) later development of inverse stratification by ~ 1.5 month; (d) an earlier overturn in spring by ~ 2 weeks; (e) earlier ice-off by ~ 1 month and $\sim 30\%$ thinner ice; (f) increased dissolved oxygen concentrations in the hypolimnion; and (g) increased nutrient concentrations originating from higher concentrations in the lower lake. The sum of nitrate and nitrite concentrations in winter and spring are decreasing at Upper Lake Zurich for the same reasons as they increase in Sihlsee. However, effects on Upper Lake Zurich are much less pronounced due to its larger volume and higher natural discharges. Local effects of PS operation in the vicinity of the intake/outlet of the PS hydropower plant are expected to be higher, but their analysis would require 3D simulations in the near field (Müller et al. 2016).

Besides these effects of PS operations, the simulations highlighted the importance of the withdrawal depth in Sihlsee. If located in the hypolimnion (reference scenario NoPS), the differences to the present PS scenario are minor. Conversely, large effects result if the outlet is placed within the epilimnion (reference scenario QNat) with: (a) hypolimnion temperatures decreasing to commonly observed values of natural lakes in that region; (b) a consequent reduction of epilimnion temperature; (c) delayed summer stratification by ~ 1.5 months; (d) therefore, reduced dissolved oxygen concentrations; (e) increased phosphate concentrations; and (f) higher sum of nitrate and nitrite concentrations due to delayed seasonal mixing.

These findings can be put into the context of previous modelling studies on pumped-storage hydropower facilities. Additional information about the systems investigated in these studies is given in Section 3.5.

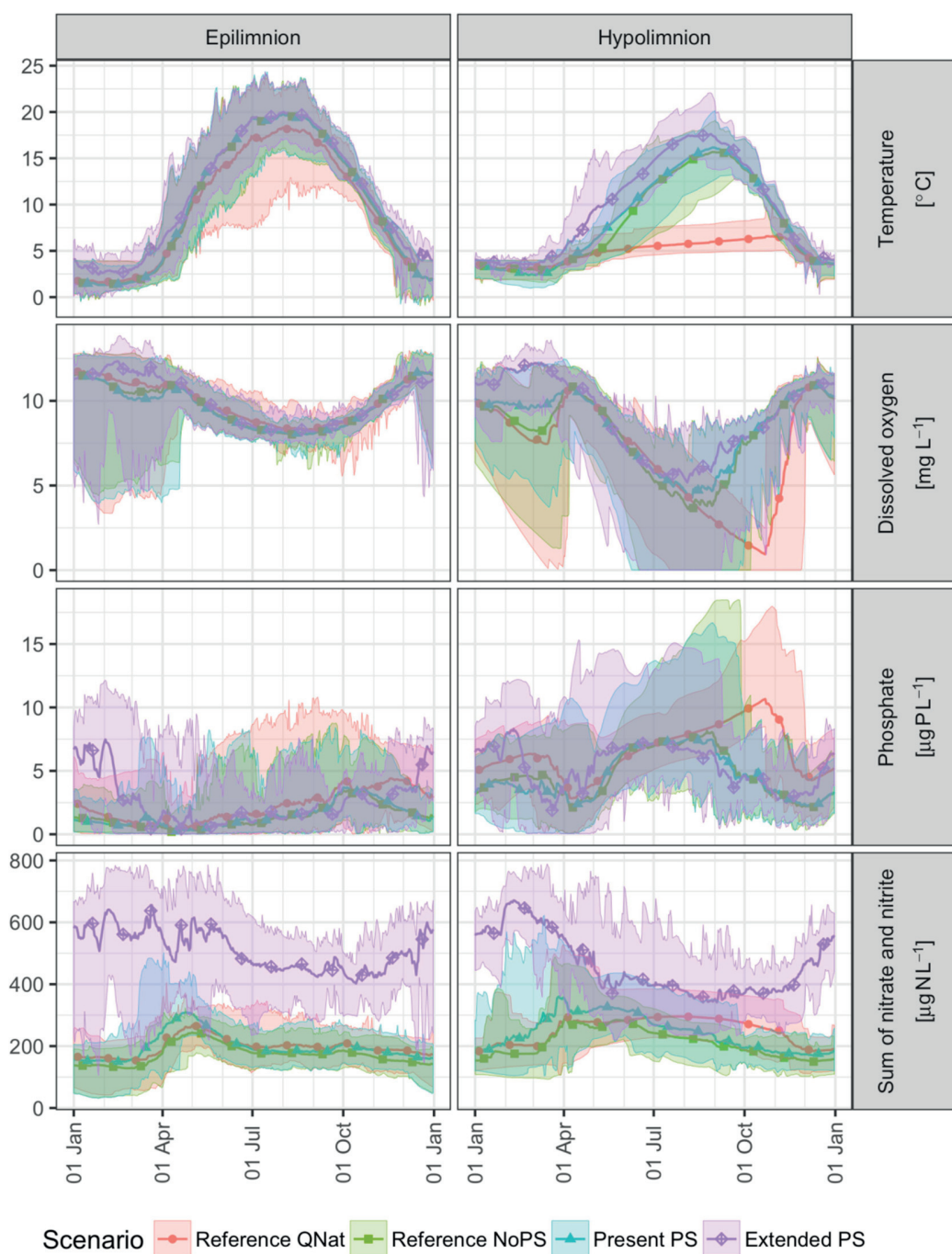


Figure 2.2 Mean (lines with markers) and range of minima and maxima (shaded areas) of simulated temperatures ($^{\circ}\text{C}$) and concentrations of dissolved oxygen (mg L^{-1}), phosphate ($\mu\text{g P L}^{-1}$) and the sum of nitrate and nitrite ($\mu\text{g N L}^{-1}$) for the two reference scenarios QNat (red) and NoPS (olive-green), the present (turquoise) and the extended PS (violet) scenarios in the epilimnion (uppermost 5 m of the water column) and the hypolimnion (lowermost 5 m of the water column) of Sihlsee.

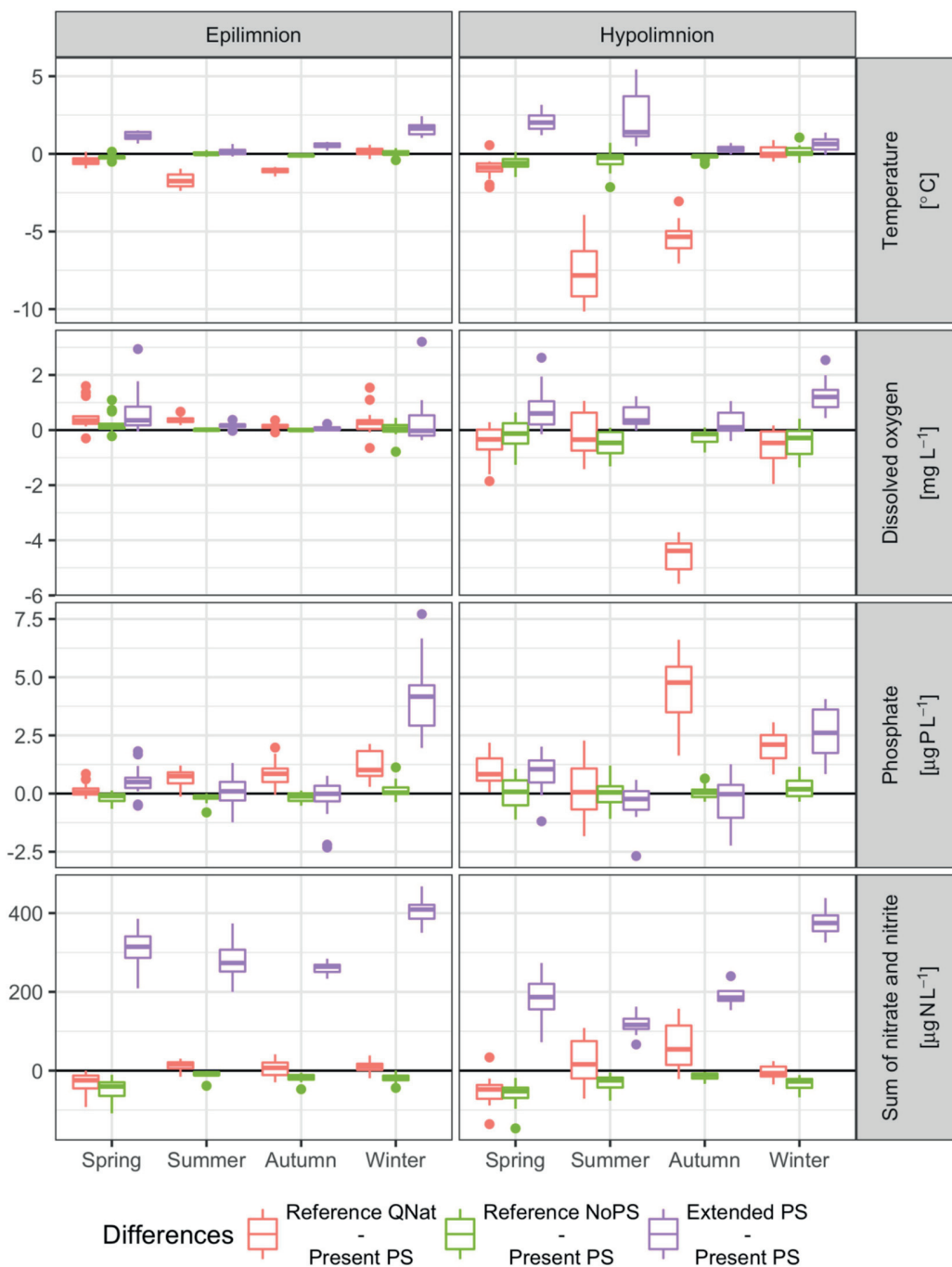


Figure 2.3 Boxplot of differences in either one of the two reference scenarios NoPS and QNat or the extended PS scenario to the present PS scenario of temperature ($^{\circ}\text{C}$) and concentrations of dissolved oxygen (mg L^{-1}), phosphate ($\mu\text{g P L}^{-1}$) and the sum of nitrate and nitrite ($\mu\text{g N L}^{-1}$) at Sihlsee. Points show outliers; values were aggregated seasonally for each year before plotting (winter: December–February; spring: March–May; summer: June–August; and autumn: September–November).

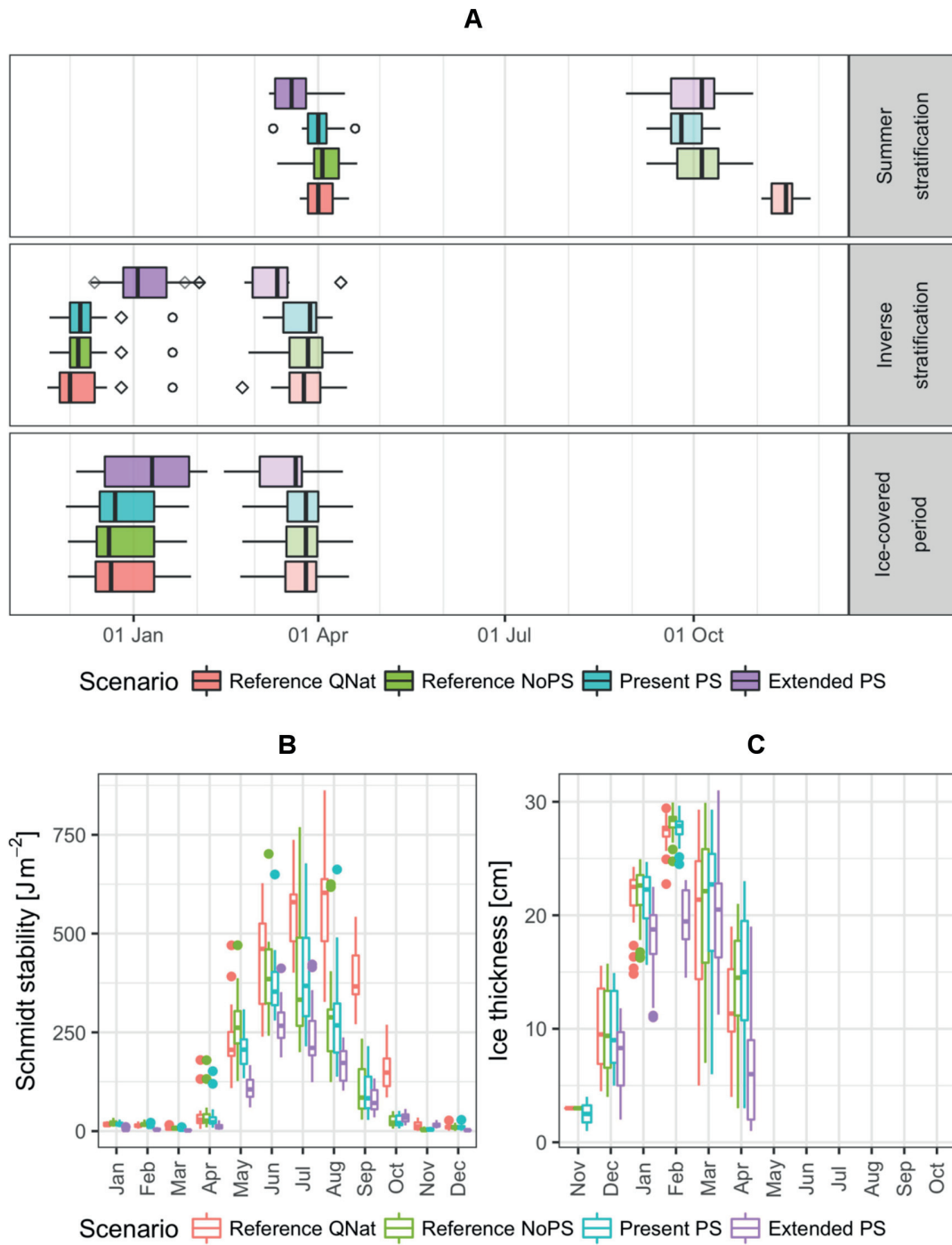


Figure 2.4 Boxplots for the two reference scenario NoPS and QNat, the present PS and the extended PS scenario at Sihlsee: (A) start and end of summer or inverse stratification as well as ice-on and ice-off; (B) monthly mean of Schmidt stability (J m^{-2}); and (C) monthly mean of ice thickness (cm). Points show outliers of start (circles) and end (squares) of summer or inverse stratification as well as ice-covered period.

Bonalumi et al. (2012) showed that both water bodies connected by a PS scheme would mostly be warmed. In autumn, 50% of this warming in the upper hypolimnion of the lower lake would be due to frictional warming of the PS flows. This effect is not as relevant for the case of Sihlsee and Upper Lake Zurich due to the much smaller head. In Lake Oconee, the water column was completely mixed in summer after the introduction of PS operation, whereas before temperature differences between epi- and hypolimnion had ranged between 5 and 13 °C (Potter et al. 1982). This is comparable to the strong reduction of Schmidt stability in Sihlsee in the extended PS scenario, but the extent of PS operations is insufficient to completely homogenize it. At Twin Lakes, the PS operation reduced the residence time from 314 to 176 days, resulted in cooling of both basins of Twin Lakes, and weakened stratification (USBR 1993). Anderson (2010) concluded that the timing of stratification at Lake Elsinore would not be affected by PS, although stratification, expressed as the temperature difference between surface and bottom waters, would be weakened by 1.2 °C in late May. Our findings confirm that summer stratification can be weakened by PS operation. Our results also suggest, in contrast to Anderson (2010) and Bermúdez et al. (2017), that the timing of stratification can be affected by PS, particularly that of inverse stratification. Regarding the PS impact on temperature, our results indicate a warming of the hypolimnion, which is contrary to the findings of USBR (1993), but similar to those of Bonalumi et al. (2012) and Potter et al. (1982).

Overall, the results of our study showed that the effects of the water exchange due to PS operations, even for extended PS, are small compared to those caused by deep-water withdrawal. Similarly, for the drinking water reservoir Grosse Dhuenn (Weber et al. 2017), selective withdrawal was shown to move the thermocline upwards, increase differences between water temperature of the epi- and hypolimnion, and thus strengthen thermal stratification, when being compared to bottom water withdrawal. These observations highlight the importance of withdrawal depth as a crucial parameter in the design of PS hydropower plants for reducing ecological impacts. However, water temperature and stratification are not the only parameters to be considered for optimizing withdrawal depth, e.g., concentrations of glacial particles might necessitate an intake/outlet placement in the hypolimnion (Bonalumi et al. 2012).

In the simulations of Bonalumi et al. (2012), PS operations were projected to significantly reduce ice cover duration. However, due to a lack of observational data for calibrating the model, this effect could not be reliably quantified. With a modified parameterization of CE-QUAL-W2, we were able to reliably reproduce ice cover duration (Figure 3.6). With this model, we could show that extended PS would strongly reduce ice thickness and ice-cover duration in Sihlsee.

Water quality parameters, such as dissolved oxygen, and nutrient concentrations, are affected by PS operations through two different mechanisms: exchange of water masses, and indirect effects due to changes in mixing and stratification. The importance of the first mechanism scales with the ratio of the exchanged water masses and the volumes of the basins as shown for example for the sum of nitrate and nitrite in Sihlsee above. Similarly, Bonalumi et al. (2012) found inorganic suspended solid concentrations to decrease in the upper reservoir and to increase in the lower

lake. At Twin Lakes, inorganic suspended solid concentrations decreased by 40 mg L^{-1} when PS operations were introduced, which was also linked to dilution (USBR 1993).

Changes in thermal stratification affect water quality in various ways. At Sihlsee, the bottom water withdrawal leads to weaker stratification, and reduces its duration by >1 month. This further affects hypolimnetic dissolved oxygen concentrations: due to less time being available to reduce dissolved oxygen to low levels, more dissolved oxygen being resupplied by mixing through the weaker thermocline, and additional supply of dissolved oxygen as river inflows plunge more easily through a weaker density gradient. Consequently, dissolved oxygen concentrations fall below the legal target of 4 mg L^{-1} in a much smaller volume and during a shorter period. This is in line with the findings of Weber et al. (2017) and Anderson et al. (2014) that the hypolimnion of a reservoir is more oxygenated when water is withdrawn at the bottom. Likewise, at Twin Lakes, the PS operation seems to have resulted in slight aeration of the hypolimnion, which was considered beneficial, as it increased habitat volume of fish (USBR 1993).

According to Anderson et al. (2014), phosphorus concentrations decrease when water is withdrawn from the hypolimnion. This is in accordance with our findings, as we found additional accumulation in autumn induced by intensified stratification for the reference scenario QNat. Nevertheless, PS impacts on nutrient concentrations are site-specific.

Our projections for effects of PS and deep-water withdrawal on temperature and stratification are robust, since they are large compared to the uncertainty of the model, and supported by an extensive data set of temperature for model calibration. The required correction of the water balance and the lack of information to divide the outflow into surface outflow and deep-water withdrawal, in the case of flood events, might somewhat affect mixing patterns for these flood events, but should not change the overall picture. The projected effects on water quality include a higher uncertainty, which is due to limited availability of hydrological and water quality forcing of inflows. Nevertheless, the projected changes in water quality yield a coherent picture of the effects of water exchange and those due to changes in thermal stratification.

When recommissioning a PS hydropower plant, a reference state needs to be defined for the environmental impact assessment. For natural lakes, this is the scenario which does not include any artificial PS flows. However, for reservoirs such as Sihlsee, this scenario is mostly a matter of definition: it might be described as the natural state without a lake, where the original river stretch needs to be analysed; it might also be an artificial state, with the reservoir remaining due to its multiple other purposes, but PS operations being removed. The simulated effects for the reference scenarios NoPS and QNat highlight that the estimated environmental impacts can depend heavily on the choice of the reference scenario. Thus, we see a need for guidelines to define such reference scenarios in the context of assessing environmental impacts of increased development or the extension of PS hydropower plants.

2.7 Conclusions

Previous studies have shown, by both pre- and post-operational observations and modelling, that PS operations can have significant impacts on temperature and thermal stratification in the connected water bodies. With the present study, we aimed at extending this assessment to indicators of water quality (oxygen and nutrient concentrations) as well as the duration and extent of ice cover. For this purpose, we projected the effects of a PS extension scenario for the case of Etzelwerk, using a directly coupled hydrodynamic and water quality model for the two connected water bodies. The results showed that PS extension would increase water temperatures in the hypolimnion of the upper reservoir by ~ 2 °C in summer. The model also projected a significant reduction of the duration and thickness of ice cover due to the PS operations. Additionally, the increased PS pumping flow would raise the nutrient concentrations in the upper reservoir and increase dissolved oxygen availability in its hypolimnion. These effects of PS operation on lake water quality are not easily transferable to other systems, as they depend on the natural, site-specific water quality. In tendency, however, PS supports a decrease of the strength and duration of stratification with correlated effects on dissolved oxygen and nutrients.

Furthermore, we aimed at disentangling the effects of PS operation and deep-water withdrawal, which has up to now not been quantified in the context of PS operations. This was achieved by analysing two reference scenarios: (i) a scenario without hydropower but with deep-water withdrawal from the upper reservoir; and (ii) a “quasi-natural” scenario with surface outflow. The scenario without hydropower showed comparably minor differences to the present PS operation. Conversely, the “quasi-natural” scenario highlighted a large effect of the withdrawal depth on the upper reservoir. Compared to the present state, the surface outflow decreased hypolimnetic water temperature by up to ~ 10 °C, and, accordingly, intensified stratification, and reduced dissolved oxygen concentrations. Thus, we can claim that at Etzelwerk the impacts of water withdrawal in the hypolimnion are more crucial than those of PS operations, especially for the present, but also for the extended PS operation. This also underlines the importance of the location of the PS intake/outlet. Consequently, withdrawal depth in the reference state defines relevant implications for the estimated environmental impacts of a PS scheme. For management purposes, it is, therefore, important to have clear guidelines for defining a reference state as a base scenario for assessing the environmental impacts of increased development or extension of PS hydropower plants. We, thus, recommend for future projects to separately analyse effects due to withdrawal depth and those due to PS operation. Although the effects on the natural lake were small in the present study, these need to be cautiously investigated at any other site.

Chapter 3

Supplementary information to Chapter 2⁵

3.1 Overview

This chapter provides supplementary information to Chapter 2. In particular, the model forcing, the available observations and the projections for Upper Lake Zurich, the lower lake of the studied system are described. Regarding the model forcing, Section 3.2 gives (a) details of the bathymetrical information, (b) information about the meteorological stations used to generate hourly time series for both Sihlsee and Upper Lake Zurich, (c) additional information on the hydrological forcing and water quality forcing. For the available observations a literature review is provided for Upper Lake Zurich, and for Sihlsee, the observations performed by Eawag from April 2014 to December 2016 are described. The latter comprise observations of temperature, inorganic suspended solids, dissolved oxygen, chlorophyll-a, nitrate, nitrite and total phosphorus. Due to both Upper Lake Zurich's larger volume and its larger share of natural inflows the PS effects on temperature and water quality do not exceed the interannual variability of these characteristics. Lastly, this chapter also provides an overview of the specifications of other PS operations, which have been studied in literature and are cited in Chapter 2.

⁵ This chapter is based on the supplementary information to "Effects of lake-reservoir pumped-storage operations on temperature and water quality" by U. G. Kobler, A. Wüest and M. Schmid published in *Sustainability*. The fieldwork, simulations and the analysis presented hereafter are original and were performed by the author of the thesis.

3.2 Model forcing and initial conditions

3.2.1 Bathymetry

The bathymetry is based on Lidar measurements (terra Vermessungen, October 2014, personal communication) for Sihlsee and on GIS-data of the Federal Institute of Topography (swisstopo Art. 30 GeoIV: 5704 000 000 / DHM25@2003) for Upper Lake Zurich.

Both water basins are divided into 200 m wide segments along the main axis and 0.5 m thick layers (depth). This results in 43 (58) segments and 47 (93) layers for Sihlsee (Upper Lake Zurich). The numbers of segments and layers include at each margin a segment or layer filled with zeros. An overview of the model grid with the positions of all in-, out- and artificial flows is given in Figure 3.1.

The Sihlsee inflows are located in segments 2 (Minster and Sihl), 10 (Eubach) and 22 (Grossbach), each entering the lake within the top 4 layers. At Upper Lake Zurich the inflows are located in segments 4 (Linth), 37 (Wägitaler Aa) and 38 (Jona). While River Linth is distributed into layers 2-28, the other inflows enter between layers 2-14. The outflow to Lower Lake Zurich is located at segment 58 and implemented as a weir.

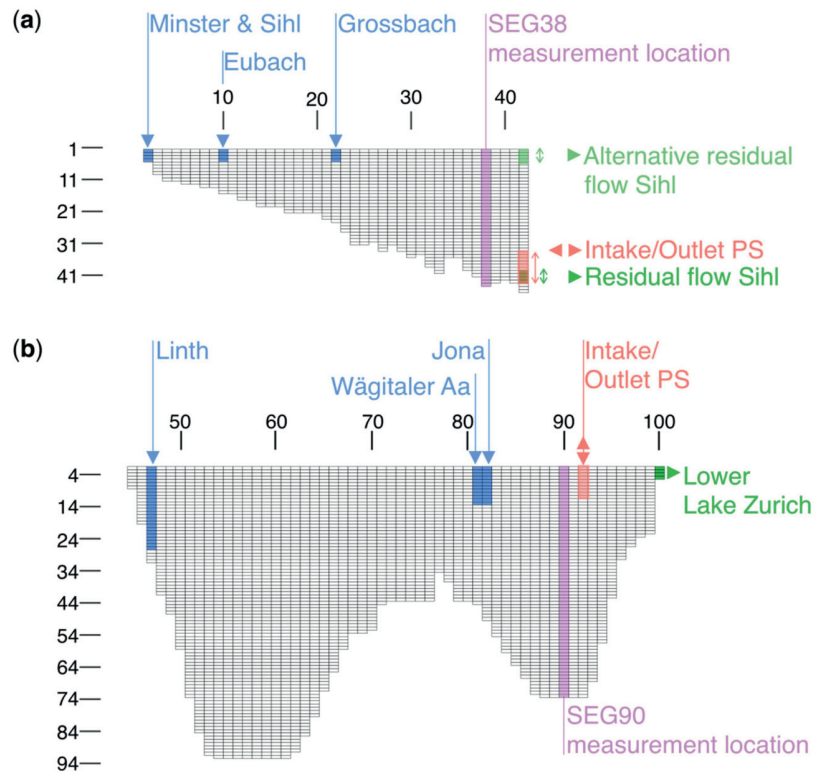


Figure 3.1 Overview of model grid: Sihlsee (a) and Upper Lake Zurich (b) including the positions of all inflows (blue), outflows (green) and artificial flows (red). The grid labels indicate segment numbers on the horizontal and layer numbers on the vertical axis. The segments with available observations (SEG38 and SEG90) are shaded in violet.

The PS intake and outlet of present and extended PS at Sihlsee is located at segment 42 and stretches from layer 33 to 43 that at Upper Lake Zurich is positioned at segment 49 and extends between layers 2 to 12.

The residual flow to River Sihl from Sihlsee is indicated in green in Figure 3.1. The regular outlet is located at segment 42 between layers 38 to 43, where water is withdrawn for the present PS, the extended PS scenario and the reference scenario NoPS. For the reference scenario QNat the outlet of the residual flow is moved to the surface (weir crest at 887.4 m a.s.l.).

3.2.2 Meteorological forcing

For calculating heat exchange at the water surface and mixing processes, the standard version of CE-QUAL-W2 requires the input of air temperature, dew point, wind speed and direction as well as cloudiness and solar radiation. Incoming long-wave radiation is then calculated internally. We replaced this procedure with an external calculation of long-wave radiation and modified the code to read in these values instead of cloudiness, which is then no longer required. Long-wave radiation was calculated according to recommendations given by Flerchinger et al. (2009). Incoming clear-sky long-wave radiation was calculated using the method of Dilley and O'Brien (1998). The cloud correction by Unsworth and Monteith (1975), and the elevation correction by Deacon (1970) were applied. The albedo of long-wave radiation was kept constant at 0.97.

Table 3.1 Overview of meteorological information used. Shown are the temporal resolution (h: hourly, d: daily), the time range which was used to generate the meteorological forcing and the order of stations of MeteoSwiss, which were used to fill data gaps: (1) Zurich Fluntern, (2) Wädenswil, (3) Schmerikon and (4) Einsiedeln.

Water body	Variable	Temporal resolution	Time period	Station	Institution	Gap treatment
Upper Lake Zurich	Air temperature	h	01.01.1997-31.12.2015	Wädenswil	MeteoSwiss	(1)
	Dew point	h	01.01.1997-31.12.2015	Wädenswil	MeteoSwiss	(1)
	Wind velocity	h	01.01.1997-31.12.2015	Schmerikon	MeteoSwiss	(2), (1)
	Wind direction	h	01.01.1997-31.12.2015	Schmerikon	MeteoSwiss	(2), (1)
	Cloudiness	d	01.01.1997-31.12.2015	Wädenswil	MeteoSwiss	(1)
	Solar radiation	h	01.01.1997-31.12.2015	Wädenswil	MeteoSwiss	(1)
Sihlsee	Air temperature	h	01.01.1997-31.01.2007	Einsiedeln	MeteoSwiss	(2), (1)
		h	01.02.2007-31.12.2015	Einsiedeln	Segelclub Sihlsee	(4), (2), (1)
	Dew point	h	01.01.1997-31.01.2007	Einsiedeln	MeteoSwiss	(2), (1)
		h	01.02.2007-31.12.2015	Einsiedeln	Segelclub Sihlsee	(4), (2), (1)
	Wind velocity	h	01.01.1997-31.01.2007	Wädenswil	MeteoSwiss	(1)
		h	01.02.2007-31.12.2015	Einsiedeln	Segelclub Sihlsee	(4), (2), (1)
	Wind direction	h	01.01.1997-31.01.2007	Wädenswil	MeteoSwiss	(2), (1)
		h	01.02.2007-31.12.2015	Einsiedeln	Segelclub Sihlsee	(4), (2), (1)
	Cloudiness	d	01.01.1997-29.04.2012	Einsiedeln	MeteoSwiss	(1)
		d	30.04.2012-31.12.2015	Wädenswil	MeteoSwiss	(1)
	Solar radiation	h	01.01.1997-07.03.2012	Wädenswil	MeteoSwiss	(1)
		h	08.03.2012-31.12.2015	Einsiedeln	MeteoSwiss	(2), (1)

The meteorological forcing for Sihlsee was mostly based on observations of MeteoSwiss at Einsiedeln and Segelclub Sihlsee (Figure 2.1, Table 3.1). Monitoring of solar radiation and wind speed at an hourly time step at Einsiedeln started only in 2007. For previous years data from the MeteoSwiss station Wädenswil were used. In 2012 the measurement of cloudiness at Einsiedeln was discontinued. Afterwards data were taken from the MeteoSwiss station Zurich Fluntern.

For Upper Lake Zurich, observations of the MeteoSwiss station Wädenswil were used for air temperature, dew point, cloudiness and solar radiation. Wind velocity and direction were taken from the MeteoSwiss station Schmerikon (Figure 2.1, Table 3.1). Gaps were filled with data from the closest station (Wädenswil, followed by Zurich Fluntern).

3.2.3 Hydrological forcing

For Sihlsee, the discharges of the rivers Minster, Eubach and Grossbach are monitored by the Federal Office for the Environment (FOEN). As inflows of River Sihl and the remaining catchment area were not available, these were estimated by scaling the inflow of Minster proportional to their catchment area. The outflows to River Sihl for present and extended PS are based on simulations of the Swiss Federal Institute for Forest, Snow and Landscape Research (Zappa et al. 2015). These simulations give the total flow in River Sihl downstream of the dam, composed of the sum of discharges through the regular outlet and those of floods over the spillway. Since all water is withdrawn from the bottom outlet in the model, the simulated flow patterns during flood events may be different to those actually occurring in the reservoir.

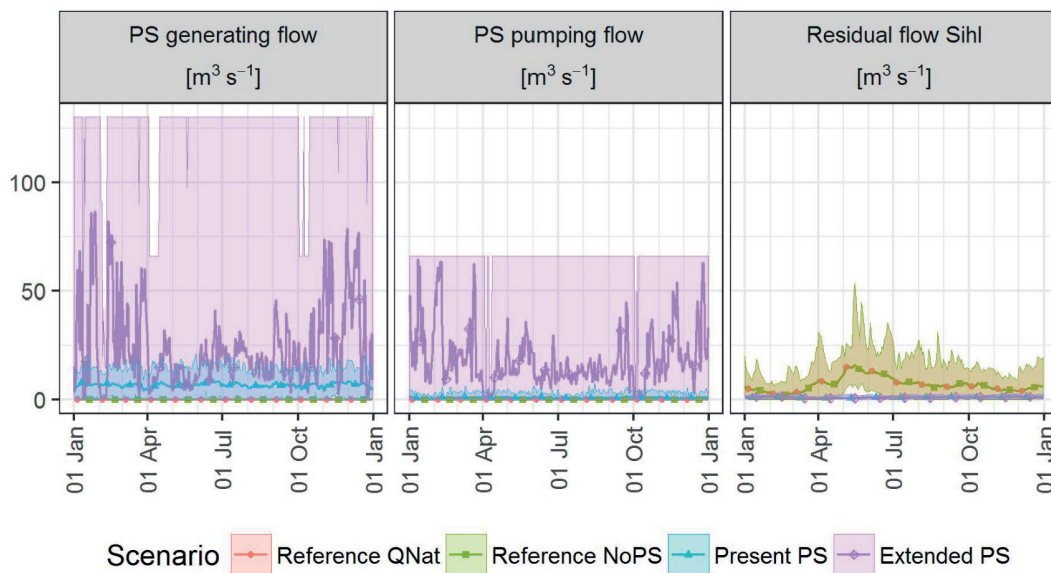


Figure 3.2 PS generating and PS pumping flow as well as residual flow to river Sihl ($\text{m}^3 \text{s}^{-1}$) for the reference scenario QNat and NoPS, the present PS and the extended PS scenario. Shown are means (lines with markers) and range of minima and maxima (shaded areas) of simulated years 1998-2012.

The outflow of the two reference scenarios (QNat and NoPS) is based on a modelling study of LIMNEX AG (personal communication). In case of QNat the outflow is implemented using a weir (Figure 3.1, upper edge at 884.7 m a.s.l., 5 m wide, weir discharge coefficient 0.7) which directly allows the computation of the discharge following the formula of Poleni (Bollrich 2007). For NoPS, the discharge computed with CE-QUAL-W2 for QNat was used, but withdrawn from the hypolimnion instead of being discharged over a weir (Figure 3.1). Figure 3.2 depicts the PS flows as well as the residual flow to river Sihl for the reference scenarios QNat and NoPS, the present PS and the extended PS scenarios.

To account for measurement errors as well as missing inflows, groundwater exchange, evaporation and precipitation at Sihlsee we estimated a correction term to achieve agreement with observed water levels. Simulated and observed water levels were converted to the corresponding volume for each day, and their difference was averaged for each month. The monthly missing volume was then implemented as a distributed tributary, which could also have negative values.

Of the inflows to Upper Lake Zurich, only the discharge of River Linth at Weesen is routinely monitored by FOEN. As no additional information was available, this discharge was used to scale the other inflows by the corresponding ratio of catchment area. The outflow to Lower Lake Zurich was implemented through a weir (upper edge at 405.5 m a.s.l., 200 m wide, weir discharge coefficient 0.5).

Both scenario-independent and scenario-dependent hydrological forcing of Sihlsee and Upper Lake Zurich are given in Table 2.1. While no PS flows are withdrawn in case of the reference scenarios (NoPS and QNat), extended PS increases PS generating and PS pumping flows by factors of ~4 and ~22, respectively (Figure 3.2). Based on the hydrological forcing the average water residence time in Sihlsee can be estimated to 150 days for the reference scenarios, 135 days for present PS and 40 days for extended PS.

The basic dataset of hourly exchange flows for the extended PS scenario was provided by the Swiss Federal Railways and considered monthly-averaged net inflows to Sihlsee. It needed adaptation to allow assessing the influence of floods and low flows. Thus, the PS flows of the extended PS scenario were adapted based on the formulation of an hourly water balance, with hourly natural in- and outflows, where the resulting water level is limited by minimum and maximum operational water levels as well as temporal restrictions for the minimal water level from June to October.

3.2.4 Inflow water quality forcing

FOEN provides water temperature observations at Rivers Alp and Linth for the considered simulation period (Figure 2.1). The River Alp was chosen to be representative for all inflows of Sihlsee and the River Linth for those of Upper Lake Zurich. Inflow temperatures for Sihlsee range from ~ 1 °C in winter to ~ 18 °C in summer. River Linth is the outflow of Walensee and thus significantly warmer in winter with average temperatures ~ 6 °C.

Inorganic suspended solid concentrations of the inflows of Sihlsee were estimated based on Keller and Weibel (1991). They derived an empirical relationship between stream flow in mm per week and suspended solid concentrations in mg L^{-1} for two sub-catchments of River Alp. Out of the two, Erlenbach (referred to as 10 in their publication) was chosen as it corresponds better to the catchment of Sihlsee. Thus, the regression listed on page 57 of their publication was used to estimate inorganic suspended solid concentrations for all inflows of Sihlsee. Inorganic suspended solid concentrations of the inflows of Upper Lake Zurich were estimated as follows: for Linth, Peters-Kümmerly (1973) determined a direct relationship between discharge and the load of suspended solids. The estimated regression follows Equation 3.1.

$$c = 1.15 \cdot Q^{0.04}$$

Equation 3.1 Regression equation of discharge and suspended solids

with c in mg L^{-1} and Q in $\text{m}^3 \text{s}^{-1}$. Additional information for the other inflows to Upper Lake Zurich was missing, thus inorganic suspended solid concentrations were estimated with the same procedure as for Sihlsee. When calibrating the model, inorganic suspended solid concentrations were scaled for both water bodies with the parameter f_{iss} .

Dissolved oxygen concentrations were estimated according to Haynes (2014), assuming equilibrium with the atmosphere, using the water temperature of the inflows. Nutrient concentrations of the sum of nitrate and nitrite, ammonium and phosphate were considered as forcing for all the inflows. For Sihlsee, these were approximated with observations at Erlenbach, a sub-catchment of River Alp (Figure 2.1). There nitrate, total nitrogen and phosphate have been observed weekly as part of a national monitoring program (NADUF) since 2003. Ammonium, not directly observed, was approximated by the difference of total nitrogen and nitrate. Weekly averages of all years between 2003 and 2015 were used to generate a mean annual forcing, which was assigned to the nutrient forcing for all simulated years. During model calibration these time series were scaled with the parameters f_{PO_4} , f_{NO} and f_{NH_4} (Section 3.3). For Upper Lake Zurich, the mean annual nutrient concentrations were calculated based on monthly observations in River Linth (1997-2014). As the observations of the other inflows to Upper Lake Zurich are not as comprehensive, these average annual nutrient concentrations were also assigned to the nutrient forcing of the other inflows. The parameters f_{PO_4} , f_{NO} and f_{NH_4} (Section 3.3) were adjusted during model calibration to scale the water quality time series for Linth and the other two inflows separately, as the concentrations differ substantially according to Gammeter and Forster (2002).

3.2.5 Initial conditions

The initial conditions for both water bodies are given in Table 3.2. The model was initialized on 01 January. At this time, Upper Lake Zurich is usually homogenized, while Sihlsee is inversely stratified. For Upper Lake Zurich, constant values corresponding to average observed winter conditions or to default values of CE-QUAL-W2 were set as initial conditions. For Sihlsee, an inversely stratified temperature profile was assumed, whereas water quality parameters were set to constant values. The first year of the simulations was excluded from the analysis, and due to the relatively short residence times, the initial conditions have only a minor impact on the simulation results in the subsequent years.

Table 3.2 Initial conditions of temperature, ice thickness and concentrations of inorganic suspended solids, phosphate, ammonium, sum of nitrate and nitrite, labile dissolved organic matter (LDOM), refractory dissolved organic matter (RDOM), labile particulate organic matter (LPOM), refractory particulate organic matter (RPOM), algal groups 1 and 2, dissolved oxygen and zooplankton. Temperature at Sihlsee was input as profile.

Variable	Layer Unit	Sihlsee										Upper Lake Zurich
		2-46	2	3	4	5	6	7	8	9	10-46	2-92
Temperature	[°C]	-	0.8	0.9	1	1.5	2	2.5	3	3.5	4	6
Ice thickness	[m]	0.1	-	-	-	-	-	-	-	-	-	0
Inorganic suspended solids	[mg L ⁻¹]	2	-	-	-	-	-	-	-	-	-	2
Phosphate	[µg P L ⁻¹]	5	-	-	-	-	-	-	-	-	-	5
Ammonium	[µg N L ⁻¹]	2	-	-	-	-	-	-	-	-	-	2
Sum of nitrate and nitrite	[µg N L ⁻¹]	300	-	-	-	-	-	-	-	-	-	700
LDOM	[mg L ⁻¹]	0.1	-	-	-	-	-	-	-	-	-	0.1
RDOM	[mg L ⁻¹]	0.1	-	-	-	-	-	-	-	-	-	0.1
LPOM	[mg L ⁻¹]	0.1	-	-	-	-	-	-	-	-	-	0.1
RPOM	[mg L ⁻¹]	0.1	-	-	-	-	-	-	-	-	-	0.1
Algae group 1	[mg L ⁻¹]	0.05	-	-	-	-	-	-	-	-	-	0.05
Algae group 2	[mg L ⁻¹]	0.05	-	-	-	-	-	-	-	-	-	0.05
Dissolved oxygen	[mg L ⁻¹]	10	-	-	-	-	-	-	-	-	-	11
Zooplankton	[mg L ⁻¹]	0.01	-	-	-	-	-	-	-	-	-	0.01

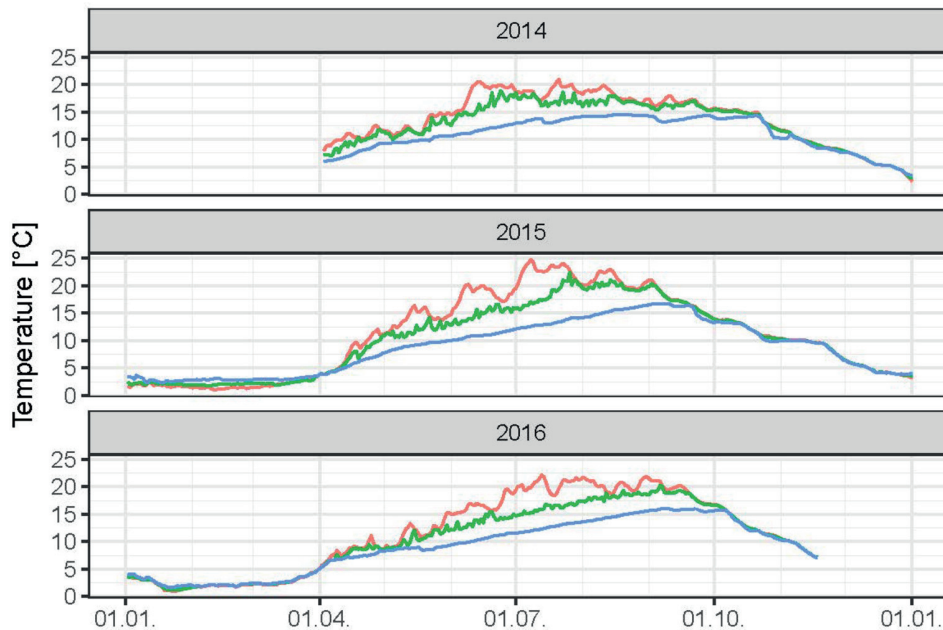


Figure 3.3 Observed water temperature in Sihlsee for 2014-2016 at three depths: 1 m below surface (red), 6 m below surface (green), 0.5 m above sediment (blue); measurements were performed at SEG38 (Figure 3.1).

3.3 Available observations at Sihlsee and Upper Lake Zurich and model calibration

3.3.1 Available observations

The observations at Sihlsee were conducted by Eawag solely for the purpose of this study from April 2014 to December 2016. Temperatures, observed quasi-continuously (Figure 3.3), show that seasonal convective mixing occurred latest in mid-October, and inverse stratification started to evolve at end-December, facilitating ice growth dependent on meteorological conditions. In winter 2014/15 the lake was ice covered, but not in winter 2015/16. Summer stratification arose between beginning and mid-April with maximum temperatures between 20 and 25 °C and 15 to 17 °C in the epi- and hypolimnion, respectively. Summer hypolimnion temperatures are high compared to most stratified Swiss lakes, where they generally remain below 10 °C throughout the year. As shown in the present study, these high hypolimnion temperatures are caused by deep-water withdrawal in the lake.

Vertical profiles of additional physical and chemical parameters were measured on a monthly basis from April 2014 to December 2016 (26 profiles for inorganic suspended solids and nitrate, 25 for dissolved oxygen, 16 for Chlorophyll-a, 24 for total phosphorus). Observed inorganic suspended solid concentrations were homogeneously distributed at ~5 mg L⁻¹ in April and from October to December. During summer stratification inorganic suspended solid concentrations

were ~ 5 and $<30 \text{ mg L}^{-1}$ in the epi- and the hypolimnion, respectively. One flood event on 22 July 2014 caused ISS concentration peaks in the thermocline. In August and September, dissolved oxygen concentrations in the hypolimnion fell below 4 mg L^{-1} , the legal requirement in Switzerland (GSchV 1998). Chlorophyll-a concentrations did not exceed $3.5 \mu\text{g L}^{-1}$, with highest values for June, August and September. Observed nitrate concentrations varied between 100 and $350 \mu\text{g N L}^{-1}$, with decreased concentrations in the epilimnion due to algal uptake from June to September. Nitrite concentrations were $<10 \mu\text{g N L}^{-1}$ for the 2 observations made. Total phosphorus was $<35 \mu\text{g P L}^{-1}$, with enriched concentrations in the hypolimnion for July and September and epilimnion concentrations $<10 \mu\text{g P L}^{-1}$ throughout the year. Thus, Sihlsee can be considered oligotrophic.

The observations at Upper Lake Zurich are part of a monitoring program by the cantonal agencies (Gammeter and Forster 2002; Schildknecht et al. 2013). The observed temperature (1994-2005) during summer stratification was $5\text{-}6^\circ\text{C}$ and $20\text{-}25^\circ\text{C}$ for the hypo- and the epilimnion, respectively (Gammeter and Forster 2002). From December to April, the lake was mixed and in some winters inversely stratified with a minimum surface temperature of $\sim 2^\circ\text{C}$. Wind protected bays can freeze over during very cold winters (Gammeter and Forster 2002). No observations are available for inorganic suspended solid concentrations. The hypolimnetic dissolved oxygen concentrations at SEG90 (Figure 2.1) for 1994-2005 fell below 4 mg L^{-1} every year during the stagnation period. Chlorophyll-a concentrations did not exceed $6 \mu\text{g L}^{-1}$ for 2006-2010. The mean annual concentrations (1996-2010) of nitrate, nitrite and ammonium were 700, 5 and $10 \mu\text{g N L}^{-1}$ and those of orthophosphate were $\sim 10 \mu\text{g P L}^{-1}$. The annual mean of the total phosphorus concentrations did not exceed $12 \mu\text{g P L}^{-1}$. Thus, Upper Lake Zurich can be classified as mesotrophic.

3.3.2 Model calibration

The model was calibrated manually with a manual trial and error approach, with the aim of minimizing root mean square errors (RMSE), mean absolute errors (MAE) and mean errors (ME) between simulated and observed quantities. Additionally, the differences between observed profile and time series data and simulations were visually inspected. Several model parameters of CE-QUAL-W2 and factors for adjusting the water quality forcing (Section 3.2) of both water bodies were calibrated, while the majority of the other parameters was either set to the default value or determined based on literature values (Bonalumi et al. 2012; Mieleitner and Reichert 2006; Mieleitner and Reichert 2008).

RMSEs are given in Table 2.2 of the main manuscript, MAEs and MEs in Table 3.3. Moreover, temperature profiles at Sihlsee and Upper Lake Zurich show a good agreement for the calibration period (2014-2015) (Figure 3.4, Figure 3.5). Similar to the RMSEs (Table 2.2) MAEs and MEs shows that dissolved oxygen and nutrient concentrations are better predicted in the epi- than in the hypolimnion.

The comparison of simulated and observed ice-thickness is shown in Figure 3.6, where observations were provided by the Swiss Federal Railways, and volumetrically averaged time

series of observed and simulated variables for epi- and hypolimnion are shown in Figure 3.7 and Figure 3.8 for Sihlsee and Upper Lake Zurich, respectively. While in the epilimnion concentrations are either overestimated (sum of nitrate and nitrite) or underestimated (total phosphorus), the average in the hypolimnion is reproduced satisfactorily. The model is, however, not capable of reproduction peak concentrations, which typically occur during floods. A list of model parameters with a description, and their corresponding default and calibrated values are given in Table 3.4.

Table 3.3 Mean absolute error (MAE) and mean error (ME) of temperature, dissolved oxygen, the sum of nitrate and nitrite as well as total phosphorus computed for the entire water column, the epilimnion and the hypolimnion of Sihlsee or Upper Lake Zurich (na: not available).

Variable	Unit	Sihlsee 2014-2015			Upper Lake Zurich 1998-2015		
		Entire water column	Epi- limnion ¹	Hypo- limnion ²	Entire water column	Epi- limnion ¹	Hypo- limnion
Mean absolute error (MAE)							
Temperature	[°C]	0.71	0.69	0.75	0.63	0.54	0.65
Dissolved oxygen	[mg L ⁻¹]	0.90	0.82	1.05	0.98	0.83	0.93
Inorg. suspended solids	[mg L ⁻¹]	2.78	1.13	4.34	na	na	na
Sum of nitrate and nitrite	[µg N L ⁻¹]	61	58	69	91	114	91
Total phosphorus	[µg P L ⁻¹]	2.86	2.03	4.14	2.95	2.96	2.88
Mean error (ME)							
Temperature	[°C]	0.41	0.58	0.28	-0.11	0.02	-0.23
Dissolved oxygen	[mg L ⁻¹]	0.36	-0.10	0.94	0.49	0.00	0.35
Inorg. suspended solids	[mg L ⁻¹]	1.55	0.56	1.90	na	na	na
Sum of nitrate and nitrite	[µg N L ⁻¹]	21	14	18	16	70	26
Total phosphorus	[µg P L ⁻¹]	-1.20	-0.76	-2.64	-1.75	-2.03	-1.76

¹ Uppermost 5 m of the water column. ² Lowermost 5 m of the water column. ³ All depths ≥20 m.

Table 3.4 Model parameters deviating from the default values of CE-QUAL-W2. Given are the values for both water bodies and the default value of CE-QUAL-W2. The column on the right indicates whether the parameters were selected from literature (in capital letters) or computed by calibration (cal). The capital letters stand for: A: Bonalumi et al. (2012), B: Mieleitner and Reichert (2006), C: Mieleitner and Reichert (2008).

		Sihlsee	Upper Lake Zurich	Default	Based on
Inorganic suspended solids					
SSS	Settling velocity [m d ⁻¹]	0.2	0.2	1	A
SEDRC	Sediment resuspension	ON	ON	OFF	
TAUCR	Critical shear stress for sediment resuspension	0.001	0.001	1	
Gas exchange					
EQN#	Equation used to calculate gas exchange	5	5	6	A
Parameters nitrification and denitrification					
NH4T1	Lower temperature for ammonia decay [°C]	0	0	5	cal
NO3T1	Lower temperature for nitrate decay [°C]	0	0	5	cal
ORGP	Organic matter stoichiometric coefficient for phosphorus [-]	0.0087	0.0087	0.005	B
ORGN	Organic matter stoichiometric coefficient for nitrogen [-]	0.08	0.08	0.08	cal
Parameters organic matter					
OMT1	Lower temperature for organic matter decay [°C]	0	0	4	cal
OMT2	Upper temperature for organic matter decay [°C]	30	30	25	
Parameters sediment					
NH4R	Sediment release rate of ammonium, fraction of SOD-rate	0.02	0.02	0.001	cal
SEDC	Detailed sediment- diagenesis-model	ON	ON	OFF	
SEDCI	Initial sediment concentration [g m ⁻²]	0.01	0.01	0	
SOD	Anaerobic sediment release rate [g m ⁻² d ⁻¹]	0.4	1		
DYNSEDK	Dynamic computation first-order-model	ON	ON	OFF	
SODT1	Lower temperature for sediment decay [°C]	0	0	4	
Mixing parameters					
FRIC	Chézy friction coefficient [m ^{0.5} s ⁻¹]	70	70		A
AX	Longitudinal Eddy-Viscosity [m ² s ⁻¹]	0.1	0.1	1	
DX	Longitudinal Eddy-Diffusivity [m ² s ⁻¹]	0.1	0.1	1	
AZMAX	Maximum vertical Eddy-Viscosity [m ² s ⁻¹]	0.1	0.1	1	
FI	Internal friction [-]	0.01	0.01	0.015	
Scaling of meteorological forcing					
SHD	Shading coefficient [-]	0.85	0.90	1	cal
WSC	Wind sheltering coefficient [-]	1.35	1.25	1	
Scaling of water quality forcing of inflows					
fiss	Multiplier inorganic suspended solids [-]	0.25	1.00 0.25 ¹		cal
fPO4	Multiplier phosphate [-]	4.58	1.00 32.5 ¹		
fNH4	Multiplier ammonium [-]	0.17 ²	0.65 0.72 ¹		
fNO	Multiplier nitrate + nitrite [-]	1.42	1.10 4.86 ¹		
Heat exchange at air water interface					
AFW	Coefficient wind function [W m ⁻² mm Hg ⁻¹]	5.87	5.87	9.2	A
BFW	Coefficient wind function [W m ⁻² mm Hg ⁻¹ (m s ⁻¹)-CFW]	2.42	2.42	0.46	
CFW	Coefficient wind function	1	1	2	
Heat exchange at sediment water interface					
TSED	Temperature sediment [°C]	5	7	10	cal
CBHE	Coefficient heat exchange [W m ⁻² °C ⁻¹]	1.0×10 ⁻⁶	1.0×10 ⁻⁶	0.3	A
Light attenuation water column					
EXH2O	Attenuation pure water [m ⁻¹]	0.2	0.2	0.25	cal
BETA	Fraction incident solar radiation absorbed at water surface [-]	0.35	0.35	0.45	

¹ The two multipliers for inflow water quality at Upper Lake Zurich were used for River Linth and the other two inflows (Jona and Wägitaler Aa), respectively.

² As ammonium was not observed, the difference of total nitrogen and nitrate and nitrite was taken as proxy and adapted with the given factor.

Continuation Table 3.4.

		Sihlsee / Upper Lake Zurich			
		Group 1	Group 2	Default	Based on
Parameters phytoplankton					
AG	Max. growth rate phytoplankton [d ⁻¹]	1.9	1.4	2	cal/C
AR	Max. respiration rate phytoplankton [d ⁻¹]	0.05	0.05	0.04	B
AE	Max. excretion rate phytoplankton [d ⁻¹]	0.015	0.015	0.04	cal
AM	Max. mortality rate phytoplankton [d ⁻¹]	0.015	0.015	0.1	cal
AS	Algal settling rate [m d ⁻¹]	0.08	0.01	0.1	C
ALGP	Algal stoichiometric coefficient for phosphorus [-]	0.0087	0.0087	0.005	B
ALGN	Algal stoichiometric coefficient for nitrogen [-]	0.08	0.08	0.08	cal
ALPOM	Fraction of algal biomass converted to POM when dying	0.9	0.9	0.8	B
AHSP	Algal half-saturation for phosphor [g m ⁻³]	0.0007	0.0013	0.003	C
AT1	Lower temperature for algal growth [°C]	0	0	5	cal
AT2	Lower temperature for max. algal growth [°C]	11	11	25	
AT3	Upper temperature for max. algal growth [°C]	15	15	35	
AT4	Upper temperature for algal growth [°C]	30	30	40	
ACHLA	Ratio algal biomass to chlorophyll a [mg Algae (µg Chl a) ⁻¹]	0.1	0.1	0.05	
Parameters zooplankton					
ZG	Max. growth rate zooplankton [d ⁻¹]	0.7		1.5	cal
ZP	Zooplankton stoichiometric coefficient for phosphorus [-]	0.0087		0.005	B
ZN	Zooplankton stoichiometric coefficient for nitrogen [-]	0.08		0.08	cal
PREFA1	Relative preference factor of zooplankton for algae 1 [-]	1		0.5	cal
PREFA2	Relative preference factor of zooplankton for algae 2 [-]	1		0.5	
ZT1	Lower temperature for zooplankton growth [°C]	0		5	
ZT2	Lower temperature for max. zooplankton growth [°C]	20		25	
ZT3	Upper temperature for max. zooplankton growth [°C]	30		35	
ZT4	Upper temperature for zooplankton growth [°C]	35		40	

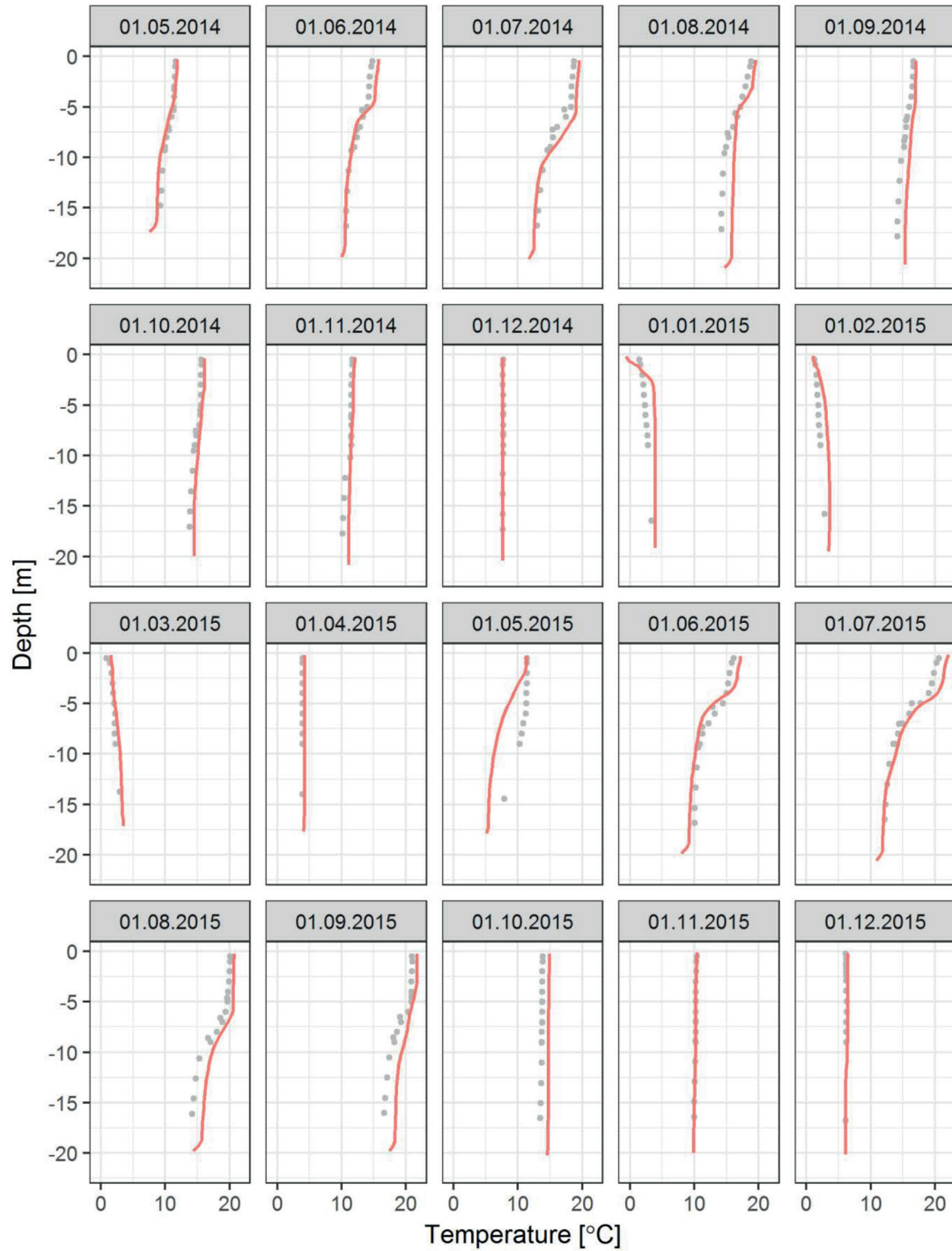


Figure 3.4 Simulated (red) and observed (grey) temperatures (°C) at Sihlsee.

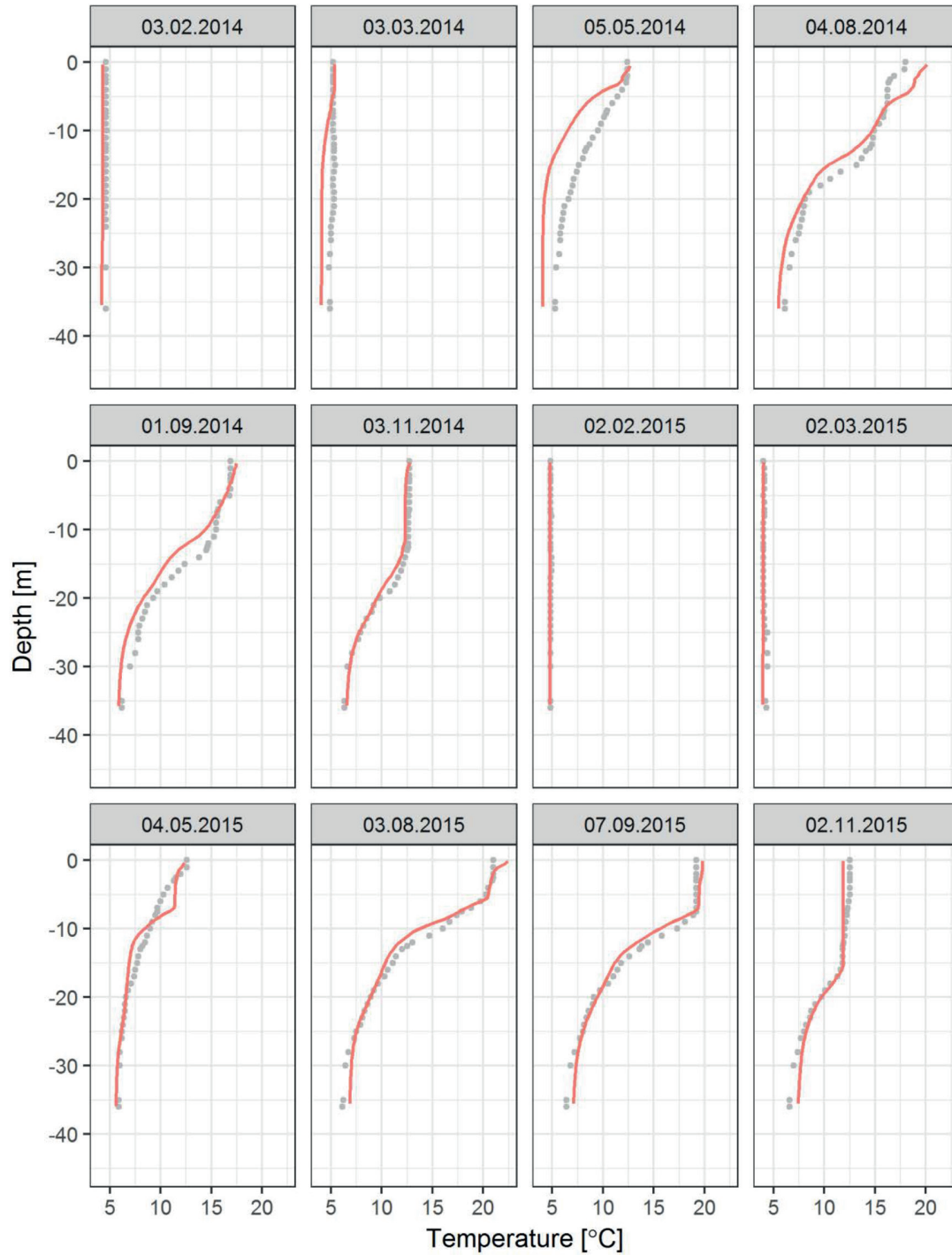


Figure 3.5. Simulated (red) and observed (grey) temperatures (°C) at Upper Lake Zurich.

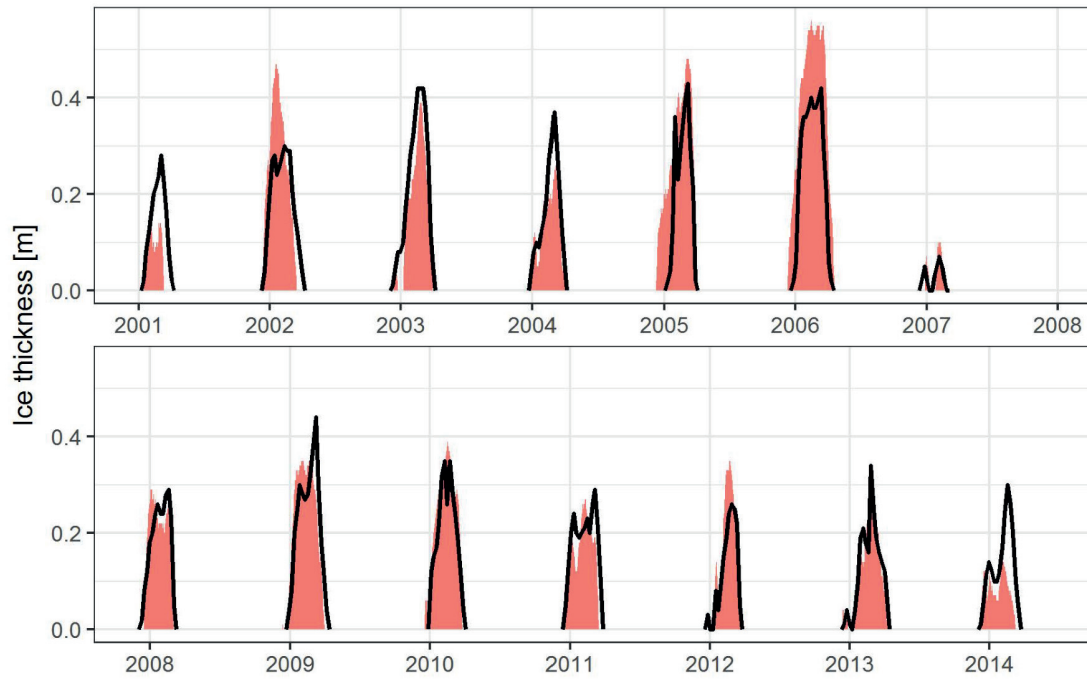


Figure 3.6. Simulated (red) and observed (black) ice thickness (m) at Sihlsee from 2001-2014.

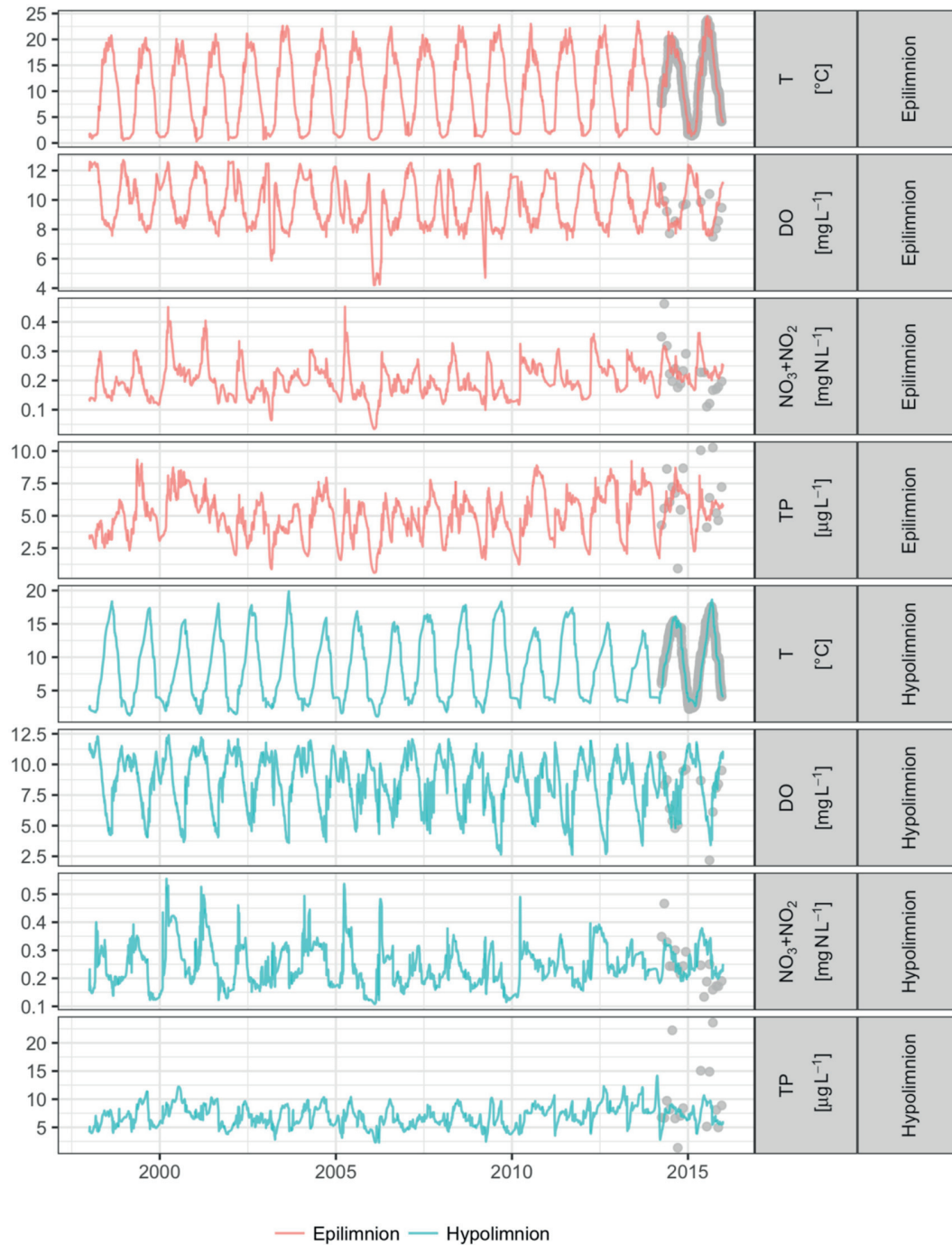


Figure 3.7 Time series of simulated (lines) and observed (grey points) variables at Sihlsee; depicted are temperature (T) in °C, dissolved oxygen (DO) in mg L⁻¹, sum of nitrate and nitrite (NO₃+NO₂) in µg N L⁻¹ and total phosphorus (TP) in µg P L⁻¹ all aggregated volumetrically for either epi- (uppermost 5 m of the water column) or hypolimnion (lowermost 5 m of the water column).

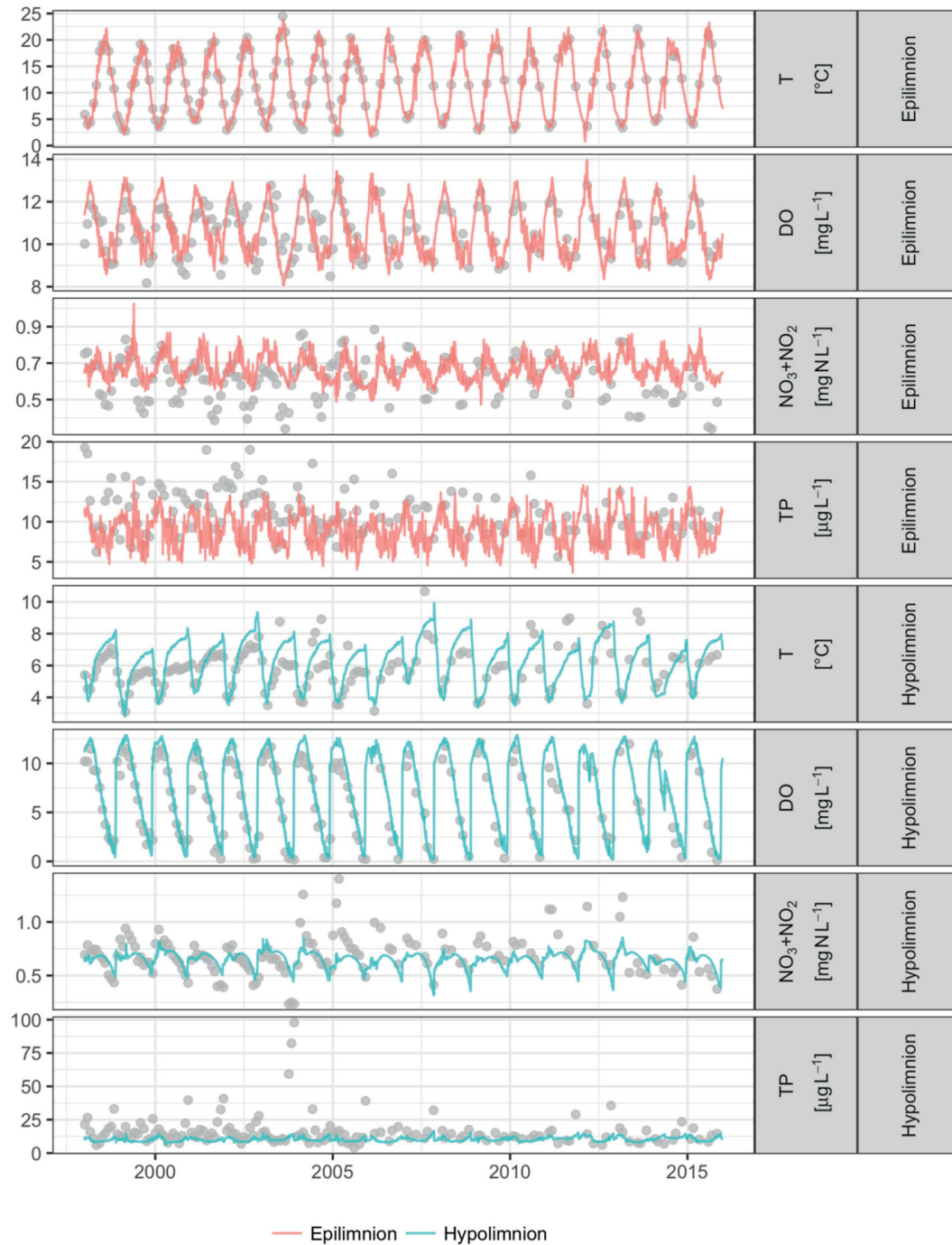


Figure 3.8 Time series of simulated (lines) and observed (grey points) variables at Upper Lake Zurich; depicted are temperature (T) in °C, dissolved oxygen (DO) in mg L⁻¹, sum of nitrate and nitrite (NO₃+NO₂) in µg N L⁻¹ and total phosphorus (TP) in µg P L⁻¹ all aggregated volumetrically for either epi- (uppermost 5 m of the water column) or hypolimnion (all depths ≥20 m).

3.4 Results at Upper Lake Zurich

Figure 3.9 shows the mean and extrema of all considered PS scenarios for Upper Lake Zurich, and Figure 3.10 shows a boxplot of seasonal differences between either the reference scenario or the extended PS scenario and the present PS scenario. Both figures are separated for epi- and hypolimnion and individually show results for temperature, dissolved oxygen and nutrients.

Effects on temperature in Upper Lake Zurich are minor, with largest deviations in winter (December-February) due to warmer hypolimnetic water from Sihlsee being released at the surface of Upper Lake Zurich. However, the warming of the entire water column in winter remains at $<0.2\text{ }^{\circ}\text{C}$ and $<0.5\text{ }^{\circ}\text{C}$ for present PS and extended PS, respectively (Figure 3.9, Figure 3.10), since the PS generating flow only accounts to $\sim 10\%$ and of natural inflows.

Schmidt stability, which is shown in Figure 3.11 B, is hardly affected due to different PS operations, while the duration of summer stratification lasts ~ 1 week longer without PS operation, (information is taken from Figure 3.11 A, which shows boxplots of start and end of summer stratification). As a consequence, the dissolved oxygen concentrations in autumn are reduced and the nutrient concentrations are increased without PS operation (Figure 3.9, Figure 3.10). The periods with dissolved oxygen concentrations $<4\text{ mg L}^{-1}$ span on average ~ 101 , ~ 100 and ~ 95 days, for the reference, present PS and extended PS scenarios, respectively. Additionally, the nutrient concentrations of the scenarios with PS are modified by the input of water with different concentrations from the hypolimnion of Sihlsee. Thus, phosphate concentrations are reduced by ~ 1 and $\sim 2\text{ }\mu\text{g P L}^{-1}$ from November to February for present and extended PS, respectively. The sum of nitrate and nitrite concentrations decrease during the entire year by $\sim 15\text{--}50\text{ }\mu\text{g N L}^{-1}$ for both present and extended PS compared to the reference scenario. Between the present and the extended PS scenario the differences remain $<15\text{ }\mu\text{g N L}^{-1}$.

In summary, however, all projected impacts on temperature, stratification, oxygen and nutrient concentrations in Upper Lake Zurich for both the present and the extended PS scenarios do not exceed the interannual variation of these parameters that occur due to variations in meteorology and streamflow. Yet, in the vicinity of the intake/outlet of the PS hydropower plant we cannot exclude the possibility of more relevant effects due to PS operation (Müller et al. 2016).

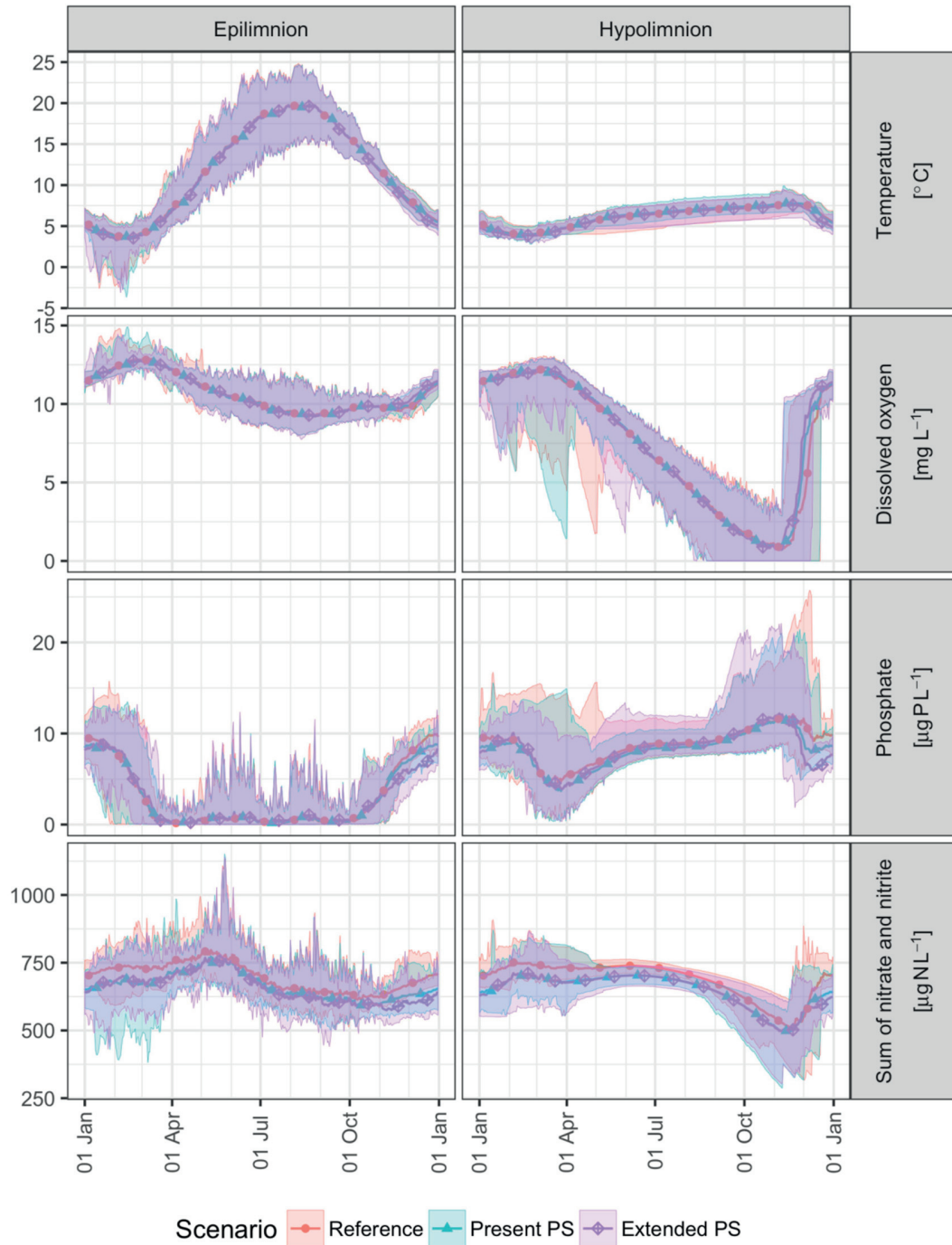


Figure 3.9 Mean (lines with markers) and range of minima and maxima (shaded areas) of simulated temperature (°C) and concentrations of dissolved oxygen (mg L⁻¹), phosphate (µg P L⁻¹) and the sum of nitrate and nitrite (µg N L⁻¹) for the reference (red), the present PS (green) and the extended PS (blue) scenario at Upper Lake Zurich.

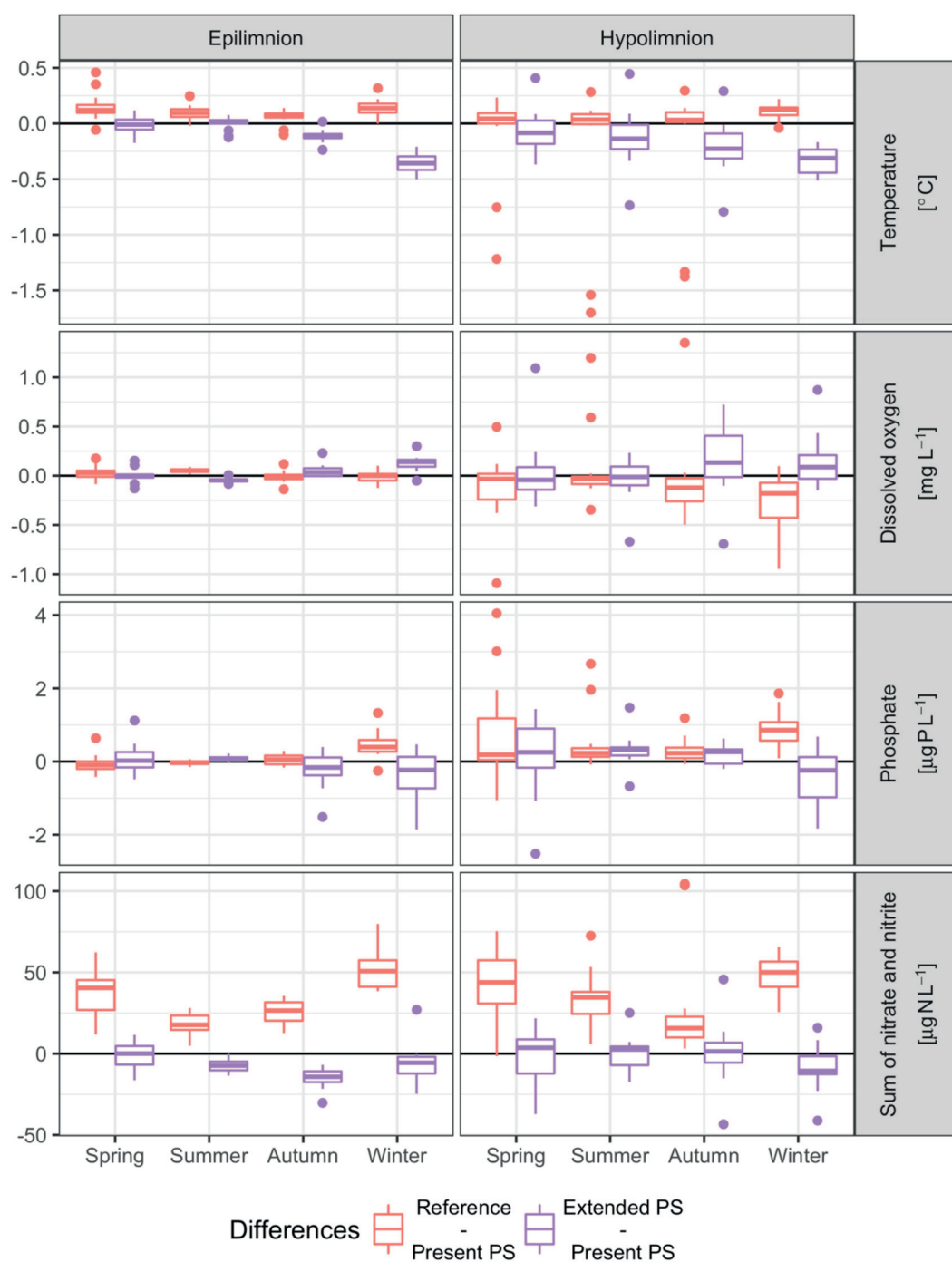


Figure 3.10 Boxplots of differences in either the reference scenarios or the extended PS scenario to the present PS scenario of temperature ($^{\circ}\text{C}$) and concentrations of dissolved oxygen (mg L^{-1}), phosphate ($\mu\text{g P L}^{-1}$) and the sum of nitrate and nitrite ($\mu\text{g N L}^{-1}$) at Upper Lake Zurich. Points show outliers; values were aggregated seasonally for each year before plotting (winter: December-February, spring: March-May, summer: June-August, autumn: September-November).

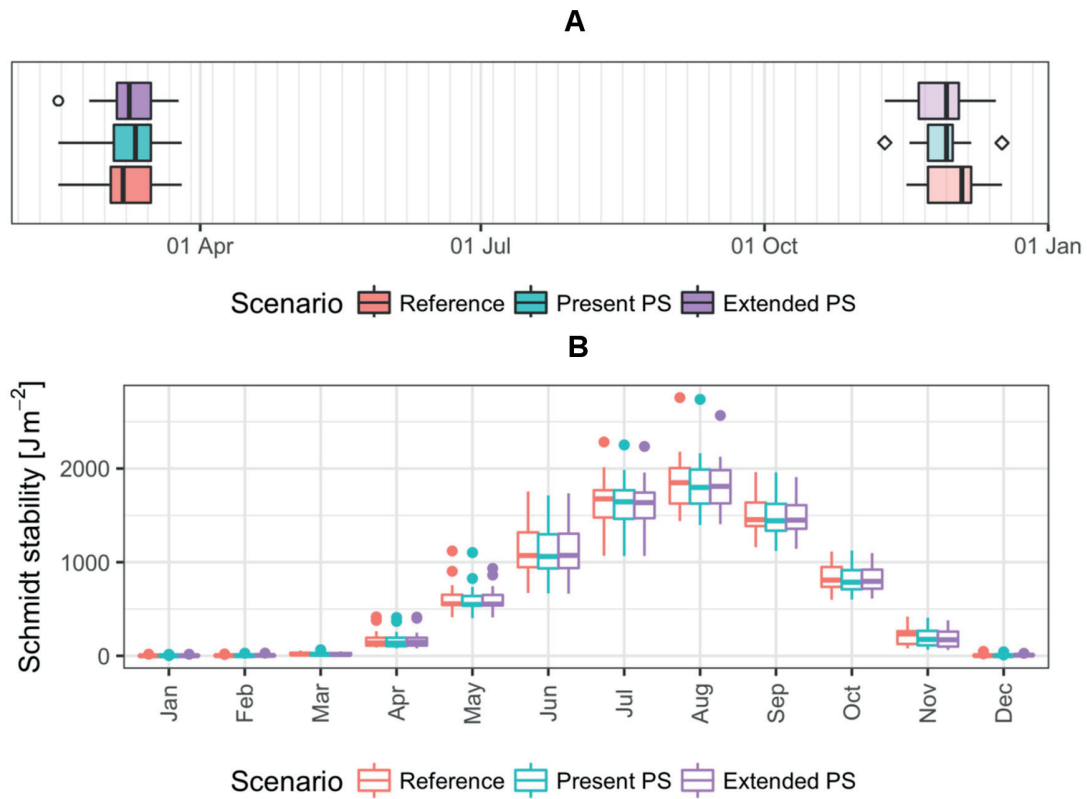


Figure 3.11 Boxplots for the reference scenario, the present PS and the extended PS scenario at Upper Lake Zurich: (A) Start and end of summer stratification; (B) Schmidt stability (J m^{-2}), aggregated to monthly mean for each year before plotting. Points show outliers of start (circles) and end (squares) of summer stratification.

3.5 Specifications of pumped-storage hydropower plants in literature review

Table 3.5 Specifications of pumped-storage hydropower plants and the connected water bodies (WB) studied in a similar context.

Publication	Head [m]	Volume		Surface area		Max. depth		Max. PS generation g flow [m ³ s ⁻¹]	Max. PS pumpin g flow [m ³ s ⁻¹]	Intake/outlet t location	
		upper WB [10 ⁶ m ³]	lower WB [10 ⁶ m ³]	upper WB [km ²]	lower WB [km ²]	upper WB [m]	lower WB [m]			upper WB	lower WB
Bonalumi et al. (2012)	~1270	~22	~111	1.43	1.95	26	85	~95	~74	Lower hypolimnion	Upper hypolimnion
Potter et al. (1982)	~27	~580 ¹	~407 ¹	~85 ¹	~62 ¹	~33 ¹	~7 ¹	~1347 ²	~991 ²	Upper hypolimnion	Upper hypolimnion
USBR (1993)	~145	~14	112.6	~1.2 ³	73	~20 ³	~27	~112	~97	Lower hypolimnion	Lower hypolimnion
Bermúdez et al. (2017)	~283	87 ⁴	72 ⁴	~7.0	~6.3	~30	~20	~150	~124	Lower hypolimnion	Upper hypolimnion
Anderson (2010)	~500	7	74	0.31	13.4	~49	~9	~40	~75	Upper hypolimnion	Upper hypolimnion

¹ https://epd.georgia.gov/sites/epd.georgia.gov/files/related_files/site_page/oc5.pdf, 28 February 2018

² Estimated with an efficiency of 0.9 and 0.8 for generating and pumping, respectively, from the installed capacities given at <http://www.energystorageexchange.org/projects/239>, 28 February 2018

³ <https://www.usbr.gov/tsc/techreferences/rec/REC-ERC-82-06.pdf>, 28 February 2018

⁴ Given is only the storage capacity

Chapter 4

Combined effects of pumped-storage operation and climate change on thermal structure and water quality⁶

4.1 Overview

In Chapter 2, PS operations were shown to cause relevant ecological effects on the connected water bodies when considering present climatic conditions. Additionally, significant modifications must be expected due to climate change as has been highlighted in Chapter 1. Consequently PS operations, which are characterised by their long concession periods, need to be analysed in combination with projected climate change. Up to now, this combination was not studied. Therefore, this chapter investigates these combined effects on water temperature and quality, as well as extent and duration of stratification and ice cover, using a site in Switzerland. For this purpose, a coupled two-dimensional hydrodynamic and water quality model for the two connected water bodies is run with 10×15-years long synthetic stochastic meteorological forcing for both current and future climate conditions under two PS and two reference scenarios. The synthetic time series are generated with the weather generator VG, and future conditions are based on the A2 emission scenario⁷ for north-eastern Switzerland towards the end of the 21st century. The results show relevant synergistic and antagonistic effects of PS operations and climate change. For example, hypolimnion temperatures in September are projected to increase by < 0.6 °C in a near-natural reference scenario and by ~2.5 °C in an extended PS scenario. Ice cover, which occurs every year under near-natural conditions in the current climate, would almost completely vanish with extended PS operation in the future climate. Conversely, the expected negative impacts of climate change on hypolimnetic dissolved oxygen concentrations are partially counteracted by extended PS operations. Therefore, the consideration of future climate conditions for the environmental impact assessment in the planning of new or the recommissioning of existing PS hydropower plants must be recommended.

⁶ This chapter is based on the scientific article “Combined effects of pumped-storage operation and climate change on thermal structure and water quality” by U. G. Kobler, A. Wüest and M. Schmid accepted for publication in *Climatic Change*. The fieldwork, simulations and the analysis presented hereafter are original and were performed by the author of the thesis.

⁷ The A2 emission scenario considers that no mitigation measures are taken into account.

4.2 Introduction

Expansion of new renewable electricity sources is an important cornerstone of strategies to mitigate anthropogenic climate change (e.g., EU 2009; Ibrahim et al. 2011). However, their intermittent nature calls for additional electricity storage, which is, still today, most efficiently realized by pumped-storage (PS) hydropower plants. Yet, these PS operations affect abiotic and biotic characteristics of the two connected water bodies (Bonalumi et al. 2011). For example, for the case of Sihlsee, PS operations have been shown to increase hypolimnetic temperature and dissolved oxygen (DO) concentrations mostly due to pumping surface water from the lower lake to the hypolimnion of the upper reservoir, and the weakened reservoir stratification (Kobler et al. 2018). Moreover, Kobler et al. (2018) estimated that ice thickness would decrease due to extended PS operation.

Climate change also alters water bodies, e.g., by raising water temperature (O'Reilly et al. 2015), prolonging summer stratification (Dokulil et al. 2010; Livingstone 2003), which further results in increased oxygen depletion and, therefore, in increased mineralization and nutrient release from sediments (Delpla et al. 2009; Xia et al. 2014). Increased temperature and prolonged summer stratification further result in shortened ice cover duration (Benson et al. 2012; Magee et al. 2016) and inverse stratification, which refers to periods with cooler water (0 to -4°C) in the epilimnion on top of warmer hypolimnetic water (-4°C). Shorter inverse stratification in turn leads to increased DO concentrations in winter and less accumulation of nutrients released from sediments in the hypolimnion. These abiotic impacts further affect lake ecology, e.g., through decreasing habitats for fish with low temperature preferences, such as trout (North et al. 2014).

Bonalumi et al. (2012) showed that PS effects on lake temperature are more pronounced in warmer years, as PS operation increased the efficiency of heat exchange with the atmosphere, further suggesting that climate change would likely aggravate PS impacts. Yet, the link between climate change and PS operation has so far not been quantified. Thus, with the present study we aim at investigating whether climate change will amplify or reduce the different impacts of PS operations on the thermal structure, ice cover and water quality of the two connected water bodies. As a study site we use Etzelwerk, where the impacts of different PS scenarios for the current climate have already been investigated in a previous study (Kobler et al. 2018). Here, we link the model applied in this previous study with climate scenarios generated with a vector-autoregressive weather generator to assess the combined effect of climate change and PS operations. The weather generator had been successfully tested at Lake Constance, where the synthetic meteorological forcing reproduced statistical dependencies of measured meteorological data, and was used to drive a lake model which could successfully emulate observed thermal and water quality dynamics (Schlabing et al. 2014).

We analyse (a) two different climate scenarios representing current and future conditions in combination with (b) four different management options. The latter include two different levels of PS operations, the present and an extended PS, and two reference cases, the quasi-natural case with surface outflow and a case with deep-water withdrawal. These PS and reference scenarios

depict a typical set considered in the environmental impact assessment for the recommissioning of a PS hydropower plant. Based on the simulation results, we discuss the relevance of including expected climate change effects in environmental impact assessments when planning or recommissioning PS hydropower plants. Concessions are usually issued for many decades within which significant climate change must be expected. These results could, therefore, further reveal ecologically relevant synergistic and antagonistic effects of climate change and PS operations.

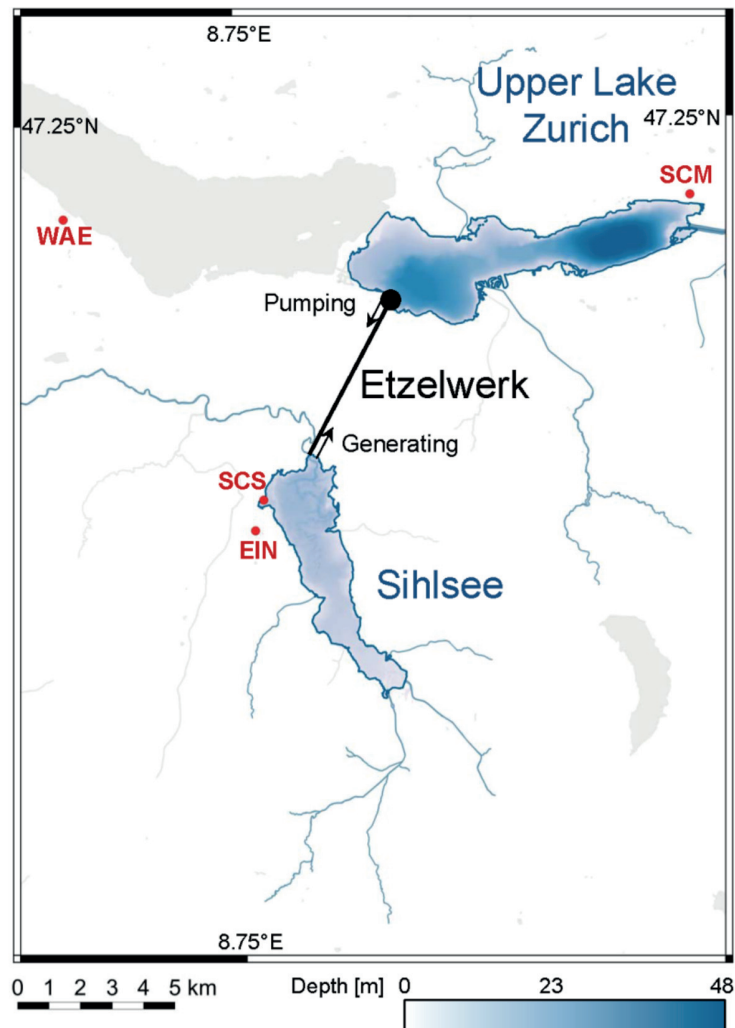


Figure 4.1 Overview of study site with meteorological observations taken from stations indicated in red: SCS meteorological stations Segelclub Sihlsee, all others are stations operated by MeteoSwiss: EIN (Einsiedeln), SCM (Schmerikon), and WAE (Wädenswil). The MeteoSwiss station SMA (Zurich Fluntern) is located outside the map at 8.56573°E, 47.37789°N.

4.3 Study sites

The considered PS hydropower plant is Etzelwerk (Figure 4.1), which is located in Switzerland. It connects Sihlsee, the upper artificial reservoir, with Upper Lake Zurich, the lower natural lake. Sihlsee is a dimictic reservoir, which is regularly inversely stratified and ice-covered in winter, whereas Upper Lake Zurich is mostly monomictic. In summer epilimnion temperatures at Sihlsee reach maxima of $\sim 25^{\circ}\text{C}$, those of the hypolimnion remain $< 17^{\circ}\text{C}$. At Upper Lake Zurich maximum epilimnion temperatures are similar to those observed at Sihlsee, whereas hypolimnion temperatures stay $\leq 6^{\circ}\text{C}$ (Kobler et al. 2018). In both lakes DO depletion throughout the stratified summer period, causes hypolimnetic DO to drop to $< 4\text{ mg L}^{-1}$. Total phosphorus concentrations remain $< 35\text{ }\mu\text{g P L}^{-1}$ at Sihlsee, and the annual mean at Upper Lake Zurich does not exceed $12\text{ }\mu\text{g P L}^{-1}$. Currently water is withdrawn from Sihlsee's hypolimnion by PS generation and discharged to the epilimnion of Upper Lake Zurich. For PS pumping water from the epilimnion of Upper Lake Zurich is brought to the hypolimnion of Sihlsee. Both basins are described in more detail in Kobler et al. (2018), and their characteristics are summarized in Table 4.1.

Table 4.1 Characteristics of Sihlsee (upper reservoir) and Upper Lake Zurich (lower lake) including their mean annual water balance (1997-2015) for the considered PS scenarios: "quasi-natural" reference (QNat), reference without PS (NoPS), present PS and extended PS scenarios.

		Sihlsee			Upper Lake Zurich		
Max. depth	[m]	23			48		
Max. surface area	[km ²]	11.3			20.25		
Max. volume	[10 ⁶ m ³]	96.1			470		
Storage capacity	[10 ⁶ m ³]	89.4			-		
Catchment area	[km ²]	156.5			1,564		
Mixing category	[-]	dimictic			monomictic		
		Reference scenarios	Present PS	Extended PS	Reference scenarios	Present PS	Extended PS
PS generating power	[MW]	0	~ 135	~ 525	0	~ 135	~ 525
PS pumping power	[MW]	0	~ 65	~ 265	0	~ 65	~ 265
Residence time	[days]	~ 150	~ 135	~ 40	~ 70	~ 70	~ 70
Sum of inflows	[10 ⁶ m ³ yr ⁻¹]	235	235	235	2410	2410	2410
Sum of outflows	[10 ⁶ m ³ yr ⁻¹]	-220	-32	-32	-2410	-2598	-2598
Correction term	[10 ⁶ m ³ yr ⁻¹]	-15	-15	-15	0	0	0
PS generating flow	[10 ⁶ m ³ yr ⁻¹]	0	-214	-778	0	214	778
PS pumping flow	[10 ⁶ m ³ yr ⁻¹]	0	26	590	0	-26	-590

4.4 Materials and methods

4.4.1 Hydrodynamic and water quality model

We applied a modified version of the two-dimensional laterally-averaged hydrodynamic and water quality model CE-QUAL-W2 which was developed by the Portland State University in cooperation with the US Corps of Engineers (Cole and Wells 2013). The model was already applied to the study site for simulating the effects of different management scenarios under current climatic conditions in a previous study (Kobler et al., 2018), which includes a detailed description of the model, the calibration procedure, and the data sources for the bathymetric, meteorological, hydrological and water quality forcing needed to drive the model. The model grid and a conceptual diagram of the main processes considered are available in Section 5.2.

In short, the model is composed of a hydrodynamic module where temperature, stratification and mixing processes are calculated using a k-epsilon model, and a water quality module that includes the inputs, outputs and transformations of inorganic suspended solids, dissolved oxygen, organic matter, nitrogen and phosphorus. In the present version, the water quality model includes two algae and one zooplankton group as well as a sediment compartment. The code of the publicly available version 3.71 of CE-QUAL-W2 was modified to enable direct input of incoming long-wave radiation with the meteorological forcing file, and to improve the performance of the ice module to reproduce observed ice cover thickness and duration (Kobler et al. 2018).

The meteorological and the hydrological forcing were obtained from several monitoring stations close to the study site (Kobler et al. 2018). The numerical grids of both water bodies were divided into segments of 200 m width (longitudinal direction) and layers of 0.5 m height (vertical direction). The model had been calibrated manually based on long-term monitoring data from Upper Lake Zurich and two years of observational data from Sihlsee collected for this purpose. The corresponding root-mean-square-errors (RMSE) for the entire water column of Sihlsee reached values of 0.94 °C, 1.2 mg L⁻¹ and 4.5 µg P L⁻¹ for temperature, DO and total phosphorus, respectively. At Upper Lake Zurich the RMSE amounted to 0.93 °C, 1.3 mg L⁻¹ and 4.1 µg P L⁻¹. These values are well within the range typically achieved with CE-QUAL-W2 for similar applications (Kobler et al. 2018).

4.4.2 Climate scenarios

Ten synthetic time series of 15 years duration for the periods 1998-2012 (current climate) and 2078-2092 (future climate) were calculated with the weather generator VG (Schlabing et al. 2014). Generated time series of future climate were not directly compared to the results from Kobler et al. (2018) to avoid systematic errors and to allow for the computation of statistics that are based on a similar sized “population”. Air temperature was increased compared to present day conditions according to regional projections of the Swiss Climate

Change Scenarios CH2011 (2011) for the IPCC A2 scenario in 2085 for north-eastern Switzerland. The projected air temperature increases vary seasonally (for each day of the year) in the range of 3 °C (April) to 4.5 °C (August). All other meteorological forcing variables and inflow water temperatures were computed by VG, maintaining the dependencies of observed values during the period 1997-2015. A detailed comparison of VG-generated and observed variables is given in Section 5.3.

4.4.3 Pumped-storage scenarios

Four different management scenarios were used in the simulations that had been previously developed to simulate the impacts of PS operations (Kobler et al. 2018). The water balance of all scenarios is shown in Table 4.1, and additional information on the position of all in- and outflows is given in Section 5.2.

The present PS scenario describes the current state, where water is withdrawn from the hypolimnion of Sihlsee for both, generating electricity and the residual flow to River Sihl, with installed capacities of ~135 MW for generating and ~65 MW for pumping. Pumping brings water from Upper Lake Zurich to the hypolimnion of Sihlsee. At Upper Lake Zurich, PS intake and outlet are situated in the epilimnion. The seasonal variation of PS operation is minor, with mean monthly flows ranging from 6.1 to 7.8 m³ s⁻¹ for generating and from 0.7 to 1.1 m³ s⁻¹ for pumping, respectively.

The extended PS scenario corresponds to an extension with installed capacities for generating and pumping increased to ~525 MW and ~265 MW, respectively. Compared to the present PS scenario, both PS flows are increased by factors of up to ~4 to 5 (generating) and of ~20 to 40 (pumping) from November to March and by factors of ~1 to 3 (generating) and ~9 to 23 (pumping) during the rest of the year.

The “quasi-natural” reference scenario (QNat) corresponds to the “natural lake state” of the reservoir, if the dam were of natural origin. The discharge to River Sihl is calculated based on a regime analysis of discharges observed before dam construction (LIMNEX AG 2016, personal communication). It is implemented with a discharge over a weir. Thus, water is withdrawn from the epilimnion in contrast to the other scenarios where all water is withdrawn from the hypolimnion. No artificial PS flows are considered for this reference scenario.

When comparing QNat and present as well as extended PS projections, it is difficult to clearly assign the observed effects to either the PS flows or to water withdrawal from the hypolimnion. To disentangle these two processes, a second reference scenario (NoPS) was designed, where water is withdrawn from the hypolimnion through the present residual flow outlet, but no PS operation takes place. The downstream discharge of River Sihl is equal to that in the reference scenario QNat. NoPS is also a possible future management option in case hydropower operations were to be discontinued.

4.4.4 Aggregation of results

The climate ensemble consisting of ten simulations with a total of 150 simulated years included in each studied period (1998-2012 for current climatic conditions, and 2078-2092 for future climatic conditions) were combined to the aggregated results as presented below. Means, minima and maxima of the simulated temperatures and concentrations of DO and phosphate were calculated for each day of the year, separately for the epilimnion (uppermost 5 m of the water column) and the hypolimnion (lowermost 5 m). The differences between the current and the future climate were calculated at each depth for each climate scenario.

The durations of summer and inverse stratification were defined similar to Kobler et al. (2018) as the longest uninterrupted periods with temperature differences $>0.2\text{ }^{\circ}\text{C}$ and $<-0.2\text{ }^{\circ}\text{C}$ between the upper- and the lowermost layer. Schmidt stability was computed according to Idso (1973). Ice-on, ice-off, duration of ice-cover and its maximum thickness were estimated for the longest uninterrupted ice-covered periods for all winters.

For the boxplots, values were aggregated to the mean of each day of the year for both the epilimnion and the hypolimnion, and for each combination of PS and climate scenarios. The results presented hereafter focus on Sihlsee, the upper reservoir of the PS plant. The results for Upper Lake Zurich, the lower lake, are summarized in Section 5.5.

4.5 Results

In the following the impacts of current and future climate conditions are discussed on the basis of projected time series (i) of water quality in the epilimnion (Figure 4.2) and hypolimnion (Figure 4.3) as well as (ii) of differences between current and future climate (Figure 4.4).

Climate change increases the water temperature at Sihlsee throughout the water column for all PS scenarios. Yet, projected temperature changes (ΔT) vary among the different PS scenarios. The earlier onset of summer stratification results in maximum ΔT in the epilimnion in April of $\sim 2.5\text{ }^{\circ}\text{C}$, $\sim 3.0\text{ }^{\circ}\text{C}$ and $\sim 2.9\text{ }^{\circ}\text{C}$ for both reference scenarios QNat and NoPS and the present PS scenario, respectively. The smallest ΔT of $\sim 1.0\text{ }^{\circ}\text{C}$ (reference scenarios QNat) and $\sim 1.3\text{ }^{\circ}\text{C}$ (reference scenario NoPS and present PS scenario) occur in February. The seasonal minima in winter can be explained by the fact that water temperature cannot fall below $0\text{ }^{\circ}\text{C}$. The seasonal minimum is less pronounced in the extended PS scenario, where the ice-covered period with surface temperatures of $0\text{ }^{\circ}\text{C}$ is already significantly shortened for the present climate. For the extended PS scenario the projected ΔT range between ~ 1.4 (January) and $\sim 2.6\text{ }^{\circ}\text{C}$ (August).

In the hypolimnion, ΔT is small in the reference scenario QNat compared to all other scenarios. For QNat, ΔT remains $<0.6\text{ }^{\circ}\text{C}$ except for November and December when it reaches a maximum of $\sim 1.0\text{ }^{\circ}\text{C}$, resulting from prolonged stratification. The reference scenario NoPS as well as the

present and the extended PS scenarios show similar behavior with a minimum hypolimnetic ΔT of $<0.4^{\circ}\text{C}$ in January and a maximum of ~ 2.4 to 2.5°C in September. Summer stratification is prolonged due to climate change (Figure 4.5). Its duration increases by ~ 33 , ~ 27 , ~ 26 and ~ 26 days for the reference scenarios QNat and NoPS and for the present and the extended PS scenarios, respectively. This is primarily due to an earlier onset of stratification in spring. The end of summer stratification is delayed by ~ 12 days from mid to end of November for QNat, and by less than one week for all other scenarios. The summer stratification is also intensified: Schmidt stability increases during the stratified period by $\sim 22\%$, $\sim 12\%$, $\sim 12\%$ and $\sim 11\%$ for the reference scenarios QNat and NoPS and the present and extended PS scenarios, respectively (Table 4.2 and Section 5.4).

Conversely, the duration and intensity of inverse stratification are reduced (Figure 4.5). For the two reference scenarios QNat and NoPS as well as the present PS scenario it is shortened by ~ 2.1 months and for the extended PS scenario by ~ 1.3 months to a remaining duration of a few days. This shortening is caused by a delayed onset and an earlier end of the inverse stratification.

With few exceptions, Sihlsee develops an ice cover with a thickness >5 cm in all 150 simulated winters under present climate conditions for the present PS and both reference scenarios. The frequency of ice coverage exceeding 5 cm thickness is reduced to $\sim 83\%$ (124 of 150 years) for the extended PS scenario (Table 4.2). Climate change is projected to reduce the frequency of an ice cover thicker than 5 cm even to values between $\sim 57\%$ and $\sim 60\%$ for the present PS and the reference scenarios, respectively, and to $\sim 13\%$ (19 of 150 years) for the extended PS. The average duration of the ice-covered period is reduced by $\sim 81\%$ for the extended PS scenario and by $\sim 71\%$ for all other scenarios. In winters with ice cover, the ice thickness is projected to decrease by $\sim 54\%$ for both reference scenarios as well as the present PS scenario, and by $\sim 64\%$ for the extended PS scenario (Section 5.4). In Figure 4.5, for the extended PS scenario the ice-covered period is depicted as lasting longer than the inverse stratification, which can be explained by the definition of the latter since we only considered the longest uninterrupted period of each winter.

The prolongation of summer stratification also causes changes of DO concentrations (Figure 4.5). In the current climate, DO concentrations fall below the 4 mg L^{-1} threshold in almost every simulated summer period of both reference scenarios. PS operations supply oxygen-rich water from Upper Lake Zurich to the hypolimnion of Sihlsee, and therefore, the occurrence of $\text{DO} < 4\text{ mg L}^{-1}$ is reduced to $\sim 92\%$ of the years (138 of 150) for the present PS scenario and to $\sim 31\%$ (47 of 150) for the extended PS scenario (Table 4.2). These frequencies increase to $\sim 99\%$ (149 of 150) and $\sim 69\%$ (103 of 150) for the future climate scenarios due to prolonged stratification. Also, the average duration of the period with DO concentrations $< 4\text{ mg L}^{-1}$ is prolonged by ~ 1 month for QNat, ~ 2 to 3 weeks for NoPS and present PS, and ~ 3 days for the extended PS.

Shortened inverse stratification and ice-covered period result in an increase of both epi- and hypolimnetic DO concentrations for the reference scenarios QNat and NoPS and the present PS scenario, whereas for the extended PS scenario, this effect is minor, as inverse stratification is already strongly reduced for current climate conditions. Throughout the rest of the year

hypolimnetic DO concentrations are reduced by up to 3.3, 1.0, 1.0 and 0.7 mg L⁻¹ for QNat and NoPS, the present and the extended PS scenario, respectively. Additionally, warmer temperature in summer causes reduced solubility and, therefore, epilimnetic DO concentrations decrease by up to 0.6 mg L⁻¹ for all PS scenarios.

Table 4.2 Aggregated differences between current (CC) and future climate conditions (FC) calculated from all 150 years for Sihlsee.

Scenario	Current climate (CC)	Future climate (FC)	$\Delta = \text{FC} - \text{CC}$	$\Delta/\text{CC} [\%]$
Years with hypolimnetic DO concentrations <4 mg L⁻¹ [-]				
Reference QNat	150	150	0	0
Reference NoPS	147	150	3	2
Present PS	138	149	11	8
Extended PS	47	103	56	119
Years with ice cover [-]				
Reference QNat	149	112	-37	-25
Reference NoPS	150	106	-44	-29
Present PS	150	118	-32	-21
Extended PS	130	39	-91	-70
Years with ice thickness >5 cm [-]				
Reference QNat	148	87	-61	-41
Reference NoPS	149	86	-63	-42
Present PS	150	91	-59	-39
Extended PS	124	19	-105	-85
Mean duration ice-covered period [days]				
Reference QNat	84	24	-60	-71
Reference NoPS	87	25	-62	-71
Present PS	89	25	-64	-71
Extended PS	47	9	-38	-81
Mean ice thickness during ice-covered period [cm]				
Reference QNat	19	9	-10	-53
Reference NoPS	20	9	-11	-55
Present PS	20	9	-11	-54
Extended PS	12	4	-8	-64
Mean Schmidt stability during periods of inverse stratification [J m⁻²]				
Reference QNat	14	8	-6	-44
Reference NoPS	17	9	-8	-47
Present PS	14	8	-6	-43
Extended PS	4	2	-2	-45
Mean Schmidt stability during periods of summer stratification [J m⁻²]				
Reference QNat	308	375	67	22
Reference NoPS	195	218	23	12
Present PS	185	208	23	12
Extended PS	93	104	11	11

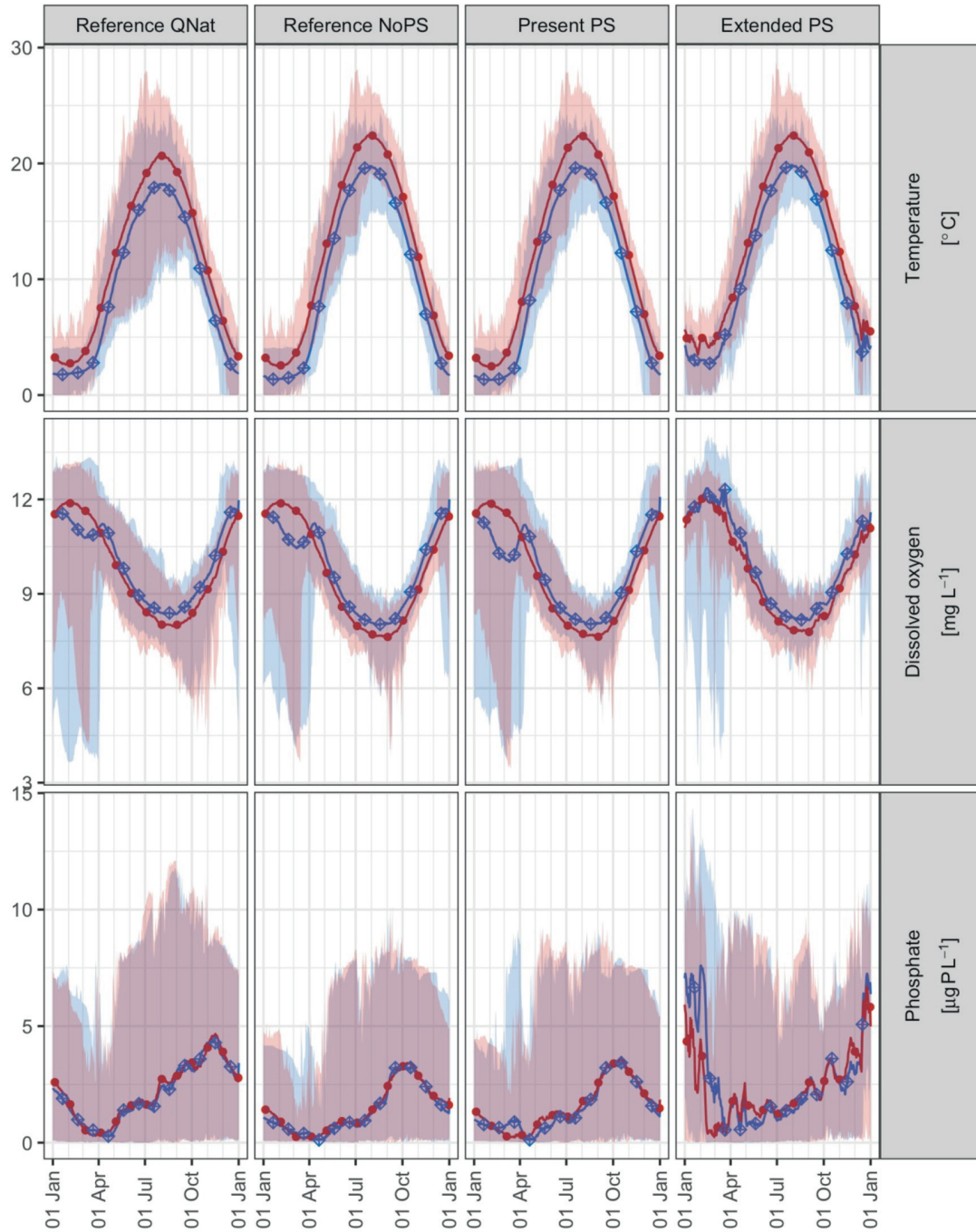


Figure 4.2 Absolute values of temperatures ($^{\circ}\text{C}$), DO (mg L^{-1}) and phosphate ($\mu\text{g P L}^{-1}$) in the epilimnion (from surface to 5 m depth) of Sihlsee for future (red) and current climate scenario (blue). Shown are means (lines and markers) as well as minima and maxima (shaded areas) for each day of the year for each PS scenario.

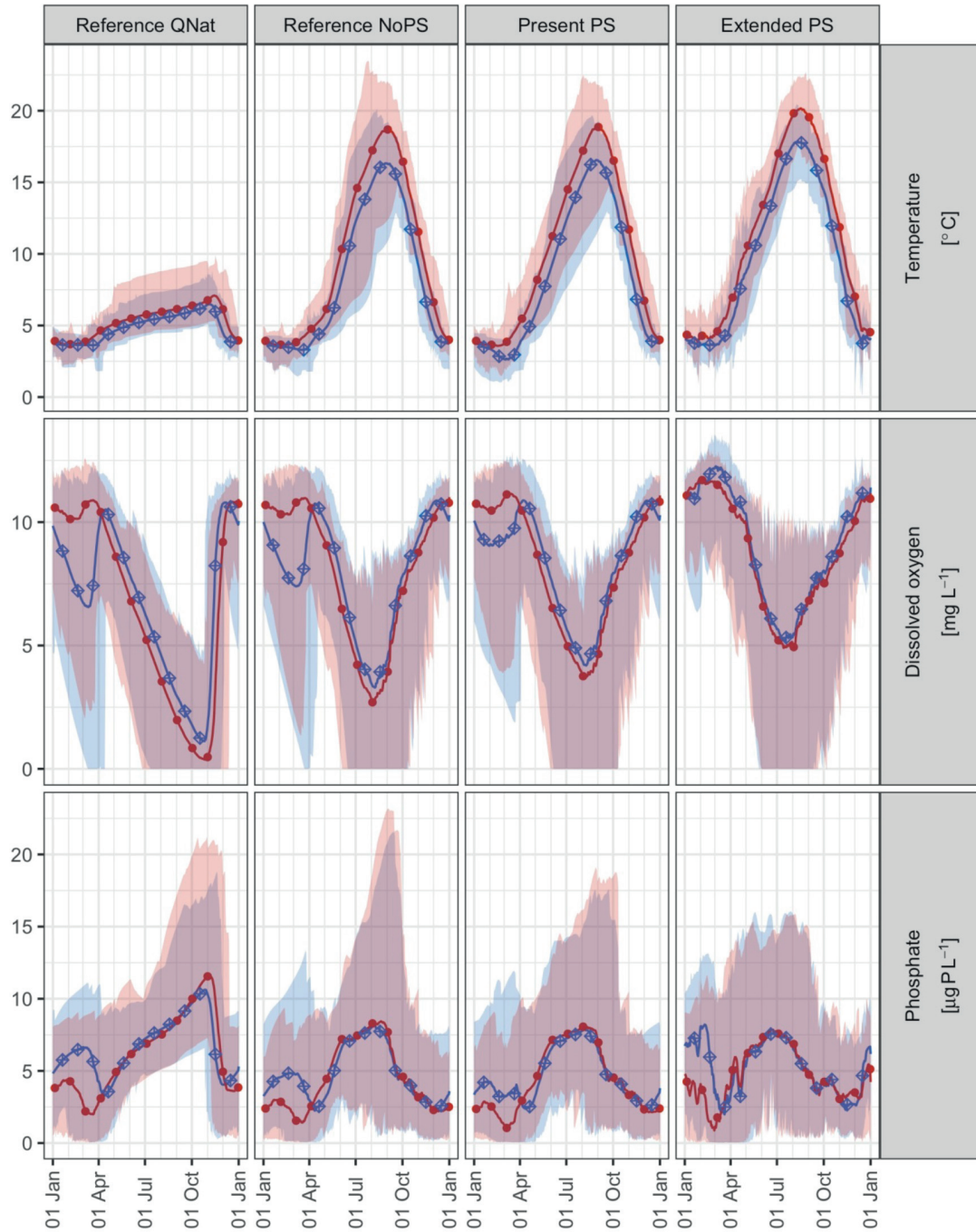


Figure 4.3 Absolute values of temperatures ($^{\circ}\text{C}$), DO (mg L^{-1}) and phosphate ($\mu\text{g P L}^{-1}$) in the hypolimnion (lowest 5 m of the water column) of Sihlsee for future (red) and current climate scenario (blue). Shown are means (lines and markers) as well as minima and maxima (shaded areas) for each day of the year for each PS scenario.

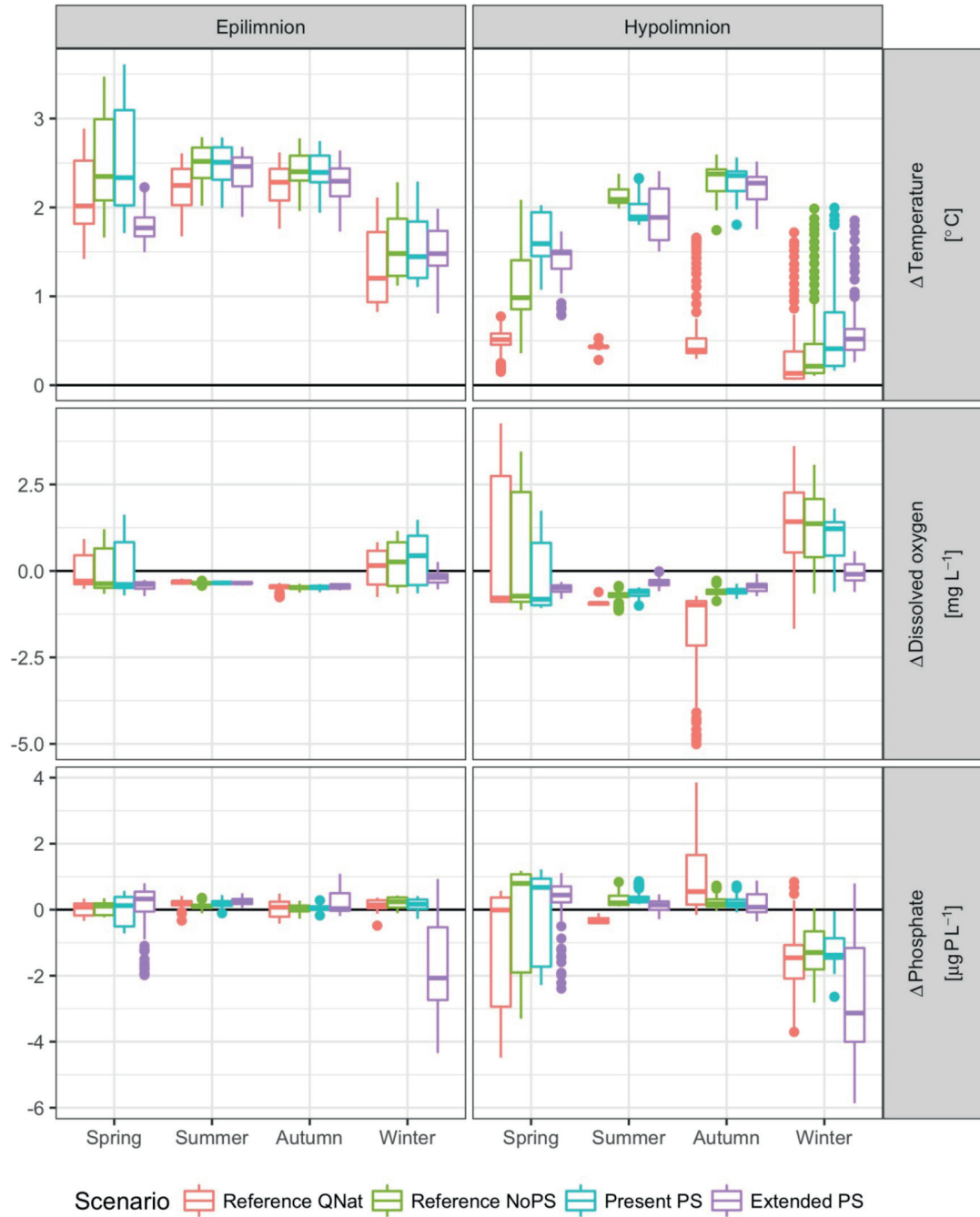


Figure 4.4 Boxplot of differences between future and current values of temperature ($^{\circ}\text{C}$), DO (mg L^{-1}) and phosphate ($\mu\text{g P L}^{-1}$) at Sihlsee for all PS scenarios and for each season (spring: March-May, summer: June-August, autumn: September-November, winter: December-February) for the epi- and the hypolimnion

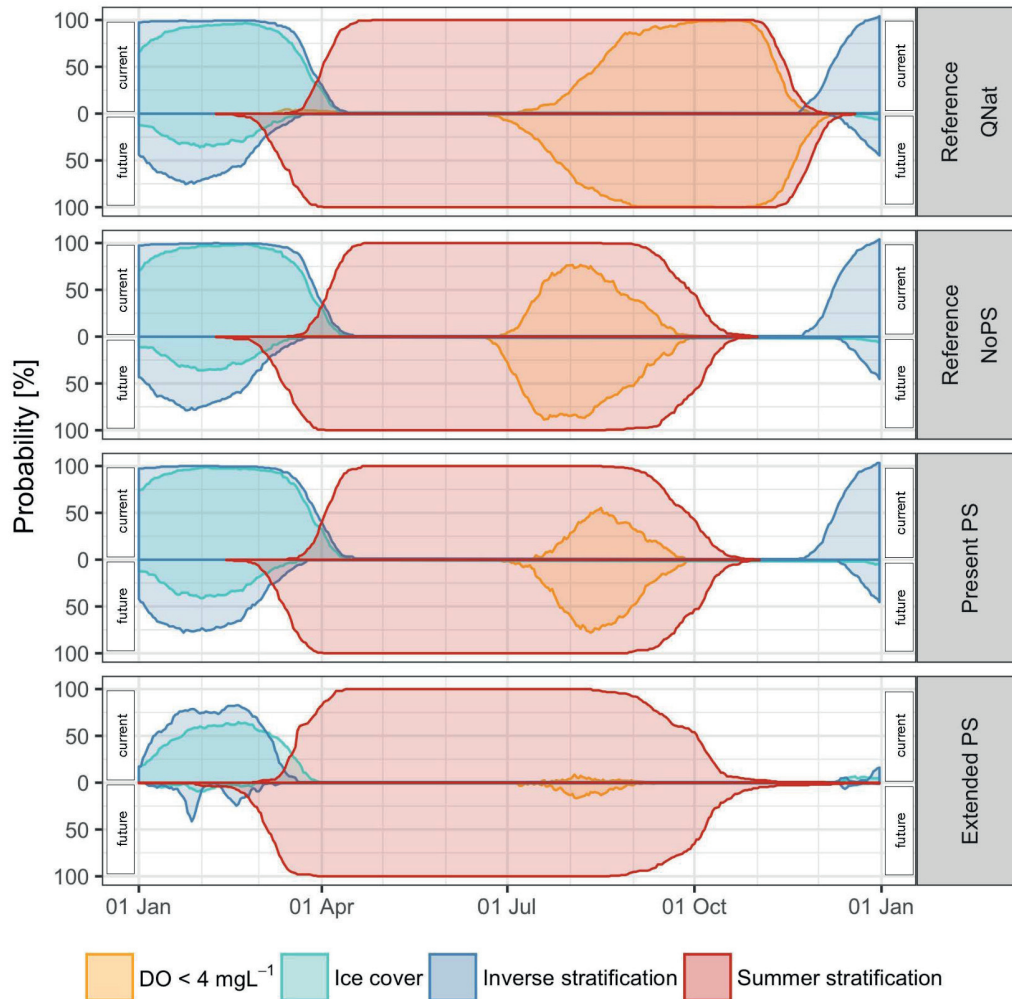


Figure 4.5 Comparison for all four PS scenarios of current (upper half) and future (lower half) probability (%) for each day of the year that the lake is ice-covered (dark blue), inversely stratified (light blue), stratified (red) or that hypolimnion DO concentrations are $<4 \text{ mg L}^{-1}$ (orange) at Sihlsee. For the extended PS scenario, the ice-covered period ends after the inverse stratification, which results from the fact that only the longest uninterrupted period of inverse stratification was considered.

The effects of changing stratification on hypolimnetic phosphate concentrations are approximately inverse to those on DO concentrations, as phosphate is released from the sediments and accumulates in the hypolimnion during stratified periods in summer. The shorter inverse stratification and the corresponding higher probability of open water conditions for future climate lead to increased DO concentrations and, thus, to reduced hypolimnetic phosphate concentrations in winter by up to ~ 3.6 , ~ 2.5 , ~ 1.9 and $\sim 4.5 \text{ } \mu\text{g P L}^{-1}$ for QNat, NoPS, the present and extended PS scenario, respectively. For the extended PS scenario, these concentrations are additionally decreasing in the hypolimnion of Sihlsee due to an earlier onset of primary production in Upper Lake Zurich. The decline of hypolimnetic phosphate concentrations can be propagated to the epilimnion where concentrations decrease by up to $3.0 \text{ } \mu\text{g P L}^{-1}$. While for QNat changing mixing dynamics can increase hypolimnetic phosphate concentrations by up to $\sim 2.6 \text{ } \mu\text{g P L}^{-1}$, concentrations remain unaffected for all other PS scenarios.

4.6 Discussion

For both Upper Lake Zurich and Sihlsee, the simulated climate change effects for the reference scenario QNat are in line with effects that have previously been observed or projected for dimictic or monomictic lakes (Ficker et al. 2017; North et al. 2014): (a) an increase in epilimnetic temperature, (b) a comparably small increase in hypolimnetic temperature as stratification decouples the hypolimnion from the atmosphere, (c) prolonged summer stratification, which further results in (d) reduced hypolimnetic DO and (e) increased hypolimnetic phosphate concentrations. For Sihlsee, climate change is projected to (f) shorten the ice-covered period, (g) reduce ice thickness, (h) shorten the duration of inverse stratification in winter, and consequently, (i) increase hypolimnetic DO and (j) decrease hypolimnetic phosphate concentrations. Again, these findings agree with observations and projections for other ice-covered lakes (Benson et al. 2012; Prowse et al. 2011).

In addition to these established effects, our simulations show relevant interactions between the effects of PS operations and those of climate change. In the PS scenarios, the projected warming rate in the hypolimnion of Sihlsee is almost as large as that in the epilimnion. This is due to deep-water withdrawal and the corresponding drawdown of surface water, as well as the transfer of epilimnetic water from Upper Lake Zurich. Hypolimnetic temperature in Sihlsee is already now increased by 5 to 10 °C throughout summer due to PS operations (Kobler et al. 2018), and our simulations show that this effect is further exacerbated by climate change. This is relevant as increasing hypolimnetic temperatures cause intensified mineralization of organic matter (Gudas et al. 2010) and may promote anoxic conditions in the surface sediments (Jensen and Andersen 1992).

The further warming of the hypolimnion results in weaker and shorter summer stratification. Altogether, the combined effects of climate change, prolonging stratification, and of PS operations, shortening it, almost compensate each other. Thus, the average duration with extended PS under future climate is similar to that of QNat under current climate. But the properties of the stratification would be very different, as it is projected to (i) start and end earlier by ~1 month, and to (ii) be significantly less stable due to the much smaller temperature difference between the epi- and the hypolimnion. Such seasonal shifts affect the timing of various processes in an ecosystem differently and thus modify interactions between them. For example, earlier warming in spring has been shown to disrupt trophic linkages between phyto- and zooplankton (Winder and Schindler 2004), especially if warming is seasonally heterogeneous (Straile et al. 2015).

The shorter duration of stratification and the input of epilimnion water from Upper Lake Zurich increase DO availability and reduce phosphate concentrations in the hypolimnion of Sihlsee (Kobler et al. 2018). These effects are partially offset by climate change, which extends the average duration of DO concentrations $<4 \text{ mg L}^{-1}$ by ~2 weeks for the present PS and by <1 week for the extended PS scenario. However, this effect, caused by climate change, is even stronger for the reference scenario QNat, where the duration of DO $<4 \text{ mg L}^{-1}$ is extended by ~1 month.

Ice-cover is already affected by PS pumping: particularly, for the extended PS scenario increased epilimnion temperatures were projected to decrease ice thickness and shorten the ice-covered period (Kobler et al. 2018). Climate change further reduces Sihlsee's ice cover by two processes: the direct impact of warmer epilimnion and air temperatures, which shortens the ice-covered period by ~71% (Table 4.2). Combined with the increased temperature of the PS pumping flow, the ice-covered period is even shortened by 82% for extended PS. The number of winters exceeding an ice thickness of 5 cm is reduced by ~17% due to extended PS and by ~40% due to climate change, but by ~85% if both effects are combined (Table 4.2). Since both PS and climate change lead to shorter inverse stratification and reduced ice cover, it is important for the ecosystem to consider their combined effects. These may include reduced likelihood of winter anoxia, but also modified survival rates of different species, leading to altered community composition (Adrian et al. 2006; Rühland et al. 2015). Additionally, changes in winter phenology could result in alterations of fish growth and reproduction (Shuter et al. 2012).

Combined effects of deep-water withdrawal and climate change were also found by Prats et al. (2018) who analysed different management scenarios for a Mediterranean drinking water reservoir. They concluded that reservoirs should be more sensitive to meteorological forcing than natural lakes as the deep-water withdrawal transports climate-induced excess heat to lower layers. For their current management scenario with deep-water withdrawal both epi- and hypolimnion temperatures would increase, while the seasonal dynamics of thermocline depth and stratification would hardly be affected (Prats et al. 2018). For a scenario with surface water withdrawal, they projected longer and more stable summer stratification as well as less warming of epi- and hypolimnion. They showed that surface water withdrawal and dam heightening combined with long-term climate change would lead to similar mean hypolimnion temperatures as with deep-water withdrawal under the present climate, which is not the case for Sihlsee.

The projected increases in epilimnion temperature in Sihlsee are ~50% of those in air temperature. According to physical principles, if only air temperature is modified and all other forcing remains equal, epilimnion temperatures in equilibrium with the atmospheric forcing should increase by ~70 to 90% of increases in air temperature (Schmid et al. 2014). An additional simulation without any inflows resulted in higher epilimnetic warming of ~60 to 70% of those of air temperature. Moreover, the weather generator projects a reduction of relative humidity, which explains the remaining difference of ~10% to the expected warming. Climate models often project a decrease of relative humidity over land (Byrne and O'Gorman 2016), which is mostly projected to occur in summer (CH2018 2018). However, the projected reduction in relative humidity by the weather generator is based on correlations between current air temperature and humidity for the present climate, and it remains uncertain whether these are also valid for future climate⁸. Similar arguments apply for the projected inflow temperatures.

⁸ Compared to the CH2018 projections those of VG (Figure 5.6 and Figure 5.7) seem to overestimate the reduction of relative humidity particularly for autumn, winter and spring, where CH2018 projects hardly any changes for the RPC8.5 scenario towards the end of the 21st century.

Besides air temperature, climate change is also likely to modify precipitation and discharge patterns. For central and north-eastern Switzerland, most regional climate models agree that precipitation will decrease during summer months, whereas the direction of changes during the rest of the year remains uncertain (Fischer et al. 2015). Significant changes in precipitation would also modify river discharge, external nutrient loading (Dokulil et al. 2010) and would require modifications of the PS operations. Furthermore, in the catchment of Sihlsee, the duration of snow cover would be reduced, leading to a change of the seasonal discharge pattern. Fenocchi et al. (2017) analysed that riverine inflows can play a crucial role for hypolimnetic temperatures for the example of Lake Maggiore. Significant changes in discharge could also have an impact on lake-internal processes and stratification in Sihlsee, especially for the reference scenario QNat. However, these effects will likely be much smaller than the differences between the “quasi-natural” scenario and the scenarios with deep-water withdrawal.

The water flows of the extended PS scenarios were derived based on the traditional operation strategies for a PS hydropower plant, which will likely change in future. Pérez-Díaz et al. (2015) summarize future trends of the operation of PS hydropower plants, and highlight the importance of providing power regulation reserves by means of variable speed design of pump-turbines or hydraulic short-circuiting. Nevertheless, as the studied PS hydropower plant is operated by the Swiss Federal Railways (SBB AG) and mainly supplies power to trains, one could argue that the future operation might not differ a lot from present conditions.

A possible option to reduce the PS effect for the hypolimnion is to shift the PS intake/outlet to the epilimnion. Bonalumi et al. (2012) showed that for a deeper inlet/outlet, a larger volume is significantly affected, as mostly the volume between the intake/outlet and the thermocline is warming. As a consequence of the large water level fluctuations, shifting the PS intake/outlet to the epilimnion, which would be favourable with respect to temperature changes, would require the construction of a multi-level offtake structure and the implementation of an adaptive withdrawal strategy as analysed by Weber et al. (2017). Including such a selective withdrawal was, however, beyond the focus of this study.

In summary, our simulations show ecologically relevant synergistic and antagonistic effects of climate change and PS operations within the typical time scale for which concessions of hydropower plants are usually issued. Without consideration of climate change scenarios, an environmental assessment for a hydropower plant, therefore, can only incompletely assess the expected impacts on ecological processes in the affected water bodies during its lifetime. We thus recommend including projections for future climate effects in environmental impact assessments. Furthermore, our results show that estimated impacts of both PS and climate change may differ for different reference scenarios, highlighting the importance to have clear guidelines for defining the reference.

4.7 Conclusions

Coupled effects of PS operations and climate change have not been studied, to our knowledge, up to now. Thus, we generated meteorological and inflow water temperature forcing using a vector-autoregressive weather generator for current and future conditions. With this forcing, we drove a two-dimensional hydrodynamic and water quality model for two different PS and two reference scenarios. This allowed us to quantify the impact of both climate change and PS operation on temperature, DO and phosphate concentrations. Our results showed a synergistic effect of PS operation and climate change on hypolimnion temperatures, whereas epilimnion temperature increased similarly in all PS scenarios.

The increased surface water temperatures were projected to cause increased water column stability, prolonged summer stratification, and subsequently lower DO concentrations. An antagonistic effect resulted for the duration of summer stratification, which is prolonged by climate change and shortened by PS operation. However, the combination of climate change and the extended PS scenario advanced summer stratification by almost one month. In winter, DO concentrations increased due to diminished ice cover and weakened inverse stratification. The projected changes further imply changes for lake ecology. The reduced phosphate availability after the ice-covered period would likely affect spring algal growth. The increased overall temperature, especially in case of climate change acting along with the extended PS operation, in combination with decreasing DO concentrations, reduces the available habitat for temperature-sensitive fish species.

For a comprehensive environmental impact assessment of PS hydropower plants, we recommend to quantify not only the changes involved due to the PS operation itself, but also those due to climate change as well as their interactions. This is especially important when the intake/outlet of the PS hydropower plant is located in the hypolimnion, as warming rates were shown to be increased by the combination of deep-water withdrawal and climate change.

Chapter 5

Supplementary information to Chapter 4⁹

5.1 Overview

This chapter provides supplementary information to Chapter 4. In Section 5.2 additional information on CE-QUAL-W2 is given by conceptual diagrams describing the hydrodynamic and the water quality features of this model. This is followed by a section describing the calibration and the validation of the weather generator VG, which shows good agreement between the projections with observed meteorological conditions and those generated with VG. Moreover, additional results are depicted for Sihlsee, and the projections for Upper Lake Zurich are summarized. The projections for Upper Lake Zurich of combined PS operation and climate change effects are comparable to those presented in literature for solely climate change with (a) a pronounced temperature increase in the epilimnion, (b) only slight changes in the hypolimnion, (c) decreasing dissolved oxygen and increasing phosphate concentrations in the hypolimnion due to prolonged summer stratification.

⁹ This chapter is based on the supplementary information to “Combined effects of pumped-storage operation and climate change on thermal structure and water quality” by U. G. Kobler, A. Wüest and M. Schmid accepted for publication in *Climatic Change*. The fieldwork, simulations and the analysis presented hereafter are original and were performed by the author of the thesis.

5.2 Additional information on model description and study site

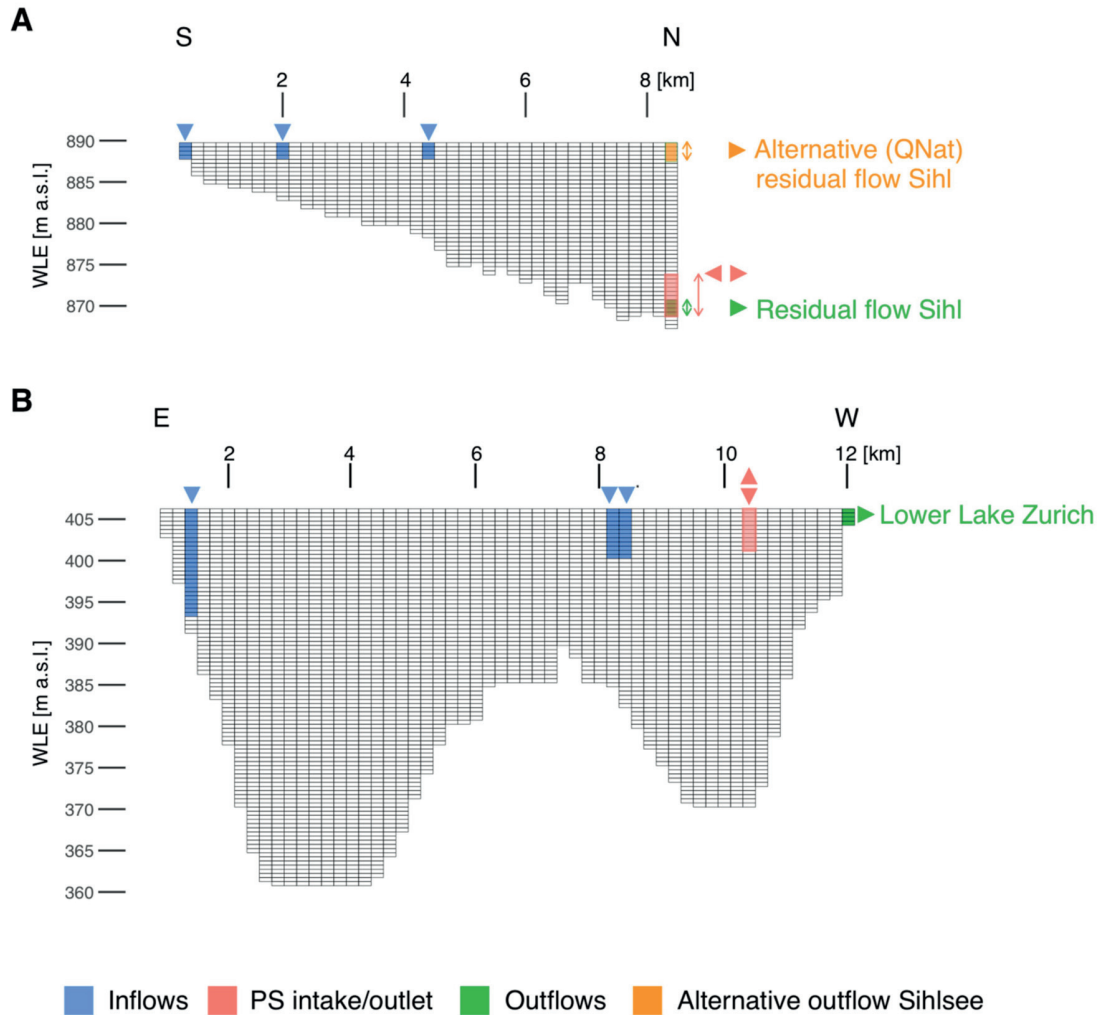


Figure 5.1 Lateral cross-section with inflow (blue), outflow (green), alternative outflow (orange), and PS generating and pumping (red) location within the model grid for (A) Sihlsee (section from south (S) to north (N); showing the distance from the southern shore in km) and (B) Upper Lake Zurich (section from east (E) to west (W); showing the distance from the eastern shore in km); vertical axis refers to the water level elevation (WLE).

5.2.1 Major equations

The major set of laterally averaged equations of CE-QUAL-W2 are described in Cole and Wells (2013), they also discuss how these equations are solved numerically.

5.2.2 Conceptual diagrams

Figure 5.2 shows the dependencies of water temperature and ice cover on meteorological, hydrological and water quality forcing. Figure 5.3 depicts the conceptual dependencies of the constituents that can be described by CE-QUAL-W2. The information was gathered from Cole and Wells (2013).

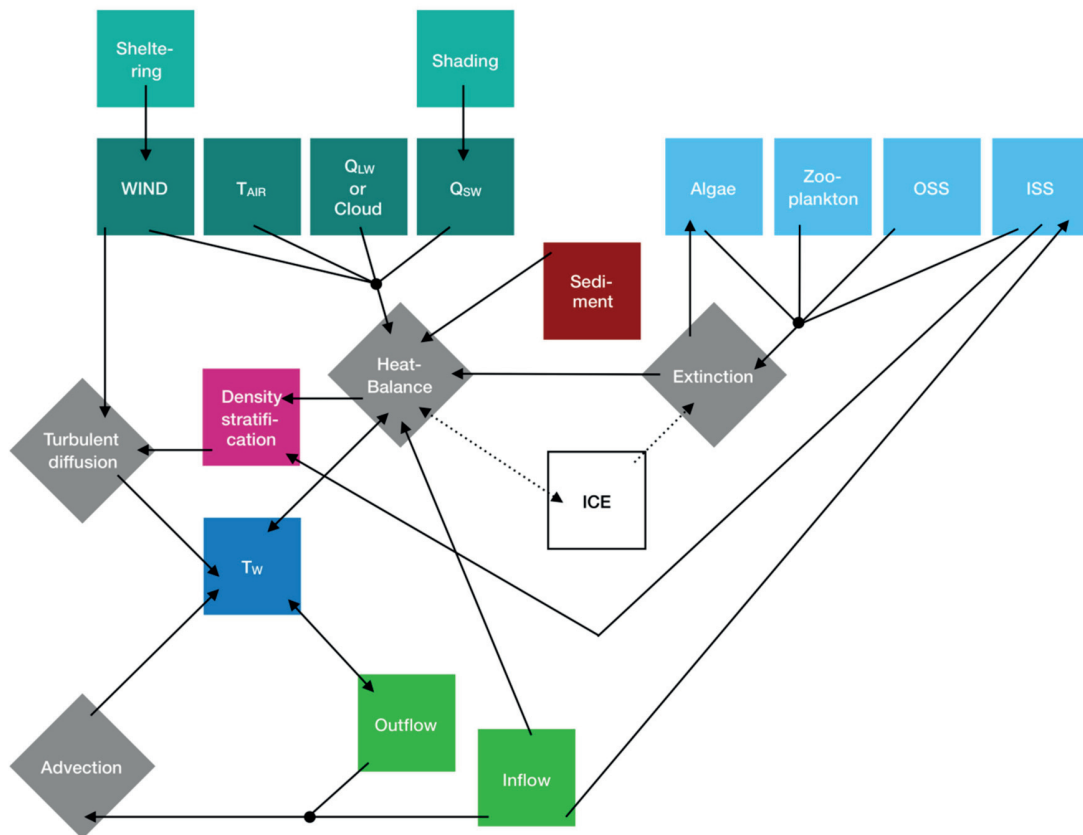
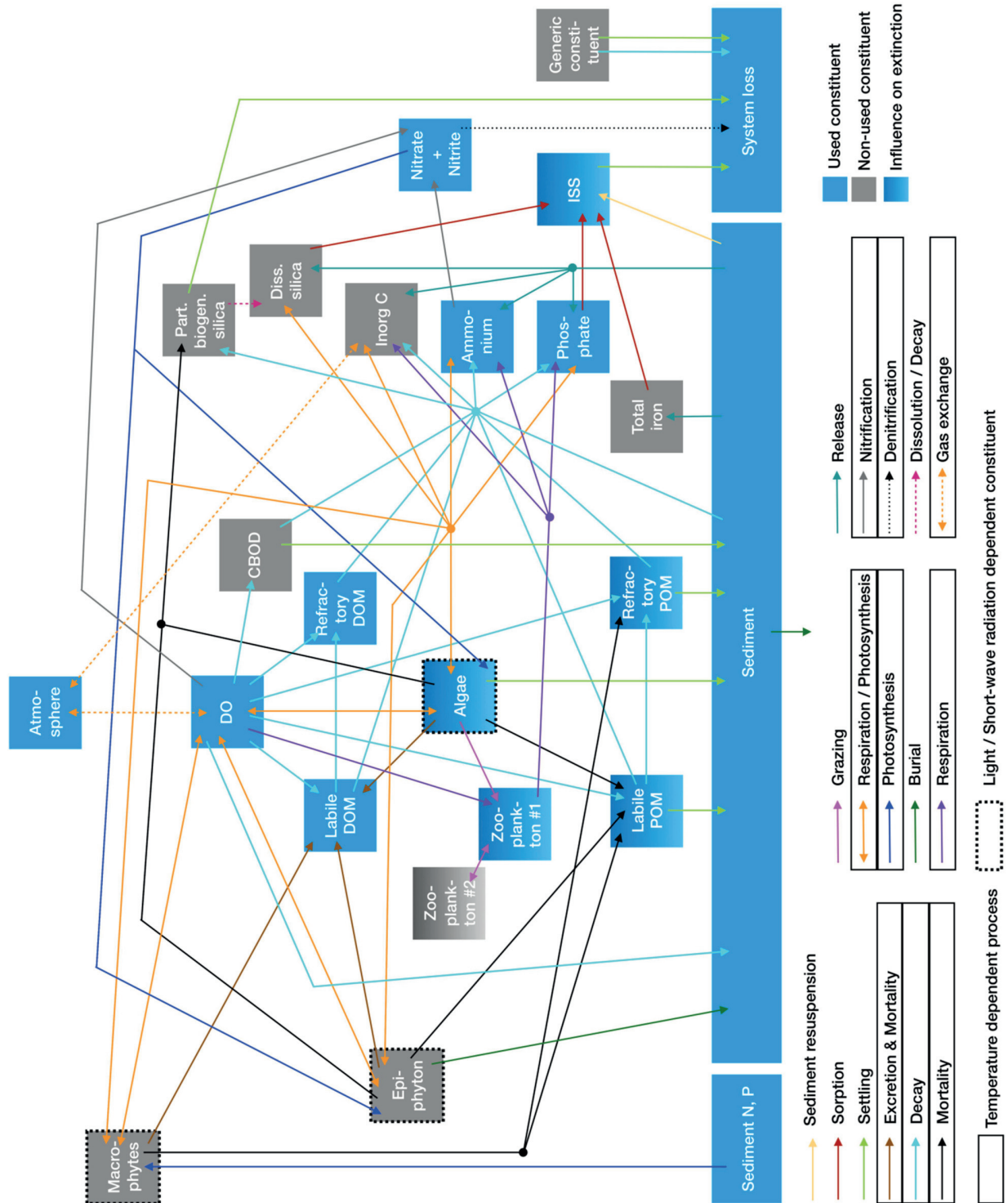


Figure 5.2 Conceptual diagram of CE-QUL-W2's interdependencies of water temperature (T_w) and ice cover (ICE) on meteorological (turquoise; wind speed and direction (WIND), air temperature (T_{AIR}), long-wave radiation (Q_{LW}), cloudiness (Cloud) and short-wave radiation (Q_{SW})) and hydrological (green) forcing as well as on other compartments of the model (part of the water quality compartment (light blue) with organic (OSS), inorganic suspended solids (ISS), algae and zooplankton as well as sediment heat release (red), density stratification (pink)); considered processes are depicted in gray. Shading in this study is taken into account with a fixed value according to Kobler et al. (2018); however, CE-QUAL-W2 would also allow to shading the surrounding landscape and vegetation.



5.3 Calibration and validation of the weather generator VG

Schlabing et al. (2014) developed a weather generator VG based on a single vector-autoregressive process, with the vector as such being composed of simulated meteorological variables at one time step. VG applies a variable transformation to allow the implementation of meteorological variables with other than normal marginal distributions. Once the observations are transformed, a vector-autoregressive process can be fitted to then allow for the generation of time series. These can either emulate the observed variables or generate future conditions by changing mean and or variability. Lastly, the simulations need to be back-transformed to the measurement domain and e.g. short-wave radiation needs to be disaggregated to allow for a typical daily cycle.

The weather generator is expected to transfer the observed correlations between the different meteorological variables. This has been previously tested for Lake Constance (Schlabing et al. 2014) and is also generally the case in the present study (Figure 5.4). The prediction of inflow water temperature with VG might be too simplified, which could explain the slightly different correlations of observations and simulations with air temperature and dew point. This can also be observed when looking at the QQ-plots (Figure 5.5). VG underestimates the occurrence of high inflow water temperatures, especially at Sihlsee. However, natural inflow only accounts for ~10% of the total water balance, and sensitivity analysis has shown that the simulated lake properties are not sensitive to inflow water temperature at Sihlsee.

The QQ-plots also indicate that VG underestimates the occurrence of dry cold conditions (very low dew points) and overestimates the frequency of extreme values (both low and high) of long-wave radiation. The observed distributions of short-wave radiation and air temperature are reliably reproduced by VG.

Wind, one of the most sensitive forcing variables, is only weakly correlated to all other meteorological variables. Thus, there might be errors involved in predicting future wind fields with VG. We decided to transform the u - (positive eastward) and v - (positive northward) wind components to a coordinate system aligned with the main axis of each lake, as these typically align with the major wind direction. For forcing CE-QUAL-W2 these wind components needed to be back-transformed to wind speed and direction.

We validated VG by comparing the mean and range of lake model projections for simulations driven with the available meteorological observations and those driven with the output of VG (Figure 5.8 and Figure 5.9). These comparisons show that the statistical properties of simulated water temperature and quality are well reproduced if VG-generated forcing is used to drive the model.

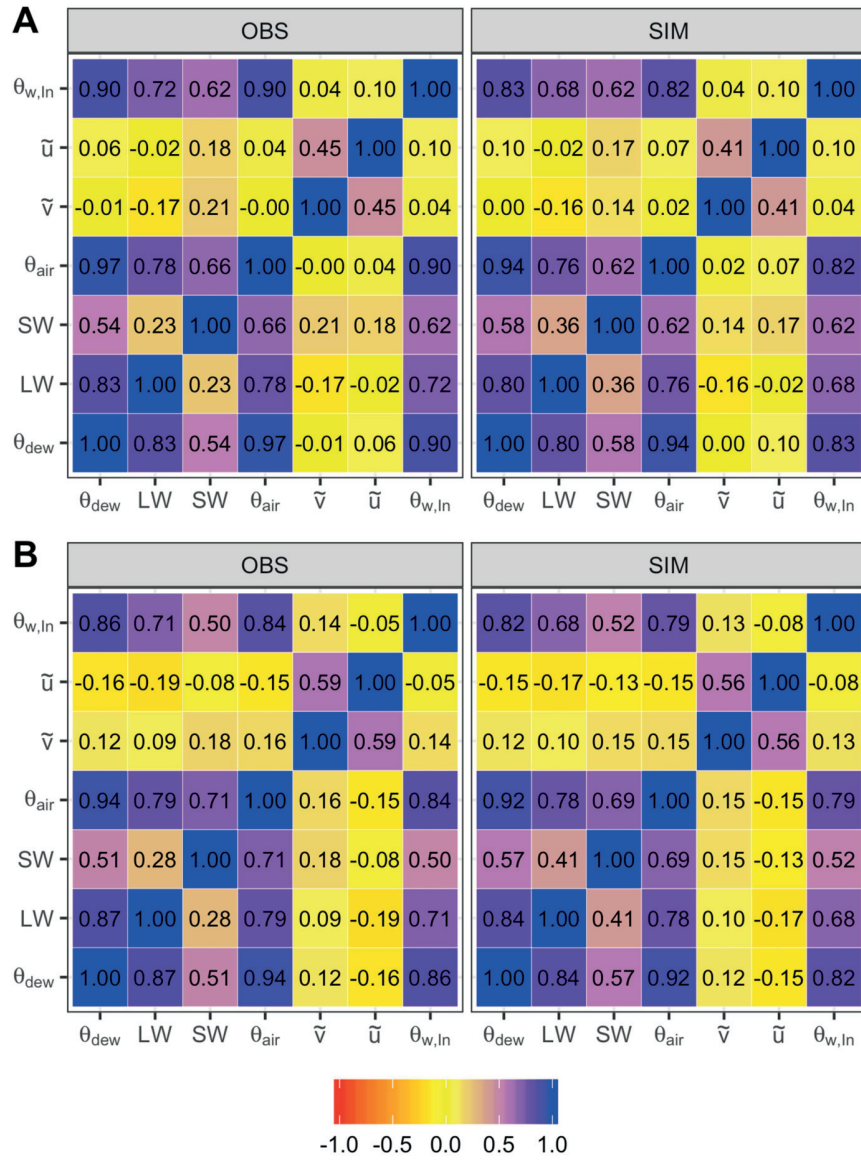


Figure 5.4 Pearson correlation between all variables (θ_{air} : air temperature, θ_{dew} : dew point, $\theta_{w,In}$: inflow water temperature, LW: long-wave radiation, SW: short-wave radiation, \tilde{v} : wind component normal to the main lake orientation, \tilde{u} : wind component along the main lake orientation) of observations (OBS) or simulations (SIM) (set of all 10 realizations) for (A) Sihlsee and (B) Upper Lake Zurich.

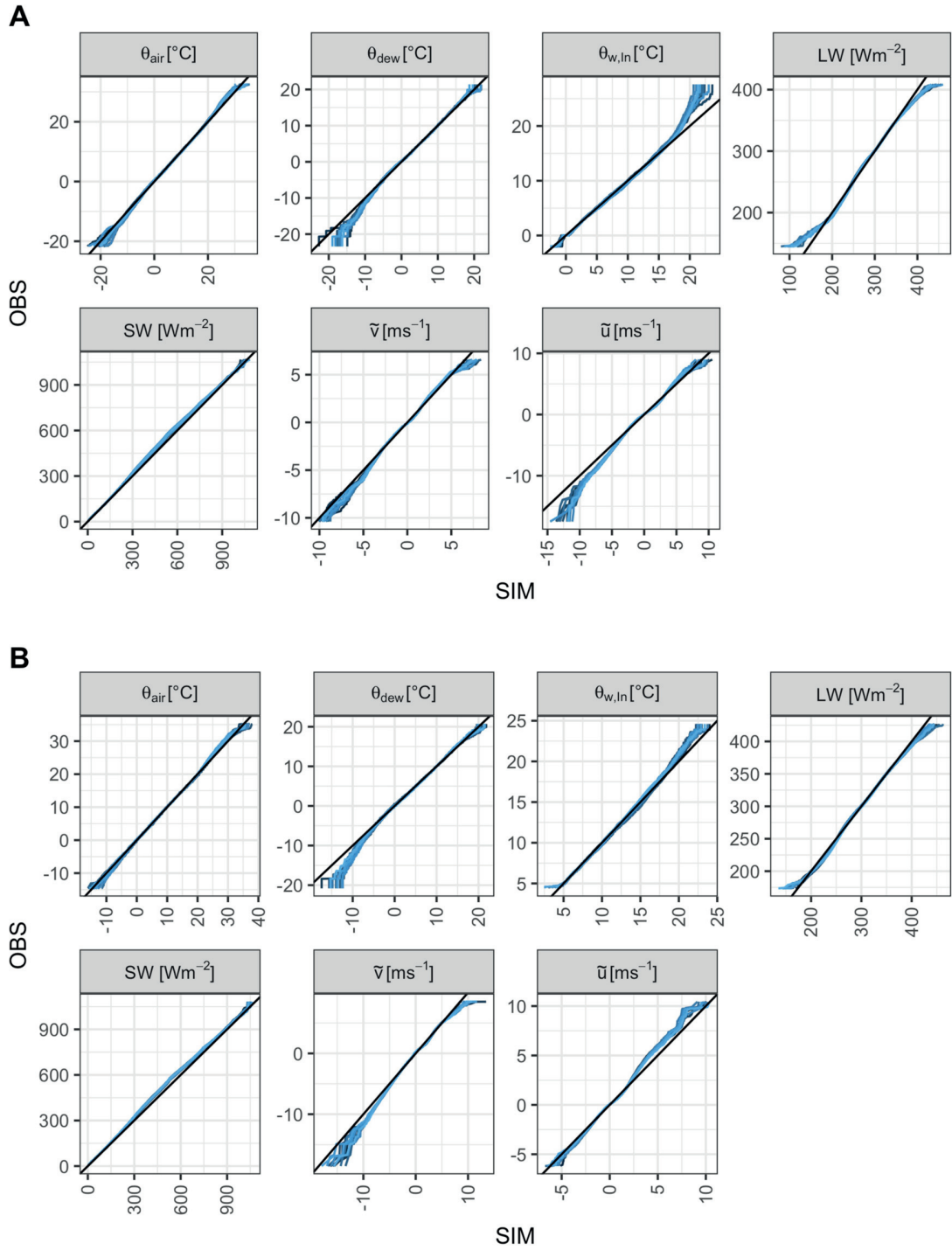


Figure 5.5 QQ-plot comparing ranked simulations (SIM) and observations (OBS) in blue for all ten realizations at (A) Sahlsee and (B) Upper Lake Zurich for each considered variable (θ_{air} : air temperature, θ_{dew} : dew point, $\theta_{w,\text{in}}$: inflow water temperature, LW: long-wave radiation, SW: short-wave radiation, \tilde{v} : wind component normal to the main lake orientation, \tilde{u} : wind component along the main lake orientation).

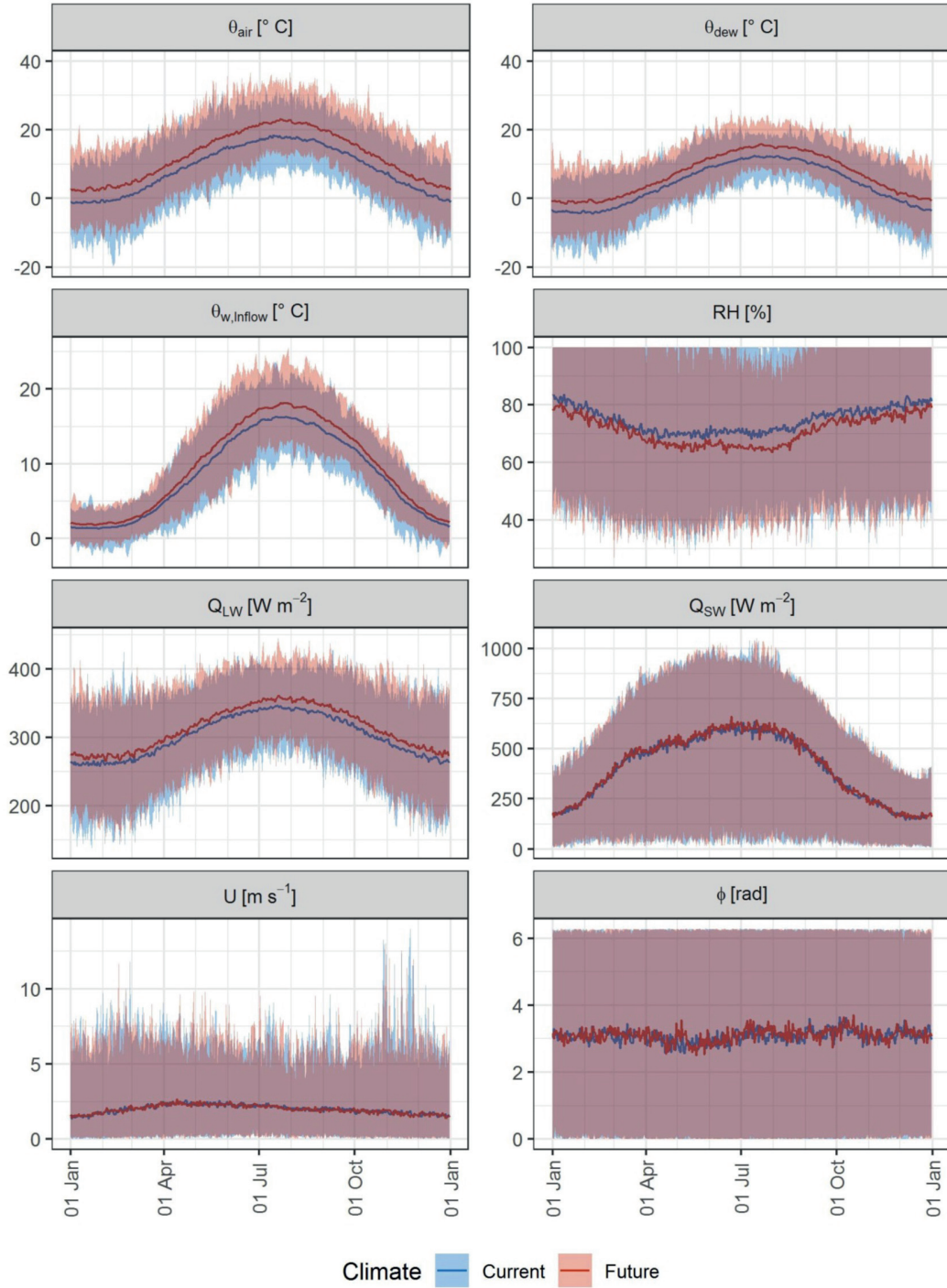


Figure 5.6 VG-generated meteorological forcing of Sihlsee; shown are aggregated mean (line) and the range of minimum and maximum (shaded area) for each day of the year and for current (blue) and future (red) climate. Panels further separate the different meteorological variables: air temperature θ_{air} ($^{\circ}\text{C}$), dew point θ_{dew} ($^{\circ}\text{C}$), inflow water temperature $\theta_{\text{w,inflow}}$ ($^{\circ}\text{C}$), relative humidity RH (%), long-wave radiation Q_{LW} (W m^{-2}), short-wave radiation Q_{SW} (W m^{-2}), wind speed U (m s^{-1}), wind direction ϕ (rad).

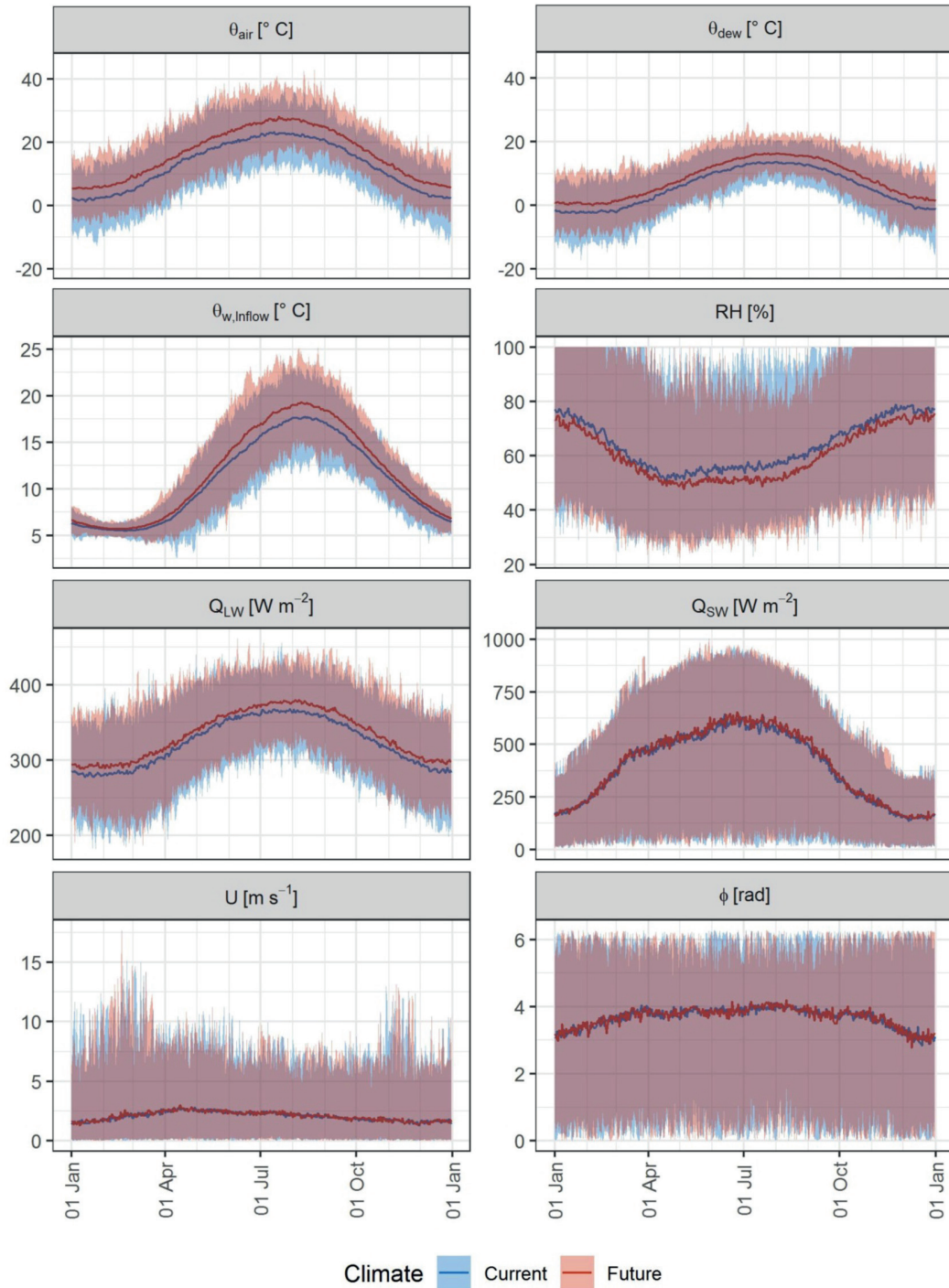


Figure 5.7 VG-generated meteorological forcing of Upper Lake Zurich; shown are aggregated mean (line) and the range of minimum and maximum (shaded area) for each day of the year and for current (blue) and future (red) climate. Panels further separate the different meteorological variables: air temperature θ_{air} ($^{\circ}\text{C}$), dew point θ_{dew} ($^{\circ}\text{C}$), inflow water temperature $\theta_{\text{w,inflow}}$ ($^{\circ}\text{C}$), relative humidity RH (%), long-wave radiation Q_{LW} (W m^{-2}), short-wave radiation Q_{SW} (W m^{-2}), wind speed U (m s^{-1}), wind direction ϕ (rad).

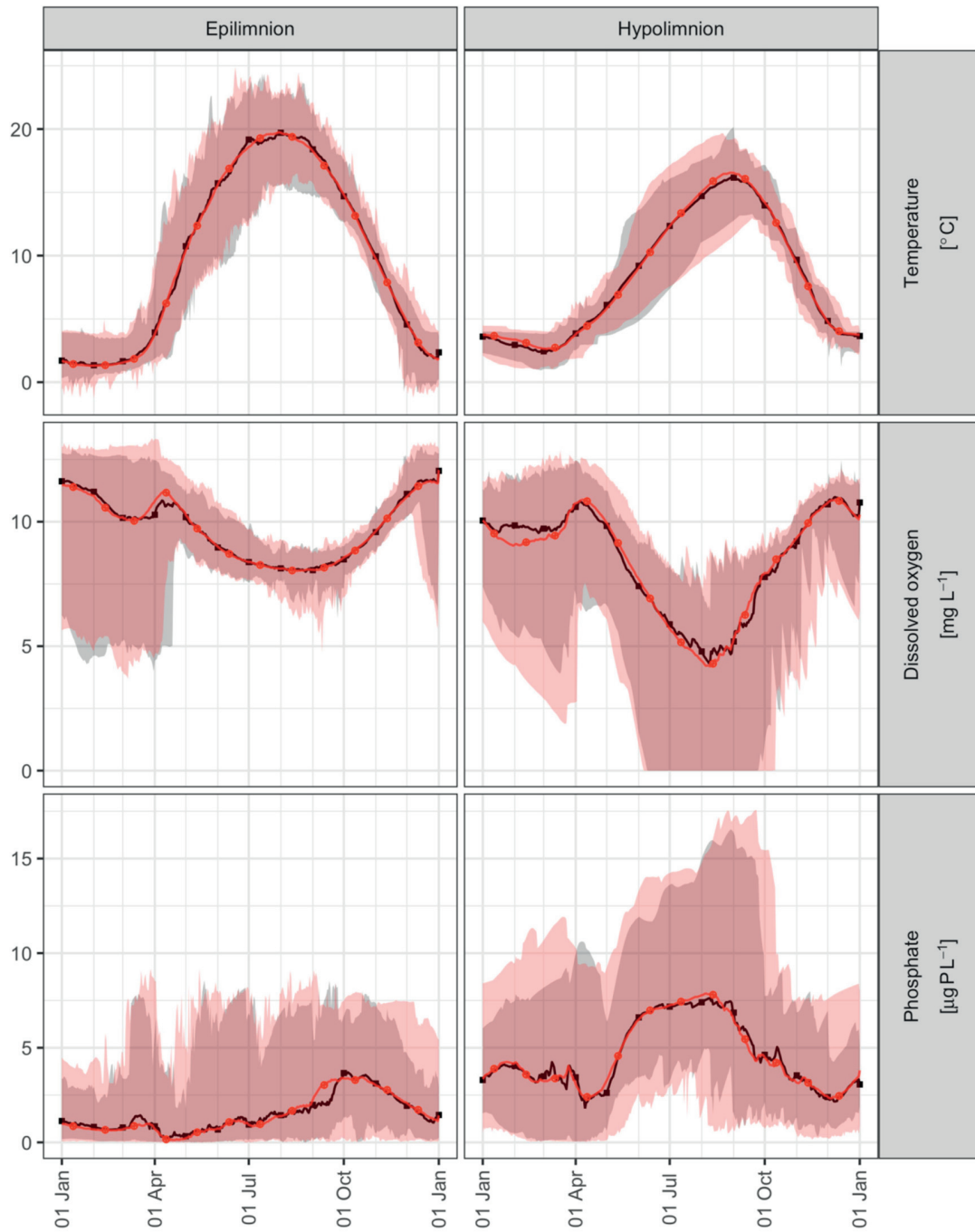


Figure 5.8 Temperature (°C) and concentrations of DO (mg L⁻¹) and phosphate (µg P L⁻¹) computed with meteorological observations (black) and ensemble of VG simulations (red) at Sihlsee. Lines depict the mean and the shaded area gives minima and maxima of the corresponding day of the year separated for epi- and hypolimnion.

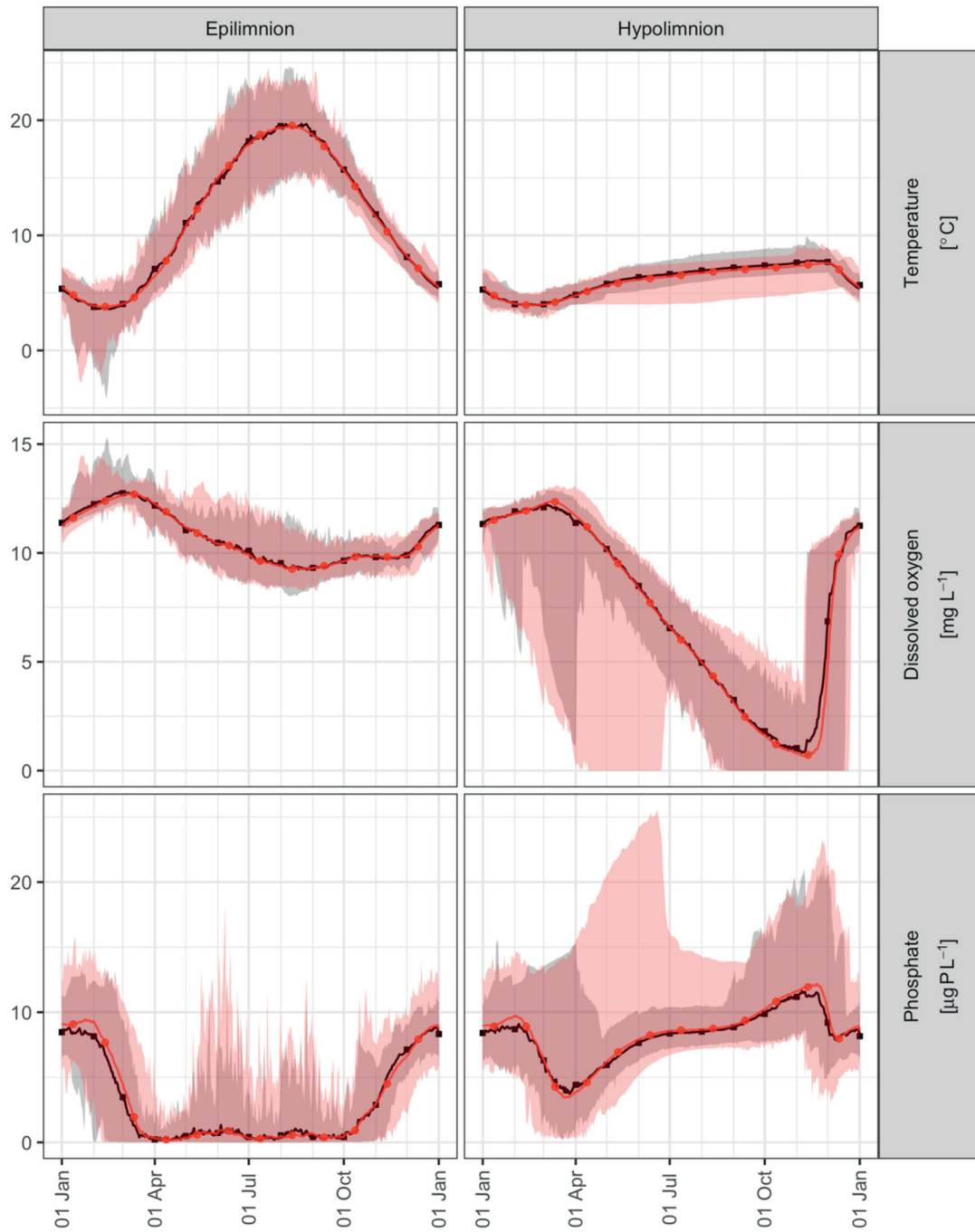


Figure 5.9 Temperature (°C) and concentrations of DO (mg L⁻¹) and phosphate (µg P L⁻¹) computed with meteorological observations (black) and ensemble of VG simulations (red) at Upper Lake Zurich. Lines depict the mean and the shaded area gives minima and maxima of the corresponding day of the year separated for epi- and hypolimnion.

5.4 Additional results Sihlsee

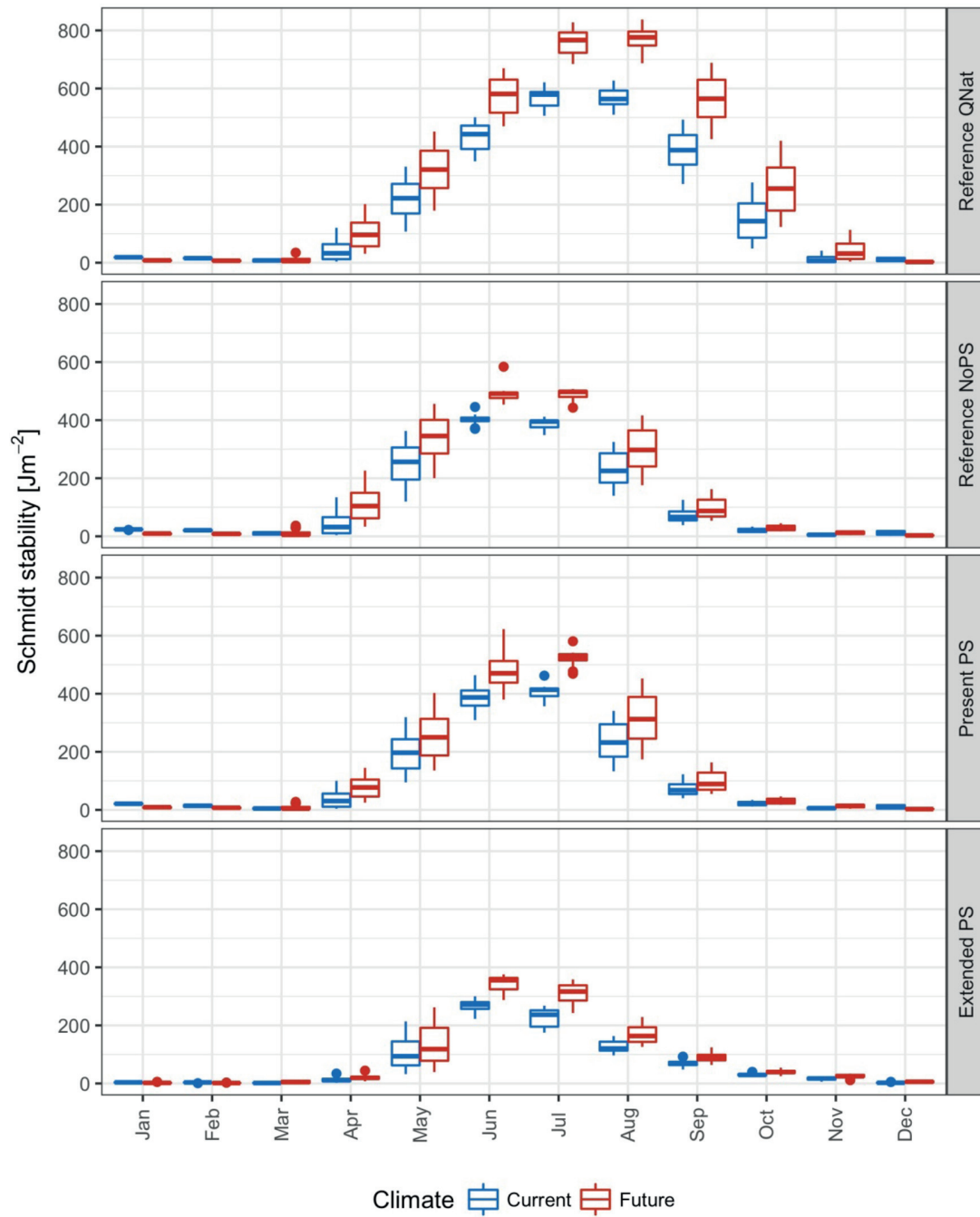


Figure 5.10 Boxplot of Schmidt stability (J m^{-2}) for the current and future climate scenario separated by month and PS scenarios.

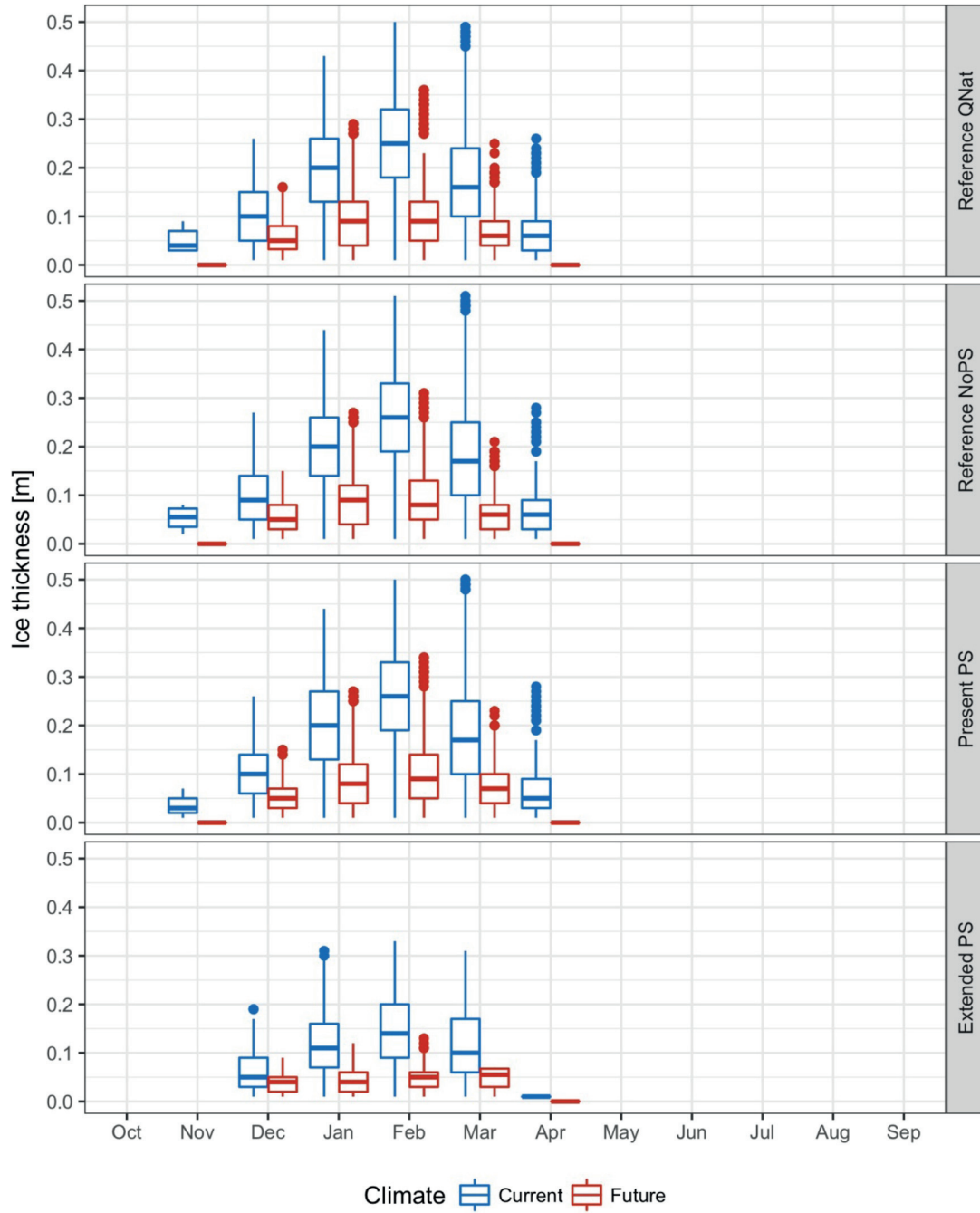


Figure 5.11 Boxplot of ice thickness (m) for the current and future climate scenario separated by month and PS scenarios.

5.5 Results Upper Lake Zurich

In general, the projected impacts of climate change on Upper Lake Zurich differ only slightly for the different PS scenarios. This has two main reasons: the PS flows are a much smaller fraction of the total inflows of Upper Lake Zurich, and the inflows are discharged to the epilimnion, where their effects on temperature can be faster equilibrated with the atmosphere.

The projected warming of epilimnion temperatures at Upper Lake Zurich due to climate change is very similar for all three PS scenarios (Figure 5.12, Figure 5.14). It reaches values from ~ 1.3 °C (May) to ~ 2.1 °C (September). Hypolimnion temperature increases by <0.6 °C from June to December, and the water temperature differences between current and future scenario reach a maximum of ~ 1.6 °C, ~ 1.5 °C and ~ 1.4 °C in January for the reference scenario QNat, the present PS and the extended PS scenario, respectively (Figure 5.13, Figure 5.14). The increased differences of hypolimnion temperature in winter can be explained by climate change delaying the mixing at Upper Lake Zurich.

The summer stratification is significantly prolonged (by ~ 13 , ~ 21 and ~ 28 days) with earlier onset and delayed end of stratification (Figure 5.15). The summer stratification is also intensified with Schmidt stability increasing by ~ 17 to $\sim 18\%$ (Figure 5.16, Table 5.1). As a consequence of prolonged stratification dissolved oxygen (DO) concentrations in autumn are deteriorating. All years of each climate ensemble show DO concentrations <4 mg L⁻¹. The duration of the period with DO concentrations <4 mg L⁻¹ increases by ~ 33 , ~ 30 and ~ 26 days for the reference scenario QNat and the present and extended PS scenario due to future climate conditions. Additionally, in winter no inverse stratification would occur for future climate conditions independent of the PS scenario (Figure 5.15).

DO concentrations in the epilimnion decline by <0.6 mg L⁻¹ independent of the PS scenario (Figure 5.12, Figure 5.14), which can be explained by lower DO solubility at higher water temperature. Hypolimnetic DO concentrations decrease most in December (by ~ 3.1 , ~ 2.8 and ~ 2.2 mg L⁻¹ for the reference scenario QNat, the present PS and the extended PS scenario, respectively) when mixing is already initiated in the current climate but stratification still persists in the future climate. Throughout the rest of the year the reduction of hypolimnetic DO concentrations remains at ~ 0.7 - 1.5 mg L⁻¹.

In the epilimnion, an earlier onset of primary production causes earlier phosphate reduction for the future climate scenario (Figure 5.12, Figure 5.14). This results in a decrease of up to ~ 3.4 , ~ 3.6 and ~ 3.9 $\mu\text{g P L}^{-1}$ for the reference scenario QNat, the present PS and the extended PS scenario from January to March. Between April and December the differences are <1.0 $\mu\text{g P L}^{-1}$ for all PS scenarios. Differences in November and December are slightly higher than for the rest of the period, which originates from prolonged stratification, thus, causing higher phosphate concentrations in the hypolimnion before the onset of mixing. In the hypolimnion prolonged and intensified summer stratification causes increased phosphate concentrations throughout the stratified period (Figure 5.13, Figure 5.14). This adds a maximum of ~ 2.8 , ~ 2.8 and ~ 2.4 $\mu\text{g P L}^{-1}$ to

current phosphate concentrations for the reference scenario QNat, the present PS and the extended PS scenario, respectively. Due to earlier primary production along with phosphate being consumed in the epilimnion, and earlier mixing in spring, the hypolimnetic phosphate concentrations decrease by a maximum of ~ 2.8 , ~ 3.0 and $\sim 3.6 \mu\text{g P L}^{-1}$ (February) for the reference scenario QNat, the present PS and the extended PS scenario, respectively.

Table 5.1 Aggregated differences between current (CC) and future climate conditions (FC) calculated from all 150 years for Upper Lake Zurich.

Scenario	Current climate (CC)	Future climate (FC)	$\Delta = \text{FC} - \text{CC}$	$\Delta/\text{CC} [\%]$
Years with hypolimnetic DO concentrations $< 4 \text{ mg L}^{-1}$ [-]				
Reference	150	150	0	0
Present PS	150	150	0	0
Extended PS	150	150	0	0
Mean Schmidt stability during periods of summer stratification [J m^{-2}]				
Reference	850	986	136	16
Present PS	851	983	132	16
Extended PS	819	940	121	15

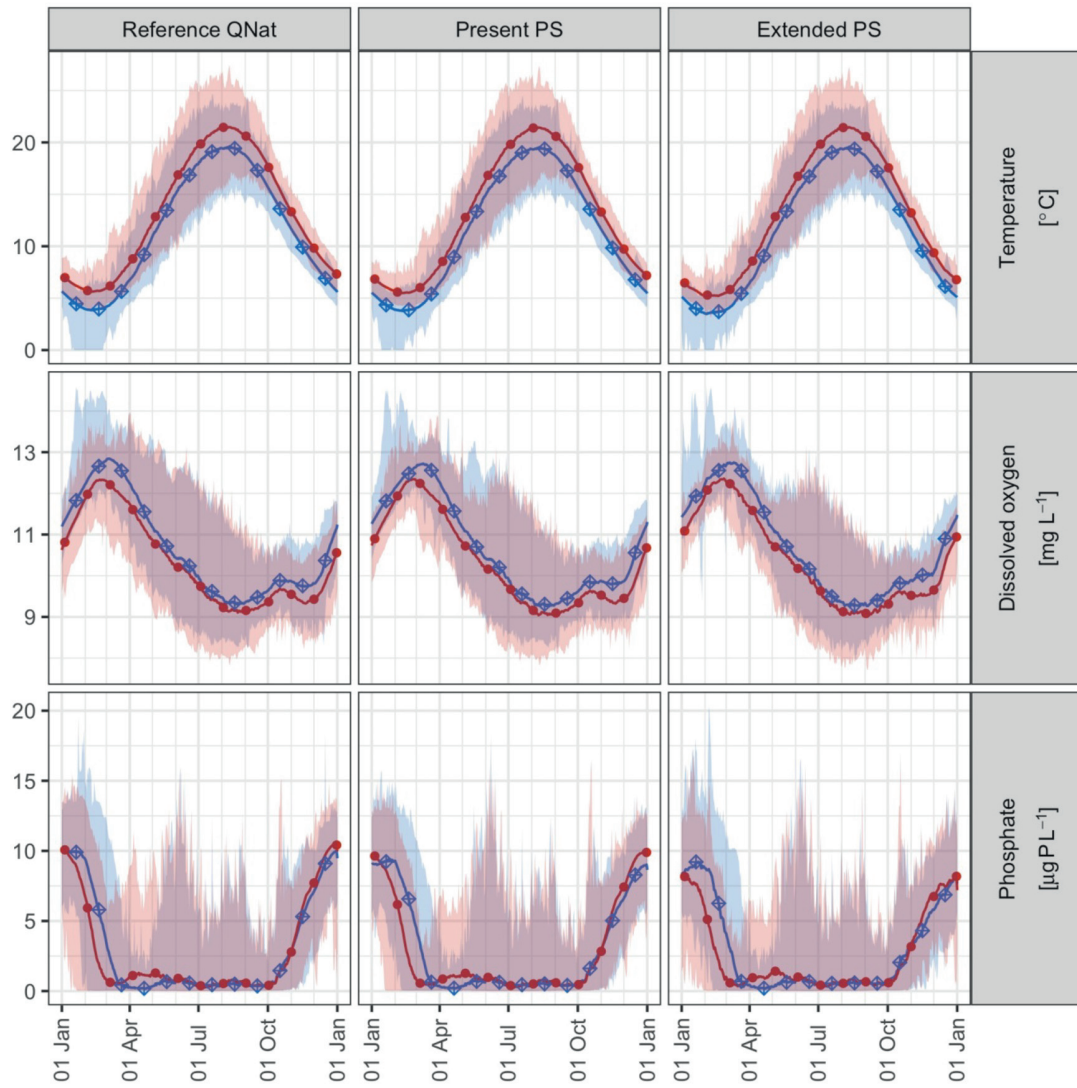


Figure 5.12 Absolute values of temperatures (°C), DO (mg L⁻¹) and phosphate (µg P L⁻¹) in the epilimnion (from surface to 5 m depth) of Upper Lake Zurich for future (red) and current climate scenario (blue). Shown are means (lines and markers) as well as minima and maxima (shaded areas) for each day of the year for each PS scenario.

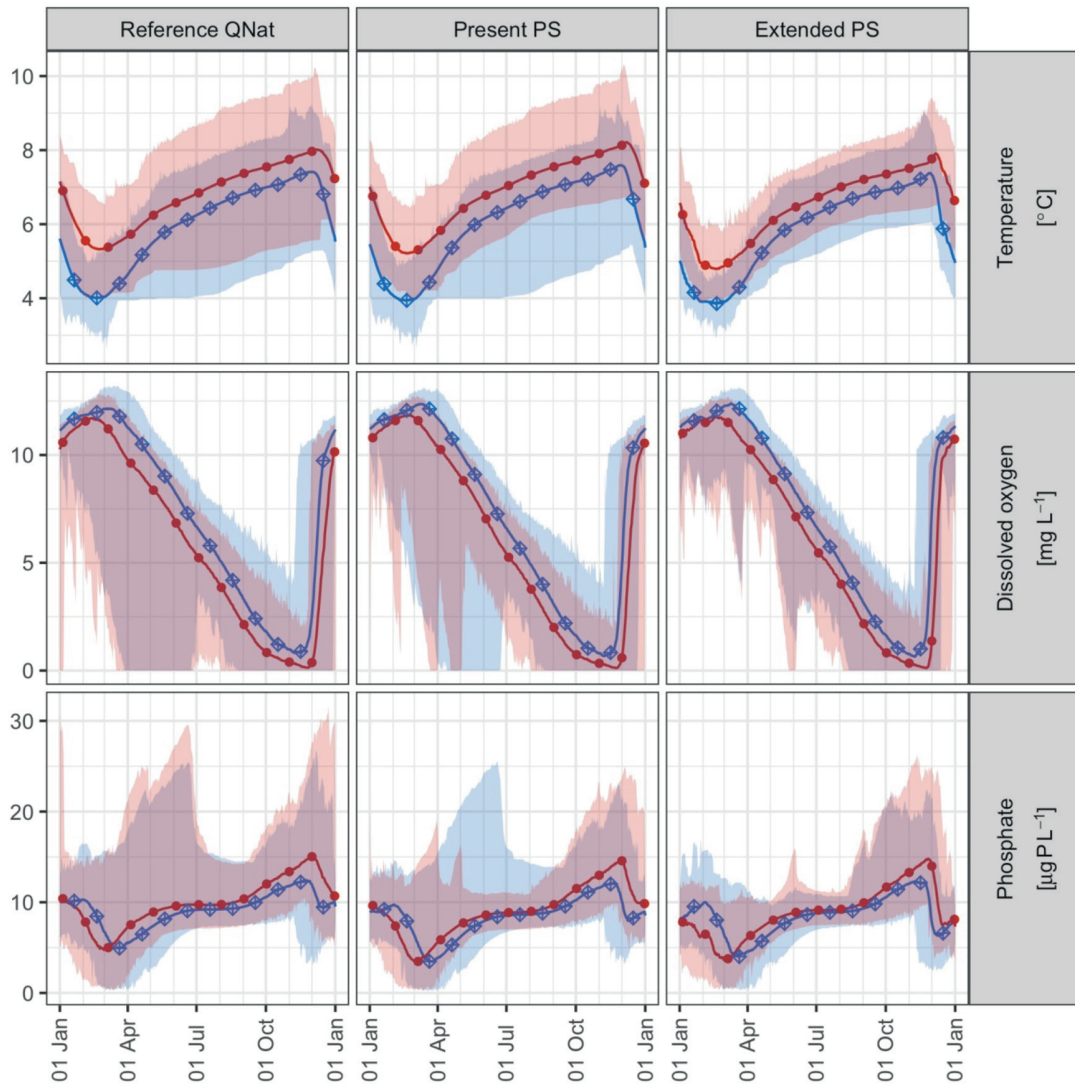


Figure 5.13 Absolute values of temperatures (°C), DO (mg L⁻¹) and phosphate (µg P L⁻¹) in the hypolimnion (lowest 5 m of water column) of Upper Lake Zurich for future (red) and current climate scenario (blue). Shown are means (lines and markers) as well as minima and maxima (shaded areas) for each day of the year for each PS scenario.

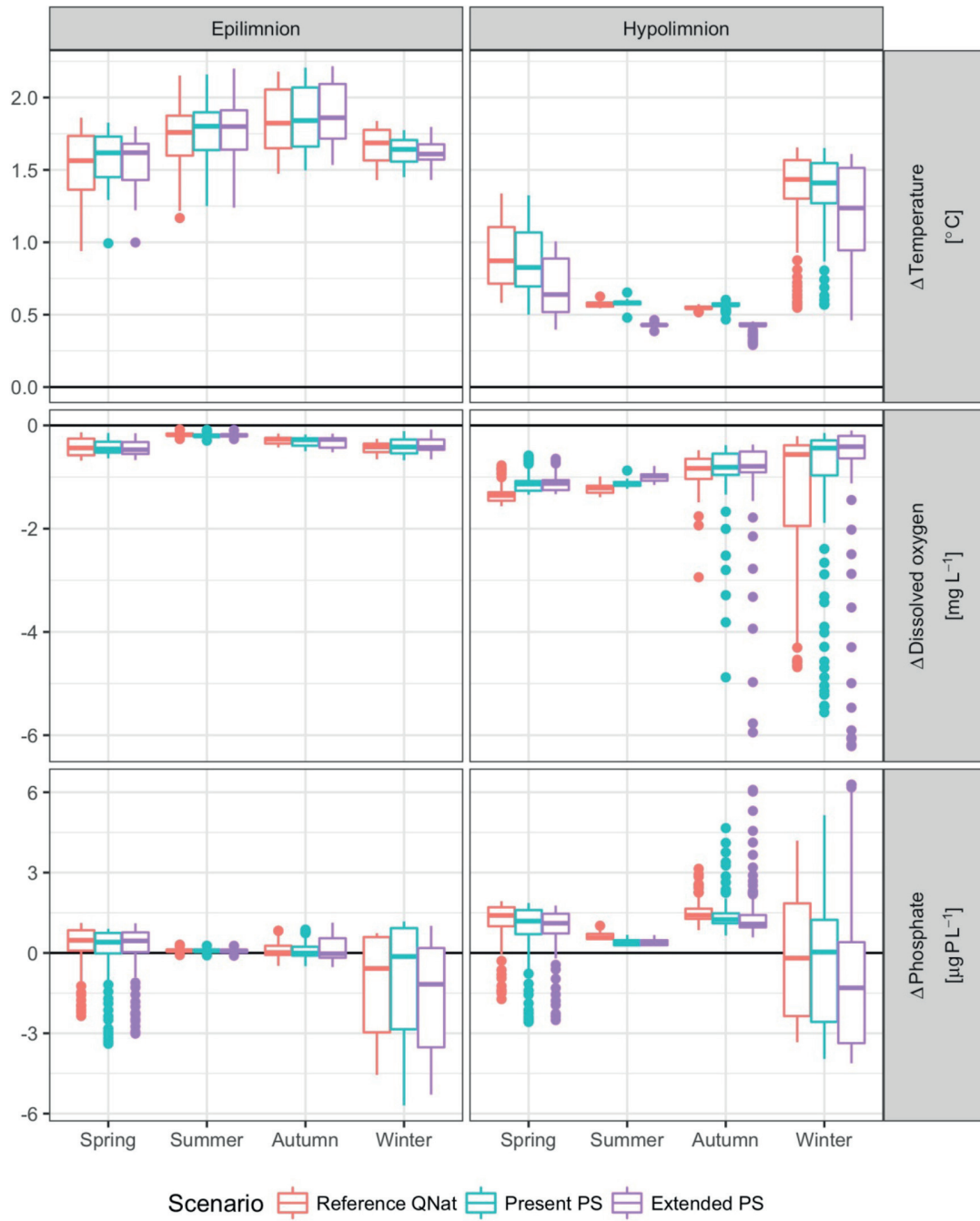


Figure 5.14 Boxplot of differences of temperature (°C), DO (mg L⁻¹) and phosphate (µg P L⁻¹) at Upper Lake Zurich for all PS scenarios and for each season (spring: March-May, summer: June-August, autumn: September-November, winter: December-February) for the epi- and the hypolimnion.

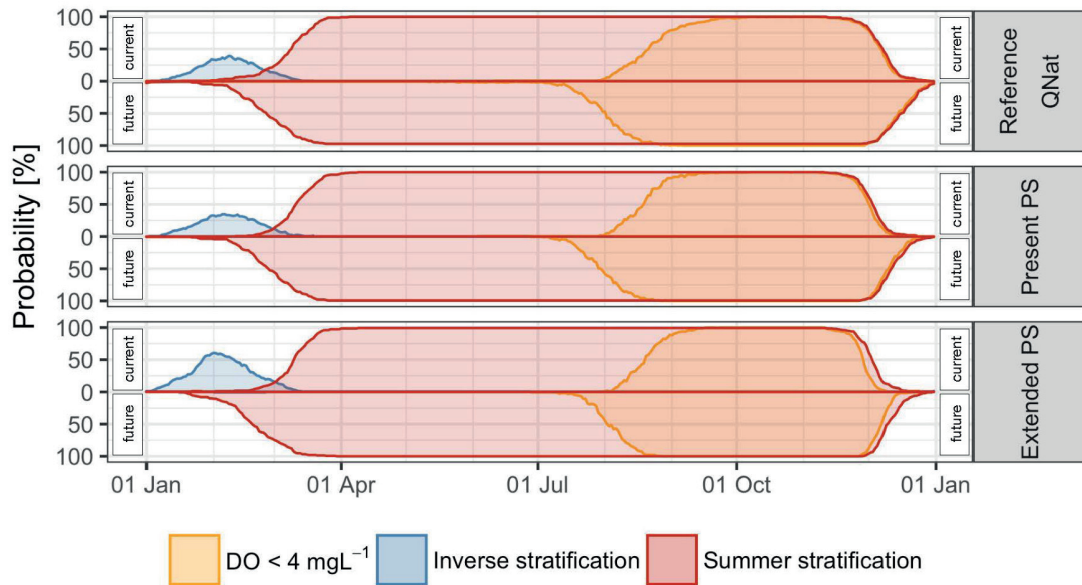


Figure 5.15 Comparison of current (upper half) and future (lower half) probability (%) of each day of the year that the lake is inversely stratified (blue), stratified (red) or that the hypolimnion reaches DO concentrations <4 mg L⁻¹ (orange) at Upper Lake Zurich.

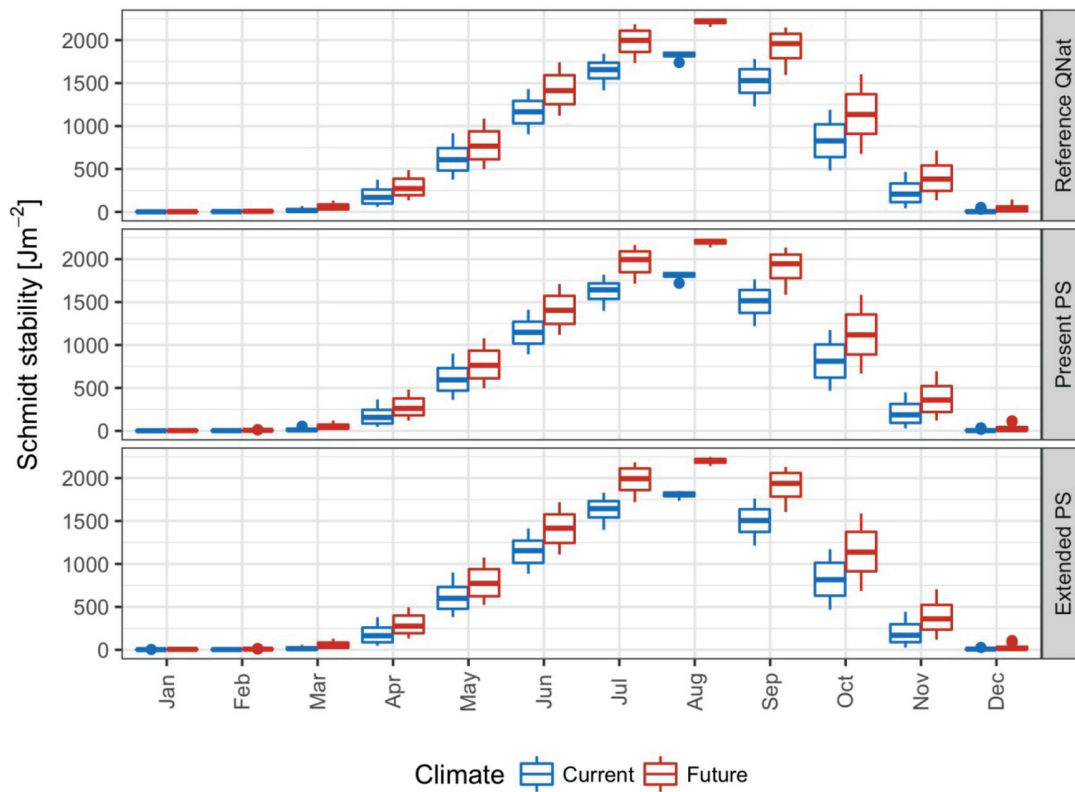


Figure 5.16 Boxplot of Schmidt stability (J m⁻²) for the current and future climate separated by month and PS scenarios.

Chapter 6

Ensemble modelling of ice cover for a reservoir affected by pumped-storage operation and climate change¹⁰

6.1 Overview

Due to the utilisation of a modified description of the ice module of the two-dimensional laterally averaged hydrodynamic model (CE-QUAL-W2), which was not tested aside from Chapters 2 and 4, the robustness of the ice thickness projections of PS operation and climate change needed to be ensured. Therefore, this chapter investigated ensemble modelling for the assessment of PS and climate change effects on the ice cover of Sihlsee. To this end, three one-dimensional models (GLM, Simstrat and MyLake) were set up in addition to CE-QUAL-W2. For the latter, the strength of the impacts with increasing distance from the dam was also investigated. Climate change effects were simulated by forcing the models with 10×15 years of synthetic meteorological time series created with a weather generator based on the available air temperature scenarios A2 for north-eastern Switzerland. Future climate by the end of the 21st century was projected to shorten the ice-covered period by ~2 months and decrease ice thicknesses by ~13 cm. Extended PS operation would already affect the ice cover under current climate conditions. For example, the average probability of ice coverage on a specific day was projected to decrease by ~13% for current climate, and could further be reduced from ~45% to ~10% for future climate. Overall, the results of all models were consistent. Although the number of winters without ice cover was projected to increase for all one-dimensional models, studying individual segments of the two-dimensional model showed that the impact was pronounced for segments close to the PS intake/outlet. In summary, the reservoir's ice cover is expected to partially vanish with higher probability of open water conditions closer to the PS intake/outlet.

¹⁰ This chapter is based on the scientific article "Ensemble modelling of ice cover for a reservoir affected by pumped-storage operation and climate change" by U. G. Kobler and M. Schmid, which is under review for publication in *Hydrological Processes* at the moment of writing this thesis. The fieldwork, simulations and the analysis presented hereafter are original and were performed by the author of the thesis.

6.2 Introduction

Due to the increasing share of new renewable electricity production, additional storage capacity is needed, which explains the renewed interest in pumped-storage (PS) hydropower plants. As of 2017, PS operations provided 95% of the electricity storage (REN21 2017). However, they are also known to affect abiotic and biotic components of the connected water bodies (Bonalumi et al. 2011). The duration and thickness of ice covers are important drivers for lake ecology (Powers and Hampton 2016; Salonen et al. 2009), yet, they have been shown to be modified by PS operation (Bonalumi et al. 2012; Kobler et al. 2018).

Climate change is another important driver affecting lake ice cover. Benson et al. (2012) analysed long-term ice phenology data of 75 lakes where ice-on was delayed by 0.3 to 1.6 days per decade and ice-off was advanced by 0.5 to 1.9 days per decade. Magee et al. (2016) showed similar trends of delayed ice-on by ~ 0.9 days per decade and earlier ice-off by ~ 1.2 days per decade.

Besides observations, also modelling approaches were used to project the effect of climate change on lake ice. Dibike et al. (2011) analysed climate change effects over a range of latitudes (40-75°N) and a period of 80 years by modifying the atmospheric forcing according to SRES A2 emission scenarios with an air temperature increase of ~ 2 to 8 °C and a precipitation increase $\sim 10\%$ to 50% in winter. They used the one-dimensional lake model MyLake and projected delayed ice-on by 5 to 20 days, advanced ice-off by ~ 10 to 30 days, and reduced ice thickness by 10 to 50 cm. Moreover, they indicated that the snow cover on top of the lake ice would change from -15 to $+5$ cm, further affecting the white ice formation by -20 to $+10$ cm. Magee et al. (2016) also set up a one-dimensional hydrodynamic lake and ice model, DYRESM-WQ-I, to project the effect of a changing climate on lake ice thickness. They projected a decrease of thickness by ~ 1.3 cm per decade for a long-term simulation of the period 1911-2014 at Lake Mendota (Wisconsin, USA).

Changes in ice cover further affect ecological and socio-economic aspects. For example, diatom composition is influenced by changes of the length of the ice-covered period (Rühland et al. 2015). Moreover, Shuter et al. (2012) summarize important implications of the under-ice lake environment: low light intensity and water temperature in combination with depleted oxygen levels, little primary production, reduced metabolism, and impediment of visual feeders from finding sparsely available prey. Therefore, changes in ice phenology could result in alterations of fish growth and reproduction (Shuter et al. 2012).

The socio-economic aspects involve recreational activities (Leppäranta 2014), and changes in ice regimes may cause potentially hazardous conditions for the seasonal use of lake ice cover for transportation (Prowse et al. 2011).

Here, we investigate the combined effects of PS operations and climate change on ice cover in Sihlsee, the upper reservoir of a PS scheme in Switzerland. These effects were previously assessed using the laterally averaged two-dimensional model CE-QUAL-W2 both for different PS scenarios (Kobler et al. 2018) and interactions with projected future climate (Kobler et al.

2019). As the modifications of the ice-module of CE-QUAL-W2 by Kobler et al. (2018) were not tested comprehensively so far, the robustness of the projected effects on ice cover needs evaluation. For this purpose, we applied two additional one-dimensional vertical models (GLM and Simstrat). This allows addressing the following research questions: (i) how reliable are the projected impact of PS operation and climate change on lake ice, and (ii) do the effects on lake ice vary in the longitudinal direction of the water body?



Figure 6.1 Overview of the artificial upper reservoir Sihlsee, with all major natural in- and outflows as well as the location of PS intake/outlet and of ice observations.

6.3 Study site

Sihlsee is the upper artificial reservoir of Etzelwerk, which is already today operated as a PS hydropower plant (Figure 6.1). This reservoir, which was inundated in the 1930s, is on average 9 m deep, has a surface area and a volume of $\sim 11.3 \text{ km}^2$ and $96.1 \times 10^6 \text{ m}^3$, respectively. Its water level varies between 889.34 and 876.84 m a.s.l., thus, the storage capacity amounts to $89.4 \times 10^6 \text{ m}^3$ (Kobler et al. 2018). It is dimictic, with temperatures up to 25 and 15 °C in the epi- and the hypolimnion during summer stratification, and it is ice-covered in winter. Detailed information on the thermal structure and the water quality of this reservoir are given in Kobler et al. (2018). Ice cover has been observed weekly by the Swiss Federal Railways since 2001 in the northern part of the reservoir, closely located to the dam (Figure 6.1). Maximum ice thickness did not exceed 0.5 m. Its mean thickness during ice-covered periods ranged between 6.4 cm (2006/07) and 29 cm (2005/06). These point observations suggest that all winters in the period 2001 to 2015 were ice-covered with mostly one freeze-thaw cycle, except in winter 2006/07, when two freeze-thaw-cycles were observed. In some winters (2011/12 and 2014/15) the major freeze-thaw cycle was preceded by another short ice cover in early winter, which lasted for ~ 2 weeks. Additional information on the meteorological conditions from November to April of each winter season can be found in Section 7.3.

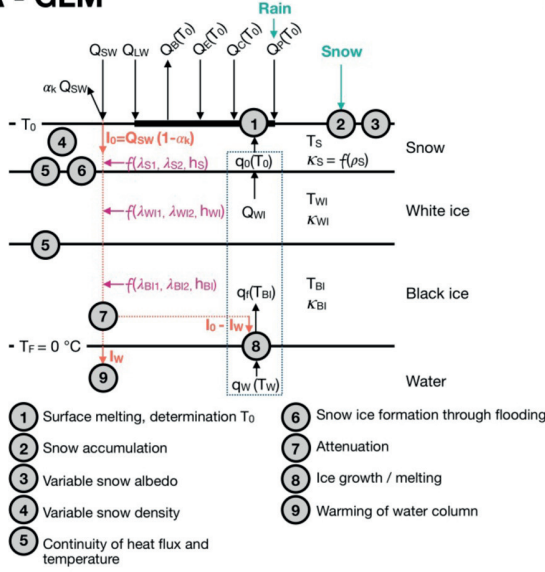
6.4 Methodology

6.4.1 Model description

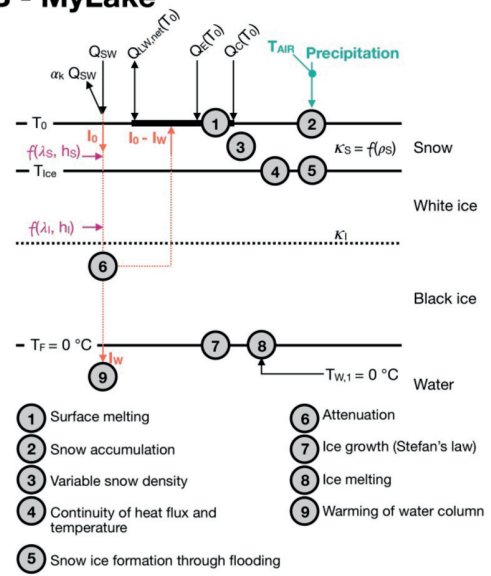
Three hydrodynamic models were set up to compare their capability of projecting the effects of PS operation and climate change on lake ice cover. A conceptual diagram of the ice modules of all four models is depicted in Figure 6.2.

The first model is CE-QUAL-W2, version 3.71. It is a two-dimensional laterally averaged hydrodynamic and water quality model, which was set up for this study site by Kobler et al. (2018), and allows for the direct coupling of the two water bodies connected by PS operation. This model was developed at Portland State University in cooperation with the US Corps of Engineers (Cole and Wells 2013), and requires bathymetric, meteorological, hydrological and water quality forcing, which has been described in detail by Kobler et al. (2018). The model is able to project stratification, dissolved oxygen and nutrient dynamics; however, the focus of this study lies on lake ice formation and decay.

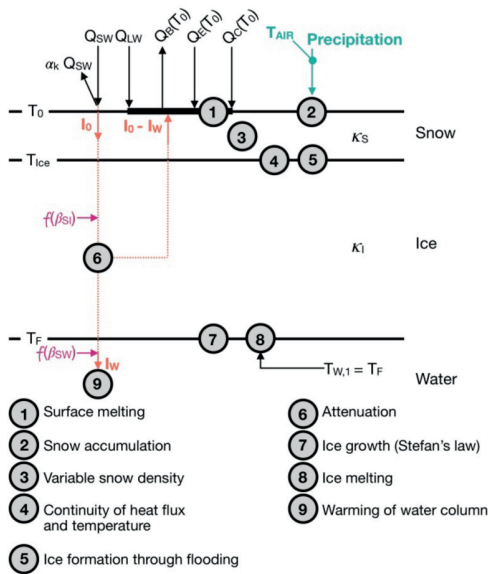
A - GLM



B - MyLake



C - Simstrat



D - CE-QUAL-W2

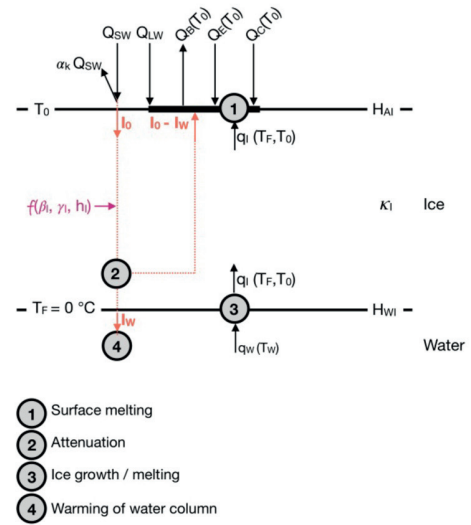


Figure 6.2 Conceptual diagrams of the ice models of (A) GLM, (B) MyLake, (C) Simstrat and (D) CE-QUAL-W2. The abbreviations refer to short-wave radiation (Q_{sw}), long-wave radiation (Q_{lw}), back (long-wave) radiation (Q_b), conductive heat flux (Q_c), latent heat flux (Q_e), net long-wave radiation ($Q_{lw,net}$), surface albedo of snow or ice (α_s), surface temperature (T_0), air temperature (T_{air}), incoming short-wave radiation entering the snow/ice layer (I_0), heat flux reaching water column (I_w), heat flux used for melting ($I_w - I_0$), snow height (h_s), height of white ice (h_{wi}), height of black ice (h_{bi}), ice height (h_i), attenuation coefficient of the visual spectrum for snow, white ice and black ice (λ_{s1} , λ_{w11} , λ_{b11}), attenuation coefficient of the infrared spectrum for snow, white ice and black ice (λ_{s2} , λ_{w12} , λ_{b12}), attenuation coefficient of snow and ice (λ_s , λ_i), conductive heat flux between snow (ice) cover and the atmosphere (q_0), heat flux in the ice at the ice-water interface (q_i), heat flux from the water column to the ice (q_w), heat flux due to white ice formation (Q_{wi}), heat flux through ice (q_i), temperature in the snow layer (T_s), temperature in the white ice layer (T_{wi}), temperature in the black ice layer (T_{bi}), temperature at the ice-snow-interface (T_{ice}), water temperature of the first layer underneath the ice cover ($T_{w,1}$), freezing temperature (T_F), conductivity snow (κ_s), conductivity white ice (κ_{wi}), conductivity black ice (κ_{bi}), conductivity ice (κ_i), density snow (ρ_s), fraction of incoming short-wave radiation absorbed in the uppermost water layer (β_{sw}), fraction of incoming short-wave radiation absorbed by snow and ice (β_{si}), fraction of incoming short-wave radiation absorbed in the ice sheet (β_i), ice extinction coefficient (γ_i).

For this purpose, we use a modified version of CE-QUAL-W2, which uses externally computed long-wave radiation forcing instead of calculating it from air temperature, vapour pressure and cloudiness. In addition some modifications were made regarding the penetration of short-wave radiation through the ice cover (Kobler et al. 2018). Within this study, we extend the work of Kobler et al. (2018, 2019), who analysed the effects of PS operation and climate change for one model segment in the deeper part of the reservoir, to the investigation of five segments with different distance from the dam, where PS flows are withdrawn and released. This allows assessing how the effects of PS operation spread throughout the reservoir.

Moreover, we set up two one-dimensional vertical hydrodynamic models. These two models were chosen based on their ability to define multiple in- and outflows, which could be specified either at a particular depth or relative to the water surface. The first of those two is the General Lake Model (GLM), version 2.4.1, which was developed at the University of Western Australia (Hipsey et al. 2018). Its lake ice module is based on the model described by Rogers et al. (1995). Comparing the publication by Rogers et al. (1995) to the source code of GLM revealed some bugs, which we corrected before model runs (Section 7.4). To be able to use a hydrological forcing as similar as possible to that prepared by Kobler et al. (2018), we also introduced the option to switch off the effect of evaporation and precipitation. Moreover, we introduced a scaling factor for the snowfall forcing, as first simulations revealed that using the entire snowfall would result in an overestimation of total ice thickness.

The second one-dimensional model is Simstrat, version 2.0, which is a modified version of the model originally published by Goudsmit et al. (2002). This model was developed at Eawag for the simulation of stratification and mixing dynamics in lakes, and its turbulence formulation is based on a k - ϵ -model. In version 2.0 of Simstrat a new lake ice module was implemented, which is based on the equations for lake ice formation and decay as used in the model MyLake (Saloranta and Andersen 2007). Regarding the penetration of solar radiation there are some differences between the two models: Simstrat assumes that the absorption of solar radiation is independent of ice and snow thickness, whereas MyLake considers a thickness-dependent exponential approach.

Therefore, we additionally set up MyLake, which, however, does not allow specifying outflows with a specific discharge or depth level different from the surface. Any withdrawal is computed internally and occurs at the surface in case of an overflow. Thus, we set up MyLake without any hydrological forcing (see also Section 6.4.4). Hourly meteorological forcing, generated with the weather generator VG (Schlabing et al. 2014) for all four models is based on previous studies of Kobler et al. (2018, 2019). For MyLake the meteorological forcing was adapted by averaging to daily resolution. Dew point was converted to relative humidity for GLM and MyLake and to water vapour pressure for Simstrat. While GLM, Simstrat and CE-QUAL-W2 use long-wave radiation as input, MyLake calculates it from cloudiness, air temperature and relative humidity following the approach of Dickey and Manov (1994). Thus, long-wave radiation projections of the weather generator were converted to cloudiness using the concept presented in section 3.3 of

Schmucki et al. (2014), and the computed long-wave radiation forcing of MyLake differs slightly from that of the other models.

For simulations with GLM, rain and snowfall were required as additional inputs. Both were computed from precipitation observed by MeteoSwiss at Einsiedeln. Rain was set equal to the observed precipitation whenever air temperature was $>0^{\circ}\text{C}$. For snow only precipitation events with air temperatures $<0^{\circ}\text{C}$ were considered, and precipitation was converted from water equivalents to snow height using a snow density of 100 kg m^{-3} . MyLake also required daily air pressure, which is provided from observations of the Federal Office of Meteorology and Climatology MeteoSwiss at Einsiedeln.

In GLM, sub-daily values can be used for the meteorological forcing¹¹, but the hydrological forcing can only be specified with a daily resolution. The water balance correction term, described in Kobler et al. (2018), needed to be adapted by a few percent for GLM and Simstrat because the volume is approximated differently for the vertical layers of these two models than it is computed based on the two-dimensional grid of CE-QUAL-W2.

The natural inflows were implemented as surface inflows. For GLM this is the standard setting for inflows, for Simstrat the surface inflows were designed to always intrude in the top 2 meters of the water column. To depict the PS pumping flows, GLM offers the option of submerged inflows at a given distance from the lake bottom. In Simstrat inflows can be placed at a specific depth level or relative to the initial water surface. It also offers the choice to distribute an inflow over a depth range where we chose 5 m (between 867.75 and 872.75 m a.s.l.) to depict the outlet/intake situation of the PS hydropower plant.

The PS generating and the residual flow of River Sihl are both withdrawn from the same depth range as the PS pumping flow. The correction term is added to the natural inflows if it is positive, and withdrawn from the top 2 m relative to the surface if it is negative. For GLM the residual outflow and the PS generating flow are withdrawn by an outlet type 1, which corresponds to an outflow from a fixed depth (870 m a.s.l.). The correction term of the water balance is treated similarly to Simstrat if positive, and withdrawn at 1 m below surface using an outlet type 2 if negative. Salinity was assumed to be constant for both GLM and Simstrat.

While GLM and MyLake compute black ice, white ice and snow thickness, the current version of Simstrat only calculates the overall ice and snow thickness, although it internally computes ice growth due to freezing of slush, which is formed whenever the weight of the snow exceeds the buoyancy of the ice. CE-QUAL-W2 solely computes the overall ice thickness without any snow coverage.

The temperature of the PS pumping flow was taken from previous projections of the epilimnion temperature of Upper Lake Zurich for either considering observed meteorological conditions (Kobler et al. 2018) or time series of current and future climate conditions developed with a weather generator (Kobler et al. 2019).

¹¹ Hourly resolution in the present study.

6.4.2 Sensitivity analysis

The sensitivity of ice formation to the model parameters is depicted in Section 7.5. The purpose of this analysis was to determine the influence of the most relevant model parameters on the snow, white ice and black ice formation. For GLM this analysis showed the necessity of introducing a scaling factor of the snow forcing.

6.4.3 Model calibration

Due to not considering any hydrological forcing, MyLake could not be calibrated with the temperature observations, since the observed temperature in the reservoir for the present PS scenario is strongly modified by the hypolimnetic withdrawal (Kobler et al. 2018).

GLM and Simstrat were both calibrated using PEST (Doherty 2010) to observed water temperatures. PEST is a model-independent parameter estimation and uncertainty analysis software package. Through a robust variant of the Gauss-Marquardt-Levenberg method, computation time can be reduced compared to other optimization methods, yet, the risk that the optimization could get trapped at a local minimum prevails (Doherty and Johnston 2003). Observed ice-thicknesses were not used for calibration.

Short-wave radiation was scaled for all four models similar to CE-QUAL-W2 with a factor of 0.85. This scaling was necessary to reproduce surface water temperature with CE-QUAL-W2. For GLM, the considered calibration parameters include a coefficient for hypolimnetic mixing (`coef_mix_hypo`), as well as factors for scaling long-wave radiation (`lw_factor`) and wind speed (`wind_factor`). Simstrat was calibrated using the following model parameters: a parameter, defining how much energy is transferred from wind to seiching (`a_seich`), and scaling factors for wind speed (`f_wind`) and long-wave radiation (`p_radin`). All model parameters and initial conditions are summarised in Section 7.6.

The root-mean-square-errors (RMSE) of simulated water temperatures using GLM were 1.35, 1.10 and 1.18 °C for the entire water column, the epi- and the hypolimnion, respectively. For Simstrat the RMSE attained values of 1.13, 0.80 and 1.31 °C. RMSE, mean absolute error (MAE) and the mean errors (ME) are summarised in Table 7.4. Altogether, these RMSEs were slightly higher than those achieved with CE-QUAL-W2 (~0.94, ~0.93, ~0.94 °C) by manual trial and error calibration (Kobler et al. 2018).

6.4.4 Pumped-storage scenarios

Four different PS scenarios were developed by Kobler et al. (2018), the present and an extended PS operation scenario as well as two reference scenarios.

Under present PS operation Etzelwerk is mostly managed like a storage hydropower plant, with mean monthly artificial flows of ~ 6 to $8 \text{ m}^3 \text{ s}^{-1}$ for generating and $\sim 1 \text{ m}^3 \text{ s}^{-1}$ for pumping. Water is withdrawn from the hypolimnion of Sihlsee and released to the epilimnion of Upper Lake Zurich during the generating cycle. Additionally, a residual flow is discharged from the hypolimnion to River Sihl (Section 7.2). The current hydraulic residence time amounts to ~ 135 days (Kobler et al. 2018).

For extended PS operation the artificial flows are increased differently for generating and pumping with factors ranging between ~ 1 to 5 and ~ 9 to 40 , respectively. The hydraulic residence time of the reservoir would change to ~ 40 days for this scenario.

The first reference scenario QNat (“quasi-natural”) depicts the “theoretical” natural state of the reservoir, if the dam were of natural origin. Regime analysis of the runoff of River Sihl before the dam was built were used to generate time series for this outflow (LIMNEX AG, 2016, personal communication), which is discharged over a weir. The residence time would increase by ~ 15 days compared to the present PS scenario. In contrast to the other scenarios, water withdrawal takes place in the epilimnion.

For the second reference scenario the outlet of the residual flow is kept in the hypolimnion, yet, the discharge rate was computed similarly to that of the reference scenario QNat. Therefore, the residence time would be similar to that of QNat. This scenario was developed originally to disentangle the effects of deep-water withdrawal and those of PS operation.

In this publication we introduce a modified version of the first reference scenario, referred to QNat*, which differs from QNat by switching off all hydrological forcing. This scenario was used exclusively for setting up MyLake.

6.4.5 Climate scenarios

Similar to Kobler et al. (2019) we generated ten synthetic time series for current (1997-2012) and future (2077-2092) climate conditions. These time series were developed using the weather generator VG (Schlabing et al. 2014), which allows emulating the observed variables or generating future conditions by changing mean or variability. Similar to Kobler et al. (2019) we increased air temperature compared to present day conditions according to regional projections of the Swiss Climate Change Scenarios CH2011 (2011) for the IPCC A2 emission scenario in 2085 for north-eastern Switzerland and each day of the year. VG was then utilized to compute all other meteorological forcing variables and inflow water temperatures, maintaining the dependencies of observed values during the period 1997-2015. The air temperature increases from CH2011 (2011) vary seasonally and range from $\sim 3^\circ \text{C}$ (Sep) to $\sim 4.5^\circ \text{C}$ (Aug).

6.4.6 Aggregation of results

All four models were run for the period 1997-2012, allowing for a spin-up phase of one year. Thus, the results presented hereafter, were generated for the time range 1998-2012. In Section 6.5.1 the simulations based on meteorological observations for that period are described. The projections for VG generated climate scenarios, each comprising a total of 10×15 years of simulations, were aggregated and are presented in Section 6.5.2.

For each day of the year, the probability of the presence of ice cover was estimated as the fraction of winters with ice on that day. Monthly means of ice thickness were calculated by averaging the projections for each scenario over the 150 simulated years.

The comparison of projections for different segments of CE-QUAL-W2 does not show the results for segment SEG 8 in case of the present PS scenario and those of segment SEG 8 and SEG 16 for the extended PS scenario, as these segments could fall dry during the ice-covered season (Section 7.2).

6.5 Results

6.5.1 Comparison of observations and simulations

Mean and maxima of observed and simulated ice thickness are given in Table 6.1. On average simulated ice thicknesses by GLM exceed observations by ~33% for the mean of each winter and by ~9% for the maximum. Simstrat's mean and maximum ice thickness simulations deviate from observations by ~9 and ~2%, those of MyLake by ~4 and ~10% and those of CE-QUAL-W2 by ~7 and ~3%. The mean absolute error of simulated and observed ice thicknesses remains below 8 cm for all models.

Observed and simulated ice-on and ice-off dates are summarized in Table 6.2. Since the time resolution of the measurements is weekly, the model reproduces are also given with this resolution. For the cases of simulated multiple freeze-thaw-cycles that do not coincide with observations, the first date of ice-on is shown in brackets (Table 6.2). GLM generally simulates an earlier ice-on and a delayed ice-off with average differences of ice-on and ice-off of ~1 and ~2 weeks, respectively. Multiple freeze-thaw cycles like in 2006/07 and those in early winter of 2012/13 and 2014/2015 are not captured by GLM simulations.

Table 6.1 Mean and maximum of observed and simulated ice thicknesses (cm) for each individual winter period as well as the mean of all winter seasons, the mean absolute error (MAE) and the mean error (ME) of simulated and observed ice thicknesses.

Winter	Observed ice thickness [cm]		Simulated ice thickness [cm]							
	Mean	Max	CE-QUAL-W2		MyLake		GLM		Simstrat	
			Mean	Max	Mean	Max	Mean	Max	Mean	Max
2000/01	14	28	12	27	16	28	19	26	12	28
2001/02	18	30	26	47	28	39	26	37	34	36
2002/03	26	42	22	39	24	37	24	39	25	39
2003/04	18	37	14	26	20	32	26	37	13	26
2004/05	22	43	29	48	22	41	30	51	22	44
2005/06	26	42	41	56	36	56	38	57	39	60
2006/07	6	18	8	25	7	17	18	24	7	20
2007/08	21	29	21	29	15	23	24	35	11	23
2008/09	25	44	24	35	22	34	28	39	30	43
2009/10	20	35	23	39	24	38	24	36	27	44
2010/11	20	29	18	27	17	23	24	33	19	26
2011/12	12	26	16	35	18	31	24	38	19	34
2012/13	15	34	15	29	20	28	23	36	15	22
2013/14	16	30	8	14	0	0	20	26	6	10
2014/15	13	25	14	25	11	18	16	23	17	27
Mean	18	33	19	33	19	30	24	36	20	32
MAE	-	-	4	7	5	7	6	5	5	7
ME	-	-	1	1	1	-3	6	3	2	-1

Table 6.2 Observed and simulated ice-on and ice-off (week number) for each individual winter and the mean of all considered winter periods as well as the mean absolute error (MAE) and the mean error (ME) in days between simulations and observations; values in brackets indicate the first week with ice out of several freeze-thaw-cycles in early winter.

Winter	Cycle	Observations [week number]		Simulations [week number]							
		Ice-on	Ice-off	CE-QUAL-W2		MyLake		GLM		Simstrat	
				Ice-on	Ice-off	Ice-on	Ice-off	Ice-on	Ice-off	Ice-on	Ice-off
2000/01	1	2	15	3	11	53	13	52	15	(51)	10
2001/02	1	50	15	50	12	50	15	50	16	50	6
2002/03	1	49	14	(50)	14	1	17	50	17	2	13
2003/04	1	51	14	52	14	51	17	49	17	(49)	12
2004/05	1	1	14	50	14	50	15	49	17	(49)	13
2005/06	1	51	16	50	16	50	18	48	19	(48)	18
2006/07	1	50	2	52	2	51	3	51	14	51	1
2006/07	2	3	9	4	9	4	8	-	-	(4)	7
2007/08	1	49	11	51	10	50	15	50	16	(46)	8
2008/09	1	52	15	(50)	14	52	16	50	16	49	14
2009/10	1	52	14	51	13	51	15	51	15	51	14
2010/11	1	50	13	51	12	50	13	49	14	50	14
2011/12	1	51	1	-	-	-	-	-	-	49	50
2011/12	2	2	13	2	13	52	16	52	15	50	11
2012/13	1	50	2	50	52					(52)	13
2012/13	2	2	16	3	15	3	16	50	17	(49)	15
2013/14	1	49	12	50	11	-	-	50	14	(48)	11
2014/15	1	52	2	(1)	(2)	52	2	-	-	52	(2)
2014/15	2	2	13	4	13	4	14	3	15	3	13
Mean		52	11	52	11	52	13	50	16	50	10
MAE [days]		-	-	8	6	7	8	10	12	15	12
ME [days]		-	-	3	-6	0	7	-7	15	-8	-11

The current version of Simstrat suffers from the fact that the ice cover disappears rapidly as soon as all overlying snow has melted independent of its thickness. This issue, particularly, appears in the winter season 2001/02 (Section 7.7), where the ice melts ~8 weeks too early. Therefore, ice-off is often simulated to occur earlier than observed with an average difference of ~1.5 weeks. Moreover, in early winter the model produces multiple freeze-thaw-cycles (e.g., 2007/08, 2011/12), which were either not captured by the weekly observations or are a numerical artefact. However, ice-on simulations differ only by ~1.1 weeks from observations.

The temporal dynamics of lake ice simulations with CE-QUAL-W2 show a slightly delayed ice-on by ~0.4 weeks and an earlier ice-off by ~0.9 weeks. The occurrence of multiple freeze-thaw-cycles matches well not only for 2006/07, but also for these episodes in early winter (2012/13 and 2015/16). Yet, the ice thickness simulations differ in some winters, which could result from the fact that only a fixed albedo is considered in this model.

For the winter period 2006/07, the ice thickness estimate exceeds the observations by between ~6 cm and ~17 cm for all considered models, which could result from the lowest average air temperatures of the entire studied period for that winter (Section 7.7).

6.5.2 Effects due to pumped-storage operation and climate change

Climate warming reduces the probability that the upper reservoir is ice-covered in winter (Figure 6.3). The average probability that the lake is ice-covered on a specific day from November to April is reduced by ~32% to ~37% for the reference scenarios QNat and QNat* (percentages for all cases are given in Section 7.8). PS operation has an additional influence on lake ice cover. Under future climate, all models show a slightly higher probability of ice coverage for the present PS scenario than for the two reference scenarios. For the extended PS scenario this probability decreases on average to ~45% considering current climate, and to ~10% for future climate. The reduced probability of lake ice coverage is least pronounced for GLM and most evident for CE-QUAL-W2 (Figure 6.4).

Due to climate change, the duration of ice-covered periods will be shortened on average by ~1.9 months for the present PS and the two reference scenarios. For QNat* MyLake projections even result in a reduction of ~2.6 months. Extended PS operation also reduces the ice cover duration by ~0.8 months (mean of all model projections, Section 7.8) already for the current climate. This reduction is most evident for the simulations of CE-QUAL-W2. Climate change results in another reduction by ~1.7 months (average of all model results), which is most pronounced for GLM.

For climate change alone, the ice-on of all models is delayed by ~2.4 to ~3.6 weeks, and three models (GLM, Simstrat and CE-QUAL-W2) project an earlier ice-off by ~3.4 to ~4 weeks. The MyLake predictions for QNat* even indicate an advancement of ice-off by ~7.1 weeks. Both an advanced ice-off (~1.1 weeks) and a delayed ice-on (~1.5 weeks) also result in a reduced duration

of the ice-covered period for extended PS operation under current climate. Considering future climate for the extended PS operation, the effects on ice-on and ice-off are even more pronounced. Our results, furthermore, suggest that the effect on ice-off is stronger than on ice-on for extended PS operation.

For climate change alone, the ice-on of all models is delayed by ~2.4 to ~3.6 weeks, and three models (GLM, Simstrat and CE-QUAL-W2) project an earlier ice-off by ~3.4 to ~4 weeks. The MyLake predictions for QNat* even indicate an advancement of ice-off by ~7.1 weeks. Both an advanced ice-off (~1.1 weeks) and a delayed ice-on (~1.5 weeks) also result in a reduced duration of the ice-covered period for extended PS operation under current climate. Considering future climate for the extended PS operation, the effects on ice-on and ice-off are even more pronounced. Our results, furthermore, suggest that the effect on ice-off is stronger than on ice-on for extended PS operation.

Ice thickness is projected to decrease on average by ~13 cm under future climate (Figure 6.4, Section 7.8). Extended PS alone already leads to reduced ice thickness ranging from ~3 to ~9 cm for current climate and future climate results in an additional decrease of ~11 cm (mean of all models).

The simulations with CE-QUAL-W2 allow assessing the effects of the distance to the dam. In general, the probability of occurrence of an ice cover decreases towards the dam (

Figure 6.5, Section 7.8). For any reference scenario under current climate conditions, the probability that the reservoir is ice-covered in the period from November to April ranges between 55 and 48% for segments SEG 8 and SEG 40, respectively (Table 7.6). Similar trends exist for all other PS scenarios, and the additional effect of climate change is also stronger closer to the dam. For example, the combination of future climate and extended PS operation results in reduced probability of ice coverage in the range of ~13 to ~1%.

Ice thickness is also projected to decrease more for segments located closer to the dam (Figure 6.6, Section 7.8). The mean reduction for future climate conditions amounts to <12 cm for the present PS and the two reference scenarios. For the extended PS operation ice thickness is already reduced on average by ~4 cm (SEG 24, SEG 32) and ~9 cm (SEG 40) for current climate. Future climate conditions would enhance this reduction by additional ~9 cm (SEG 24, SEG 32) and ~7 cm (SEG 40).

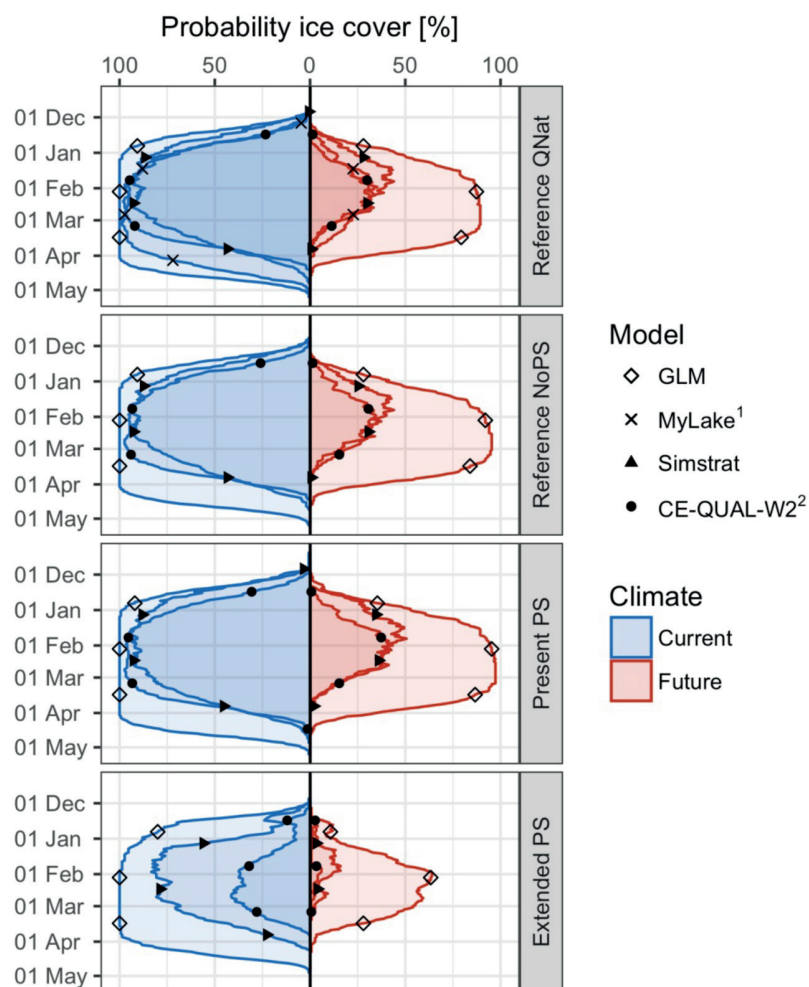


Figure 6.3 Probability (%) of lake ice coverage for current (blue) and future (red) climate conditions for each day from mid-November to end of April, separated by model (markers) and by PS scenario (rows). ¹For MyLake only the scenario QNat* is depicted. ²For CE-QUAL-W2 the projections for segment SEG 40 are depicted.

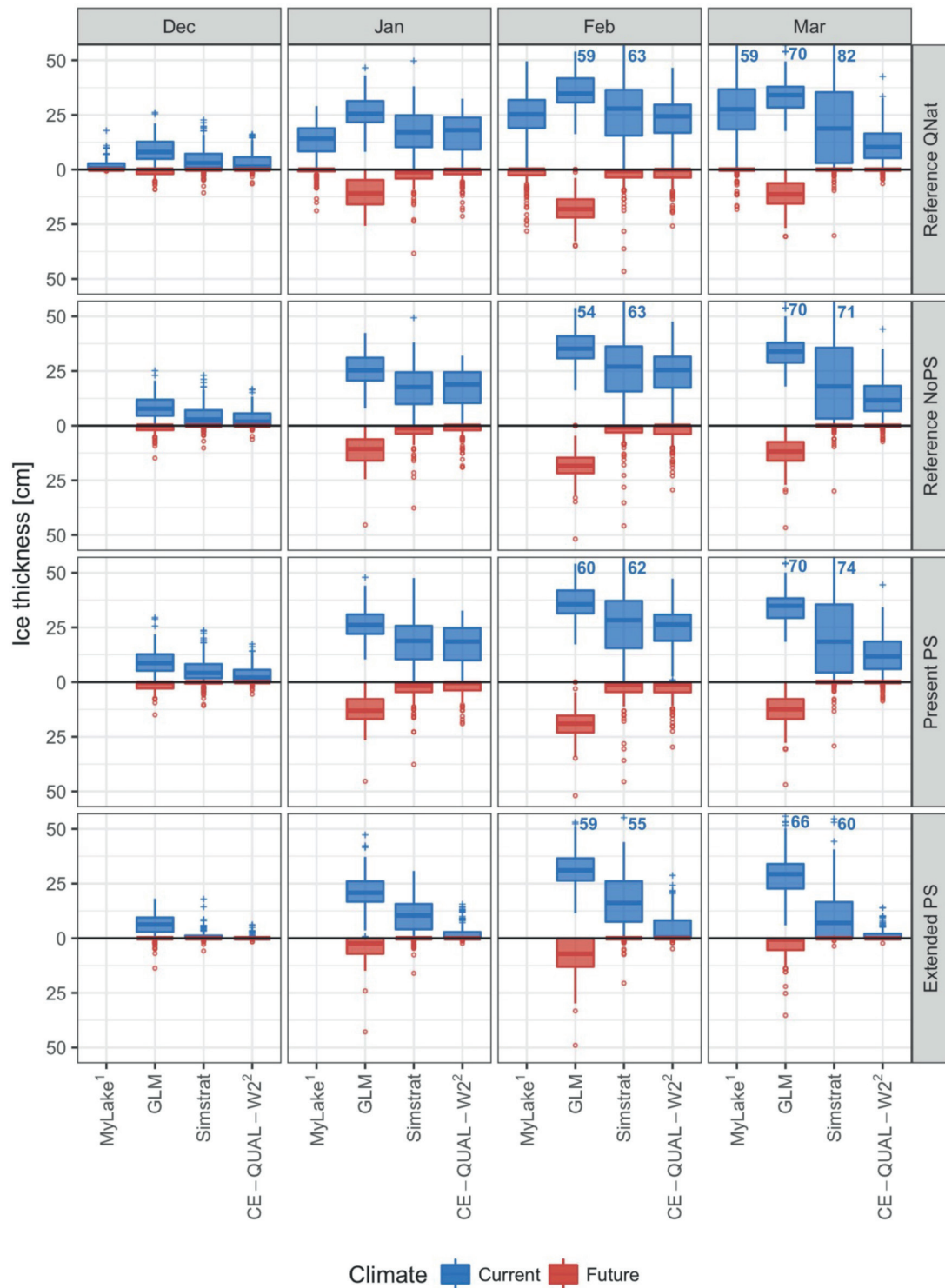


Figure 6.4 Boxplot of ice thicknesses (cm) from December to March under current (blue) and future (red) climate conditions, separated by model (columns) and by PS scenario (rows). Numbers in blue indicate the maximum value out of the range of the y-axis. ¹For MyLake the scenario QNat* is depicted. ²For CE-QUAL-W2 the projections for segment SEG 40 are depicted.

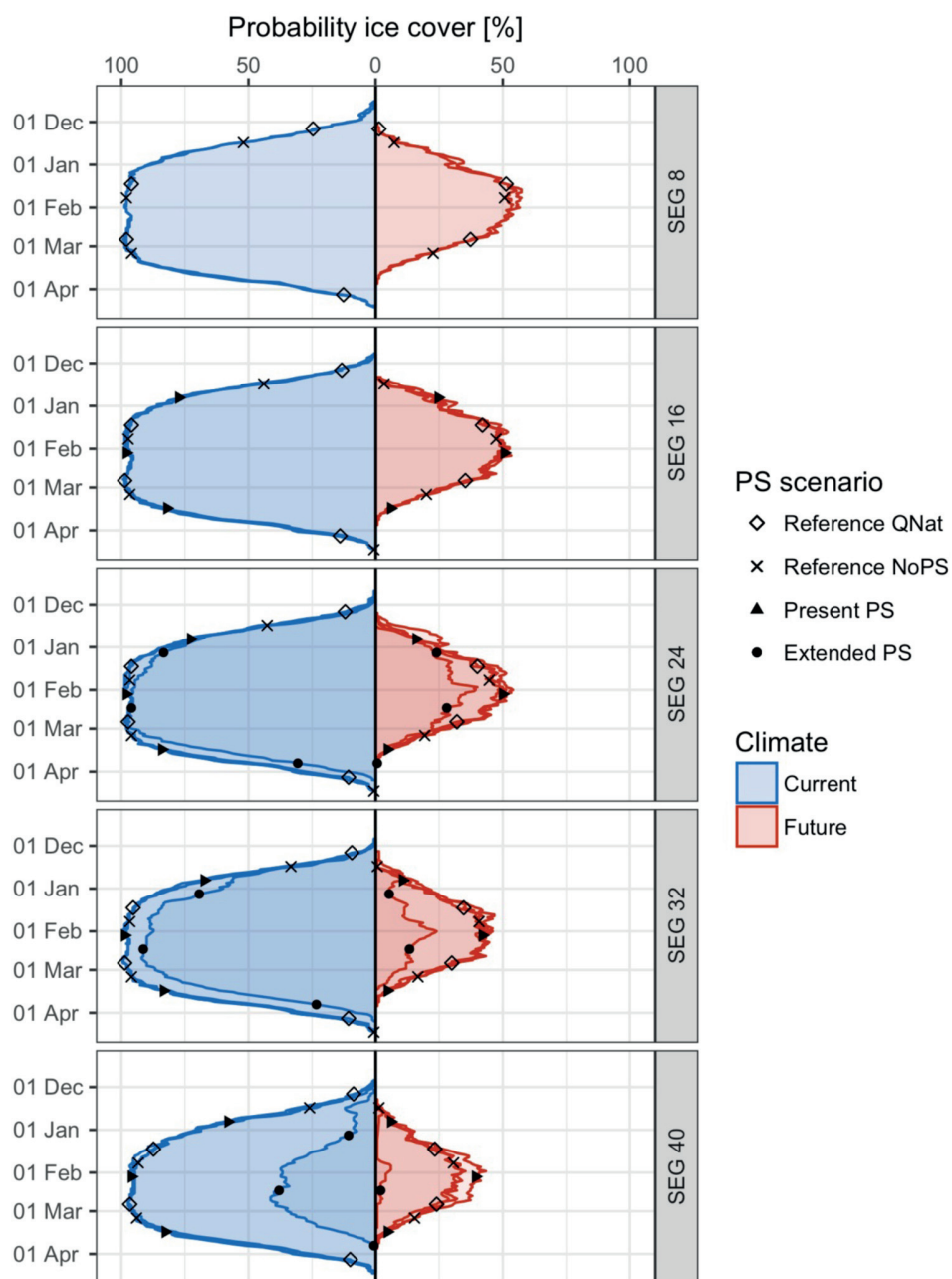


Figure 6.5 Probability (%) of lake ice coverage for current (blue) and future (red) climate conditions for each day from mid-November to mid-April, separated by model segments of CE-QUAL-W2 (rows) and by PS scenario (markers). For segment SEG 8 both PS scenarios are not depicted, and for SEG 16 the extended PS scenario is not shown.

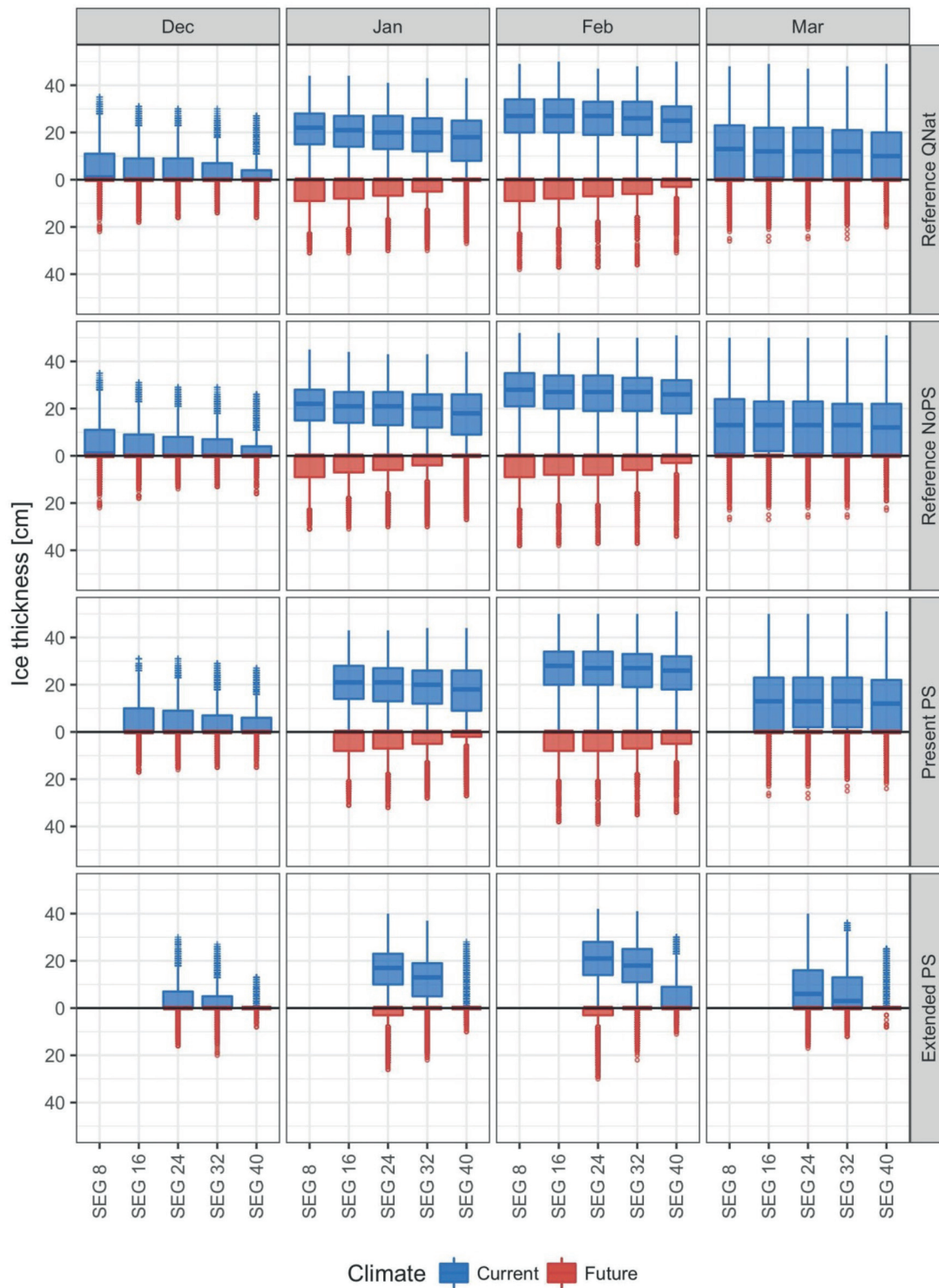


Figure 6.6 Boxplot of ice thicknesses (cm) for each month of the period December to March under current (blue) and future (red) climate conditions, separated by model segments of CE-QUAL-W2 (columns) and by PS scenario (rows).

6.6 Discussion

All models project a decreasing probability of ice coverage with climate change. In the reference scenarios and the present PS scenario, less than every second winter will see ice cover under future climate, as estimated with CE-QUAL-W2 and Simstrat. Results from MyLake even suggest that an ice cover would form only about every fourth winter. This difference for MyLake might be explained by the fact that no hydrological forcing besides the natural inflows was considered. The projected ice coverage by GLM contrasts with the other three models, with the probability of ice cover formation remaining at ~90% or higher (Figure 6.3). This is also reflected in different ice thickness: while for GLM ice thickness amounts to ~16 cm for both reference scenarios and the present PS scenario under future climate, the average ice thickness remains <10 cm for the other three models.

All models consistently project that extended PS would slightly delay ice-on and advance ice-off already under current climate. For all models, the shift in ice-off is more pronounced than that in ice-on, which is further enhanced by future climate. The average probability that the reservoir is ice-covered on a specific day in winter is reduced by ~16% for Simstrat and by a range of ~5% to ~36% for CE-QUAL-W2, dependent on the distance to the PS intake/outlet, but not significantly affected according to GLM (~7%). A reduction of the mean ice thickness by ≤ 5 cm is projected by GLM and Simstrat as well as for the segments of CE-QUAL-W2 located farther from the PS intake/outlet. For segments closer to the intake, the projections show a decrease by up to ~9 cm. Mean absolute ice thicknesses drop to ~25 cm (GLM), ~19 cm (Simstrat) and ~11 to 17 cm (CE-QUAL-W2).

The combination of extended PS operation and future climate results for all models in a massively reduced probability of ice coverage. For GLM the average probability of ice cover on a specific day between November and April would be reduced to ~21%, for Simstrat even to ~3%, and for CE-QUAL-W2 this value ranges from ~1% to ~13% with larger values for segments located farther away from PS intake/outlet. While the projections of Simstrat and GLM suggest that there will still be ice cover during some winters for the entire lake, those of CE-QUAL-W2 draw a spatially variable picture. Ice cover is expected to completely vanish in segments close to the PS intake/outlet but will still occur occasionally in segments located further away.

Regarding climate change impacts on the ice cover, our findings are in line with those of Gebre et al. (2014a). They analysed climate change impacts on lake ice with regionally downscaled output of global climate models, with an air temperature increase for the 2080s ranging between 2.2 °C and 5.7 °C, and set up MyLake for a variety of hypothetical lakes all over Scandinavia. Their projections show a reduction of mean annual maximum ice thickness in a range of ~3 to 59 cm, along with a delayed ice-on (5 to 26 days) and a progressing ice-off (11 to 73 days). These projections are not significantly affected by the depth of these hypothetical lakes.

Similarly, Yao et al. (2014) projected shortening of the ice-covered seasons by ~48 days and decreases of ice thickness by 17 cm (average projections of all models) towards the end of the

century, which corresponds to reductions of ~40% for ice cover duration and ~52 % for ice thickness. Their climate scenarios were based on the Canadian Regional Climate Model with an increase of the annual mean air temperature by ~6 °C but no significant changes for precipitation. Their projections varied quite strongly between different models for both ice duration and ice thickness.

While both Yao et al. (2014) and Gebre et al. (2014a) considered a climate change effect on precipitation, our study did not include this forcing factor. In general the future climate impact on precipitation suggests for north-eastern Switzerland a small increase of winter precipitation (CH2011 2011) with an expected shift from snow to rain. The reduction of snowfall would result in thinner snow cover on top of the ice sheet, and, therefore, less white ice could be expected. Moreover, with less snow on top of the ice sheet the albedo would decrease, which further enhances the declining trend of ice thickness for future climate conditions. The increasing amount of liquid precipitation would also enhance the trend of a decreasing ice thickness.

Out of the four models in the study of Yao et al. (2014), GLM was least sensitive to climate change. This is supported by our findings, where GLM predicts only a slight reduction of the probability of ice coverage. Thus, the recommendation of Bueche et al. (2017) to apply GLM for studying climate change effects needs to be considered with care, particularly for the winter period.

Regarding the effects of PS operation on lake ice cover, our findings support the reduction of ice thickness described by Kobler et al. (2018) and Bonalumi et al. (2012). However, the analysis of additional segments adds another dimension to the conclusions given in Kobler et al. (2018, 2019). These two studies showed a decreasing trend of lake ice thickness of ~30% for a segment located close to the PS intake/outlet considering current climate and concluded that these results were valid for the entire reservoir. Yet, the more detailed analysis herein shows that this reduction mainly occurs close to the PS intake/outlet. Thus, only the probability of winters with a partial ice cover would increase and not that of completely ice-free winters. Similarly, the projection by Kobler et al. (2018) that ice cover would completely vanish for the combination of extended PS operation and climate change is only valid for locations close to the intake/outlet, whereas ice cover is expected to still occur in some winters in other parts of the reservoir.

In general, the differences between modelled and observed ice-on, ice-off and ice thickness are in the range referred to in Dibike et al. (2011), who showed mean absolute deviations of 6.2 and 5.8 days for ice-on and ice-off, respectively, and 11 cm for ice thickness. However, our results suggest that the computed ice-on of GLM advances observations by ~2 weeks, which is contrary to the good agreement between GLM projections and observations described by Yao et al. (2014). Yet, they are in line with the results of Bueche et al. (2017), who applied GLM to Lake Ammersee, which only froze over once during their studied period. Although they had only qualitative information of the ice coverage for that specific winter, their results suggest that the projected ice-on preceded the observations. In our study, ice-on is best predicted with MyLake, followed by CE-QUAL-W2 and then on par by Simstrat and GLM. Ice-off is predicted best with

CE-QUAL-W2, followed by MyLake, Simstrat and GLM, in line with the results of Yao et al. (2014), where GLM was outperformed by two other models.

Some models were able to project the occurrence of multiple freeze-thaw-cycles. Particularly, CE-QUAL-W2, Simstrat and MyLake, were able to capture the observed dynamics of two freeze-thaw-cycles in 2006/07. In 2014/15 these three models reproduced the development of a freeze-thaw-cycle prior to the development of the main ice-covered period.

Although the ice model of Simstrat is based on MyLake, there are some relevant differences. Particularly in Simstrat, ice melts quickly once snow cover has disappeared, which is not projected with MyLake. One possible reason is the different formulation of the absorption of short-wave radiation in the ice cover (Section 7.7). In case of MyLake, and also for GLM and CE-QUAL-W2, the attenuation is implemented through an exponential thickness-dependent approach, whereas for Simstrat a constant value is assumed independent of the ice thickness and the actual condition of the surface (ice or snow). Although MyLake does not consider different albedos for black and white ice (Cheng et al. 2008), it would be interesting to consider this for the further development of Simstrat. In summary, there is still potential for improving the physical description of the lake ice cover in all models used in the present study.

6.7 Conclusions

To assess the robustness of previous projections of the impact of PS operation and climate change on timing, duration and thickness of the ice cover on Sihlsee with the two-dimensional model CE-QUAL-W2, we applied three one-dimensional vertical models, GLM, Simstrat and MyLake. Two of these models (GLM and Simstrat) were calibrated with PEST and could well reproduce observed water temperatures, particularly in the epilimnion.

Overall, these three models projected a reduction of ice thickness and the duration of the ice-covered period due to climate change ranging from ~1.4 months for GLM to ~2.6 months for MyLake. Mean ice thickness was projected to decline by up to ~16 cm (Simstrat). Projected impacts of extended PS differ between the models already under current climate conditions. While GLM only shows minor effects on both the thickness and duration of the ice cover, Simstrat and CE-QUAL-W2 project reductions of the ice thickness of ~5 cm and up to ~9 cm, respectively. For the combination of extended PS operation and future climate, the divergences between models are further amplified. For example, the longest uninterrupted ice-covered period remains up to ~40 days longer in GLM than in Simstrat and CE-QUAL-W2. The major differences between GLM and the other models might be explained by the fact that the overall ice thickness seems to be overestimated by GLM.

In addition, we assessed the spatial variability of ice cover projections in different segments of CE-QUAL-W2. Results show that the ice thickness is decreasing less for segments located farther

from the dam. Considering, only extended PS operation the longest uninterrupted ice-covered period would decrease by ~10, ~17 and ~60 days for segments 24, 32 and 40, respectively. Climate change on the other hand would reduce this period by another ~38 days. Yet, the combination of climate change and PS impacts would still result in a partial ice cover for most winters. Additionally, we want to stress that, so far, no mechanistic ice model has been applied to PS reservoirs. As our projections have, however, already shown an impact on the ice thickness in late winter, it would be interesting to study how this decreasing ice thickness would further affect ice movement induced by wind and currents.

Chapter 7

Supplementary material to Chapter 6¹²

7.1 Overview

This chapter provides supplementary information to Chapter 6. In the first section of this chapter an overview of the selected segments of CE-QUAL-W2 is depicted, which also shows, which segments are falling dry and therefore, are not presented in Chapter 6. Additionally, this chapter presents (a) the meteorological forcing for each winter season (referring to the period from November to April), (b) how the source code of GLM was adapted, (c) the results of sensitivity analysis of all four models, (d) information on the calibration of GLM and Simstrat with comparative figures of epi- and hypolimnetic temperatures, information on the RMSE, MAE and ME, parameter values and initial conditions, (e) the simulation results for black ice, white ice and snow using observed meteorological conditions, which are described and discussed in Chapter 6 in detail. Moreover, tables with values for (a) the mean duration of the longest uninterrupted ice-covered periods, (b) the average probability that the lake is ice covered on a specific day during the winter period (November to April), and (c) the mean ice thickness over all ice-covered periods is provided for all four models and for each combination of PS and climate scenario.

¹² This chapter is based on the supplementary information to “Ensemble modelling of ice cover for a reservoir affected by pumped-storage operation and climate change” by U. G. Kobler and M. Schmid, which is under review for publication in Hydrological Processes at the moment of writing this thesis. The fieldwork, simulations and the analysis presented hereafter are original and were performed by the author of the thesis.

7.2 Selected segments in CE-QUAL-W2

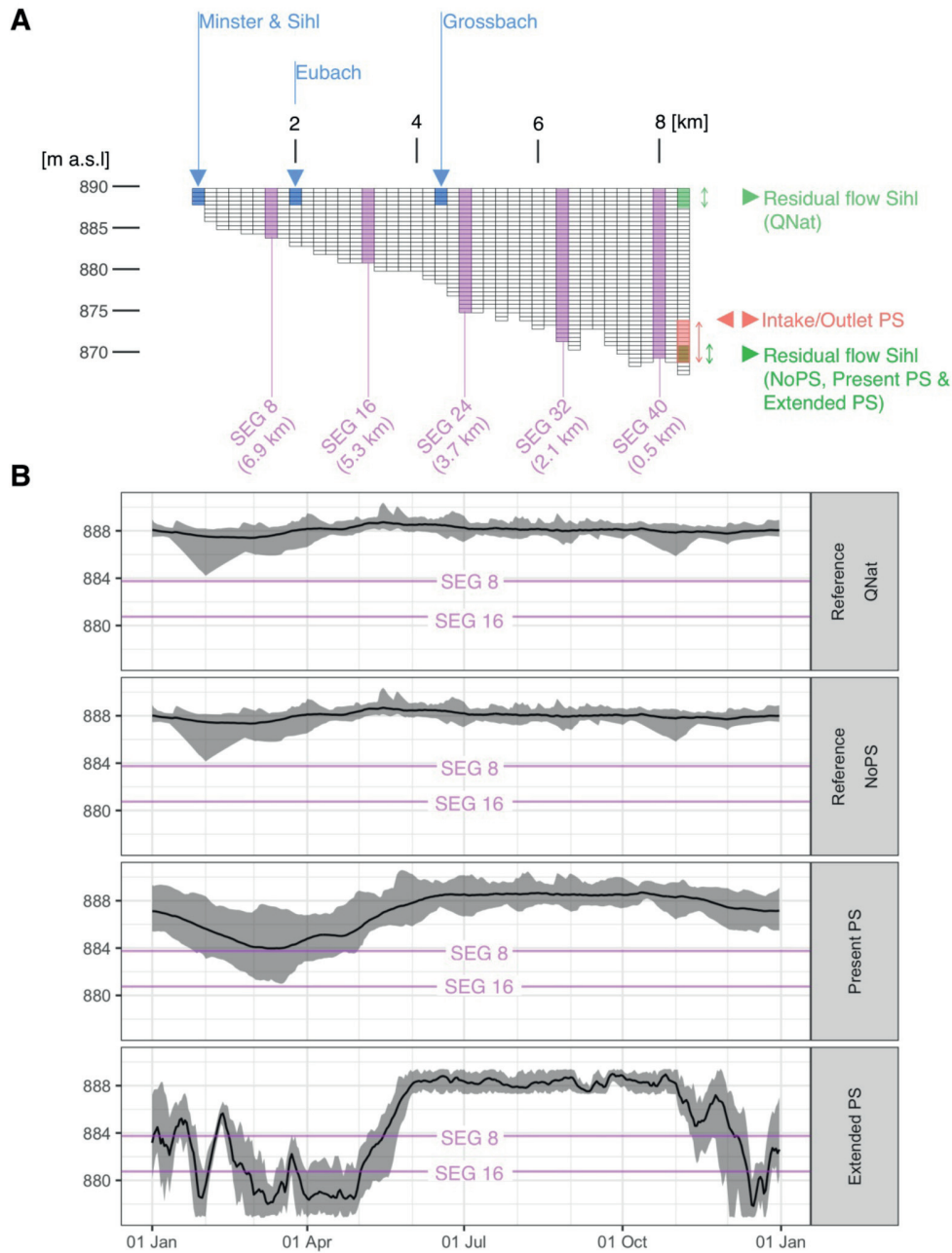


Figure 7.1 (A) Overview bathymetry of CE-QUAL-W2, with the location of all in- and outflows: natural inflows (blue), residual flow (green), and artificial intake/outlet (red); violet shows the selected segments and their distance from the dam is shown in brackets. (B) Water level elevation (m a.s.l.) for all four PS scenarios over the period 1998-2012: depicted are mean (black line) and range of minimum and maximum (shaded area) for each day of the year; in violet the minimal possible water level for segments SEG 8 and SEG 16 are shown.

7.3 Meteorological forcing

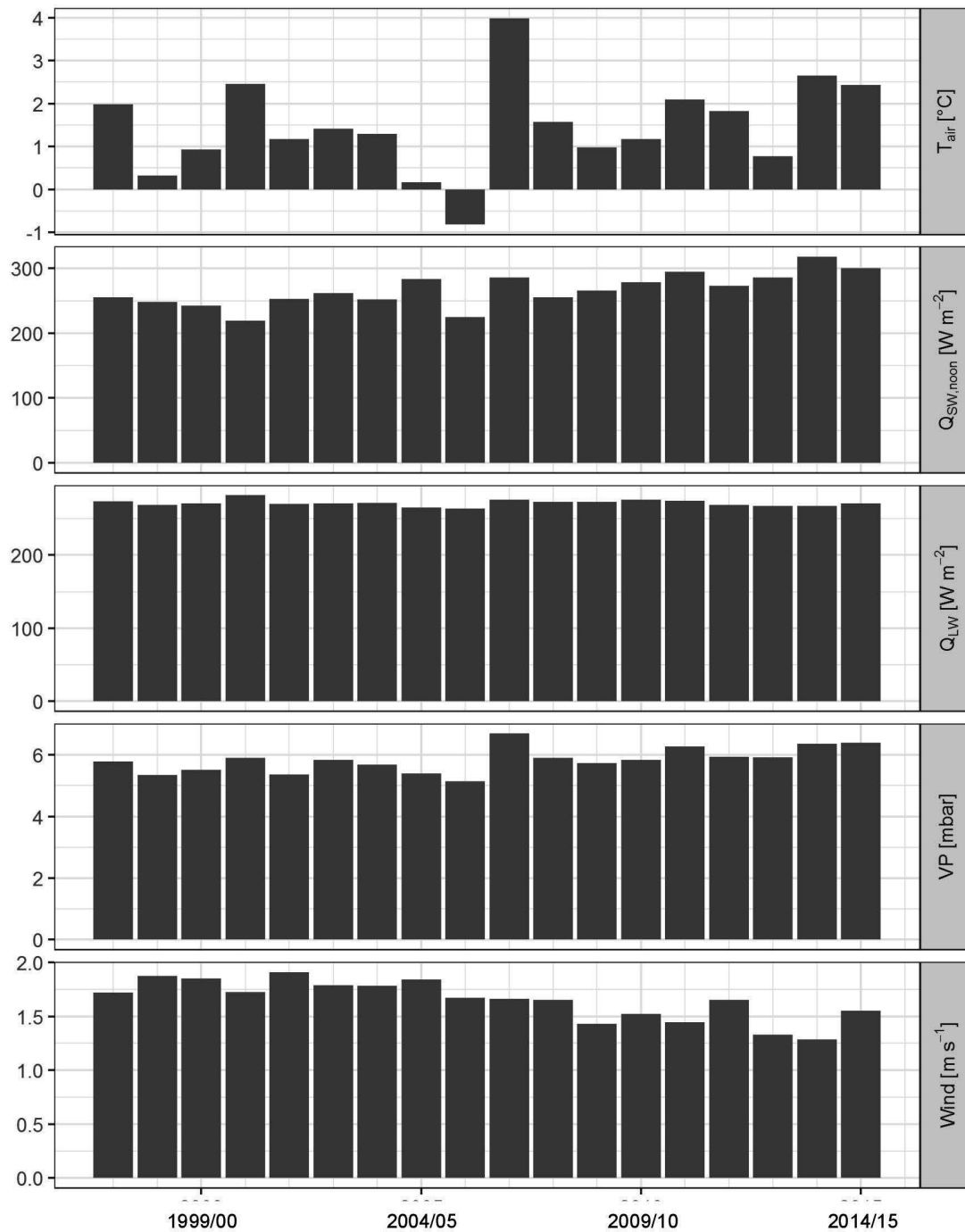


Figure 7.2 Means of meteorological forcing for each winter period (November to April) from 1997/98 to 2014/15; depicted are values for air temperature T_{air} ($^{\circ}\text{C}$), noon values of short-wave radiation $Q_{SW,noon}$ (W m^{-2}), downward long-wave radiation Q_{LW} (W m^{-2}), vapor pressure VP (mbar) and wind speed Wind (m s^{-1}).

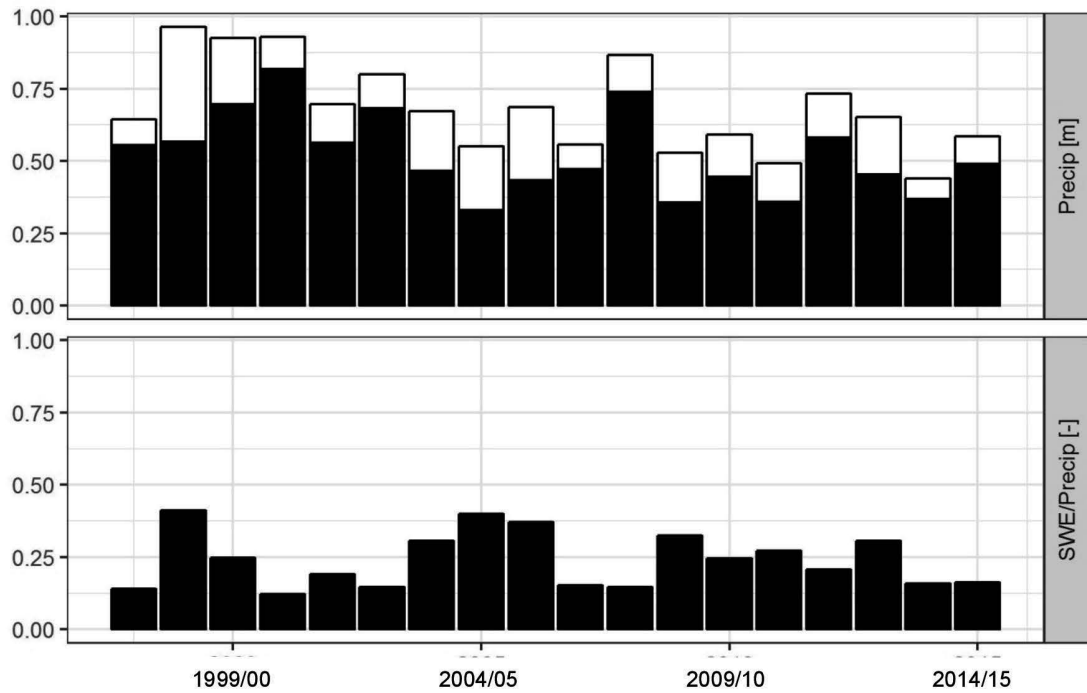


Figure 7.3 Totals of each winter period (November to April) for precipitation Precip (m), which is separated for rain (black) and snow water equivalent SWE (white) as well as the fraction of the snow-water-equivalents (SWE) of the entire precipitation.

7.4 Adaptation GLM

The original source of GLM, version 2.4.1, was adapted in the following way:

- A Boolean variable was introduced which allowed to switch off the effect of precipitation on the water balance.
- The indices for computing the new surface temperature were differing from those of equation 4 presented in Rogers et al. (1995). Thus, correction was needed for the variables BBB, FFF, DDD, GGG and EEE of the source code (File: glm_surface.c).
- Originally, evaporation from snow and white ice were computed as long as snow height and the height of white ice were larger than zero. Yet, the computed evaporation, given in water equivalents, could exceed the height of snow or white ice. Thus, we changed this in the following way: evaporation from snow (white ice) is now only computed when the snow height (height of white ice) exceeds the computed value of evaporation.

7.5 Sensitivity analysis

All model parameters and the considered range of variation for the sensitivity analysis are depicted in Table 7.1. Before model calibration a sensitivity analysis on lake ice model parameters was conducted. Therefore, the models were run with several variations of lake ice model parameters. The corresponding figures are presented for some selected years in Section 7.5. These results suggest that the projected ice thickness with GLM is not sensitive to the choice of maximum and minimum density of snow. Yet, the variation of the scaling factor of the snowfall results in ice thickness differences of up to ~25 cm (2005). Nevertheless, the variation of the snowfall forcing is of key importance to reproducing the ice thickness. This could, if this factor is set to 1 even lead to differences of observations and projections of ~40 cm (2005). Snow thickness on top of the ice sheet is also not affected by any density variation, which in turn is also valid for white ice formation. The scaling factor of snowfall forcing of 0.35 reduces white ice thickness by ~40 cm. Cheng et al. (2008) mentioned that GLM is known to overestimate white ice formation, which seems to be linked to the overestimated overall ice thicknesses.

Simstrat was least sensitive to the variation of the ice albedo. Variations of parameters affecting the snow on top of the ice sheet (snow albedo, fraction of solar radiation that is absorbed at the air-ice/snow-interface, scaling factor of precipitation) resulted in some years in a multiple instead of a single freeze-thaw-cycle (2011). Also the variation of freezing temperature could cause this shift of temporal ice dynamics. Projections suggest, in general, that lake ice tends to appear quite fast, once all overlying snow has melted. Therefore, the snow thickness is sensitive to similar parameter set than the ice thickness.

MyLake projections suggest that the model is rather robust to parameter variations, only the variation of precipitation input and the snow (in some cases also the ice) albedo would affect ice, white ice and snow thickness by ~5 to 10 cm, <5 cm and ~10 cm, respectively.

For CE-QUAL-W2 the variation of the ice albedo resulted in different ice thickness ranging between ~30 to ~70 cm in 2005. The variation of all other parameters affected the thickness less, however, for some years (2004) the ice-on was shifted. The results of the variation of three parameters, the fraction of the incoming solar radiation absorbed at the air-ice-interface, the ice extinction coefficient and the heat exchange coefficient at the water-ice-interface, show rather similar behaviour. This could highlight a parameter identification problem.

Table 7.1 Parameters and the analysed ranges for the sensitivity analysis for all models.

Model	Parameter abbreviation	Explanation	Unit	Analysed range
GLM	$Q_{\max, \text{snow}}$	Maximum density snow	[kg m ⁻³]	300-450
	$Q_{\min, \text{snow}}$	Minimum density snow	[kg m ⁻³]	50-175
	f_{asnow}	Scaling factor snow albedo	[-]	0.50-1.20
	f_{snow}	Scaling factor snowfall	[-]	0.15-1.00
Simstrat	α_{ice}	Ice albedo	[-]	0.15-0.45
	α_{snow}	Snow albedo	[-]	0.64-0.90
	$\beta_{\text{snow,ice}}$	Fraction of the incoming solar radiation absorbed at the air-ice/snow-interface	[-]	0.30-0.50
	T_{freeze}	Freezing temperature	[°C]	0.00-0.20
	f_{precip}	Scaling factor precipitation	[-]	0.80-1.20
MyLake	α_{ice}	Ice albedo	[-]	0.15-0.45
	α_{snow}	Snow albedo	[-]	0.64-0.90
	λ_{ice}	Attenuation coefficient ice	[m ⁻¹]	4-6
	λ_{snow}	Attenuation coefficient snow	[m ⁻¹]	12-18
	f_{precip}	Scaling factor precipitation	[-]	0.80-1.20
CE-QUAL-W2	α_{ice}	Ice albedo	[-]	0.20-0.90 ¹
	β_{ice}	Fraction of the incoming solar radiation absorbed at the air-ice-interface	[-]	0.20-0.80
	γ_{ice}	Ice extinction coefficient	[m ⁻¹]	0.01-10.0
	$H_{\text{water,ice}}$	Heat exchange coefficient at water-ice-interface	[W m ⁻² °C ⁻¹]	5-500

¹ The range used for the ice albedo of CE-QUAL-W2 is different from the other models, as this model does not allow discriminating between snow and ice cover.

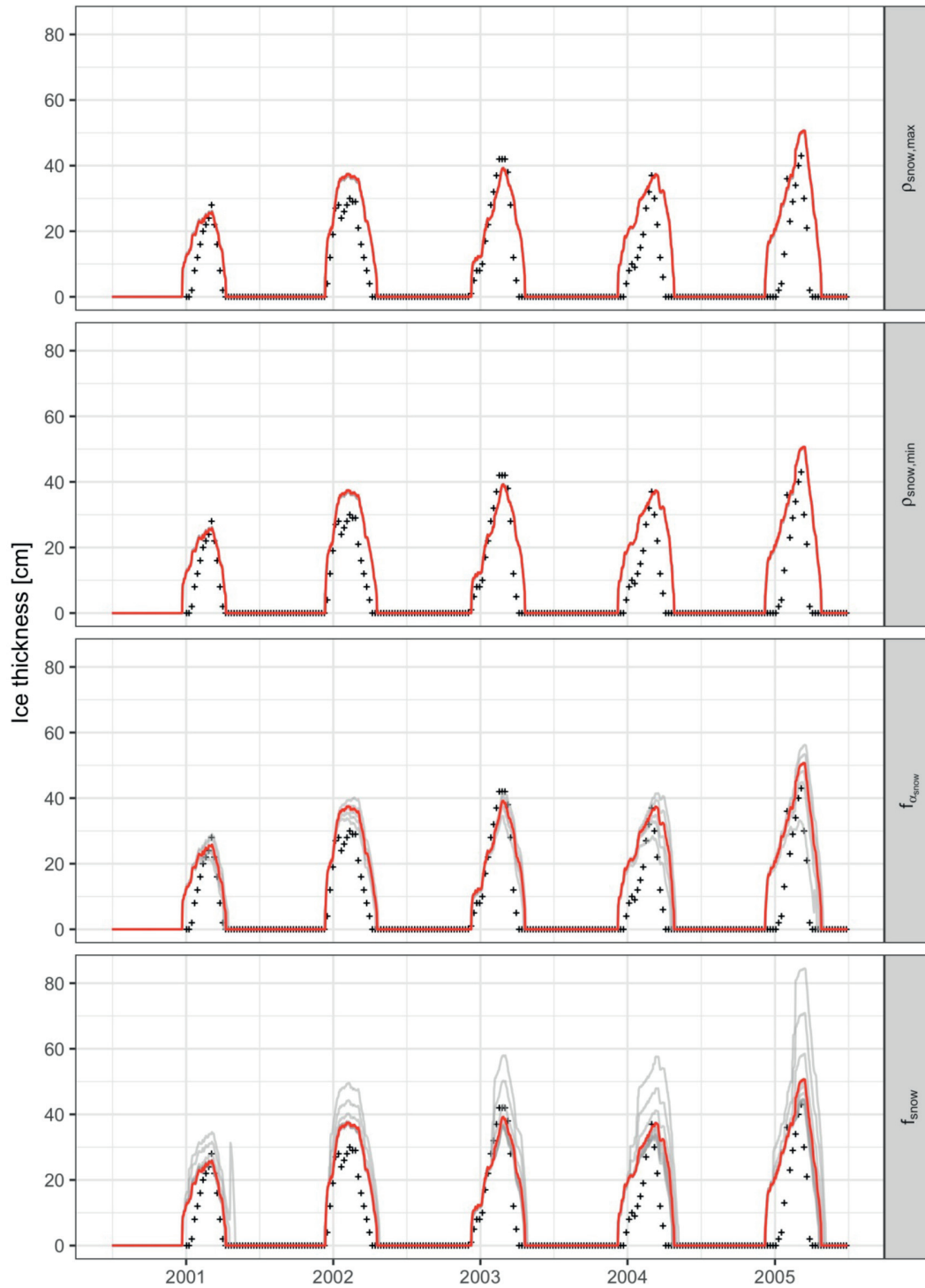


Figure 7.4 Sensitivity of ice thickness to parameter variation for GLM; shown are projections with varying model parameters (grey lines) and projections with the chosen parameter combination (red line) as well as observed ice thicknesses (black markers). Parameters were varied in a range of 300 to 450 kg m⁻³ ($\rho_{\text{max,snow}}$: maximum density snow) and 50 to 175 kg m⁻³ ($\rho_{\text{min,snow}}$: minimum density snow), 0.5 to 1.2 ($f_{\alpha\text{snow}}$: scaling factor of snow albedo), 0.15 to 1.00 (f_{snow} : scaling factor snowfall).

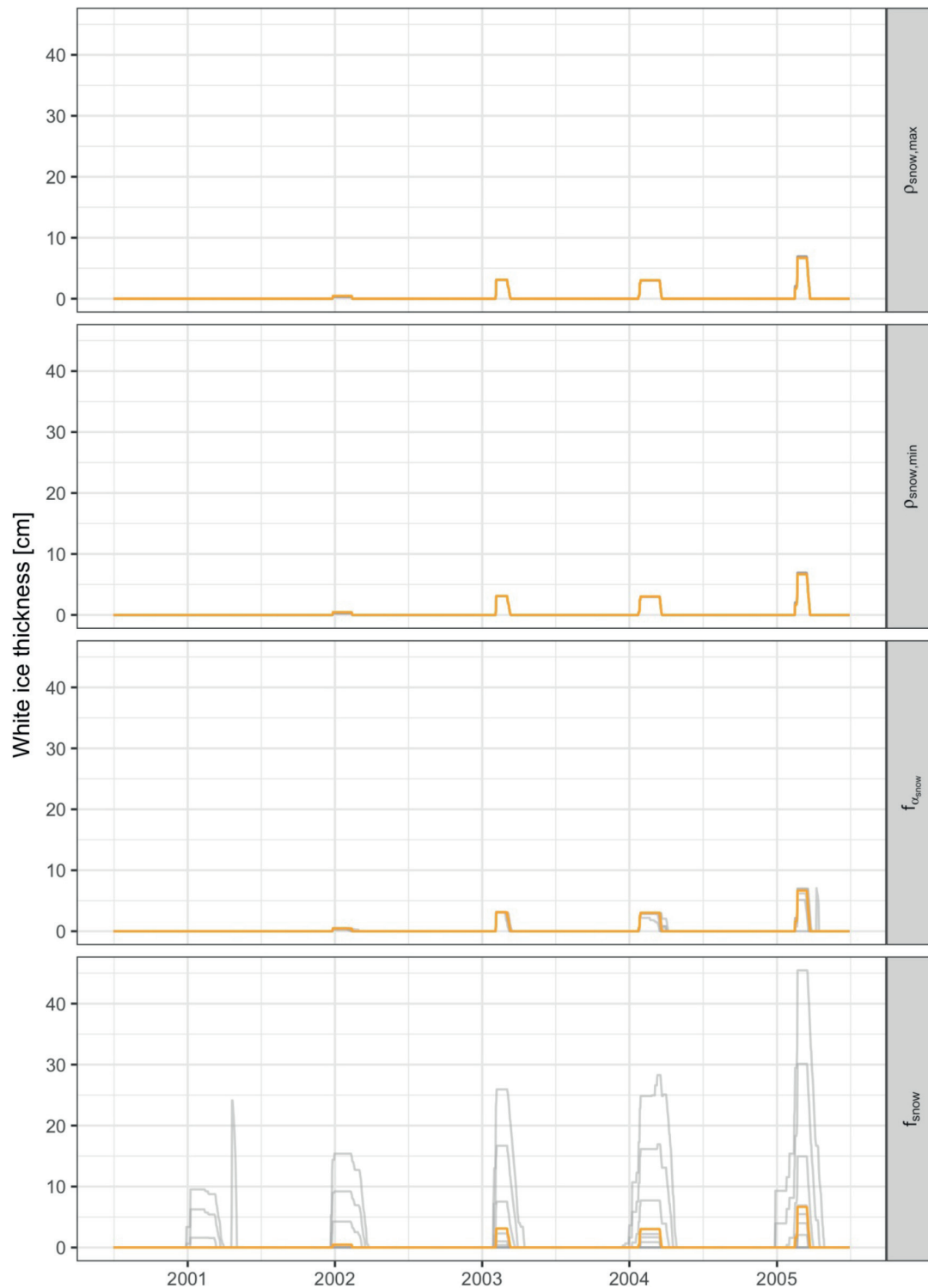


Figure 7.5 Sensitivity of white ice thickness to parameter variation for GLM; shown are projections with varying model parameters (grey lines) and projections with the chosen parameter combination (orange line). Parameters were varied in a range of 300 to 450 kg m⁻³ ($\rho_{\text{max,snow}}$: maximum density snow) and 50 to 175 kg m⁻³ ($\rho_{\text{min,snow}}$: minimum density snow), 0.5 to 1.2 (f_{asnow} : scaling factor of snow albedo), 0.15 to 1.00 (f_{Isnow} : scaling factor snowfall).

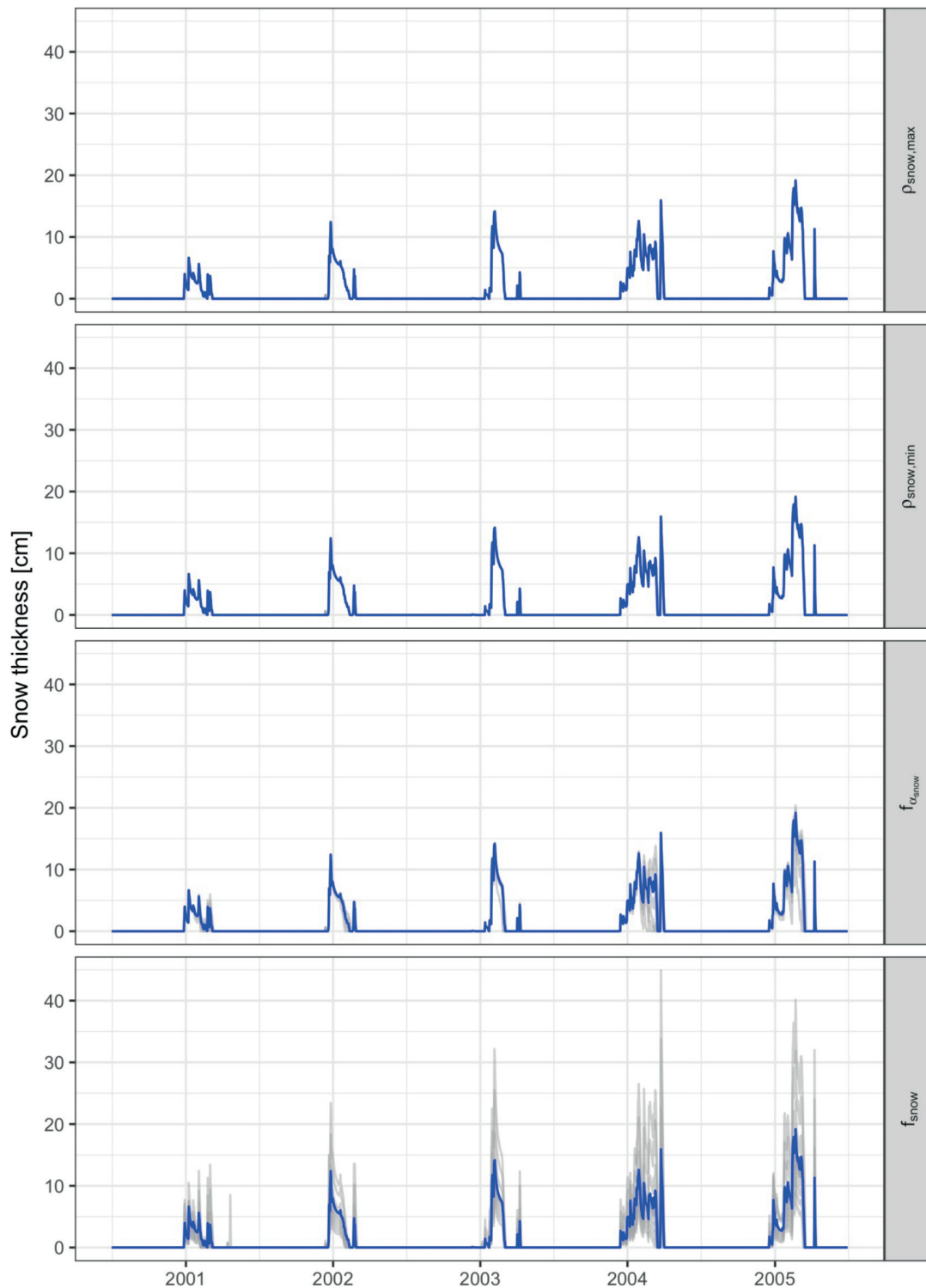


Figure 7.6 Sensitivity of snow thickness to parameter variation for GLM; shown are projections with varying model parameters (grey lines) and projections with the chosen parameter combination (blue line). Parameters were varied in a range of 300 to 450 kg m⁻³ ($\rho_{\text{max,snow}}$: maximum density snow) and 50 to 175 kg m⁻³ ($\rho_{\text{min,snow}}$: minimum density snow), 0.5 to 1.2 (f_{Gsnow} : scaling factor of snow albedo), 0.15 to 1.00 (f_{snow} : scaling factor snowfall).

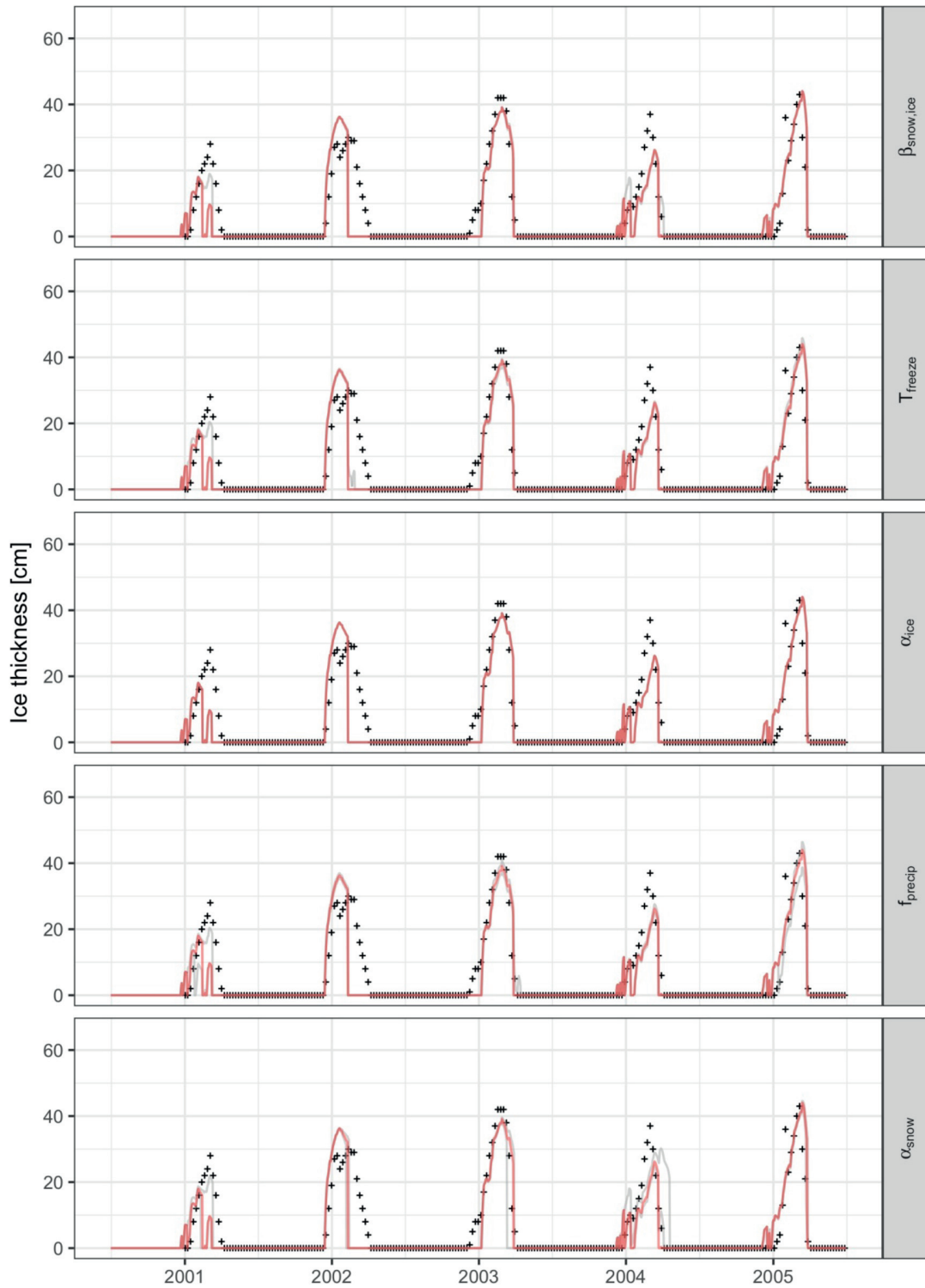


Figure 7.7 Sensitivity of ice thickness to parameter variation for Simstrat; shown are projections with varying model parameters (grey lines) and projections with the chosen parameter combination (red line) as well as observed ice thicknesses (black markers). Parameters were in a range of 0.3 to 0.5 ($\beta_{\text{snow,ice}}$: fraction of the incoming solar radiation absorbed at the air-ice/snow-interface), 0.0 to 0.2 °C (T_{freeze} : freezing temperature), 0.15 to 0.45 (α_{ice} : ice albedo), 0.8 to 1.2 (f_{precip} : scaling factor precipitation) and 0.64 to 0.90 (α_{snow} : snow albedo).

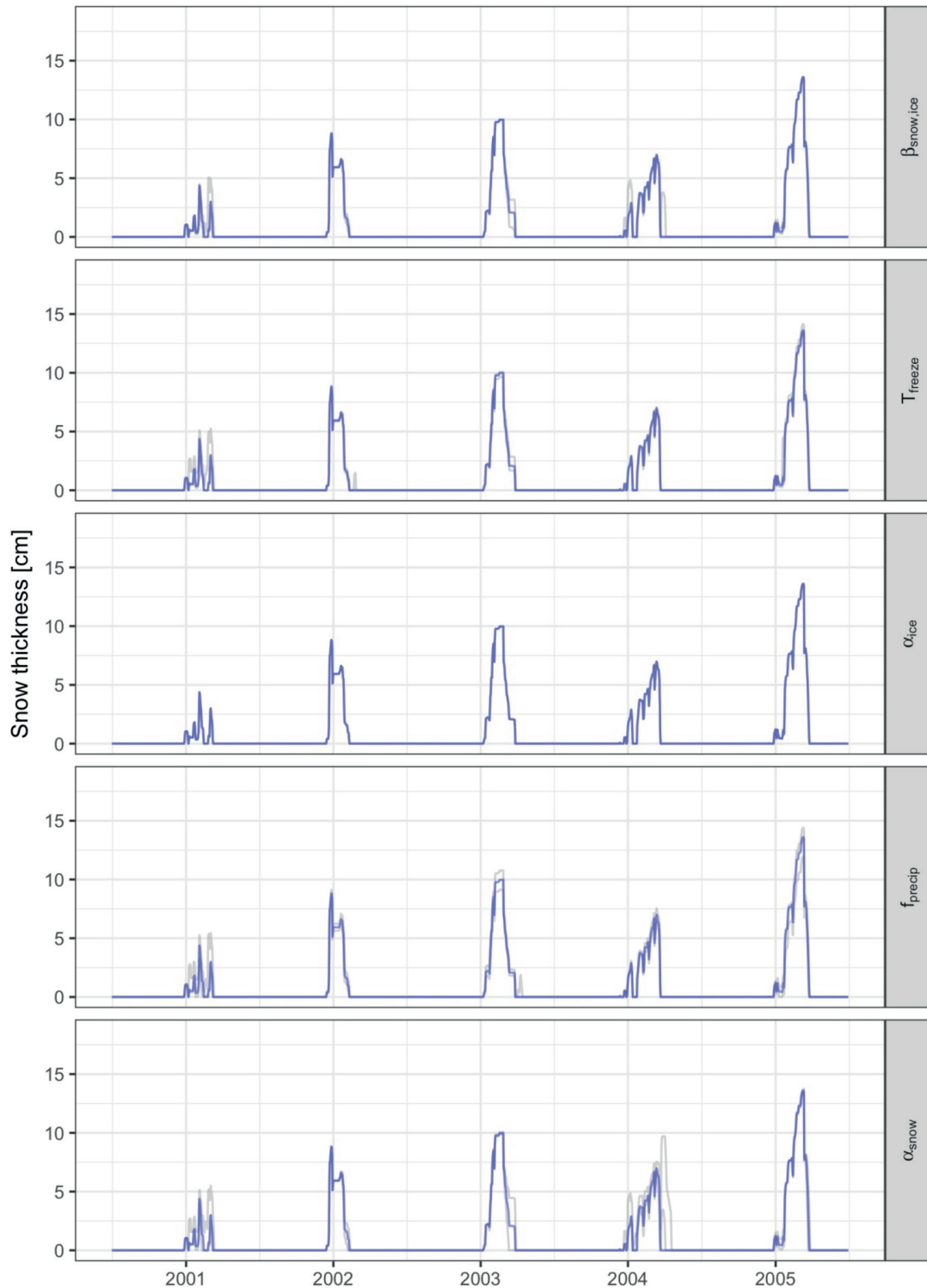


Figure 7.8 Sensitivity of snow thickness to parameter variation for Simstrat; shown are projections with varying model parameters (grey lines) and projections with the chosen parameter combination (blue line). Parameters were varied in a range of 0.3 to 0.5 ($\beta_{\text{snow,ice}}$: fraction of the incoming solar radiation absorbed at the air-ice/snow-interface), 0.0 to 0.2 °C (T_{freeze} : freezing temperature), 0.15 to 0.45 (α_{ice} : ice albedo), 0.8 to 1.2 (f_{precip} : scaling factor precipitation) and 0.64 to 0.90 (α_{snow} : snow albedo).

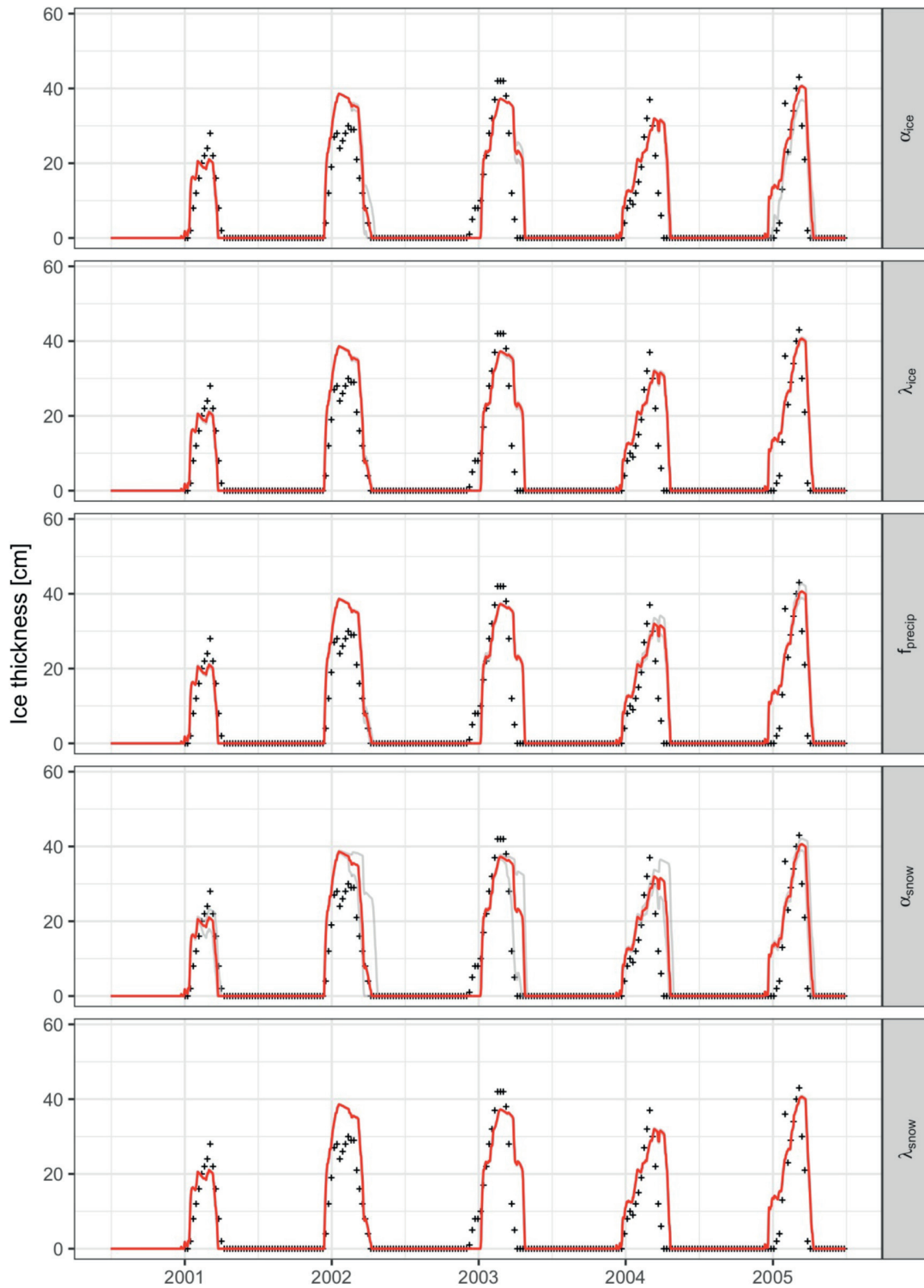


Figure 7.9 Sensitivity of ice thickness to parameter variation for MyLake; shown are projections with varying model parameters (grey lines) and projections with the chosen parameter combination (red line) as well as observed ice thicknesses (black markers). Parameters were varied in a range of 0.15 to 0.45 (α_{ice} : ice albedo), 4 to 6 m^{-1} (λ_{ice} : attenuation coefficient ice), 0.8 to 1.2 (f_{precip} : scaling factor precipitation), 0.64 to 0.90 (α_{snow} : snow albedo) and 12 to 18 m^{-1} (λ_{snow} : attenuation coefficient snow).

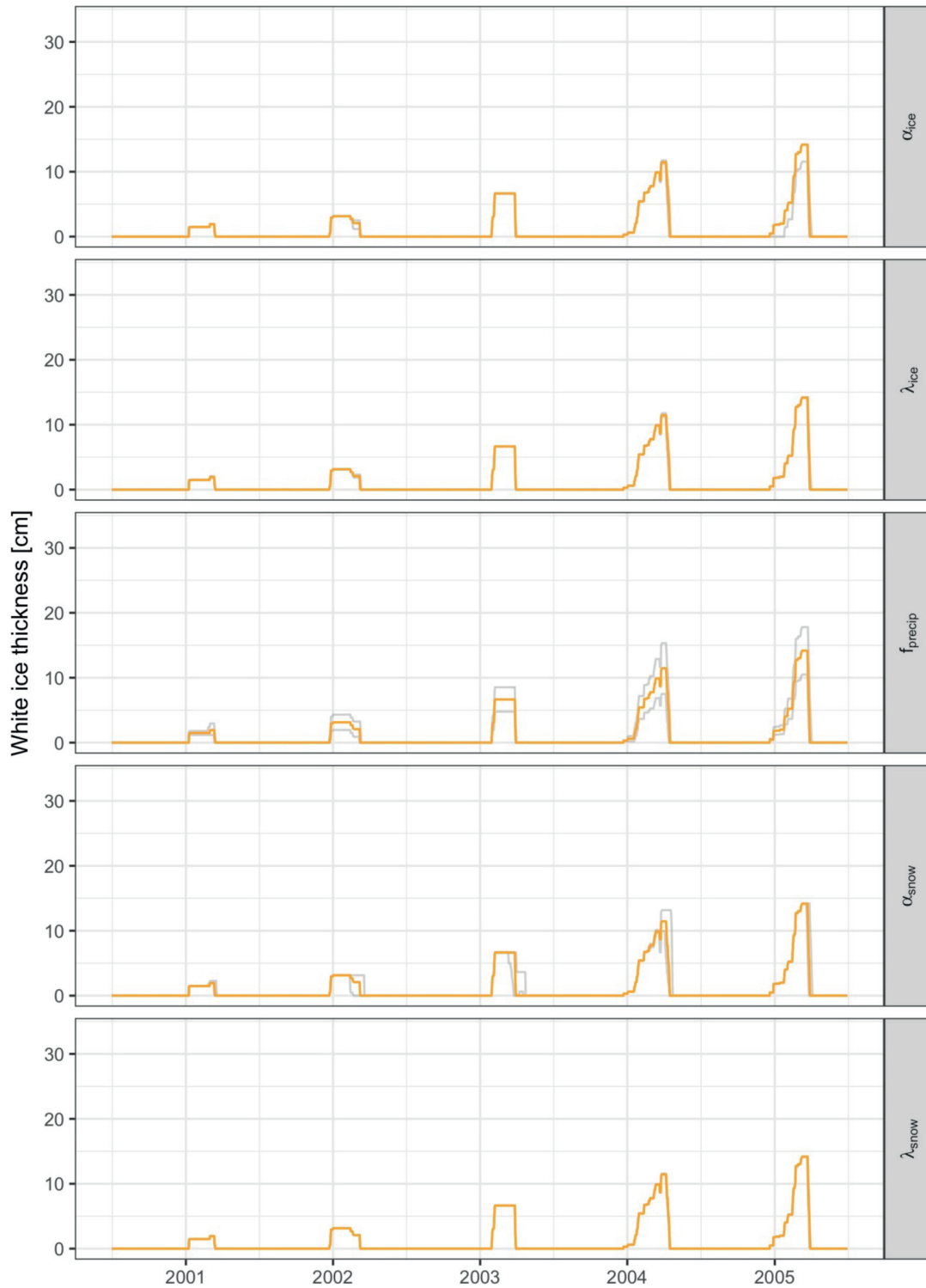


Figure 7.10 Sensitivity of white ice thickness to parameter variation for MyLake; shown are projections with varying model parameters (grey lines) and projections with the chosen parameter combination (orange line). Parameters were varied in a range of 0.15 to 0.45 (α_{ice} : ice albedo), 4 to 6 m^{-1} (λ_{ice} : attenuation coefficient ice), 0.8 to 1.2 (f_{precip} : scaling factor precipitation), 0.64 to 0.90 (α_{snow} : snow albedo) and 12 to 18 m^{-1} (λ_{snow} : attenuation coefficient snow).

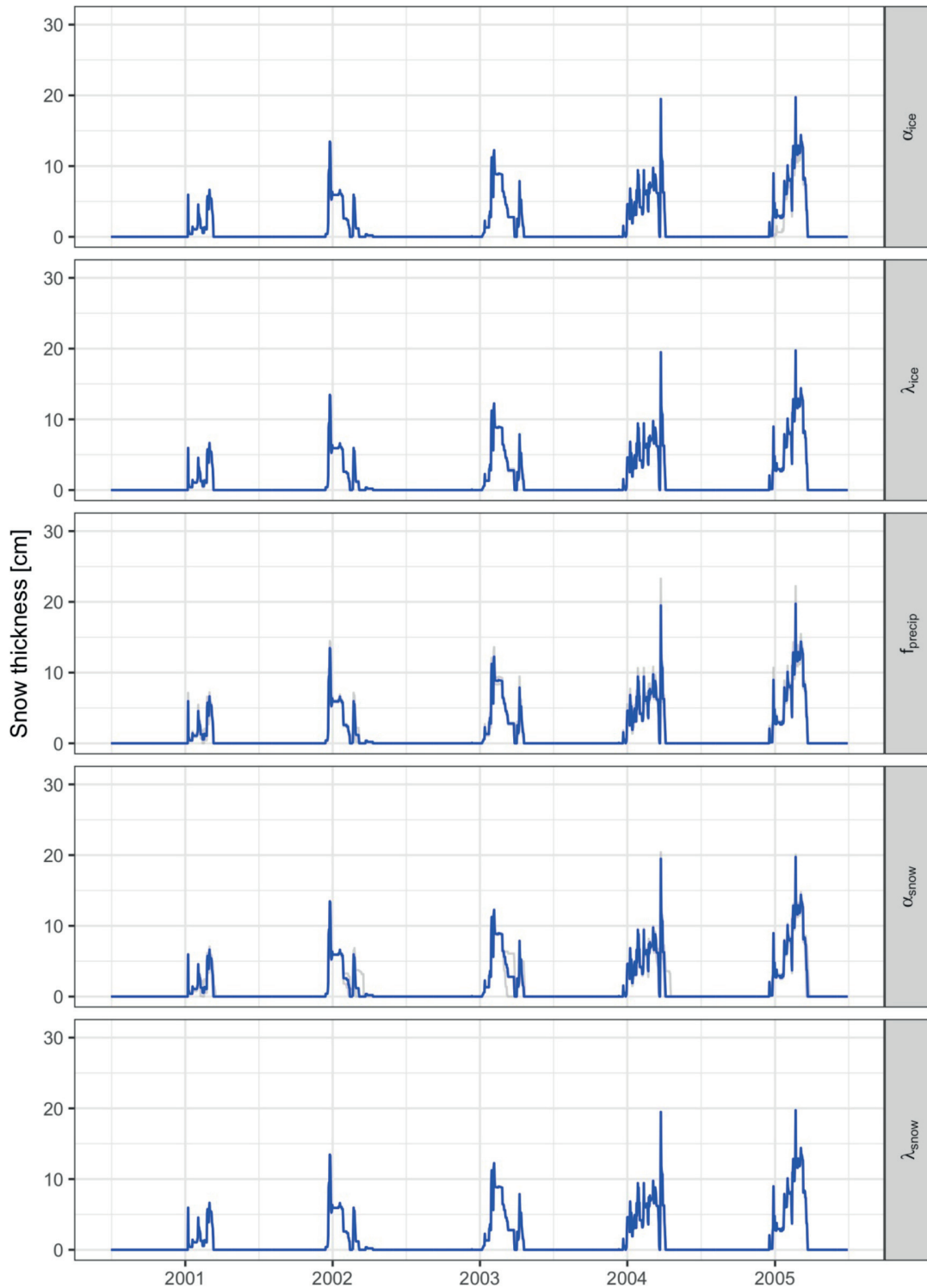


Figure 7.11 Sensitivity of snow thickness to parameter variation for MyLake; shown are projections with varying model parameters (grey lines) and projections with the chosen parameter combination (blue line). Parameters were varied in a range of 0.15 to 0.45 (α_{ice} : ice albedo), 4 to 6 m^{-1} (λ_{ice} : attenuation coefficient ice), 0.8 to 1.2 (f_{precip} : scaling factor precipitation), 0.64 to 0.90 (α_{snow} : snow albedo) and 12 to 18 m^{-1} (λ_{snow} : attenuation coefficient snow).

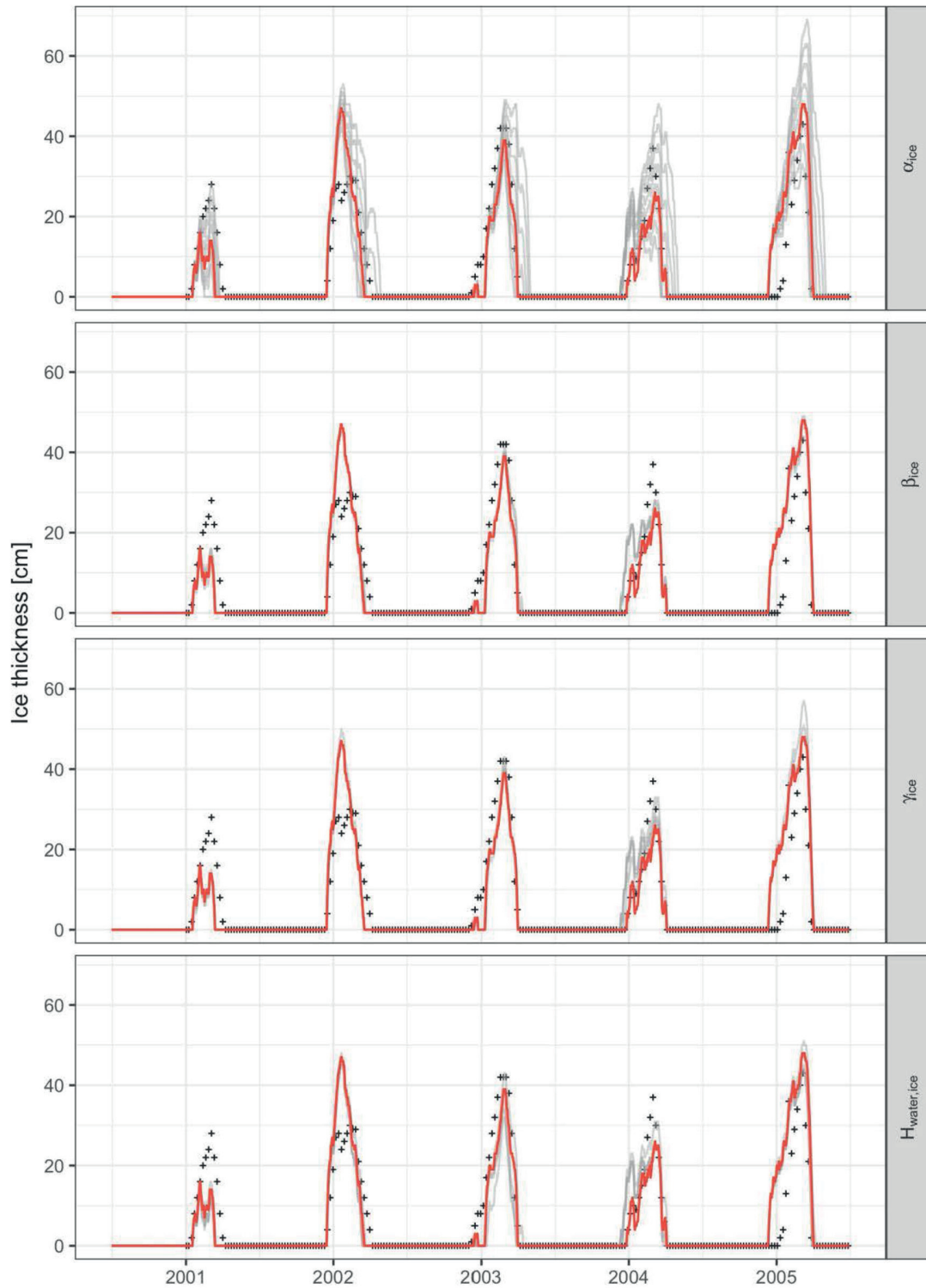


Figure 7.12 Sensitivity of ice thickness to parameter variation for CE-QUAL-W2; shown are observed ice thicknesses (black markers), projections with varying model parameters (grey lines) and projections with the chosen parameter combination (red line). Parameters were varied in a range of 0.2 to 0.9 (α_{ice} : ice albedo), 0.2 to 0.8 (β_{ice} : fraction of the incoming solar radiation absorbed at the air-ice-interface), 0.01 to 10 (γ_{ice} : ice extinction coefficient) and 5 to 500 $W\ m^{-2}\ ^{\circ}C^{-1}$ ($H_{water,ice}$: heat exchange coefficient at water-ice-interface).

7.6 Additional information model calibration

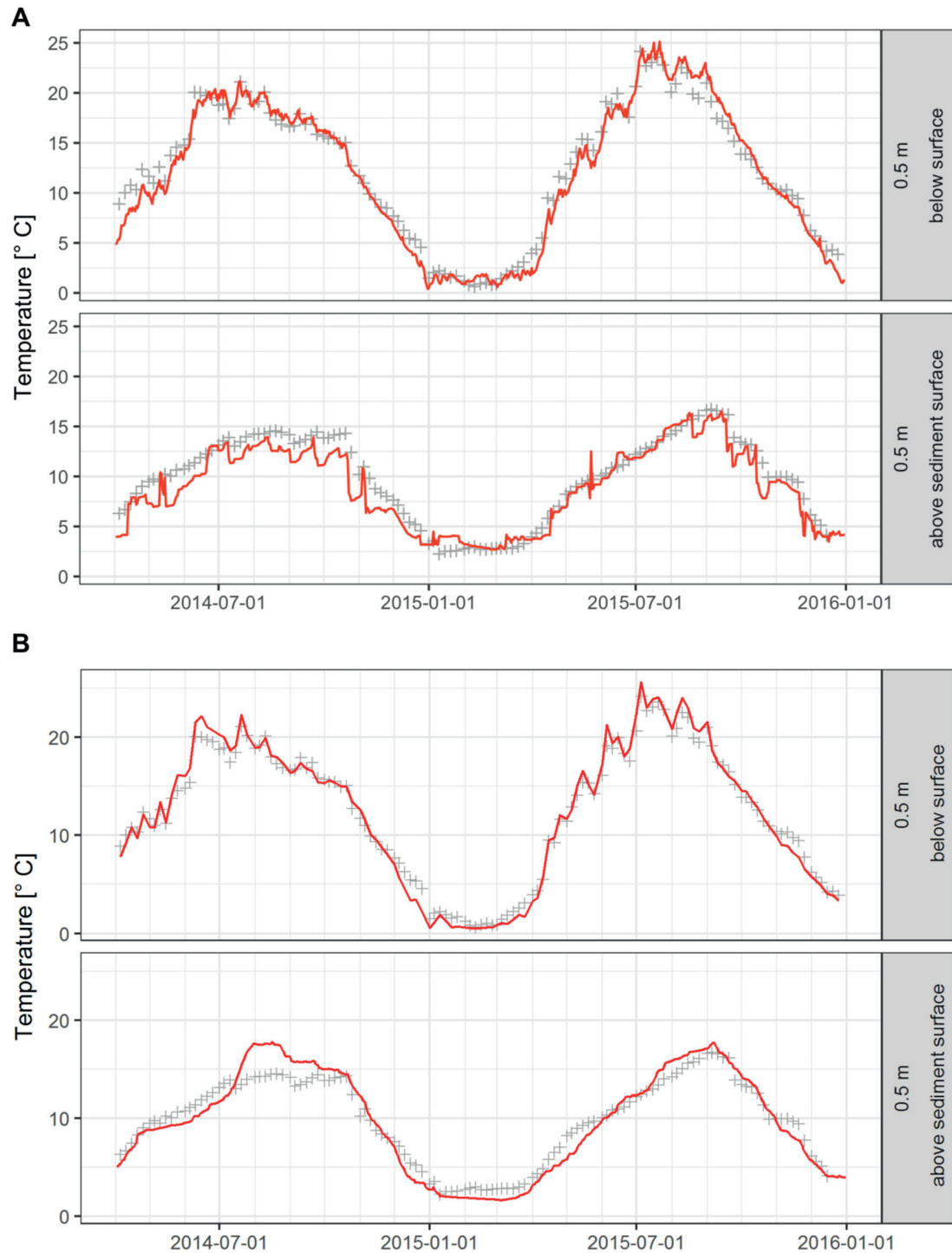


Figure 7.13 Projections of (A) GLM and (B) Simstrat (red lines) as well as observations (grey markers) of water temperatures (°C) in Sihlsee for the present PS scenario; depicted temperatures are taken in the specified distance from either the surface or the sediment surface.

The model parameters and initial conditions of GLM and Simstrat are shown in Table 7.2 and Table 7.3. For the model parameters of MyLake similar values than those proposed for the test case of Lake Vansjø were taken; initial conditions were taken similar to those presented in Table 7.3.

Table 7.2 Model parameters for GLM and Simstrat; values estimated with PEST are highlighted in red, those chosen after a sensitivity analysis in blue.

Parameter	Description	Value		Method
		Simstrat	GLM	
Kw	Extinction coefficient [m ⁻¹]	0.708	0.708	Observed
p_radin	Scaling factor long-wave radiation [-]	0.9539	-	CAL
albsw	Albedo open water [-]	0.090	-	Default
ice_albedo	Albedo ice	0.300	-	Default
snow_albedo	Albedo snow [-]	0.770	-	Default
freez_temp	Freezing temperature [°C]	0.100	-	Adapted ¹
beta_snowice	Absorption of short-wave radiation in snow and ice [-]	0.400	-	Default
beta_sol	Absorption of short-wave radiation in first cell [-]	0.350	-	Default
cd	Bottom friction coefficient [-]	1.50×10 ⁻³	-	Default
f_wind	Scaling factor wind speed [-]	0.3816	-	CAL
p_windf	Parameter for fitting wind function [-]	1.000	-	Default
c10	Wind drag coefficient [-]	1.000	-	Default
a_seiche	Fraction of wind energy to seiche energy [-]	5.282×10 ⁻³	-	CAL
q_nn	Parameter for the distribution of seiche energy [-]	1.100	-	Default
k_min	Minimal value for TKE [J kg ⁻¹]	1.00×10 ⁻⁹	-	Default
lat	Latitude [°]	47.1	-	Observed
p_air	Air pressure [mbar]	912	-	Observed
hgeo	Geothermal heat flux [W m ⁻²]	0.080	-	Default
coef_mix_conv	Mixing efficiency convective overturn	-	0.125	Default
coef_mix_stir	Mixing efficiency wind stirring	-	0.230	Default
coef_mix_shear	Mixing efficiency unsteady turbulence effects	-	0.200	Default
coef_mix_turb	Mixing efficiency shear production	-	0.510	Default
coef_mix_KH	Mixing efficiency Kelvin-Helmholtz turbulent billows	-	0.300	Default
coef_mix_hyp	Mixing efficiency	-	0.4778	CAL
deep_mixing	Model description deep mixing	-	2	
wind_factor	Scaling factor wind speed	-	0.9445	CAL
sw_factor	Scaling factor short-wave radiation	-	0.850	Kobler et al. (2018)
lw_factor	Scaling factor long-wave radiation	-	0.9497	CAL
at_factor	Scaling factor air temperature	-	1.000	Default
rh_factor	Scaling factor relative humidity	-	1.000	Default
rain_factor	Scaling factor rain	-	1.000	Default
snow_factor	Scaling factor snow	-	0.350	Sensitivity analysis
ce	Bulk aerodynamic coefficient for latent heat transfer	-	1.50×10 ⁻³	Default Delft3D
ch	Bulk aerodynamic coefficient for sensible heat transfer	-	1.50×10 ⁻³	Default Delft3D
cd	Bulk aerodynamic coefficient for momentum transfer	-	1.50×10 ⁻³	Default Delft3D
snow_rho_min	Minimum density snow [kg m ⁻³]	-	100	Default
snow_rho_max	Maximum density snow [kg m ⁻³]	-	350	Default
snow_albedo_factor	Scaling factor snow albedo	-	1.000	Default

¹ As temperature is only resolved vertically by 0.5 m, the freezing temperature was adapted to avoid the occurrence of negative water temperatures, that could occur although the temperature of the first layer beneath the ice sheet is fixed to 0 °C during melting.

Table 7.3 Initial conditions for all GLM and Simstrat simulations, with depth-dependent current velocities U and V (m s^{-1}), temperature ($^{\circ}\text{C}$), salinity ($\%$), turbulent kinetic energy k (J kg^{-1}), and dissipation rate of turbulent kinetic energy ε (W kg^{-1}).

	GLM & Simstrat	GLM	Simstrat				
Depth [m]	Temperature [$^{\circ}\text{C}$]	Salinity [psu]	Salinity [%]	U [m s^{-1}]	V [m s^{-1}]	k [J kg^{-1}]	ε [W kg^{-1}]
0.00	0.8	0.075	0.075	0.000	0.000	3.0×10^{-6}	5.0×10^{-10}
1.00	1.0	0.075	0.075	0.000	0.000	3.0×10^{-6}	5.0×10^{-10}
2.00	2.0	0.075	0.075	0.000	0.000	3.0×10^{-6}	5.0×10^{-10}
3.00	3.0	0.075	0.075	0.000	0.000	3.0×10^{-6}	5.0×10^{-10}
4.00	4.0	0.075	0.075	0.000	0.000	3.0×10^{-6}	5.0×10^{-10}
Maximum depth	4.0	0.075	0.075	0.000	0.000	3.0×10^{-6}	5.0×10^{-10}

Table 7.4 Root-mean-square error (RMSE), mean absolute error (MAE) and mean error (ME) in $^{\circ}\text{C}$ for the entire water column, the epilimnion (uppermost 5 m of the water column) and the hypolimnion (lowermost 5 m of the water column) of Sihlsee.

Model		Entire water column	Epilimnion	Hypolimnion
GLM	RMSE [$^{\circ}\text{C}$]	1.35	1.10	1.18
	MAE [$^{\circ}\text{C}$]	1.01	0.87	0.94
	ME [$^{\circ}\text{C}$]	-0.01	-0.01	-0.67
Simstrat	RMSE [$^{\circ}\text{C}$]	1.13	0.80	1.31
	MAE [$^{\circ}\text{C}$]	0.85	0.60	1.02
	ME [$^{\circ}\text{C}$]	-0.11	-0.16	-0.08

7.7 Temporal dynamics lake ice projections

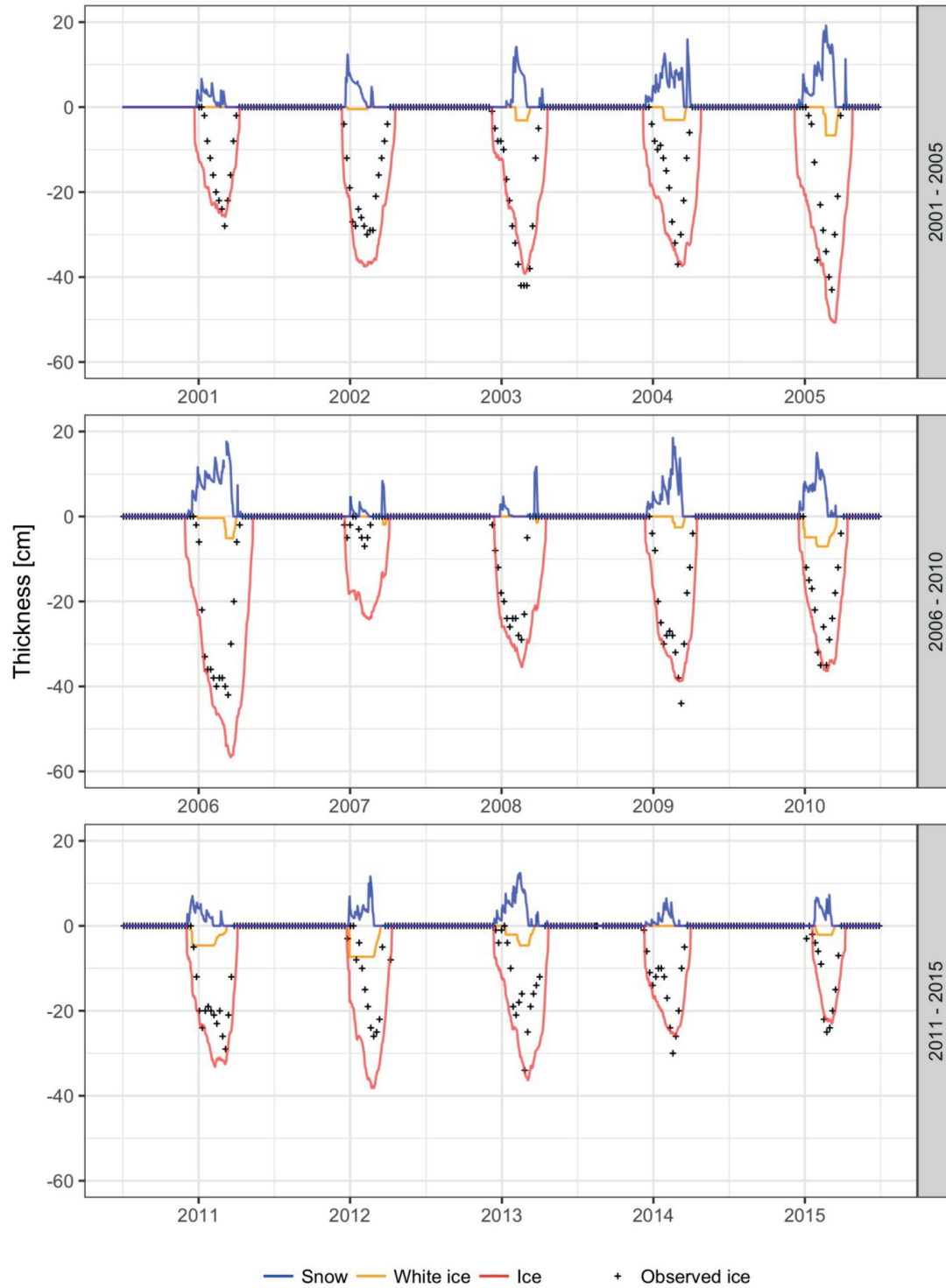


Figure 7.14 Observed ice thickness (black markers, depicted with negative values) and GLM projections of ice (red, depicted with negative values), white ice (orange, depicted with negative values) and snow (blue) thickness (cm).

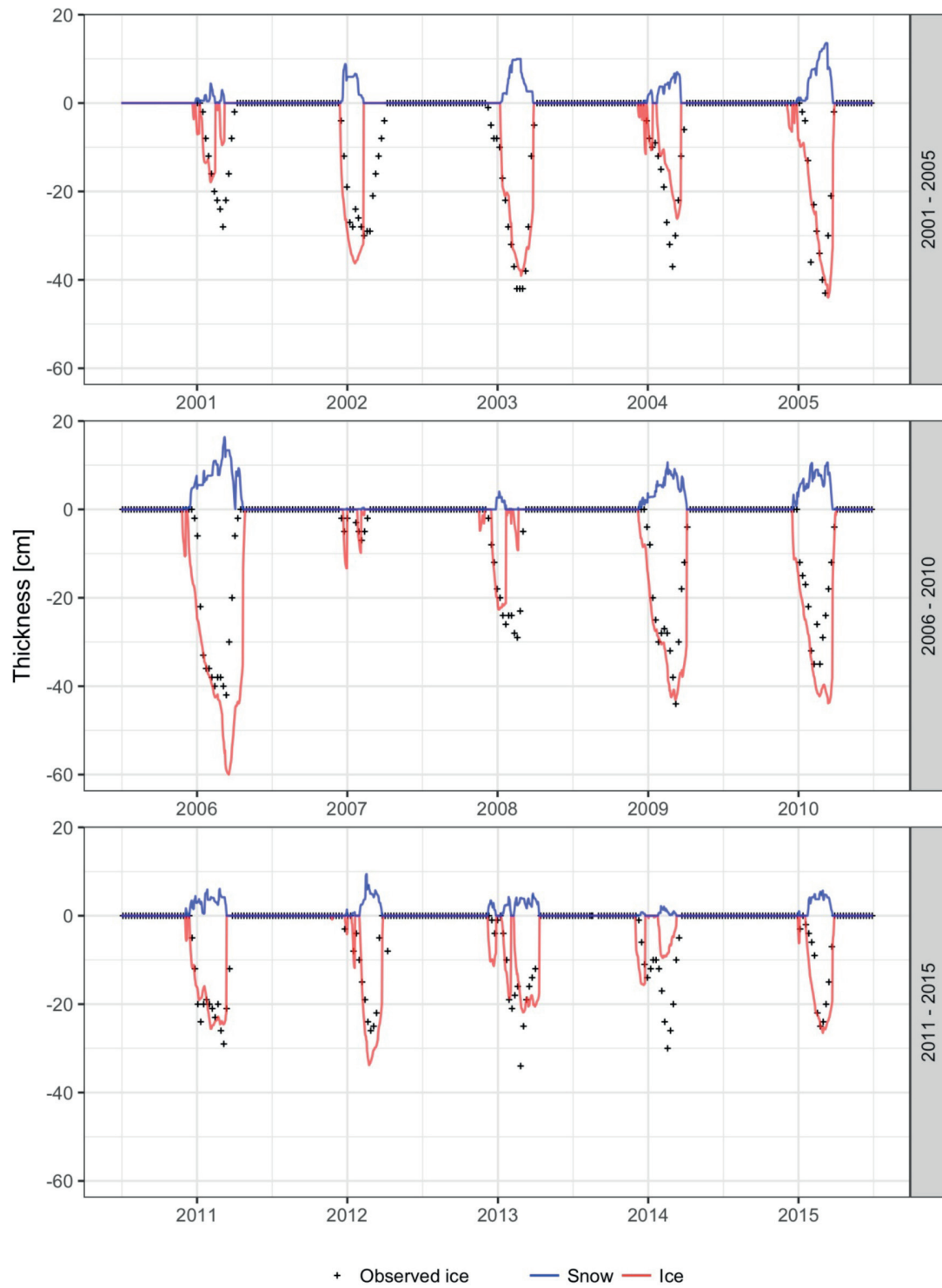


Figure 7.15 Observed ice thickness (black markers, depicted with negative values) and Simstrat projections of ice (red, depicted with negative values) and snow (blue) thickness (cm).

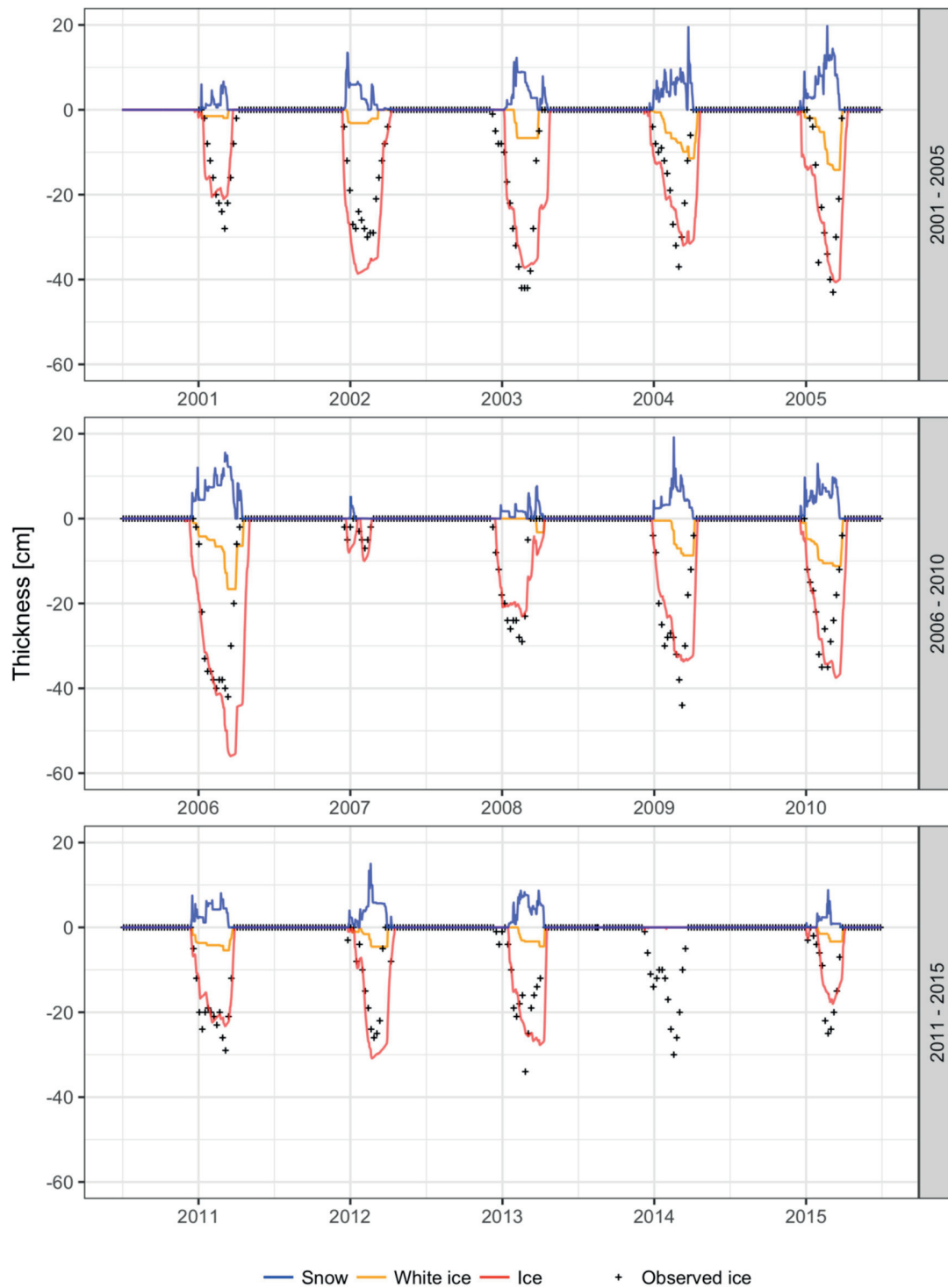


Figure 7.16 Observed ice thickness (black markers, depicted with negative values) and MyLake projections of ice (red, depicted with negative values), white ice (orange, depicted with negative values) and snow (blue) thickness (cm).

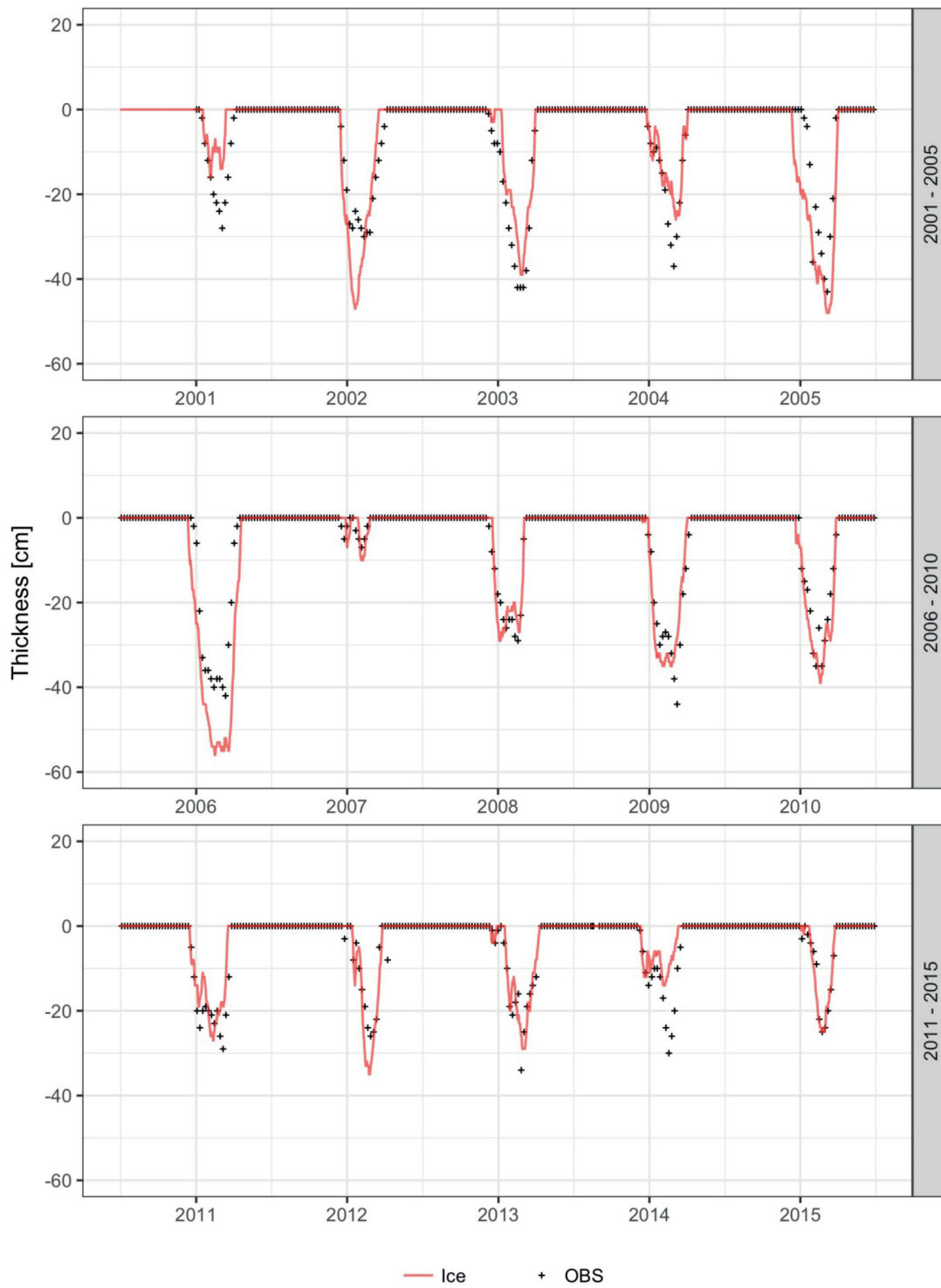


Figure 7.17 Observed ice thickness (black markers, depicted with negative values) and CE-QUAL-W2 projections of ice thickness (red, depicted with negative values) (cm).

7.8 Additional information on the effects due to PS operation and climate change

Table 7.5 Mean duration of the longest uninterrupted ice-covered periods (days) for the different models and the combination of different climate conditions (CC: current climate, FC: future climate) and PS scenarios.

		Reference QNat		Reference NoPS		Present PS		Extended PS	
		CC	FC	CC	FC	CC	FC	CC	FC
GLM		126	82	125	81	126	84	113	47
Simstrat		75	18	74	17	76	19	53	8
MyLake		102 ¹	23 ¹	-	-	-	-	-	-
CE-QUAL-W2	SEG 8	94	33	95	32	-	-	-	-
	SEG 16	92	30	94	31	92	31	-	-
	SEG 24	91	28	92	30	92	31	82	34
	SEG 32	89	27	91	27	91	27	74	17
	SEG 40	84	22	85	24	87	26	17	9
	Mean	90	28	91	29	91	29	58	20
Mean of all models		98	38	97	42	98	44	75	25

¹ Without any in- and outflows

Table 7.6 Average probability (%) that the lake is ice covered on a specific day during the winter period (November to April), for the different models and the combination of different climate conditions (CC: current climate, FC: future climate) and PS scenarios.

		Reference QNat		Reference NoPS		Present PS		Extended PS	
		CC	FC	CC	FC	CC	FC	CC	FC
GLM		71	41	70	44	71	46	64	21
Simstrat		49	13	48	13	51	16	35	3
MyLake		58 ¹	10 ¹	-	-	-	-	-	-
CE-QUAL-W2	SEG 8	54	19	55	19	-	-	-	-
	SEG 16	53	17	53	17	53	18	-	-
	SEG 24	52	16	52	16	53	17	48	13
	SEG 32	51	14	51	14	52	14	43	6
	SEG 40	48	10	48	10	49	12	13	1
	Mean	52	15	52	15	52	15	35	7
Mean of all models		57	20	57	24	58	26	45	10

¹ Without any in- and outflows

Table 7.7 Mean ice thickness (cm) over all ice-covered periods for the different models and the combination of different climate conditions (CC: current climate, FC: future climate) and PS scenarios.

		Reference QNat		Reference NoPS		Present PS		Extended PS	
		CC	FC	CC	FC	CC	FC	CC	FC
GLM		27	16	27	16	28	17	25	13
Simstrat		25	9.3	25	9.1	24	9.0	19	6.3
MyLake		22 ¹	8.4 ¹	-	-	-	-	-	-
CE-QUAL-W2	SEG 8	21	9.5	21	9.6	-	-	-	-
	SEG 16	20	9.6	21	9.6	21	9.5	-	-
	SEG 24	20	9.3	20	9.4	21	9.4	17	8.1
	SEG 32	20	9.1	20	9.2	20	9.3	16	7.2
	SEG 40	19	8.7	20	9.1	20	8.9	11	4.2
	Mean	20	9.2	20	9.4	21	9.3	15	6.5
Mean of all models		24	11	24	11	24	12	20	8.6

¹ Without any in- and outflows

Chapter 8 Conclusions

8.1 Achieved results

In a first step, the effects of pumped-storage operation on temperature, ice cover and water quality have been assessed with a laterally-averaged two-dimensional hydrodynamic and water quality model (CE-QUAL-W2). This model was calibrated for current climatic conditions. Afterwards four different PS scenarios were defined and analysed. In a next step, the model was combined with synthetic weather projections for current and future climate. The latter were developed using a weather generator, described in detail by Schlabin et al. (2012). This combined approach allowed to assess the coupled effect of PS operation and climate change. Lastly, to evaluate the robustness of the projections of lake ice dynamics, additional simulations were performed with three vertical one-dimensional models (GLM, MyLake, Simstrat). The effects on water temperature, water quality and the upper reservoir's ice cover can be summarized as follows:

- When extending the PS operation¹³, hypolimnetic temperatures are projected to increase by ~2 °C in summer, the ice-covered period would be shortened, ice thickness would decline, nutrient concentrations would be raised, and hypolimnetic dissolved oxygen concentrations would increase in the upper reservoir.
- The aforementioned effects of extended PS operation are site-specific; yet, the results presented in Chapter 2 suggest that PS operation supports a decrease in strength and duration of stratification with correlated effects on dissolved oxygen and nutrients.
- To disentangle the effects of deep-water withdrawal versus those of PS operation, the analysis of two reference scenarios allowed concluding that the differences between the reference scenario with deep-water withdrawal and those of present PS are minor. For the reference scenario with surface water withdrawal, the hypolimnetic water temperatures were, on the other hand, projected to be reduced by up to ~10 °C with further effects on stratification and dissolved oxygen.
- Minor PS effects were projected for the downstream natural lake of the considered PS hydropower plant, which need not be the case for any other plant.
- The findings from Chapter 2 highlight the urge for clear guidelines to define a reference state as a base scenario for assessing the environmental impacts of increased development or extension of PS hydropower plants.

¹³ From 135 MW to 525 MW for generating and from 65 MW to 265 MW for pumping

- The results, presented in Chapter 4, showed a synergistic effect of PS operation and climate change on hypolimnion temperatures, whereas epilimnion temperature increased similarly in all scenarios independent of PS operation.
- Because of raised surface water temperatures, increased water column stability and prolonged summer stratification dissolved oxygen concentrations are subsequently lowered due to climate change.
- An antagonistic effect resulted for the duration of summer stratification, which is prolonged by climate change and shortened by PS operation.
- The combination of future climate with extended PS operation resulted in advancing summer stratification by ~1 month.
- Decreasing ice-thickness and weakened inverse stratification resulted in increasing dissolved oxygen concentrations and reduced phosphate release for future climate conditions, which could further affect lake ecology.
- For a comprehensive environmental impact assessment, the findings from Chapter 4 resulted in the recommendation to investigate PS in combination with climate change effects for the connected water bodies. Chapter 4 particularly highlights this need for PS operations with hypolimnetic water withdrawal, which promotes hypolimnetic warming more easily.
- Ensemble modelling with four different hydrodynamic models (Chapter 6) showed that the effect of PS operation and climate change results for all scenarios in shortening of ice-covered periods as well as declining ice thicknesses. Some of the model projections would result in the conclusion that lake ice would vanish, when considering both climate change and extended PS operation.
- The analysis of longitudinal variation in ice-cover projected by CE-QUAL-W2 showed that Sihlsee would likely become completely ice free only close to the PS intake/outlet. Nevertheless, the partially open lake surface would allow increased gas exchange with the atmosphere and cause enhanced mixing due to wind.

8.2 Outlook

PS operation is an important tool accompanying the increasing production of time-varying new renewable electricity. The latter is mostly implemented today (i) to avoid further global warming, and (ii) to bridge the gap between electricity demand and production arising when nuclear power plants are phased out at the end of their lifetime. PS operations can increase production flexibility, needed to cover hydropower production losses due to climate change (Schaepli 2015; Schaepli et al. 2019). Although, economic market conditions discourage investment in the development of PS hydropower plants at the moment (Björnsen Gurung et al. 2016), research is needed to increase the knowledge of PS effects on the connected water bodies today. Therefore, this section gives an overview of topics that would be interesting to study.

As highlighted in Chapter 2 the intake/outlet location of a PS hydropower plant is crucial. It strongly affects the thermal characteristics of a lake, oxygen depletion in the hypolimnion and the release of nutrients from the sediment. Therefore, to minimise environmental impacts it would be interesting to study selective withdrawal for PS operations, which have to my knowledge not been assessed. Yet, other studies successfully showed how selective withdrawal needs to be operated to avoid thermo-peaking in downstream rivers, and to increase hypolimnetic dissolved oxygen concentrations in a reservoir (e.g., Weber et al. 2017). This would extend the work of Bonalumi et al. (2012), who assessed the influence of different, fixed locations of PS intake/outlet on temperature and inorganic suspended solids.

To compensate hydropower production losses, dam heightening can also be considered. This topic was discussed in several talks during the annual conference of the Swiss Competence Center for Energy Research – Supply of Electricity in 2018 (SCCER-SoE 2018). Due to this increasing interest, it would be important to study how water temperature and quality as well as lake ecology would be affected. This analysis could follow Prats et al. (2018), who investigated how dam heightening of a Mediterranean reservoir would affect stratification dynamics when additionally considering climate change.

Furthermore, the future operation of PS hydropower plants might differ from that of today. For future operation, power reserve regulation through means of variable design of pump-turbines and hydraulic short-circuiting are becoming more relevant (Pérez-Díaz et al. 2015). Therefore, these new PS operations would need to be considered for a comprehensive view on how abiotic and biotic characteristics of the connected water bodies are affected.

In some cases, the meteorological forcing had to be taken from stations that are located quite far from the study sites. This causes sometimes inaccurate surface heat balances. Consequently, lake ice projections could not be well reproduced, i.e., MyLake projections for 2014. To overcome this issue, a weather generator, such as AEW-GEN-2d (Peleg et al. 2017) could be utilised for generating current climate forcing. This weather generator is not only based on a stochastic approach, but it also involves physical relationships, often needed for the description of sub-daily processes. It also offers the advantage of high spatial and temporal resolution.

Our assessment of the coupled effects of PS operation and climate change solely focused on increasing air temperatures. Therefore, effects related to precipitation changes might have been missed. Yet, any modification of precipitation would further affect the water balance and would call for a different PS operation. Moreover, a changing climate affects snowfall, which needs to be considered to enhance the reliability of projected effects on the ice-covered period. Thus, there is still more potential for studying these impacts, particularly, as the uncertainty of climate projections is decreasing. For Switzerland, new climate projections (CH2018) were just recently released, which would allow a more comprehensive assessment of precipitation changes.

Lastly, the testing of different models for the impact assessment on ice cover revealed that the formulations of physical processes in most ice modules currently implemented in hydrodynamic models have some deficiencies. Due to time restrictions and some concerns with regard to the source code of the ice model Delft3D was, therefore, not included in the studies as was originally planned. This would be another future step to take, since it includes a mechanical model to compute the spatial ice movement. This would particularly be interesting, as modified ice dynamics must be expected not only due to climate change, but also do to extended PS operation.

PS effects on temperature and water quality of the connected water bodies need to be studied in any case when recommissioning of existing PS hydropower plants takes place. In accordance to the outcomes of this thesis, climate change effects should be considered as well. Whether the worst case scenario¹⁴ needs to be taken into account for developing future climate projections remains questionable and was not addressed in this thesis. Nevertheless, the use of a weather generator has proven to be a reliable tool for developing such climate projections. The consideration of future climate scenarios is, therefore, feasible for other sites. Yet, this requires more model runs (and computation time) as well as additional memory compared to the current approach that just considers meteorological observations to force the model.

¹⁴ Herein the A2 emission scenario which does not consider any mitigation measures is considered.

References

- Adrian R, Wilhelm S, Gerten D (2006) Life-history traits of lake plankton species may govern their phenological response to climate warming. *Global Change Biology* 12:652-661.
- Ammann MA (1987) Herkunft und Zusammensetzung von Silt in fließenden Gewässern und Stauseen - Geotechnische Abtragungsanalysen im Alpenraum, ETH Zürich, Zurich.
- Amt für Umwelt Kanton St. Gallen (2018) Umwelt im Kanton St. Gallen: Kenngrößen für den Zürichobersee. <http://www.umwelt.sg.ch/home/Themen/wasser/seen/zuerich-obersee.html>, accessed on 2018-10-15.
- Anderson MA (2006) Technical analysis of the potential water quality impacts of LEAPS on Lake Elsinore. Department of Environmental Sciences, University of California Riverside, Riverside, CA.
- Anderson MA (2010) Influence of pumped-storage hydroelectric plant operation on a shallow polymictic lake: Predictions from 3-D hydrodynamic modeling. *Lake and Reservoir Management* 26:1-13.
- Anderson MA, Komor A, Ikehata K (2014) Flow routing with bottom withdrawal to improve water quality in Walnut Canyon Reservoir, California. *Lake and Reservoir Management* 30:131-142.
- AQUAPLUS (2013) Seegrunduntersuchungen Bätzimatt (Tuffen SZ. Zürichsee). Amt für Natur, Jagd und Fischerei Kanton SZ.
- Barbour E, Grant Wilson IA, Radcliffe J, et al. (2016) A review of pumped hydro energy storage development in significant international electricity markets. *Renewable and Sustainable Energy Reviews* 61:421-432.
- Basler & Hofmann AG (2014) Konzessionserneuerung Pumpspeicherkraftwerk Etzelwerk - Voruntersuchung mit Pflichtenheft zum Umweltverträglichkeitsbericht 1. Stufe, im Auftrag der SBB AG.
- Bell E, Kramer S, Zajanc D, et al. (2008) Salmonid fry stranding mortality associated with daily water level fluctuations in Trail Bridge Reservoir, Oregon. *North American Journal of Fisheries Management* 28:1515-1528.
- Bellmore RJ, Duda JJ, Craig LS, et al. (2017) Status and trends of dam removal research in the United States. *Wiley Interdisciplinary Reviews: Water* 4:e1164.
- Benson BJ, Magnuson JJ, Jensen OP, et al. (2012) Extreme events, trends, and variability in Northern Hemisphere lake-ice phenology (1855-2005). *Climatic Change* 112:299-323.
- Bermúdez M, Cea L, Puertas J, et al. (2017) Numerical modeling of the impact of a pumped-storage hydroelectric power plant on the reservoirs' thermal stratification structure: A case study in NW Spain. *Environmental Modeling & Assessment* 23:71-85.
- Björnsen Gurung A, Borsdorf A, Füreder L, et al. (2016) Rethinking pumped storage hydropower in the European Alps. *Mountain Research and Development* 36:222-232.
- Bollrich G (2007) Technische Hydromechanik 1. Verlag Bauwesen, Berlin.
- Bonalumi M, Anselmetti FS, Kägi R, et al. (2011) Particle dynamics in high-Alpine proglacial reservoirs modified by pumped-storage operation. *Water Resources Research* 47:W09523.

- Bonalumi M, Anselmetti FS, Wüest A, et al. (2012) Modeling of temperature and turbidity in a natural lake and a reservoir connected by pumped-storage operations. *Water Resources Research* 48:W08508.
- Bruce LC, Frassl MA, Arhonditsis GB, et al. (2018) A multi-lake comparative analysis of the General Lake Model (GLM): Stress-testing across a global observatory network. *Environmental Modelling & Software* 102:274-291.
- Bueche T, Hamilton DP, Vetter M (2017) Using the General Lake Model (GLM) to simulate water temperatures and ice cover of a medium-sized lake: a case study of Lake Ammersee, Germany. *Environmental Earth Sciences* 76:461.
- Butcher JB, Nover D, Johnson TE, et al. (2015) Sensitivity of lake thermal and mixing dynamics to climate change. *Climate Change* 129:295-305.
- Byrne MP, O'Gorman RA (2016) Understanding decreases in land relative humidity with global warming: conceptual model and GCM simulations. *Climate Change* 124:301-315.
- CH2011 (2011) Swiss climate change scenarios CH2011. C2SM, MeteoSwiss, ETH, NCCR Climate and OcCC, Zurich, Switzerland.
- CH2014 (2014) Toward quantitative scenarios of climate change impacts in Switzerland. OCCR, FOEN, MeteoSwiss, C2SM, Agroscope, and ProClim, Bern, Switzerland, p. 136 pp.
- CH2018 (2018) CH2018 – Climate Scenarios for Switzerland, Technical Report. National Centre for Climate Services, Zurich, p. 271.
- Cheng B, Zhang Z, Vihma T, et al. (2008) Model experiments on snow and ice thermodynamics in the Arctic Ocean with CHINARE 2003 data. *Journal of Geophysical Research* 113:C09020.
- Cole TM, Wells SA (2013) CE-QUAL-W2: A two-dimensional, laterally averaged, hydrodynamic and water quality model, version 3.71. User manual. Department of Civil and Environmental Engineering, Portland State University.
- de Goede E, Wagner T, de Graaff R, et al. (2014) Modelling of ice growth and transport on a regional scale, with application to Fountain Lake, Minnesota, USA. ASME 2014 33rd International Conference on Ocean, Offshore and Arctic Engineering. American Society of Mechanical Engineers.
- Deacon EL (1970) The derivation of Swinbank's long-wave radiation formula. *Quarterly Journal of the Royal Meteorological Society* 96:313-319.
- Deane JP, Gallachoir BÒ, McKeogh E (2010) Techno-economic review of existing and new pumped hydro energy storage plant. *Renewable and Sustainable Energy Reviews* 14:1293-1302.
- Deliman PN, Gerald JA (2002) Application of the two-dimensional hydrothermal and water quality model, CE-QUAL-W2, to the Chesapeake Bay - Conowingo Reservoir. *Lake and Reservoir Management* 18:10-19.
- Delpla I, Jung A-V, Baures E, et al. (2009) Impacts of climate change on surface water quality in relation to drinking water production. *Environment International* 35:1225-1233.
- Dibike Y, Prowse T, Saloranta T, et al. (2011) Response of Northern Hemisphere lake-ice cover and lake-water thermal structure patterns to a changing climate. *Hydrological Processes* 25:2942-2953.
- Dickey TD, Manov DV (1994) Determination of longwave heat flux at the air-sea interface using measurements from buoy platforms. *Journal of Atmospheric and Oceanic Technology* 11:1057-1078.
- Diem T, Koch S, Schwarzenbach S, et al. (2012) Greenhouse gas emissions (CO₂, CH₄, N₂O) from several perialpine and alpine hydropower reservoirs by diffusion and loss in turbines. *Aquatic Sciences* 74:619-635.

- Dilley AC, O'Brien DM (1998) Estimating downward clear sky long-wave irradiance at the surface from screen temperature and precipitable water. *Quarterly Journal of the Royal Meteorological Society* 124:1391-1401.
- Doherty J (2010) PEST - Model-independent parameter estimation. User manual: 5th edition. Watermark Numerical Computing.
- Doherty J, Johnston JM (2003) Methodologies for calibration and predictive analysis of a watershed model. *Journal of the American Water Resources Association* 39:251-265.
- Dokulil MT (2014) Impact of climate warming on European inland waters. *Inland Waters* 4:27-40.
- Dokulil MT, Teubner K, Jagsch A, et al. (2010) The impact of climate change on lakes in Central Europe. in George G (ed.) *The impact of climate change on European Lakes*. Springer, Dordrecht, pp. 387-409.
- EU (2009) Directive 2009/28/EC of the European Parliament and of the Council of 23 April 2009 on the promotion of the use of energy from renewable sources and amending and subsequently repealing Directives 2001/77/EC and 2003/30/EC.2009.
- EU Commission (2011) Energy Roadmap 2050, COM 2011, 885(2).
- Evans A, Strezov V, Evans TJ (2012) Assessment of utility energy storage options for increased renewable energy penetration. *Renewable and Sustainable Energy Reviews* 16:4141-4147.
- Fenocchi A, Rogora M, Sibilla S, et al. (2017) Relevance of inflows on the thermodynamic structure and on the modeling of a deep subalpine lake (Lake Maggiore, Northern Italy/Southern Switzerland). *Limnologia* 63:42-56.
- Ficke AD, Myrick CA, Hansen LJ (2007) Potential impacts of global climate change on freshwater fisheries. *Reviews in Fish Biology and Fisheries* 17:581-613.
- Ficker H, Luger M, Gassner H (2017) From dimictic to monomictic: Empirical evidence of thermal regime transitions in three deep alpine lakes in Austria induced by climate change. *Freshwater Biology* 62:1335-1345.
- Fink G, Schmid M, Wahl B, et al. (2014) Heat flux modifications related to climate-induced warming of large European lakes. *Water Resources Research* 50:2072-2085.
- Fink G, Wessels M, Wüest A (2016) Flood frequency matters: Why climate change degrades deep-water quality of peri-alpine lakes. *Journal of Hydrology* 540:457-468.
- Fischer A, Liniger M, Appenzeller C (2015) Climate scenarios of seasonal means: extensions in time and space, CH2011 Extension Series No. 2. Zurich, p. 18.
- Flerchinger GN, Xaio W, Marks D, et al. (2009) Comparison of algorithms for incoming atmospheric long-wave radiation. *Water Resources Research* 45:W03423.
- Fowler HJ, Blenkinsop S, Tebaldi C (2007) Linking climate change modelling to impacts studies: Recent advances in downscaling techniques for hydrological modelling. *International Journal of Climatology* 27:1547-1578.
- Gammeter S, Forster R (2002) *Langzeituntersuchungen im Zürichersee 1972-2000*. Wasserversorgung Zürich, Zürich.
- Gebre S, Boissy T, Alfredsen K (2014a) Sensitivity of lake ice regimes to climate change in the Nordic region. *The Cryosphere* 8:1589-1605.
- Gebre S, Boissy T, Alfredsen K (2014b) Sensitivity to climate change of the thermal structure and ice cover regime of three hydropower reservoirs. *Journal of Hydrology* 510:208-227.

- Goudsmit G-H, Burchard H, Peeters F, et al. (2002) Application of $k-\epsilon$ turbulence models to enclosed basins: the role of internal seiches. *Journal of Geophysical Research C: Oceans* 107(C12):3230
- GSchV (1998) Gewässerschutzverordnung vom 28. Oktober 1998 (GSchV), SR 814.201.
- Gudasz C, Bastviken D, Steger K, et al. (2010) Temperature-controlled organic carbon mineralization in lake sediments. *Nature* 466:478-481.
- Harby A, Sauterleute J, Korpås M, et al. (2013) Pumped storage hydropower. in Stolten D, Scherer V (eds.) *Transition to renewable energy systems*. Wiley-VCH Verlag GmbH & Co. KGaA, Weinheim, Germany, pp. 597-618.
- Hauck FR, Edson QA (1976) Pumped storage: Its significance as an energy source and some biological ramifications. *Transactions of the American Fisheries Society* 105:158-164.
- Haynes W (2014) *CRC Handbook of chemistry and physics*. CRC press., Boca Raton, FL.
- Helland I, Finstad AG, Forseth T, et al. (2011) Ice-cover effects on competitive interactions between two fish species. *Journal of Animal Ecology* 80:539-547.
- Hipsey MR, Bruce LC, Boon C, et al. (2018) A General Lake Model (GLM 2.4) for linking with high-frequency sensor data from the Global Lake Ecological Observatory Network (GLEON). *Geoscientific Model Development Discussions*.
- Hirsch PE, Eloranta AP, Amundsen P-A, et al. (2017) Effects of water level regulation in alpine hydropower reservoirs: An ecosystem perspective with a special emphasis on fish. *Hydrobiologia* 794:287-301.
- Hovel RA, Carlson SM, Quinn TP (2016) Climate change alters the reproductive phenology and investment of a lacustrine fish, the three-spine stickleback. *Global Change Biology* 23:2308-2320.
- Huisman J, Codd GA, Paerl HW, et al. (2018) Cyanobacterial blooms. *Nature Reviews Microbiology* 16:471-483.
- Ibrahim H, Ghandour M, Dimitrova M, et al. (2011) Integration of wind energy into electricity systems: Technical challenges and actual solutions *Energy Procedia* 6:815-824.
- Ibrahim H, Ilinca A, Perron J (2008) Energy storage systems - characteristics and comparisons. *Renewable and Sustainable Energy Reviews* 12:1221-1250.
- Idso SB (1973) On the concept of lake stability. *Limnology and Oceanography* 18:681-683.
- Immendoerfer A, Tietze I, Hottenroth H, et al. (2017) Life-cycle impacts of pumped hydropower storage and battery storage. *International Journal of Energy and Environmental Engineering* 8:231-245.
- IPCC (2014) *Climate change 2014: Synthesis report. Contribution of working groups I, II and III to the fifth assessment report of the Intergovernmental Panel on Climate Change*. IPCC, Geneva, Switzerland.
- Jensen HS, Andersen FØ (1992) Importance of temperature, nitrate, and pH for phosphate release from aerobic sediments of four shallow, eutrophic lakes. *Limnology and Oceanography* 37:577-589.
- Jeppesen E, Mehner T, Winfield IJ, et al. (2012) Impacts of climate warming on the long-term dynamics of key fish species in 24 European lakes. *Hydrobiologia* 694:1-39.
- Keller D, Fischer A, Frei C, et al. (2015) Implementation and validation of a Wilks-type multi-site daily precipitation generator over a typical Alpine river catchment. *Hydrological Earth System Sciences* 19:2163-2177.
- Keller DE, Fischer AM, Liniger MA, et al. (2017) Testing a weather generator for downscaling climate change projections over Switzerland. *International Journal of Climatology* 37:928-942.

- Keller H, Weibel P (1991) Suspended sediments in streamwater - indicators of erosion and bed load transport in mountainous basins. *IAHS Publication* 203:53-61.
- Kobler UG, Wüest A, Schmid M (2018) Effects of lake-reservoir pumped-storage operations on temperature and water quality. *Sustainability* 10:1968.
- Kobler UG, Wüest A, Schmid M (2019) Combined effects of pumped-storage operation and climate change on thermal structure and water quality. *Climatic Change*. Accepted.
- Kraemer BM, Anneville O, Chandra S, et al. (2015) Morphometry and average temperature affect lake stratification responses to climate change. *Geophysical Research Letters* 42:4981-4988.
- Kuo J-T, Lung W-S, Yang C-P, et al. (2006) Eutrophication modelling of reservoirs in Taiwan. *Environmental Modelling & Software* 21:829-844.
- Laybourn-Parry J, Tranter M, Hodson A (2012) The ecology of snow and ice environments. Oxford University Press, Oxford.
- Leppäranta M (2014) Freezing of lakes and the evolution of their ice cover. Springer Science & Business Media, Heidelberg.
- Liu LX, Wu JC (1999) Research on ice formation during winter operation for a pumped storage station. in Shen HT (ed.) *Ice in Surface Waters*. A. A. Balkema, Rotterdam, pp. 753-759.
- Liu W-C, Chen W-B, Kimura N (2009) Impact of phosphorus load reduction on water quality in a stratified reservoir-eutrophication modeling study. *Environmental Monitoring and Assessment* 159:393-406.
- Livingstone DM (2003) Impact of secular climate change on the thermal structure of a large temperate Central European lake. *Climatic Change* 57:205-225.
- Magee MR, Wu CH, Robertson DM, et al. (2016) Trends and abrupt changes in 104 years of ice cover and water temperature in a dimictic lake in response to air temperature, wind speed, and water clarity drivers. *Hydrology and Earth System Sciences* 20:1681-1702.
- Maykut GA, Untersteiner N (1969) Numerical prediction of the thermodynamic response of Arctic sea ice to environmental changes. The Rand Corporation, Santa Monica, California, USA.
- Me W, Hamilton DP, McBride CG, et al. (2018) Modelling hydrology and water quality in a mixed land use catchment and eutrophic lake: Effects of nutrient load reductions and climate change. *Environmental Modelling & Software* 109:114-133.
- Menshutkin VV, Rukhovets LA, Filatov. NN (2013) Ecosystem modeling of freshwater lakes (Review): 1. Hydrodynamics of lakes. *Water Resources* 40:606-620.
- Menshutkin VV, Rukhovets LA, Filatov. NN (2014) Ecosystem modeling of freshwater lakes (Review): 2. Models of freshwater lake's ecosystem. *Water Resources* 41:32-45.
- Mieleitner J, Reichert P (2006) Analysis of the transferability of a biogeochemical lake model to lakes of different trophic state. *Ecological Modelling* 194:49-61.
- Mieleitner J, Reichert P (2008) Modelling functional groups of phytoplankton in three lakes of different trophic state *Ecological Modelling* 211:279-291.
- Mooij WM, Hülsmann S, De Senerpont Domis LN, et al. (2005) The impact of climate change on lakes in the Netherlands: A review. *Aquatic Ecology* 39:381-400.
- Mooij WM, Trolle D, Jeppesen E, et al. (2010) Challenges and opportunities for integrating lake ecosystem modelling approaches. *Aquatic Ecology* 44:633-667.

- Moore MV, Hampton SE, Izmet'eva LR, et al. (2009) Climate change and the world's "Sacred Sea" — Lake Baikal, Siberia. *BioScience* 59:405-417.
- Müller M, De Cesare G, Schleiss AJ (2016) Flow field in a reservoir subject to pumped-storage operation – in situ measurement and numerical modeling. *Journal of Applied Water Engineering and Research*:1-16.
- North RP, Livingstone DM, Hari RE, et al. (2013) The physical impact of the late 1980s climate regime shift on Swiss rivers and lakes. *Inland Waters* 3:341-350.
- North RP, Livingstone DM, Köster O, et al. (2014) Long-term changes in hypoxia and soluble reactive phosphorus in the hypolimnion of a large temperate lake: Consequences of a climate regime shift. *Global Change Biology* 20:811-823.
- O'Reilly CM, Sharma S, Gray DK, et al. (2015) Rapid and highly variable warming of lake surface waters around the globe. *Geographical Research Letters* 42:10773-10781.
- Oveisy A, Boegman L, Imberger J (2012) Three-dimensional simulation of lake and ice dynamics during winter. *Limnology and Oceanography* 57:43-57.
- Park JC, Um M-J, Song Y-I, et al. (2017) Modeling of turbidity variation in two reservoirs connected by a water transfer tunnel in South Korea. *Sustainability* 9:993.
- Peleg N, Fatichi S, Paschalis A, et al. (2017) An advanced stochastic weather generator for simulating 2-D high-resolution climate variables. *Journal of Advances in Modeling Earth Systems* 9:1595-1627.
- Pérez-Díaz JI, Chazarra M, García-González J, et al. (2015) Trends and challenges in the operation of pumped-storage hydropower plants. *Renewable and Sustainable Energy Reviews* 44:767-784.
- Persson I, Jones I, Sahlberg J, et al. (2005) Modeled thermal response of three European lakes to a probable future climate. *Internationale Vereinigung für theoretische und angewandte Limnologie: Verhandlungen* 29:667-671.
- Peters-Kümmerly B (1973) Untersuchung über Zusammensetzung und Transport von Schwebstoffen in einigen Schweizer Flüssen. *Geographica Helvetica* 28:137-151.
- Potter DU, Stevens MP, Meyer JL (1982) Changes in physical and chemical variables in a new reservoir due to pumped storage operations. *JAWRA Journal of the American Water Resources Association* 18:627-633.
- Powers SM, Hampton SE (2016) Winter limnology as a new frontier. *Limnology and Oceanography Bulletin* 25:103-108.
- Prats J, Salençon M-J, Gant M, et al. (2018) Simulation of the hydrodynamic behaviour of a Mediterranean reservoir under different climate change and management scenarios. *Journal of Limnology* 77:62-81.
- Prowse T, Alfredsen K, Beltaos S, et al. (2011) Effects of changes in Arctic lake and river ice. *Ambio* 40:63-74.
- Råman Vinnå L, Wüest A, Zappa M, et al. (2018) Tributaries affect the thermal response of lakes to climate change. *Hydrology and Earth System Sciences* 22:31-51.
- Ramos-Fuertes A, Palau A, Dolz J (2018) Application of a two-dimensional water quality model (CE-QUAL-W2) to the thermal impact assessment of a pumped-storage hydropower plant project in a mountainous reservoir (Matalavilla, Sil River, Spain). in Gourbesville P, Cunge J, Caignaert G (eds.) *Advances in Hydroinformatics*. Springer Water. Springer, Singapore, pp. 301-314.
- Rehman S, Al-Hadhrami LM, Alam MM (2015) Pumped hydro energy storage system: A technological review. *Renewable and Sustainable Energy Reviews* 44:586-598.
- Reid PC, Hari RE, Beaugrand G, et al. (2016) Global impacts of the 1980s regime shift. *Global Change Biology* 22:682-703.

- REN21 (2017) Renewables 2017: Global status report. REN21 Secretariat, Paris.
- Rogers CK, Lawrence GA, Hamblin PF (1995) Observations and numerical simulation of a shallow ice-covered mid-latitude lake. *Limnology and Oceanography* 40:374-385.
- Romero JR, Antenucci JP, Imberger J (2004) One- and three-dimensional biogeochemical simulations of two differing reservoirs. *Ecological Modelling* 174:143-160.
- Rühland KM, Paterson AM, Smol JP (2015) Lake diatom responses to warming: reviewing the evidence. *Journal of Paleolimnology* 54:1-35.
- Salonen K, Leppäranta M, Viljanen M, et al. (2009) Perspectives in winter limnology: closing the annual cycle of freezing lakes. *Aquatic Ecology* 43:609-616.
- Saloranta TM, Andersen T (2007) MyLake—A multi-year lake simulation model code suitable for uncertainty and sensitivity analysis simulations. *Ecological Modelling* 207:45-60.
- SCCER-SoE (2018) SCCER-SoE Science Report. Swiss Competence Center for Energy Research - Supply of Electricity, Zurich.
- Schaeffli B (2015) Projecting hydropower production under future climates: A guide for decision-makers and modelers to interpret and design climate change impact assessments. *Wiley Interdisciplinary Reviews: Water* 2:271-289.
- Schaeffli B, Manso P, Fischer M, et al. (2019) The role of glacier retreat for Swiss hydropower production. *Renewable Energy* 132:615-627.
- Schildknecht A, Köster O, Koss M, et al. (2013) Gewässerzustand von Zürichsee, Zürichobersee und Walensee - Auswertungen der Untersuchungsergebnisse bis 2010, Tech. Bericht der Stadt Zürich. Wasserversorgung Zürich, Zürich.
- Schlabing D, Frassl MA, Eder MM, et al. (2014) Use of a weather generator for simulating climate change effects on ecosystems: A case study on Lake Constance. *Environmental Modelling & Software* 61:326-338.
- Schmid M, Hunziker S, Wüest A (2014) Lake surface temperatures in a changing climate: A global sensitivity analysis. *Climatic Change* 124:301-315.
- Schmid M, Köster O (2016) Excess warming of a Central European lake driven by solar brightening. *Water Resources Research* 52:8103-8116.
- Schmucki E, Marty C, Fierz C, et al. (2014) Evaluation of modelled snow depth and snow water equivalent at three contrasting sites in Switzerland using SNOWPACK simulations driven by different meteorological data input. *Cold Regions Science and Technology* 99:27-37.
- Semptner AJJ (1976) A model for the thermodynamic growth of sea ice in numerical investigations of climate. *Journal of Physical Oceanography* 6:379-389.
- Shuter BJ, Finstad AG, Helland IP, et al. (2012) The role of winter phenology in shaping the ecology of freshwater fish and their sensitivities to climate change. *Aquatic Sciences* 74:637-657.
- Smith EA, Kiesling RL, Galloway JM, et al. (2014) Water quality and algal community dynamics of three deepwater lakes in Minnesota utilizing CE-QUAL-W2 models: U. S. Geological Survey Scientific Investigations 2014-5066. p. 73.
- Solvang E, Harby A, Killingtveit Å (2012) Increasing balance power capacity in Norwegian hydroelectric power stations. SINTEF Energy Report TR A7126, SINTEF Energi, Trondheim.

- Stanford JA, Hauer FR (1992) Mitigating the impacts of stream and lake regulation in the Flathead River catchment, Montana, USA – an ecosystem perspective. *Aquatic Conservation: Marine and Freshwater Ecosystems* 2:35-63.
- Stepanenko VM, Martynov A, Jöhnk KD, et al. (2013) A one-dimensional model intercomparison study of thermal regime of a shallow, turbid midlatitude lake. *Geoscientific Model Development* 6:1337-1352.
- Straile D, Kerimoglu O, Peeters F (2015) Trophic mismatch requires seasonal heterogeneity of warming. *Ecology* 96:2794-2805.
- Trolle D, Skovgaard H, Jeppesen E (2008) The Water Framework Directive: Setting the phosphorus loading target for a deep lake in Denmark using the 1D lake ecosystem model DYRESM-CAEDYM. *Ecological Modelling* 219:138-152.
- Unsworth MH, Monteith JL (1975) Long-wave radiation at the ground. *Quarterly Journal of the Royal Meteorological Society* 101:13-24.
- USBR (1993) Aquatic ecology studies of Twin Lakes, Colorado, 1971-1986: Effects of a pumped-storage hydroelectric project on a pair of montane lakes. 200 Monograph No. 43, Denver, CO.
- van der Linden L, Daly RI, Burch MD (2015) Suitability of a coupled hydrodynamic water quality model to predict changes in water quality from altered meteorological boundary conditions. *Water* 7:348-361.
- Weber M, Rinke K, Hipsey MR, et al. (2017) Optimizing withdrawal from drinking water reservoirs to reduce downstream temperature pollution and reservoir hypoxia. *Journal of Environmental Management* 197:96-105.
- Wildman RA, Chan NW, Dalleska NF, et al. (2010) Effect of changes in water level on sediment pore water redox geochemistry at a reservoir shoreline. *Applied Geochemistry* 25:1902-1911.
- Winder M, Schindler DE (2004) Climate change uncouples trophic interactions in an aquatic ecosystem. *Ecology* 85:2100-2106.
- Woolway RI, Dokulil MT, Marszelewski W, et al. (2017) Warming of Central European lakes and their response to the 1980s climate regime shift. *Climatic Change* 142:505-520.
- Xia XH, Wu Q, Mou XL, et al. (2014) Potential impacts of climate change on the water quality of different water bodies. *Journal of Environmental Informatics* 25:85-98.
- Yao H, Samal NR, Joehnk KD, et al. (2014) Comparing ice and temperature simulations by four dynamic lake models in Harp Lake: past performance and future predictions. *Hydrological Processes* 28:4587-4601.
- Zappa M, Andres N, Kienzler P, et al. (2015) Crash-Tests for forward-looking flood control in the city of Zürich (Switzerland). *Proc. IAHS* 370:235-242.
- Zou R, Carter S, Shoemaker L, et al. (2006) Integrated hydrodynamic and water quality modeling system to support nutrient total maximum daily load development for Wissahickon Creek, Pennsylvania. *Journal of Environmental Engineering* 132:555-566.

Curriculum Vitae

CONTACT INFORMATION

Ulrike Gabriele Kobler
Grossmatt 4
6052 Hergiswil NW
Switzerland

+41 76 796 44 70
ulrike.kobler@icloud.com

PERSONAL INFORMATION

Date of birth	05.03.1986
Place of birth	Wels
Nationality	Austria
Civil status	Single

EMPLOYMENT HISTORY

03/2013 - 10/2014	Partial employee at Architekturbüro Dipl.-Ing. Kobler
03/2008 - 07/2008	Tutor at Vienna University of Technology, Institute of Building Construction and Technology, Research Division of Mechanics and Structural Dynamics
10/2008 - 02/2009	Tutor at Vienna University of Technology, Institute of Building Construction and Technology, Research Division of Mechanics and Structural Dynamics
2002 - 2012	Internships at Architekturbüro Dipl.-Ing. Kobler
07/2001 - 08/2001	Internship at Max Häuserer Bauunternehmen GmbH

EDUCATION

10/2014 – 01/2019	Ph.D. thesis at the Swiss Federal Institute of Aquatic Science and Technology (Eawag), Kastanienbaum, Switzerland
08/2011 - 03/2014	Vienna University of Technology, Austria Master in Civil Engineering Thesis: Rainfall-runoff modelling: Dependence of model parameters on time and objective functions
08/2006 - 07/2011	Vienna University of Technology, Austria Bachelor in Civil Engineering Thesis: Bewertung des Einflusses der Poliereinwirkung auf die Bestimmung der Polierresistenz von Sanden mit dem Prüfverfahren nach Wehner/Schulze
08/2006	Change of Degree Programme
10/2005 - 08/2006	Johannes Kepler University Linz, Austria
09/2000 - 06/2005	Higher Technical School Linz Goethestrasse, Austria

PROFESSIONAL QUALIFICATIONS

LANGUAGE SKILLS: German (native), English (very good command), French (basic)

COMPUTER SKILLS:

PROGRAMMING LANGUAGES: Python (experienced), Fortran (experienced), C++ (basic)
HYDRODYNAMIC MODELS: GLM, Simstrat, MyLake, CE-QUAL-W2, Delft3D
DATA PROCESSING: R, Python
DATABASE: SQLite, PostgreSQL
GIS: QGIS, SAGA

PUBLICATIONS

PAPERS IN ISI JOURNALS

Kobler, U. G.; Wüest, A.; Schmid, M. (2019) Combined effects of pumped-storage operation and climate change on thermal structure and water quality, *Climatic Change*.
DOI: 10.1007/s10584-018-2340-x

Kobler, U. G.; Wüest, A.; Schmid, M. (2018) Effects of lake-reservoir pumped-storage operations on temperature and water quality, *Sustainability*, 10(6), 1968.
DOI: 10.3390/su10061968

CONFERENCE PRESENTATIONS

Trento, IT – 5th European Congress of the International Association for Hydrology, 2018
Kobler, U.G.; Wüest, A.; Schmid, M.:
Coupled climate change and pumped-storage effects on temperature and stratification

Olomouc, CZ - 10th Symposium for European Freshwater Sciences, 2017
Kobler, U.G.; Schmid, M.; Wüest, A.:
Water quality impacts in the context of changing operation mode of a pumped-storage hydropower plant

Torino, IT – 23rd Congress of the International Society of Limnology, 2016
Kobler, U.G.; Schmid, M.; Wüest, A.:
Assessing the impacts of pumped-storage operations

San Francisco, US - Fall Meeting of the American Geophysical Union, 2014
Parajka, J.; Rogger, M.; Kobler, U.; Salinas, J.; Nester, T.; Blöschl, G.:
TUWmodel: an educational hydrologic model in R

INTERESTS

Hiking, Pilates, Traveling, Graphic design, Photography

